

Contract No. DTFACT-15-D-00007
Delivery Order 005 NAPTF Support
Deliverable 4.9.5.1
National Airport Pavement Construction Cycle 1 (CC1)
Comprehensive Report

December 2019

Submitted by General Dynamics Information Technology
Prepared by Applied Research Associates, Inc.

GENERAL DYNAMICS
Information Technology

TABLE OF CONTENTS

	Page
1. INTRODUCTION	1
1.1 National Airport Pavement Test Facility (NAPTF)	1
1.2 Objectives	3
1.3 Construction Cycle 1 (CC1) Experimental Design	4
2. DESIGN, CONSTRUCTION AND INSTRUMENTATION OF CC1	7
2.1 NAPTF Design	7
2.1.1 Geometry Design	7
2.1.2 CC1 Pavement Design	13
2.2 Material Properties and Construction	13
2.2.1 Subgrade	14
2.2.2 P-501 Portland Cement Concrete (PCC)	16
2.2.3 P-154 Subbase and P-209 Base Material	17
2.2.4 P-306 Cement Stabilized Base (Econcrete)	20
2.2.5 Hot Mix Asphalt Materials	20
2.3 Instrumentation	21
2.3.1 Multi-Depth Deflectometer (MDD)	23
2.3.2 Asphalt Strain Gauge (ASG)	25
2.3.3 Concrete Strain Gauge (CSG)	28
2.3.4 Pressure Cell (PC)	29
2.4 Uniformity Test	31
2.4.1 Testing Method and Equipment	31
2.4.2 Data Collection	32
2.4.3 Findings for Rigid Pavement	33
2.4.4 Findings for Flexible Pavement	39
2.4.5 Summary	40
3. PAVEMENT RESPONSE AND TRAFFIC TESTING	41
3.1 Traffic Testing of Rigid Pavement	44
3.1.1 Traffic Testing	44

3.2 Pavement Response and Traffic Testing of Flexible Pavement	50
3.2.1 Static Response Test	50
3.2.2 Traffic Testing	54
3.2.3 Slow-Speed Traffic Tests	73
4. POST-TRAFFIC TESTING	77
4.1 Trenching	78
4.1.1 Data Collections	78
4.1.2 Findings	81
4.2 Test Pit and Coring	100
4.2.1 Data Collection	100
4.2.2 Findings from Test Pit Investigation	104
4.3 Summary of Post-Traffic Testing	113
5. SUMMARY	113
5.1 Rigid Pavement	113
5.2 Flexible Pavement	114
6. REFERENCES	115
Appendix A – Material Properties	
Appendix B – Stasis Sensor Types and Locations	
Appendix C – Dynamic Sensor Types and Locations	
Appendix D – Post-Traffic Trench Data	
Appendix E – Construction Cycle 1 Historical Record Drawings	

LIST OF FIGURES

Figure	Page
1 NAPTF Building Construction	1
2 NAPTF During Construction (www.airporttech.tc.faa.gov)	2
3 National Airport Pavement Test Vehicle (NAPTV)	3
4 Construction Cycle (CC) at the NAPTF	3
5 Plan View of the NAPTF Test Items during CC1	5
6 Cross-Sectional Views of CC1 Rigid Test Items (Garg 2003)	5
7 Cross-Sectional Views of the CC1 Stabilized Base Flexible Test Items (Garg 2003)	6
8 Cross-Sectional Views of CC1 Conventional Base Flexible Text Items (Garg 2003)	6
9 Initial Design Profile for Items on Low Strength Subgrade	8
10 Initial Design Profile for Items on Medium Strength Subgrade	9
11 Initial Design Profile for Items on High Strength Subgrade	10
12 Historical Record Pavement Cross Section for Items on Low Strength Subgrade	11
13 Historical Record Pavement Cross Section for Items on Medium Strength Subgrade	12
14 Historical Record Pavement Cross Section for Items on High Strength Subgrade	13
15 CC1 Concrete Placement for Test Section Construction, Completed May 1999	17
16 Resilient Modulus Test Results for P-154 Subbase Material (Garg 1999)	19
17 Resilient Modulus Test Results for P-209 Base Material (Garg 1999)	20
18 HSDAS Schematic (Hayhoe, et al. 2001)	23
19 Installation of Multi-Depth Deflectometer (MDD) (Garg 2003)	24
20 Horizontal Locations of the MDDs in MFC Test Section (Hayhoe and Garg 2002)	25
21 Vertical Location of the MDD Sensors (CTL 1998)	25
22 Asphalt CSG (Garg and Hayhoe 2001)	26
23 ASG Installation	26
24 ASG Locations in Flexible Test Sections (CTL 1998)	27
25 Locations of CSGs in Rigid Pavement Test Items (Guo et al. 2002)	28
26 CSG Installation	29
27 6-inch Pressure Cell (CTL 1998)	29
28 2-inch Pressure Cell (CTL 1998)	30
29 PC Locations in Flexible Test Sections (CTL 1998)	31
30 FAA's KUAB Model 240 HWD Equipment	32
31 Location of the Deflection Sensors	33
32 Comparison of FWD Deflections D0 and D5 at Center of Slab for the Three Rigid Test Items (Hayhoe, et al. 1999)	35
33 Locations of HWD Joint Tests for NAPTF Rigid Test Items (Brill and Guo 2000)	36
34 Average Deflections D0 and D5 at the Center of the Slabs (Guo and Marsey 2001)	37
35 Deflection D0 at the Joints and Corners (Load = 24,000 lbs.) (Guo and Marsey 2001)	38
36 6-Wheel and 4-Wheel Wander Patterns (Guo et al. 2002)	42
37 Wander Distribution (Hayhoe and Garg 2002)	42
38 Gear Configurations	44
39 Coordinate System for Rigid Pavement Test Items (Hayhoe et al. 2001)	45
40 Crack Patterns in Rigid Test Items (Guo et al. 2002)	47
41 Definition of Corner Crack Dimensions in Table 14 (Guo et al. 2002)	48
42 Typical Strain Responses in LRS for the 4-Wheel Load (Guo et al. 2002)	49
43 Strain Responses in HRS, Lane 3 (4-Wheel Load) (Guo et al. 2002)	50

44 MDD Locations and Gear Configuration for Static Tests (Garg and Marsey 2002)	51
45 A Typical MDD Time History for Static Test (Test Item LFC) (Garg and Marsey 2002)	51
46 Typical Deflection Response from MDD for 6-Wheel Loading (Hayhoe et al. 2004)	52
47 Recovered Surface Deflections from Static Load Tests for the Flexible Test Items (Garg and Marsey 2002)	53
48 Recovered Subgrade Deflections for the Flexible Test Items from Static Load Tests (Garg and Marsey 2002)	53
49 Subgrade Contribution to the Pavement Surface Deflection (Garg and Marsey 2002)	54
50 Longitudinal ASG Response Signal (Dual Loading) (Garg and Hayhoe 2001)	57
51 Longitudinal ASG Response Signal (6-Wheel Loading) (Garg and Hayhoe 2001)	57
52 Transverse ASG Response Signal (Single Axle Load Gear) (Garg and Hayhoe 2001)	57
53 Transverse ASG Response Signal (6-wheel) (Garg and Hayhoe 2001)	58
54 Location of HWD Test Lanes Results	59
55 Comparison of Average Deflections D0 for Flexible Test Items (Garg and Marsey 2002)	60
56 Comparison of Average Deflections D5 for Flexible Test Items (Garg and Marsey 2002)	61
57 Profile Line Locations	62
58 Straightedge Used for Rut Depth Measurements in CC1	62
59 TSP Rut Depth vs. N for Profile Line 1	63
60 TSP Rut Depth Measurements	64
61 Straight Edge Rut Depth Measurements for Low Strength Subgrade Test Items (Hayhoe and Garg 2004)	65
62 Straight Edge Rut Depth Measurements for Medium Strength Subgrade Test Items (Hayhoe and Garg 2004)	66
63 Permanent Deformation from MDD for Test Item LFC under 4-Wheel Loading (Hayhoe and Garg 2004)	67
64 Permanent Deformation from MDD for Test Item LFS under 6-Wheel Loading (Hayhoe and Garg 2004)	68
65 Permanent Deformation from MDD for Test Item MFC under 6-Wheel Loading (Hayhoe and Garg 2004)	69
66 Permanent Deformation from MDD for Test Item MFC under 4-Wheel Landing Gear (Hayhoe and Garg 2004)	70
67 Permanent Deformation from Test Items MDD for MFS under 6-Wheel Loading (Hayhoe and Garg 2004)	71
68 Permanent Deformation from MDD for Test Item MFS under 4-Wheel Loading (Hayhoe and Garg 2004)	71
69 Average Temperature in the HMA Layer of Test Item MFS (Hayhoe and Garg 2004)	72
70 Permanent Deformation from MDD for HFC Test Item under 6-Wheel Loading (Hayhoe and Garg 2004)	73
71 Peak AC Strains from Longitudinal ASGs for Test Item HFS (Test Date 4/20/00; Gauge Depth = 9.5 inches; Wheel Load = 36,000 lbs.) (Garg and Hayhoe 2001)	74
72 Peak AC Strains from Transverse ASGs for Test Item HFS (Test Date 4/20/00; Gauge Depth = 9.5 inches; Wheel Load = 36,000 lbs.) (Garg and Hayhoe 2001)	74
73 AC Strains – Time of Loading Relationship for Test Item HFS from Longitudinal ASGs (Test Date 4/20/00; Gauge Depth = 9.5 inches) (Garg and Hayhoe 2001)	75
74 AC Strains – Time of Loading Relationship for Test Item HFS from Transverse ASGs (Test Date 4/20/00; Gauge Depth = 9.5 inches) (Garg and Hayhoe 2001)	75

75 Post-Traffic Trench Locations	79
76 Post-Traffic Trench Test Pit Layout	80
77 Profile Measurements on a Trench Wall	80
78 CBR Test Locations at the Subgrade Surface	81
79 LFC Trench Section	82
80 Trench Layer Interface Profiles, LFC-E (West Face of Trench)	83
81 Trench Layer Interface Profiles, LFC-E (East Face of Trench)	83
82 Trench Layer Thicknesses, LFC-E (West Face of Trench)	84
83 Trench Layer Thicknesses, LFC-E (East Face of Trench)	84
84 LFS-E Trench Views	86
85 Trench Layer Interface Profiles, LFS-E (West Face of Trench)	87
86 Trench Layer Interface Profiles, LFS-E (East Face of Trench)	87
87 Trench Layer Thicknesses, LFS-E (West Face of Trench)	88
88 Trench Layer Thicknesses, LFS-E (East Face of Trench)	88
89 Pavement Layer Profile Measurements, MFC East (West Face of Trench)	89
90 Pavement Layer Profile Measurements, MFC East (East Face of Trench)	89
91 Pavement Layer Thickness in the MFC East Trench (West Face of Trench)	90
92 Pavement Layer Thickness in the MFC East Trench (East Face of Trench)	91
93 P-401 from Maximum Rutting Location (Center of 6-Wheel Traffic Path)	91
94 Lateral Movement of P-154 Subbase in Test Item MFC at the Center of 4-Wheel Traffic Path (South Side) (Garg 2003)	92
95 Lateral Movement of P-154 Subbase in Test Item MFC at the Center of 6-Wheel Traffic Path (Garg 2001)	93
96 Post-Traffic CBR Results on Subgrade Surface in MFC-E Trench	94
97 MFS East Trench Section	95
98 Layer Profile Measurements, MFS East (West Face of Trench)	96
99 Layer Profile Measurements, MFS East (East Face of Trench)	96
100 MFS West Trench Section in the 6-Wheel Traffic Path (Hayhoe and Garg 2004)	98
101 MFS West Trench Section in the 4-Wheel Traffic Path (Hayhoe and Garg 2004)	99
102 Layer Profile Measurements, MFS West (West Face of Trench)	100
103 Schematic of Testing Areas	101
104 Location of Test Pits in Each Area	101
105 Location of 12-inch Sand Cone Density Tests in P-209 Crushed Stone Base	101
106 Sand Cone Test	102
107 Schematic of Test Locations on P-154 in Test Pits	103
108 Location of DCP Tests on P-154 Layer	103
109 Test Locations within Test Pits in the Subgrade	104
110 Moisture and Dry Density Variation with Depth in LFC East Trench	105
111 Moisture and Dry Density Change with Depth in LFS East Trench	106
112 P-401 Surface Exhibiting Delamination	107
113 Core Showing Crack Location	108
114 P-401 Removal	108
115 Subgrade Penetration into P-154 Subbase in 4-Wheel Traffic Path	109
116 Variation in Subgrade Dry Density and Moisture Content with Depth in MFC East Trench	110

Contract No.: DTFACT-15-D-00007

117 Variation in Subgrade Dry Density and Moisture Content with Depth in MFS East Trench	111
118 Moisture and Dry Density Change with Depth in the MFS West Trench	112

LIST OF TABLES

Table	Page
1 CC1 Test Items Designations	5
2 CC1 Pavement Cross-Sectional Detail (Gervais et al. 2004)	6
3 Initial CBR and Soil Classification for Each Subgrade (McQueen 2000)	15
4 Test Pit CBR Results (McQueen 2000)	16
5 P-154 Gradation Data and Requirements for Argillite Screenings Subbase (Gagnon and Garg 2010)	18
6 P-209 Gradation Data and Requirements for Crushed Aggregate Base (Gagnon and Garg 2010)	18
7 Sensor Types Installed in the CC1 Pavement	22
8 Summary of FWD Basin Tests on Rigid Pavement Test Items (Hayhoe et al. 1999)	33
9 LTE for NAPTF Longitudinal Joints (Doweled Joints) (Brill and Guo 2000)	38
10 LTE for NAPTF Transverse Joints (Dummy Joints) (Brill and Guo 2000)	39
11 Summary of Uniformity Tests on Flexible Pavements at the NAPTF (Garg and Marsey 2002)	40
12 Transverse Gear Centerline (CL) Positions in a Complete Wander Cycle (Hayhoe et al. 2004)	43
13 Summary of Traffic Tests for Rigid Test Items in CC1	45
14 Summary of Average Crack Sizes for Rigid Test Items (Guo et al. 2002)	48
15 Summary of Traffic Tests for Flexible Test Items in CC1	56
16 TSP Rut Depth Measurements	64
17 Summary of Tests Performed	77
18 Post-Traffic Trench Identification and Location	79
19 Field Density and Moisture Results for LFC	104
20 CBR Change with Depth in LFC East Trench	105
21 CBR Change with Depth in LFS East Trench	106
22 Field Density and Moisture Results for MFC	109
23 CBR Change with Depth in the MFC East Trench	110
24 Subgrade CBR in the MFS East Trench	111
25 Subgrade CBR in the MFS West Trench	112

LIST OF ACRONYMS

AASHTO	American Association of State Highway and Transportation Officials
AC	Advisory Circular
ADC	Analog to Digital Converter
ASG	Asphalt Strain Gauge
ASTM	American Society for Testing and Materials
ATREL	Advanced Transportation Engineering Laboratory
B777	Boeing 777
CBR	California Bearing Ratio
CSG	Concrete Strain Gauge
CC	Construction Cycle
COV	Coefficients of Variation
CTL	Construction Technology Laboratories
DCP	Dynamic Cone Penetrometer
DT	Displacement Transducer
ERI	Engineering and Research International, Inc.
FAA	Federal Aviation Administration
FEM	Finite Element Method
FWD	Falling Weight Deflectometer
HMA	Hot Mix Asphalt
HSDAS	High Speed Data Acquisition System
HWD	Heavy Falling Weight Deflectometer
JG	Joint Gauge
LEDFAA	Layered Elastic Design Federal Aviation Administration
LET	Layered Elastic Theory
LTE	Load Transfer Efficiency
MDD	Multiple Depth Deflectometer
NAPTF	National Airport Pavement Test Facility
NAPTV	National Airport Pavement Test Vehicle
NDT	Non-Destructive Testing
NGA	New Generation Aircraft
PC	Pressure Cell
PCC	Portland Cement Concrete
QC	Quality Control
SPU	Signal Processing Unit
SHRP	Strategic Highway Research Program
TG	Temperature Gauges
TSP	Transverse Surface Profile

1. INTRODUCTION

1.1 National Airport Pavement Test Facility (NAPTF)

The introduction of new generation aircraft (NGA) such as the Boeing 777 (B777) in 1995 created a need to develop new airport pavement design procedures based on sound theoretical principles and with rational models verified from full scale test data. The new generation of aircraft have more wheels and a different landing gear configuration than the previous models causing concern that the existing pavement design procedures did not accurately predict pavement performance for the new generation of aircraft.

The National Airport Pavement Test Facility (NAPTF) was commissioned on April 12, 1999 as a public private partnership between the US Federal Aviation Administration (FAA) and the Boeing Company to generate full-scale pavement performance data for the development and verification of airport pavement thickness design procedures. The primary purpose of the NAPTF was to provide full-scale pavement response and performance data to support new computer based pavement thickness design procedures being developed by the FAA (Layered Elastic Design – FAA 1995).

The NAPTF is a 1200 ft. (365.8 m) long and 100 ft. (30.5 m) wide with a 900 ft. (274.3 m) long and 60 ft. (18.3 m) wide test area, fully enclosed, instrumented test track located at the FAA's William J. Hughes Technical Center, Atlantic City International Airport, New Jersey. Figure 1 and Figure 2 show the NAPTF building during construction.



Figure 1. NAPTF Building Construction

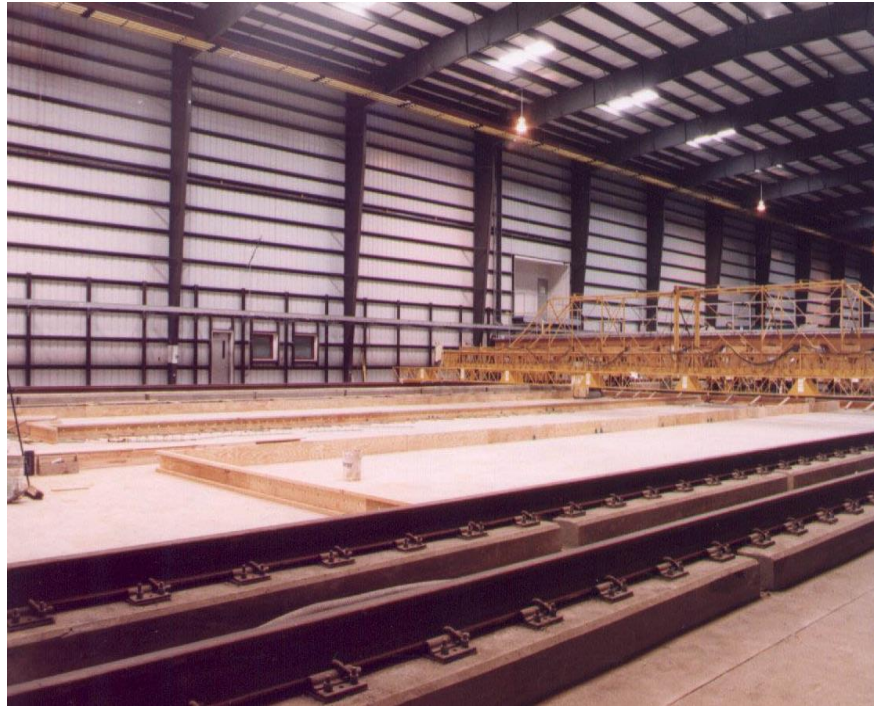


Figure 2. NAPTF During Construction (www.airporttech.tc.faa.gov)

As built, the NAPTF features fully instrumented rigid and flexible test pavements. Data from the test pavements is collected using a High Speed Data Acquisition System (HSDAS). The HSDAS uses high scan rates to collect dynamic response data and data loggers that used low scan rates for monitoring and recording static measurements. The NAPTF also features a unique test vehicle for loading the pavements. The National Airport Pavement Test Vehicle (NAPTV) can accommodate up to 75,000 lbs. (34.02 tonnes) per wheel on two independent load carriages (Figure 3). The vehicle travels on rails and is approximately 75 ft. (22.9 m) long and 80 ft. (24.4 m) wide, weighing about 1.1 million lbs. (500 tonnes). Wheel loads are provided by hydraulic actuators reacting against the dead weight of the vehicle. The lateral position of the landing gears is variable up to +/- 5 ft. (1.5 m) from the nominal travel lanes allowing the NAPTV to simulate aircraft wander.



Figure 3. National Airport Pavement Test Vehicle (NAPTV)

As constructed in 1995-1999, the NAPTV has up to 6 wheels on each carriage, arranged as three independent modules. The NAPTV can be configured to represent a range of landing gear types, from single wheel (S) to 6 wheel (3D) gears. Data collection and testing at the NAPTF are arranged by construction cycles (CCs). A construction cycle (CC) includes test pavement construction with embedded instrumentation, materials testing data, traffic testing to failure, post-traffic testing, and pavement removal (Figure 4).

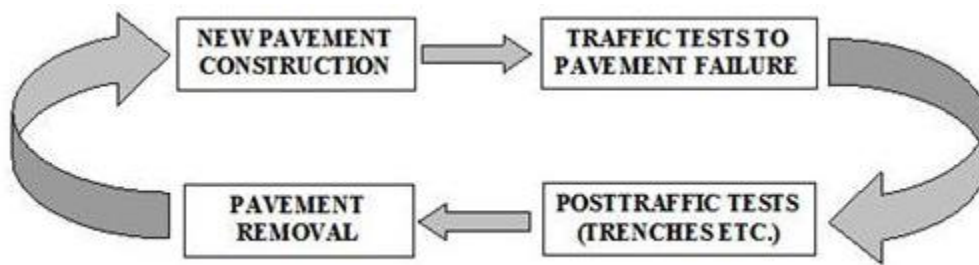


Figure 4. Construction Cycle (CC) at the NAPTF

1.2 Objectives

The primary objectives of Construction Cycle 1 (CC1) are to:

- Provide full scale test data to support new computer-based thickness design procedures then under development by the FAA (FAA 1995)
- Provide full-scale pavement response and data for use in airplane landing gear design and configuration studies

- Provide full-scale test data for re-evaluation of load repetition (alpha) factors used in the California Bearing Ratio (CBR) method of design for flexible pavements

Due to the contemporaneous introduction into service of the Boeing B-777 aircraft, particular emphasis was placed on determining the level of pavement damage expected from the B-777 airplane (6-wheel landing gear) relative to the B-747 airplane (4-wheel landing gear).

1.3 Construction Cycle 1 (CC1) Experimental Design

The CC1 test pavement was built at the same time as the NAPTF. Test item construction was completed in May 1999, shortly after the opening of the facility in April 1999. The CC1 experiment included nine pavement test items: six flexible and three rigid. The nine test items were constructed on three different subgrade strengths characterized as low (target CBR 4), medium (target CBR 8), and high (target CBR 20). The flexible test items were either stabilized (asphalt on P-401 asphalt stabilized base) or conventional (asphalt on P-209 crushed aggregate base). The rigid pavement test items were constructed on P-306 Econocrete base. Table 1 lists the test item designations. The specifications for the materials used were based on the FAA Advisory Circular (AC) 150/5370-10A. Test item designations in table 1 include three characters. The first character indicates the subgrade strength: L for low, M for medium, and H for high. The second character indicates the test pavement type: F for flexible and R for rigid. Figure 5 gives an overview of the CC1 experiment design. North and south sides of the test items were subjected to different traffic loading while having similar structures.

Properties of all of the materials used in each of the test item component layers were measured before, during, and after construction and stored in a database available for download or direct access on the FAA Airport Pavement Technology website:

<https://www.airporttech.tc.faa.gov/Airport-Pavement/National-Airport-Pavement-Test-Facility-/NAPTF-Databases/CC-1>.

To access to the database from the website, navigate to the CC1 homepage and scroll to the bottom of the page. At the bottom of the “Results & Analysis” table is a direct link to the CC1 Test Database. The database is an historical record of all of the testing conducted on the pavement materials and contains information about material properties of the component layers from quality control (QC), acceptance and material characterization tests. The QC tests were conducted primarily to ensure uniformity of quality and compliance with the design (Hayhoe and Garg 2001).

Table 1. CC1 Test Items Designations

Test Item Designation	Subgrade Type	Pavement Type	Base
LFS	Low Strength (Design CBR 4)	Flexible	P-401 asphalt stabilized
LFC			P-209 crushed stone
LRS		Rigid	P-306 Econocrete
MFS	Medium Strength (Design CBR 8)	Flexible	P-401 asphalt stabilized
MFC			P-209 crushed stone
MRS		Rigid	P-306 Econocrete
HFS	High Strength (Design CBR 20)	Flexible	P-401 asphalt stabilized
HFC			P-209 crushed stone
HRS		Rigid	P-306 Econocrete

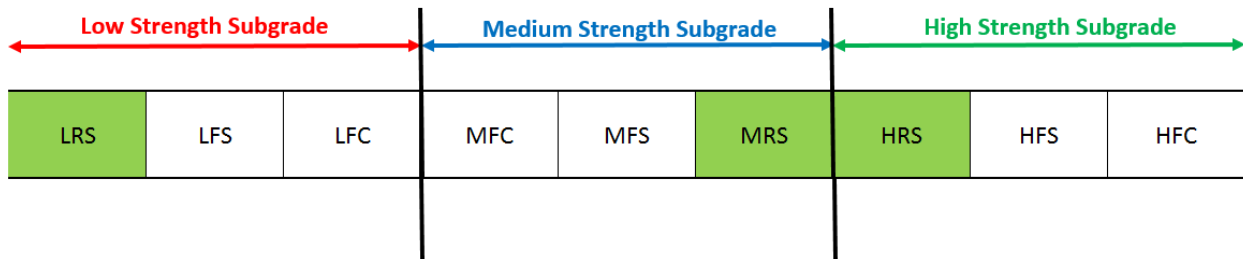


Figure 5. Plan View of the NAPTF Test Items during CC1

The thickness of the layers varied among test items. The design thickness of each test item is discussed in section 2.1. Figure 6, 7, and 8 (Garg 2003) illustrate the cross sections of the three rigid and six flexible pavement test items. Table 2 presents the cross sectional details of the CC1 test items (Hayhoe et al. 2004). Material properties were according to the FAA advisory circular AC 150/5370-10A.

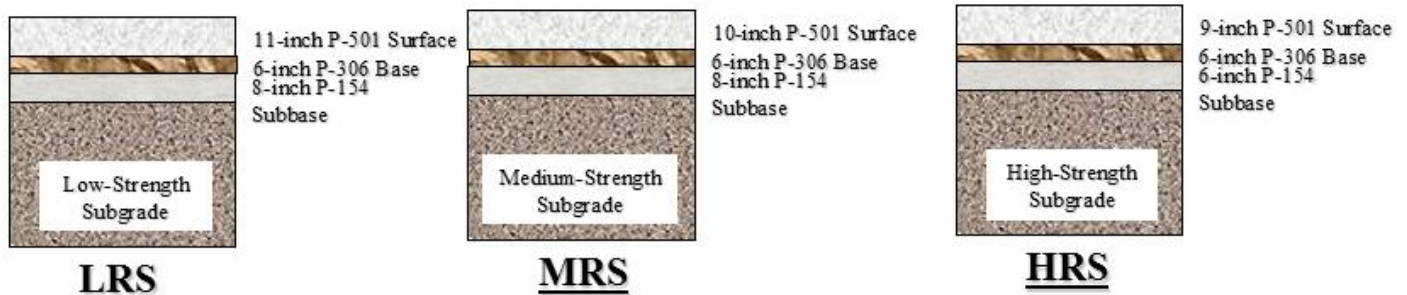


Figure 6. Cross-Sectional Views of CC1 Rigid Test Items (Garg 2003)

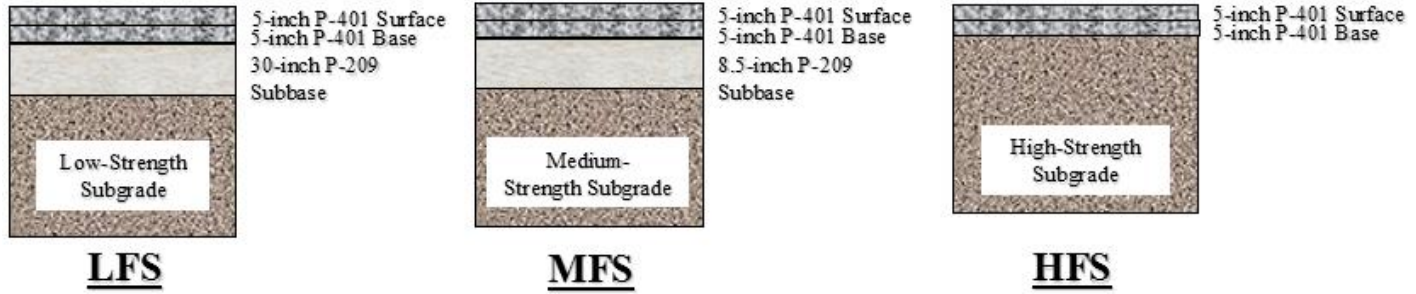


Figure 7. Cross-Sectional Views of the CC1 Stabilized Base Flexible Test Items (Garg 2003)

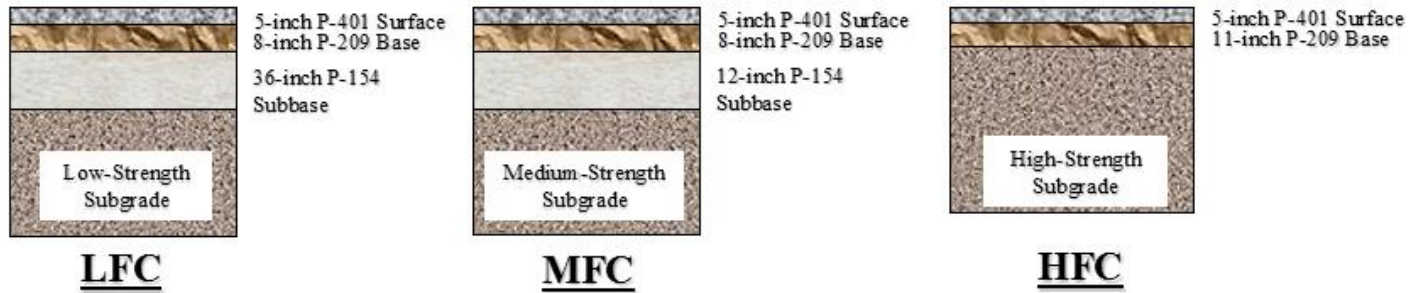


Figure 8. Cross-Sectional Views of CC1 Conventional Base Flexible Text Items (Garg 2003)

Table 2. CC1 Pavement Cross-Sectional Detail (Gervais et al. 2004)

Item ID	Surface Layer		Base Layer		Subbase Layer		Subgrade		
	Type	Thickness (in.)	Type	Thickness (in.)	Type	Thickness (in.)	Soil Type	CBR	Strength
LRS	P-501	11	P-306	6	P-154	8	MH-CH	4	Low
LFS	P-401	5	P-401	5	P-209	30	MH-CH	4	Low
LFC	P-401	5	P-209	8	P-154	36	MH-CH	4	Low
MFC	P-401	5	P-209	8	P-154	12	CL-CH	8	Medium
MFS	P-401	5	P-401	5	P-209	8.5	CL-CH	8	Medium
MRS	P-501	10	P-306	6	P-154	9	CL-CH	8	Medium
HRS	P-501	9	P-306	6	P-154	6	SW-SM	20	High
HFS	P-401	5	P-401	5	None	-	SW-SM	20	High
HFC	P-401	5	P-209	11	None	-	SW-SM	20	High

2. DESIGN, CONSTRUCTION AND INSTRUMENTATION OF CC1

2.1 NAPTF Design

2.1.1 Geometry Design

NAPTF Width

In designing the dimensions of CC1 test items, the width of the test track was influenced by factors such as wheel spacing, wander pattern, and boundary condition. A typical wheel configuration consists of two tracks, each containing one to three dual wheel axles in tandem.

An Industry Working Group consisting of pavement experts from the FAA, Boeing Company, U.S. Army, Navy, Air Force, Federal Highway Administration, university professors and engineering consultants, specified the maximum lateral spacing between the center lines of the tracks to be at least 20 ft. (6 m). The required spacing between the extreme outside wheels was estimated to be 26 ft. (8 m) (McQueen 2000). The panel also determined a wander width of approximately 60 to 80 inches (50 to 200 cm).

To determine the minimum distance required from the outer wheel of the test gear to the edge of the foundation wall, both layered elastic theory (LET) and finite element method (FEM) analysis were performed on a variety of pavement structures, as documented by Hayhoe, et al. 1993. Based on the results, it was decided to keep 10 ft. (3 m) as the minimum distance in addition to the shoulder pavement, planned at 3 ft. (1 m) on each side of the test pavement (McQueen 2000). After consideration of data acquisition requirements, a 20 ft. (6 m) slab pattern was specified by the working group. This required a minimum width of 60 ft. (18.5m) for a three slab width. With two 3 ft. (1 m) wide shoulders, the total recommended width was set to 66 ft. (20.5 m).

NAPTF Length

The overall length of the facility was set to the sum of the individual lengths of 9 test items, plus the lengths of all transition areas between adjacent test items, plus additional lengths required for run-up of the test vehicle, and for the ramp for construction and support vehicle access. Minimum test item lengths of 60 ft. (18 m) and 100 ft. (30 m) were established for flexible pavements and rigid pavements respectively and the transition length of 25 ft. (7.6 m) was selected. Therefore, the length of the CC1 experiment added up to 900 ft. (274 m) (McQueen 2000).

Subgrade Depth

Figure 9 through Figure 11 present the plan and profile layouts of test items with low, medium and high strength subgrade, respectively. These plans were provided by the government based on the earlier assumption of design subgrade CBRs of 4, 8, and 14 for low, medium, and high strength subgrade test items, respectively. Transition pavements were located between the test items to minimize the effects of impact loading and progression of damage from one test item to adjacent ones. Design thicknesses were adjusted based on CBR measurements on completed subgrade. Figure 12 through Figure 14 present the historical record plans for low, medium, and high strength subgrade test items.

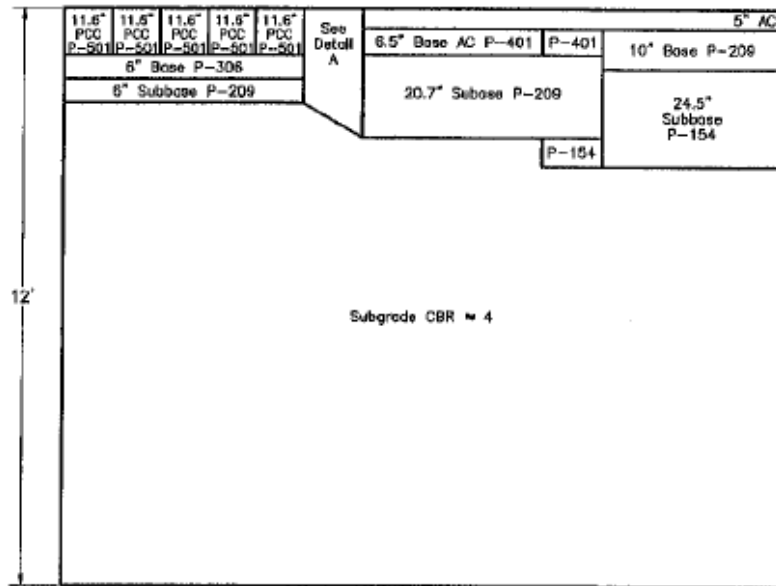
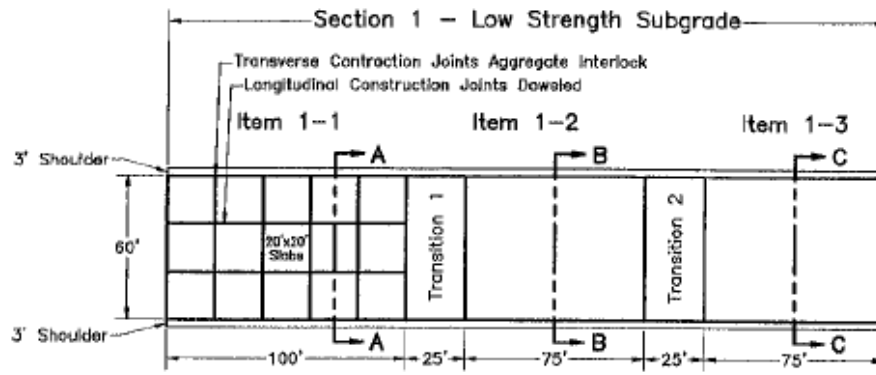


Figure 9. Initial Design Profile for Items on Low Strength Subgrade

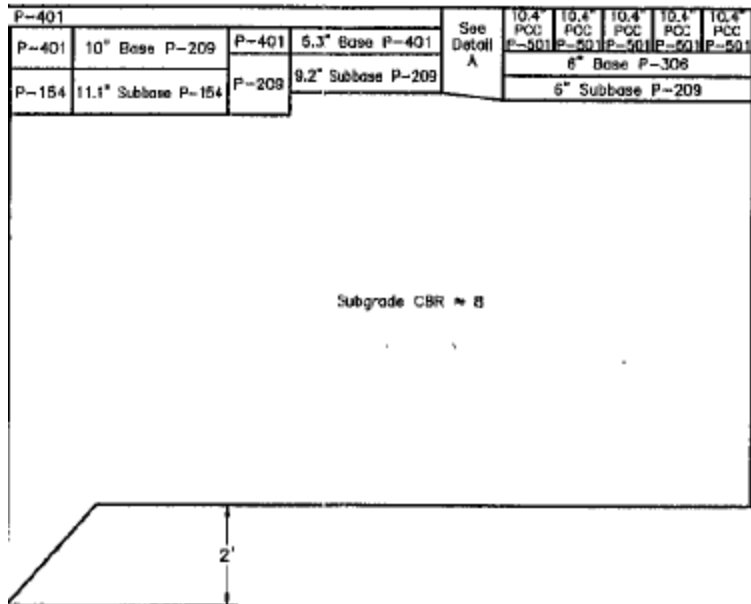
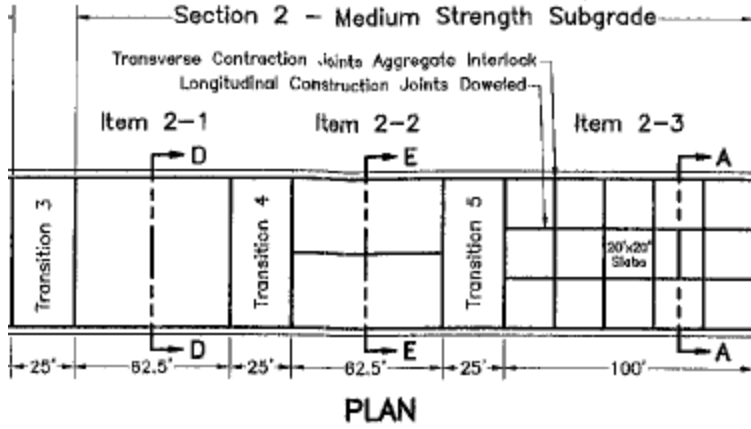


Figure 10. Initial Design Profile for Items on Medium Strength Subgrade

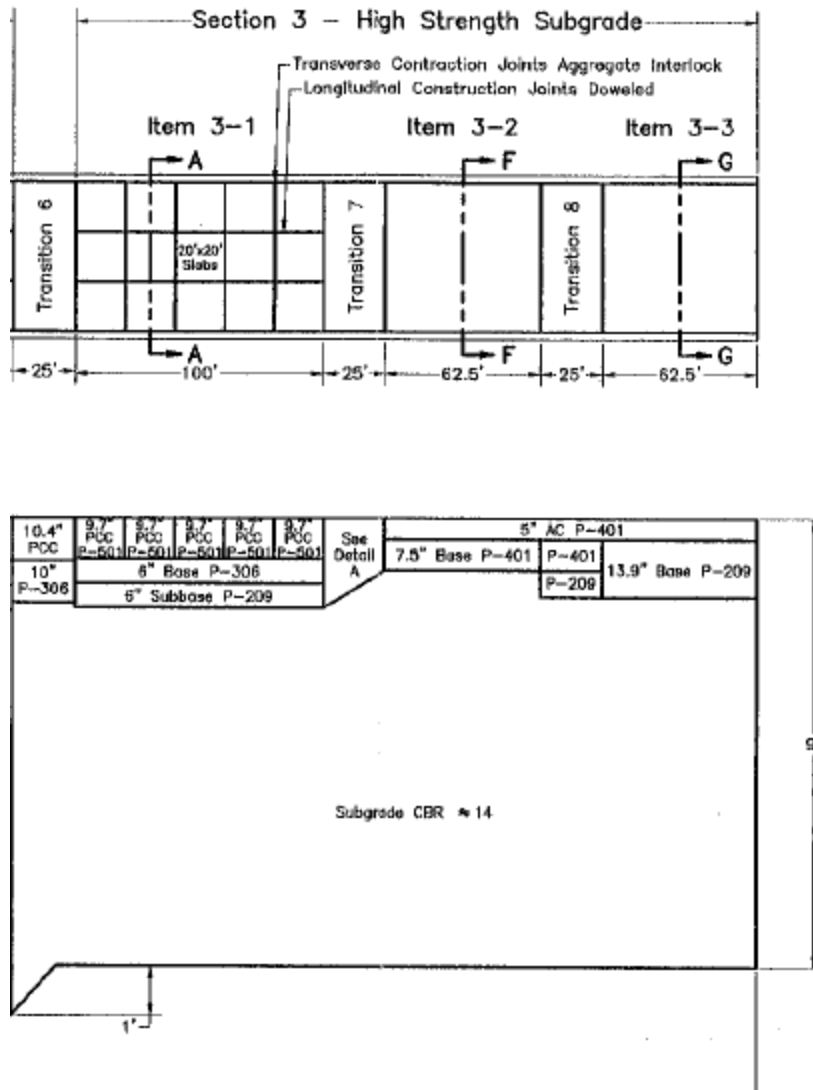


Figure 11. Initial Design Profile for Items on High Strength Subgrade

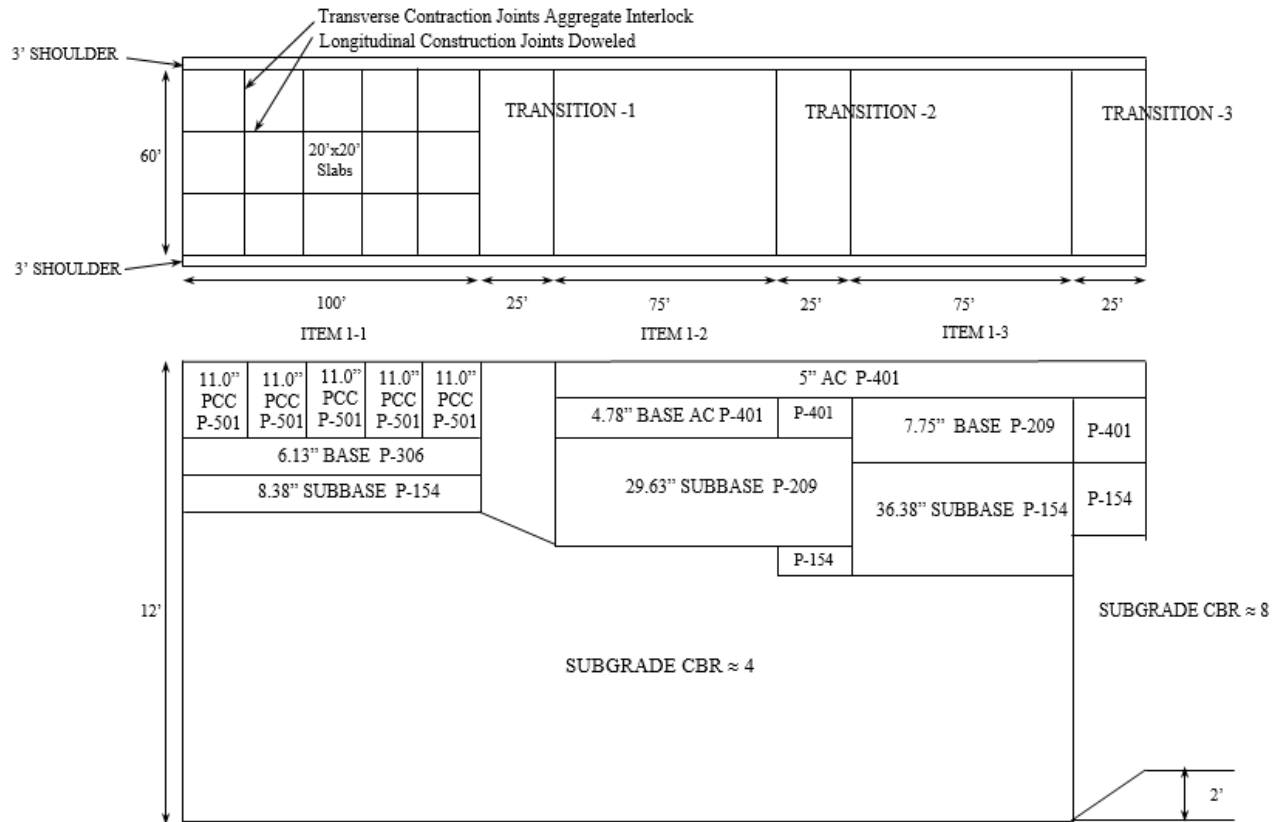


Figure 12. Historical Record Pavement Cross Section for Items on Low Strength Subgrade

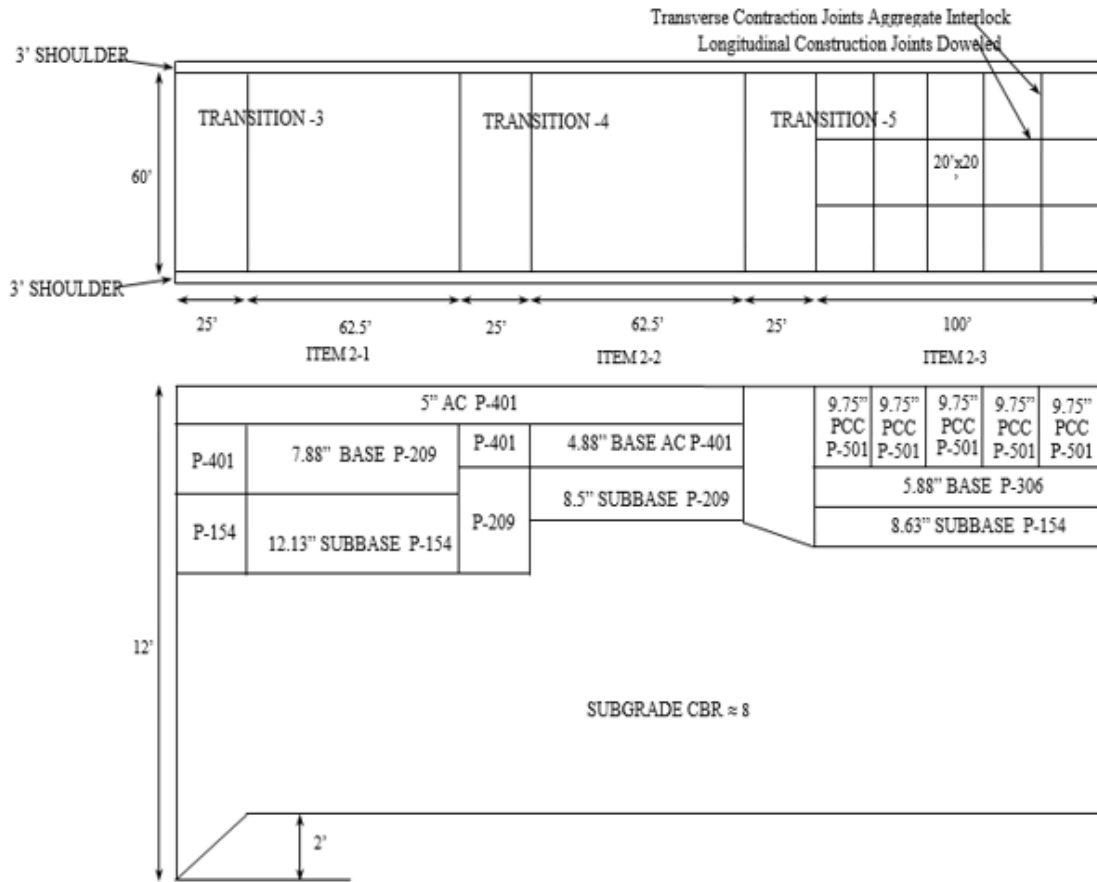


Figure 13. Historical Record Pavement Cross Section for Items on Medium Strength Subgrade

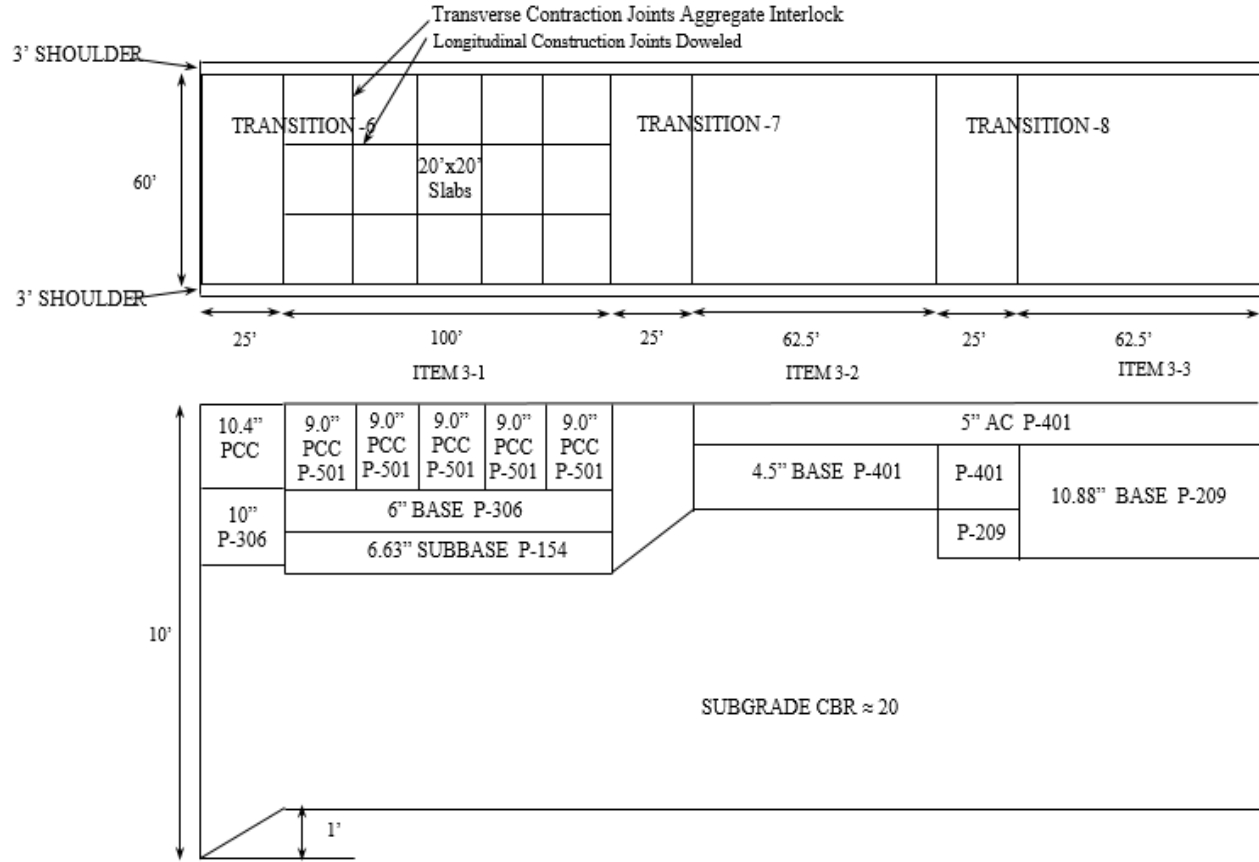


Figure 14. Historical Record Pavement Cross Section for Items on High Strength Subgrade

2.1.2 CC1 Pavement Design

For the design of CC1, the FAA CBR design procedure contained in AC 150/5320-6C was initially used to design flexible and Westergaard model for rigid pavement. For the case of the B777, the FAA method did not support triple tandem gear. Therefore, the DC-10 aircraft (which had similar loads as the B777) was used as the design aircraft with 50% increase in passes to account for the additional two wheels in the triple tandem. However, it was found that this method was conservative as compared to LET and FEM methods. Therefore, in designing CC1, Layered Elastic Design Federal Aviation Administration (LEDFAA 1.2) software was used with 10,000 passes to failure, 4-wheel loading gear configuration, and 45,000 lbs. wheel load. LEDFAA 1.2 was introduced as a design standard in 1995 along with AC 150/5320-6D. The core of LEDFAA 1.2 program was JULEA, which was a layered elastic computational program. Since prior full-scale testing programs were performed at coverage levels of 3,000 or less, higher coverage levels were selected to better quantify failure mechanisms.

2.2 Material Properties and Construction

A considerable number of measurements of the physical properties of the NAPTF test pavements were made before, during, and after construction was completed. Material properties of each material was collected for three reasons: construction QC, construction acceptance, and material

characterization. Tests were conducted on the subgrade materials, base, subbase, and surface layers.

2.2.1 Subgrade

The original soil at NAPTF site was described by the Cape Atlantic Soil Conservation District as Downer Loamy sand and Aura Loamy sand. The site was underlain by tertiary age sediments of Cohansey sand, which consists of predominantly light colored, medium to coarse-grained quartz sand containing small amounts of gravel, fine to coarse-grained sand, silty and clayed sand, and interbedded clay. Kirkwood sand consisting of fine micaceous sand with local beds of dark clay, underlay the Cohansey sand. A geotechnical investigation of the NAPTF site was made in July 1996. A total of 26 borings were placed at the site with 14 borings within the test pavement area. Evaluation of the in-situ soil at the NAPTF site included laboratory tests for soil classification, plasticity, compaction, CBR, and in situ moisture content. The details of laboratory test results for in-situ site soil can be found in table A-1 of Appendix A. Test results showed that the in-situ silty sand would drain rapidly and could not maintain the higher levels of moisture. It would also densify under test load applications causing an increase in CBR. Therefore, it was found not suitable for use in subgrades, and it was decided to replace sands with imported material.

A material known as County Sand and Stone Clay (CS&SC) purchased from County Sand & Stone Inc. in Norma, New Jersey was used for low strength subgrade with the target CBR of 4. A material called DuPont Clay sourced from Woodstown, New Jersey was used for medium strength subgrade with the target CBR of 8. For the high strength subgrade, the locally available sand was used with a target CBR of 20. Designers were forced with the problem of not only obtaining a minimum subgrade strength for each type of material but also of controlling the CBR for each material within a relatively small range. This was achieved by controlling the water content of the material.

Construction of the subgrades for the test pavement consisted of processing each of the three subgrades to uniform conditions of consistency and water content. Rigorous requirements were developed to provide the desired subgrade strengths and maintain uniformity within each lift. Achieving uniformity was important in order to obtain reliable load response data. Pavement distresses caused by non-uniformity in pavement or subgrade construction could be misinterpreted as being caused by loading. This could have undesirable consequences during the analysis of the test data to develop the structural design requirements for large, multiple wheel aircraft. A detailed quality assurance inspection and testing program was initiated during the placement of controlled subgrade and construction of pavement test items to ensure that the required degree of uniformity was achieved (McQueen 2000). The specification for pavement and subgrade construction was modeled after the FAA specification contained in AC 150/5370-10A, with subgrade acceptance primarily based on CBR, and moisture/density measurements used for QC.

The investigation of the NAPTF site indicated the depth of the water table to be 17-20 ft. below the existing ground level. To avoid potential difficulties in the subgrade preparation due to water table proximity, the FAA chose to elevate the design grade approximately 4 ft. above the existing grade. All of the in-situ material was removed to a depth of 12 ft. below the new finished pavement grade for low strength subgrade, 10 ft. for medium strength subgrade and 9 ft. for high strength subgrade.

In construction of the subgrade, material was placed in 8-inch lifts or thicker and compacted to the required density to achieve the design CBR range. Acceptance of each lift of the subgrades was based on CBR tests. Four groups of three or more CBR penetrations were performed on each subgrade lift. Lifts were typically 6 inches (15.2 cm) to 8 inches (20.3 cm) thick before proceeding to placement of the next lift. The locations of the CBR test groups were determined according to American Society for Testing and Materials (ASTM) D 3665. The lifts were covered with plastic film after compaction and the film kept wet to minimize moisture loss from the surface of the subgrade. The CBR tests were usually started as soon as the plastic film was in place, although there were frequent delays of hours to days because of other construction activities. Uniformity of subgrade strength across the four groups was considered to be more important for acceptance of a lift than deviation of the lift average from the target value. The lowest lifts were typically significantly higher in strength than the target value because the construction procedures and the relationships between in-place CBR and moisture content were being developed as the lower lifts were placed (Hayhoe and Garg 2001). Table 3 contains the strengths and soil classification for each subgrade after construction (McQueen 2000).

Table 3. Initial CBR and Soil Classification for Each Subgrade (McQueen 2000)

Subgrade	Average CBR (%)	Soil Classification
Low	3.5	ML/CL
Medium	7.5	CH
High	20 < CBR < 30	SP/SM

Tests performed during construction were in-situ moisture content (ASTM D 2216), density (ASTM D 2937) and CBR (ASTM D 4429). Dynamic Cone Penetrometer (DCP) tests measured the rate of penetration through various layers to characterize change of subgrade strength with depth. Table A-1 through A-5 are representative of the data collected during subgrade construction. Comprehensive QC test data are available at <https://www.airporttech.tc.faa.gov/Airport-Pavement/National-Airport-Pavement-Test-Facility-/NAPTF-Databases/CC-1>. Summaries of field testing results including CBR, moisture content, density, degree of compaction and DCP tests on low, medium and high strength test items during the construction of subgrade, are provided in Figure A-1 through Figure A-10 in Appendix A (Garg 1999).

Prior to the initiation of full scale testing, about 6 months after the initial construction, test pits were opened to a depth of 4 ft. (1.2 m) to 5 ft. (1.5 m) below the surface of the flexible pavements on stabilized base. CBR tests were performed at several depths of the subgrade. The CBR results are summarized in table 4 (McQueen 2000).

Table 4. Test Pit CBR Results (McQueen 2000)

Subgrade	Average CBR (%)
Low	5
Medium	6
High	45

After acceptance of the subgrade, resilient modulus tests (ASTM D1587) were conducted on low and medium strength subgrade soils using Shelby thin-wall tube samples extracted from in-place material. Results for each of the test items are presented in figure A-11 through figure A-16 of Appendix A. The subgrade resilient modulus values varied from approximately 2,600 to 7,500 psi (14 to 52 MPa for low-strength soils and from 5,000 to 12,500 psi (34 to 86 MPa) for medium-strength soils.

2.2.2 P-501 Portland Cement Concrete (PCC)

Plain (unreinforced) concrete slabs were constructed on a prepared base in accordance with Item P-501 in AC 150/5370-10A. Following the P-501 specification, the minimum flexural strength allowable for airport pavements was 600 psi (4.1 MPa). The mix design was developed to target a flexural strength of approximately 650 to 700 psi (4.5 to 4.8 MPa). Several mix designs were produced to obtain the targeted flexural strength but proved to be difficult with local available aggregate. The final mix design was based on a 50% sand and 50% No. 57 stone blend with a cement content of 500 lbs/ cy (290 kg/cm). This resulted in a target strength of 740 psi (5.1 MPa) at a water cement ratio of 0.47 (McQueen 2000). Appendix A, figure A-17 (Garg 1999) gives the 28-day flexural strength test results for P-501 concrete in the CC1 surface layers.

Figure 15 shows the placement of concrete for the slabs during construction of the test sections, completed in May 1999. QC for Item P-501 PCC was based on slump, air content, and compressive strength. This data is available for download on FAA Airport Pavement Technology website (<https://www.airporttech.tc.faa.gov/Airport-Pavement/National-Airport-Pavement-Test-Facility-/NAPTF-Databases/CC-1>).



Figure 15. CC1 Concrete Placement for Test Section Construction, Completed May 1999

2.2.3 P-154 Subbase and P-209 Base Material

The base and subbase courses were composed of granular materials constructed on the finished, prepared subgrade following AC 150/5370-10A, Items P-209, and P-154. The P-209 base material used at the NAPTF were partial blend coarse Milestone Materials (obtained from Hanson Aggregates in Glen Mills, Pennsylvania, formally known as Milestone Materials) and fine Maryland Materials obtained from northeast Maryland. The P-154 subbase material was a uniformly graded, manufactured argillite screenings product called Grey Quarry Blend Fines.

Table 5 and Table 6 summarize the specified gradation requirements for P-154 and P-209 and the gradation used at the NAPTF (Gagnon and Garg 2010). For both P-154 and P-209, the material passing the No. 40 sieve was required to have a maximum liquid limit of 25 and maximum plasticity index of 6. For P-154, the actual liquid limit and plasticity index values were 16 and 3.1, respectively. Therefore, the requirements were met.

Table 5. P-154 Gradation Data and Requirements for Argillite Screenings Subbase (Gagnon and Garg 2010)

Sieve Size	Percentage by Passing by Weight Sieve	
	Specification	NAPTF CC1
3 in	100	100
No. 10	20-100	44.2
No. 40	5-60	11.7
No. 200	0-8	5.6

Table 6. P-209 Gradation Data and Requirements for Crushed Aggregate Base (Gagnon and Garg 2010)

Sieve Size	Design Range Percentage by Weight	Job Mix Tolerance, Percent	Percentage Passing by Weight
2 in.	100	0	100
1-1/2 in.	95-100	+/- 5	95.9
1 in.	70-95	+/- 8	86.2
3/4 in.	55-85	+/- 8	79.5
No. 4	30-60	+/- 8	46.5
No. 30	12-30	+/- 5	17.7
No. 200	0-8	+/- 3	6.7

QC testing and inspection was conducted to ensure uniformity and quality of the subbase material. The QC plan for the subbase P-154 material consisted of gradations on bulk samples from the compacted lifts, moisture and density measurements on the compacted lifts, thickness measurements, grade, and surface condition. The compacted subbase thicknesses were measured using rod and level survey equipment at intervals of 10 ft. in each direction. The database structure for P-209 and P-154 are similar. QC data for P-154 and P-209 are presented in table A-6 of Appendix A. The dry densities and moisture contents for P-209 base and P-154 subbase aggregates

were determined using the modified Proctor test (AASHTO T180). Appendix A, figure A-18 and figure A-19 gives moisture content data for P-154 subbase and P-209 base materials, respectively.

Resilient modulus tests were conducted following the Strategic Highway Research Program (SHRP) Protocol P-46 testing procedure (Hayhoe and Garg 2001). Current AASHTO test procedures did not exist at that time. AASHTO adopted SHRP P-46 as AASHTO T 294 in 1994 but have since withdrawn it. The current standard for resilient modulus of soils is AASHTO T 307 (20123). Resilient modulus test results for subbase and base material are presented in Figure 16 and Figure 17 (Garg 1999).

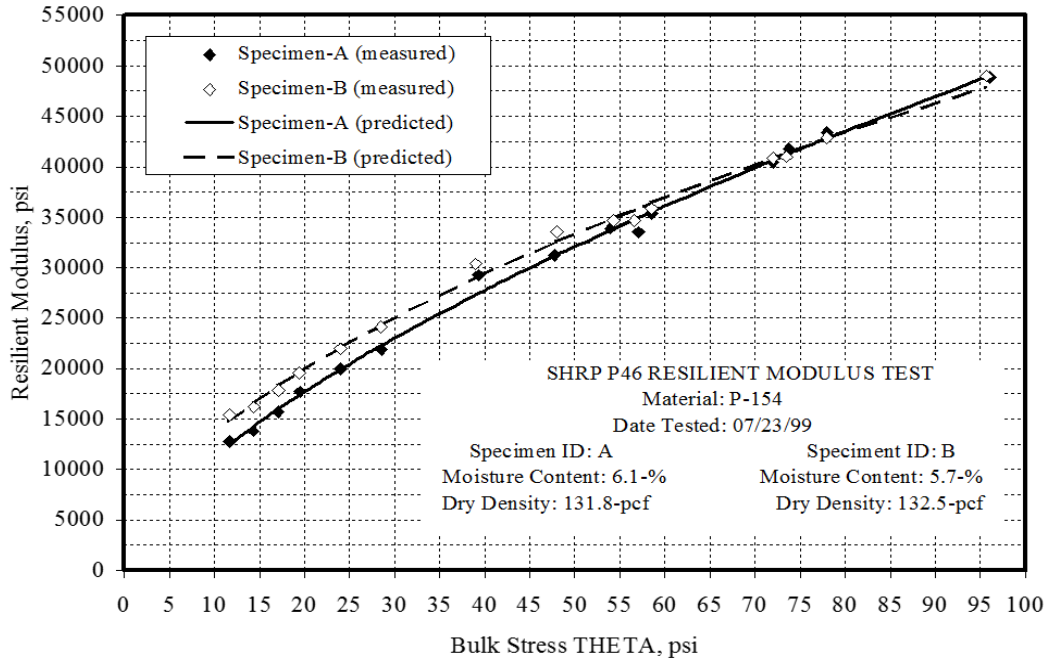


Figure 16. Resilient Modulus Test Results for P-154 Subbase Material (Garg 1999)

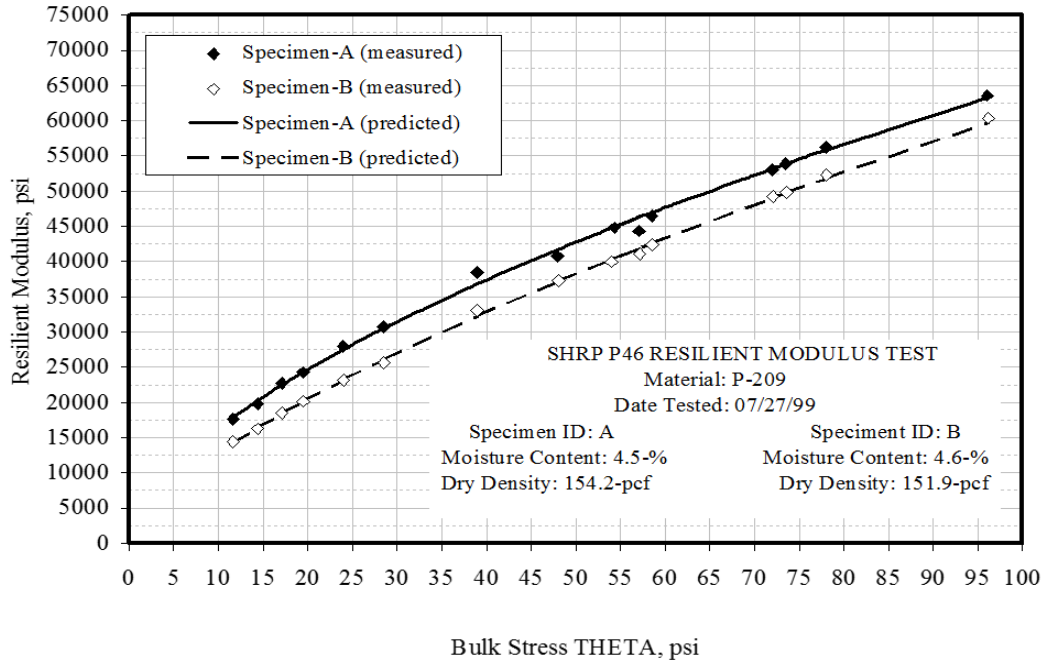


Figure 17. Resilient Modulus Test Results for P-209 Base Material (Garg 1999)

2.2.4 P-306 Cement Stabilized Base (Econocrete)

Econocrete base for rigid pavements was mixed and placed following Item P-306, Econocrete Base, in AC 150/5370-10A. The QC for the P-306 Econocrete base was based on slump, air content, and compressive strength. A mix comprised of 50% sand and 50% stone with a cement content of 200 lbs./cy (115 kg/cm) was used. This resulted in an average 28-day compressive strength of approximately 600 psi (4.1 MPa). Appendix A, tables A-7 and A-8, and figure A-20, contain material test data including compressive strength test results for P-306 Econocrete.

2.2.5 Hot Mix Asphalt Materials

Hot Mix Asphalt (HMA) in CC1 was produced in accordance with Advisory Circular 150/5370-10A, Item P-401. The same material was used for both HMA surface and HMA stabilized base layers. QC testing of the P-401 material during production was required to ensure that the final product met P-401 specifications. During production, aggregate gradation, binder content, mix temperature and mixture properties were monitored. The QC tests for P-401 HMA included aggregate gradation, mat and joint density, asphalt content, air voids, and stability. Appendix A, table A-9 gives an example of aggregate gradation and binder content available from P-401 mix component database. Appendix A, table A-10 gives an example of mixture properties such as densities and air voids from field cores.

The Marshall Test properties of the P-401 mixtures from the truck were measured during production using the Asphalt Institute MS-2 method. The field densities of P-401 cores extracted from NAPTF flexible test items were measured using ASTM D 2726 procedure. The NAPTF

database is available for download or direct access on the FAA Airport Pavement Technology web site (<https://www.airporttech.tc.faa.gov/Airport-Pavement/National-Airport-Pavement-Test-Facility-NAPTF-Databases/CC-1>). Resilient modulus tests (ASTM D 4123) and fatigue tests (AASHTO TP 8-94) were conducted at the University of Illinois Advanced Transportation Engineering Laboratory (ATREL) facility. A total of seven cores were extracted from the NAPTF flexible test items for resilient modulus testing. The average laboratory measured P-401 AC resilient modulus at 77°F (25°C) was 426 ksi (2940 MPa) (Hayhoe and Garg 2001). The primary acceptance test results for the HMA are summarized as follows (McQueen 2000):

- Average asphalt content = 5.4%
- Average compaction = 98% of 75 blow Marshall density
- Average plant air voids = 3.6%

The asphalt content, air voids and % compaction for P401 AC and base layer for each test item are presented in figure A-21 through figure A-23 in Appendix A.

2.3 Instrumentation

Sensors were embedded in the test items to collect data. Sensors were classified as two types: static: for slow response measurements, and dynamic: for fast response measurements. Static sensors monitored temperature, moisture, and crack status on an hourly basis. Dynamic sensors were triggered by the vehicle operations and measured pavement responses such as strain and deflection due to the applied loads.

Each of the six flexible pavement test items had three sets of dynamic sensors. The first set consisted of multiple depth deflectometers (MDDs), pressure cells (PCs) and asphalt strain gauges (ASGs) in the south traffic path. The second set consisted of the same set of instrumentation in the north traffic path; and the third set consisted of one MDD located in the centerline. Flexible test items included static sensors in addition to measure the environmental condition of the pavement structure at different levels. Pavement temperatures in the AC layer were monitored using Omega Thermistor temperature gauges. The temperature gauges (TGs) were placed at 0.5 inches (13 mm), 2.5 inches (64 mm), and 4.5 inches (114 mm) below the AC surface. In the case of pavements with asphalt stabilized-base, TGs were placed at the bottom of the asphalt stabilized-base layer (Garg and Hayhoe 2001).

Each rigid pavement test item had also three sets of instrumentation. The first set of instrumentation installation consisted of the concrete strain gauges (CSGs) and joint gauges (JGs) in the south traffic path. The second set of instrumentation installation consisted of the CSGs and JGs in the north traffic path, and the third instrumentation installation consisted of a single JG in the centerline. The sensor types installed in the test items are listed in table 7. The flexible pavement test items on conventional base (i.e, LFC, MFC, and HFC), had approximately three moisture and six temperature sensors. The flexible pavement test items on stabilized base each had approximately one moisture and ten temperature sensors. The rigid pavement test items each had one moisture and six temperature sensors. Additionally, each of the three rigid pavement test items had approximately thirteen resistance sensors to identify when the Econcrete base cracked. Static data were collected continuously at hourly intervals (Teubert, et al. 2002). Appendix B includes a full list of static sensors and their installation locations.

Table 7. Sensor Types Installed in the CC1 Pavement

Sensor Type	Number Installed
MDD (CTL Design)	30
Potentiometer for MDD (Data Instruments)	210
Asphalt Strain Gauge (CTL Design)	96
PCC Strain Gauge (CTL Design)	463
Pressure Cell 6 inch (Geokon 3650 EPC)	60
Pressure Cell 2 inch (Kulite 0234 SPC)	84
Joint Clip Gauge (TML PI-5-100)	25
Total Dynamic	968
Moisture Gauge (Campbell C5615-L)	15
Temperature Gauge (Omega Thermistor)	66
Total Static	81

Data was acquired, processed, stored, and disseminated from the individual sensors using 6 data collection systems interconnected by wire and wireless local area networks (Teubert, Brill et al. 2002). The signal processing units (SPUs) and test vehicle computer were located in the test building; however, they could be remotely operated from the control room, located in the administrative building. The HSDAS was used to collect data from the dynamic pavement sensors and transmit the data to a computer in the control room. The HSDAS consisted of six Hewlett Packard VXI Mainframe SPUs. Each SPU had a 133- MHz Pentium computer system card and three analog to digital converter (ADC) cards with a 64-channel multiplexer on each card. Each rigid test item had a dedicated SPU. Each pair of flexible test items on a given strength subgrade had a dedicated SPU. The schematic for data collection is shown in Figure 18 (Hayhoe, et al. 2001).

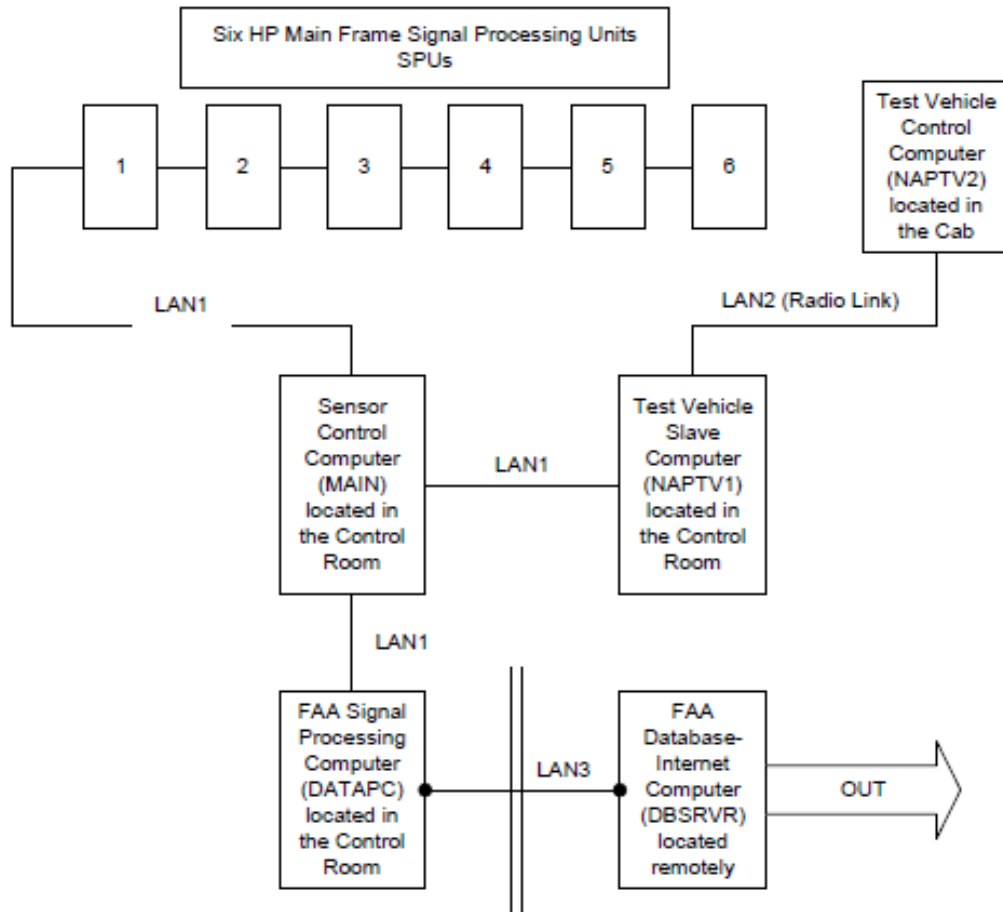


Figure 18. HSDAS Schematic (Hayhoe, et al. 2001)

Collection of data in dynamic sensors was triggered by vehicle movement on the test items. Data was collected at a sampling rate of 20 Hz (one sample per 0.05 sec). Three data files were created for each test item for each vehicle pass (Teubert, et al. 2002). The following sections present more details on each sensor type and installation.

2.3.1 Multi-Depth Deflectometer (MDD)

MDDs, manufactured by Construction Technology Laboratories (CTL), were used to measure deflections of pavement layers at multiple vertical locations referenced to a stable point. Each MDD is an array of seven potentiometer Displacement Transducer (DT) physically connected via a graphite rods to snap anchor discs placed at strategic locations to capture the multiple-wheel load interaction (Figure 19). The MDDs work by recording the deflection of the individual sensors in relation to an anchor sensor that is buried below the zone of influence of the anticipated loads. The anchor depth is 9-feet (2.7 m) for the medium-strength subgrade test sections. The surface sensor is actually the only sensor to be directly connected to the anchor; the other sensors measure deflections in relation to the surface sensor. The absolute movement of an individual sensor is then calculated by subtracting the sensor reading from the surface sensor reading. Accordingly, individual layer response is calculated by subtracting the lower sensor reading from the higher sensor reading.



Figure 19. Installation of Multi-Depth Deflectometer (MDD) (Garg 2003)

Five MDDs were embedded within each flexible test item. Figure 20 shows the horizontal locations of the MDDs (Hayhoe and Garg 2002). Each wheel path had two MDDs designated as NW-MDD, SW-MDD (west side MDDs), NE-MDD and SE-MDD (east side MDDs). One MDD was located in the centerline (CL) of pavement test item designated as CL-MDD aligned with the west side MDDs. Figure 21 shows the vertical location of the MDDs within the flexible test sections (CTL 1998). The separation of the sensors across the subbase/subgrade interface is approximately 2 inches (50 mm).

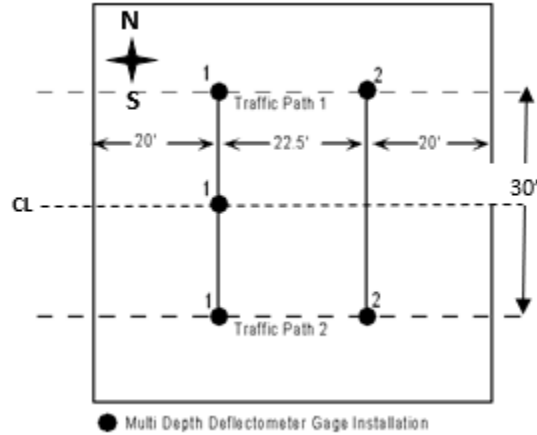


Figure 20. Horizontal Locations of the MDDs in MFC Test Section (Hayhoe and Garg 2002)

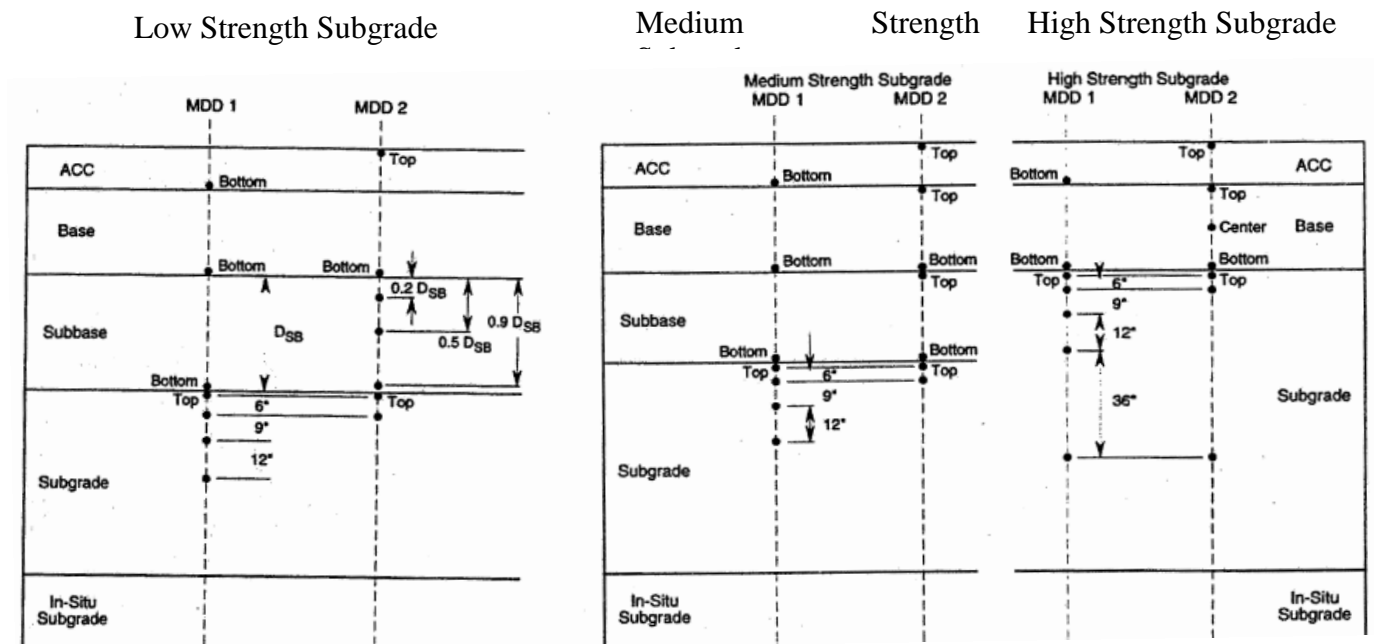


Figure 21. Vertical Location of the MDD Sensors (CTL 1998)

2.3.2 Asphalt Strain Gauge (ASG)

The ASGs for the NAPTF were fabricated by the manufacturer (CTL). Each ASG is a full-bridge assembly consisting of four foil gauges affixed to a 5/16 inch polyester rod as shown in Figure 22. Due to the configuration (polyester rod joining two steal flanges), the ASGs are referred to as “H-bar”. According to manufacturer specifications, the ASG instrument had an accuracy of 1 microstrain and a resolution of 0.1 microstrain. The measurement range was 2000 microstrain and the temperature range was from 0 to 150°C.

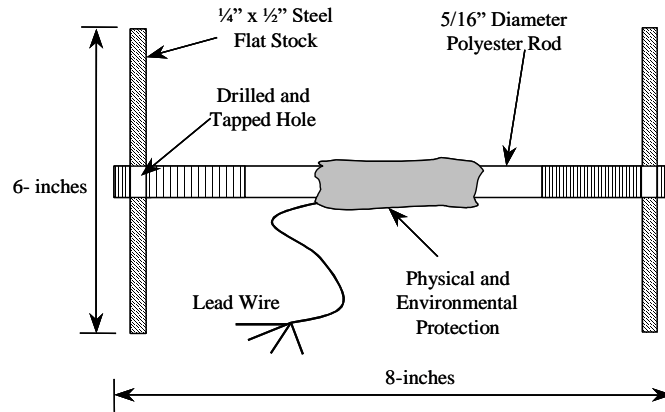


Figure 22. Asphalt CSG (Garg and Hayhoe 2001)

ASGs were installed in both longitudinal and transverse directions at the bottom of the surface asphalt layer and at the bottom of the stabilized base asphalt layer of the stabilized base test items. Figure 23 shows the installation of ASG in the AC layer. A total of 96 H-bar type ASGs (transverse and longitudinal) were installed at the time of construction. Figure 24 shows the location of the ASGs in flexible test sections (CTL 1998).



Figure 23. ASG Installation

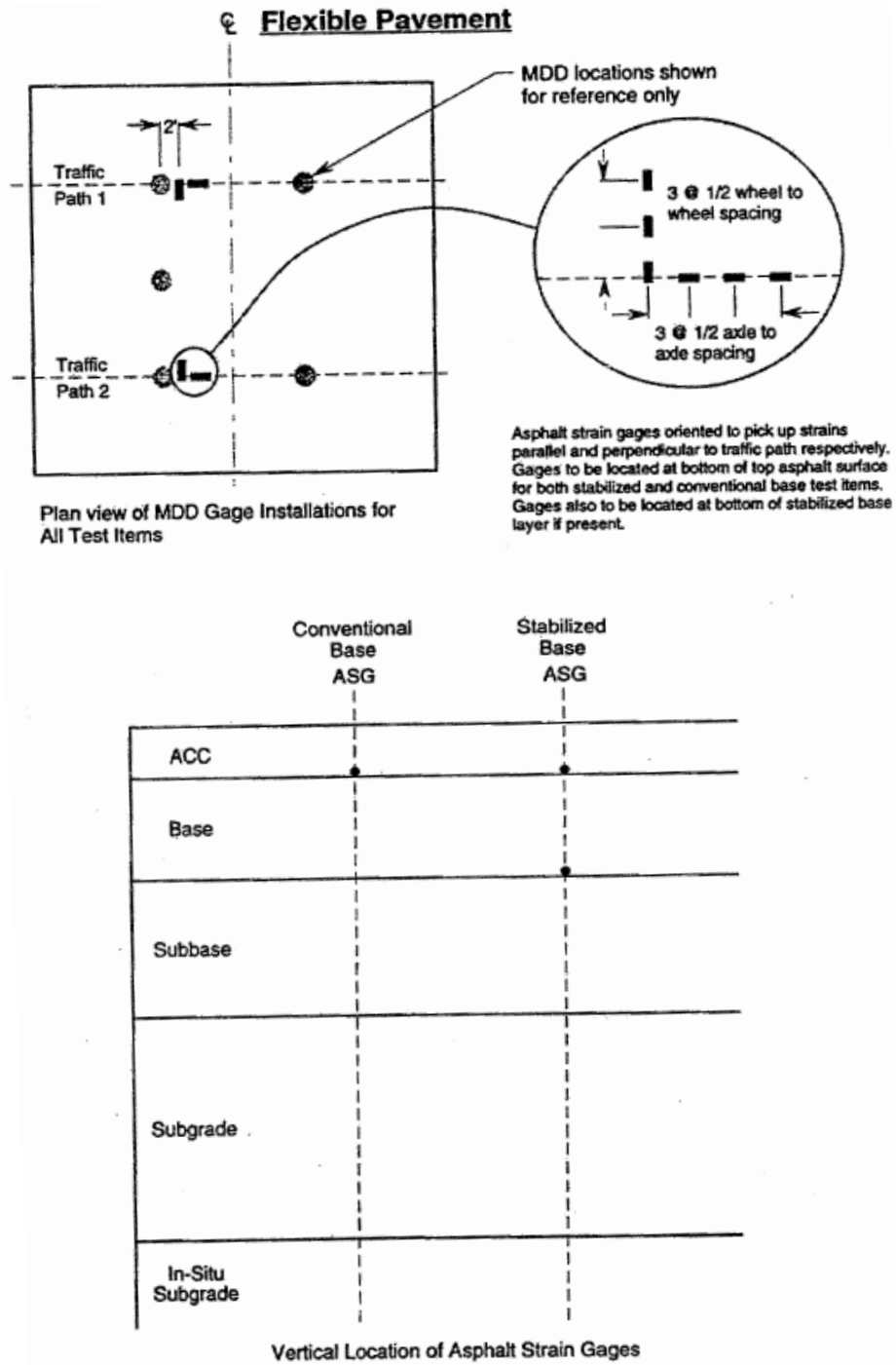


Figure 24. ASG Locations in Flexible Test Sections (CTL 1998)

2.3.3 Concrete Strain Gauge (CSG)

CSGs were of the same basic design as the ASGs, except that the foil gauges were affixed to steel bars.

Figure 25 shows the strain gauge locations in the rigid pavement test items (Guo et al. 2002). Only slabs 2 and 3 in each lane were instrumented. Sensors were installed near both the top and bottom surfaces of the slabs to provide measurements of the tensile and the compressive strains that developed during loading. Figure 26 shows the installation of CSGs in the NAPTF rigid pavement test items. A total of 154, 156, and 153 CSGs were installed in test items LRS, MRS, and HRS, respectively. Of the total of 463 CSGs, 40 were found to be not performing, including 14 sensors (9.1%) in LRS, 12 sensors (7.7%) in MRS and 14 sensors (9.1%) in HRS (Guo et al. 2002). The details about the location of the sensors are documented by Guo et al. (2002).

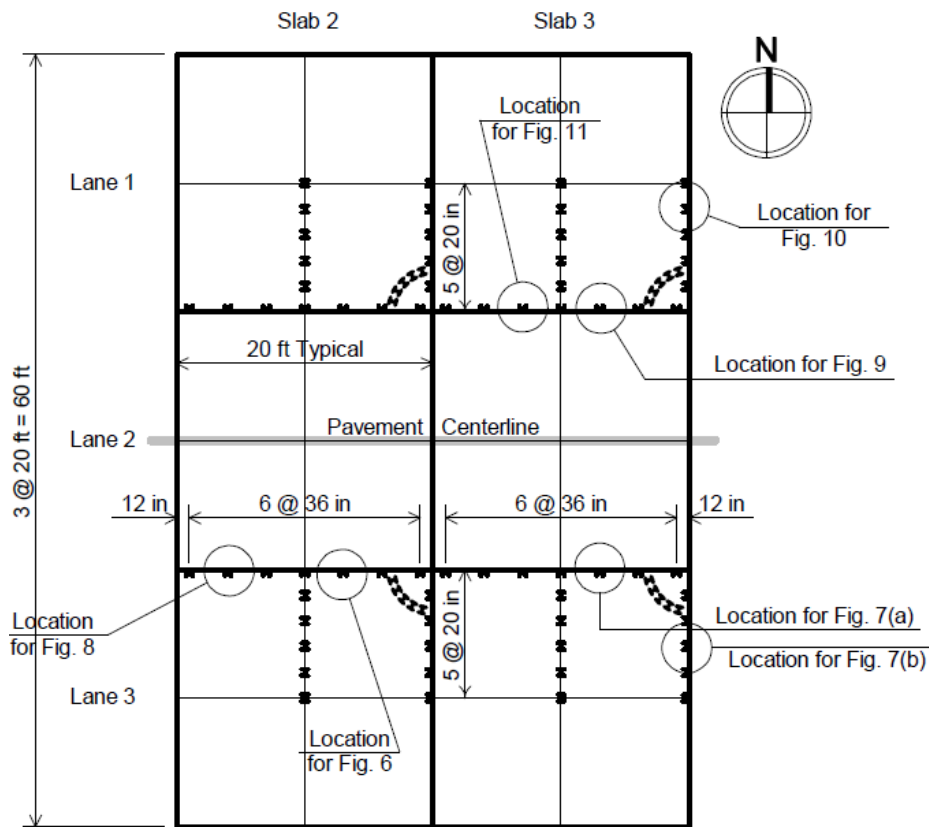


Figure 25. Locations of CSGs in Rigid Pavement Test Items (Guo et al. 2002)



Figure 26. CSG Installation

2.3.4 Pressure Cell (PC)

Two types of PCs were used, designated PC2 and PC6. The PC2 were Kulite Model Soil Pressure Cells. They were small diameter soil pressure cells consisting of a liquid-filled hollow steel cell of approximately 2 inches (5.1 cm) in diameter and 0.5 inches (1.3 cm) thick with an electrical pressure transducer housed within the cell. The PC6 were Geokon Model Earth Pressure Cells. They were large diameter soil pressure cells consisting of two welded steel plates of 6 inches (15.3 cm) diameter and 0.5 inches (1.3 cm) thick. The space between the two plates were filled with liquid connected to an electrical pressure transducer with a steel tube. Any change in the soil pressure where the cell was embedded, was measured by pressure transducer (CTL 1998). The 6-inch and 2-inch pressure cells are displayed in Figure 27 and Figure 28Figure 30, respectively (CTL 1998).

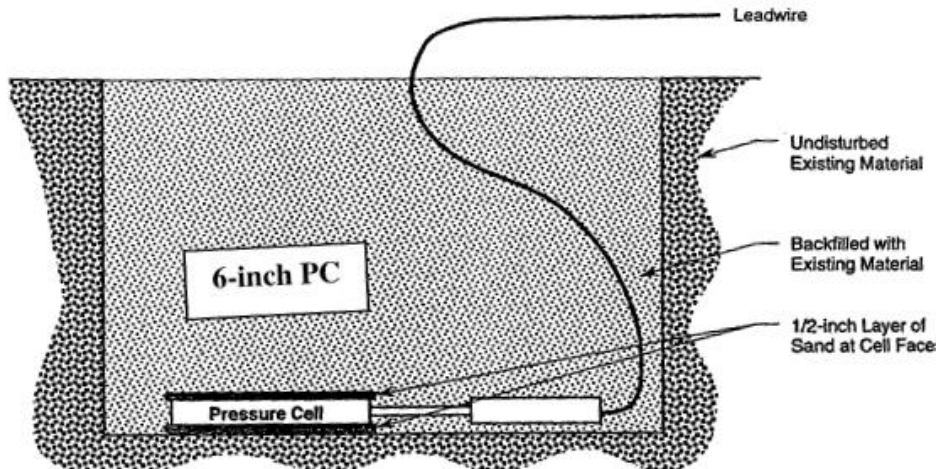


Figure 27. 6-inch Pressure Cell (CTL 1998)

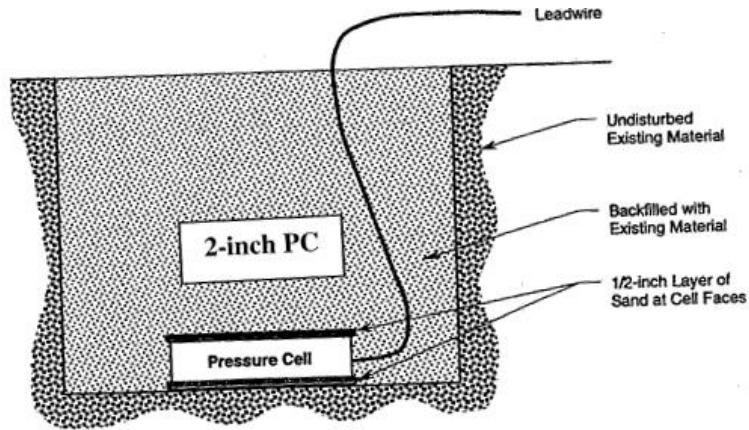


Figure 28. 2-inch Pressure Cell (CTL 1998)

The PC6 sensors were installed in the unbound granular base and subbase and the PC2 sensors were installed in the subgrade. All the PCs were located near the west side MDDs. Figure 29 shows the location of PCs within the flexible test sections (CTL 1998).

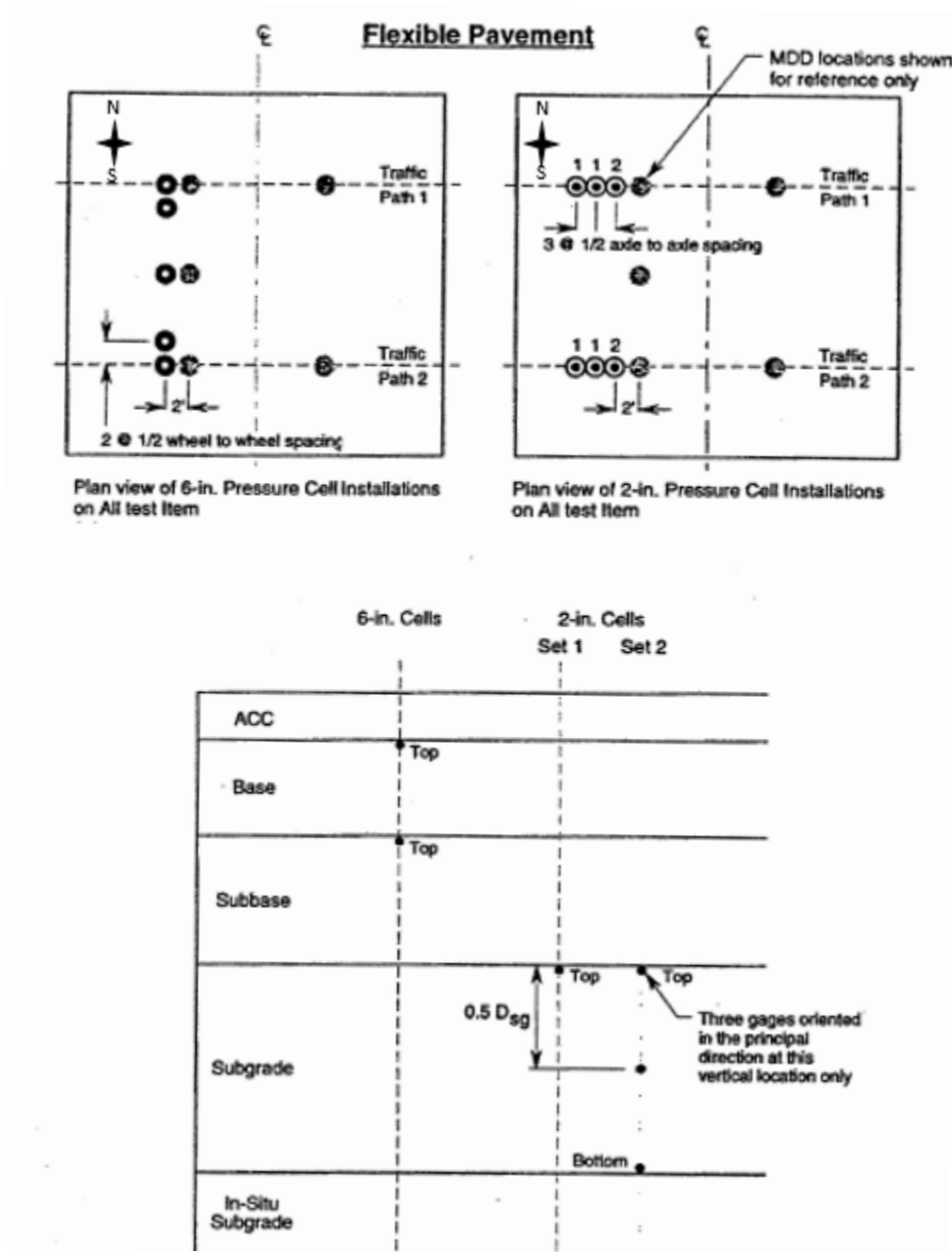


Figure 29. PC Locations in Flexible Test Sections (CTL 1998)

2.4 Uniformity Test

2.4.1 Testing Method and Equipment

In 1999, the FAA purchased a KUAB Model 240 Heavy Falling Weight Deflectometer (HWD) device for evaluation of the test pavements at the NAPTF (Figure 30). The KUAB operates on the principle of dropping weights on a series of hard, rubber buffers separated by a second series of weights and buffers which are connected to a loading plate resting on the pavement surface. In the

KUAB device, the loading plate is segmented into quarters to ensure that the loading force is evenly distributed. Weights and buffers can be added or removed as necessary to adjust peak load and loading time. The loading pulse shape is also influenced by the combination of weights and buffers used. The main objectives of conducting HWD tests were to verify the uniformity of the pavement construction, particularly subgrade strength before the start of traffic testing.



Figure 30. FAA's KUAB Model 240 HWD Equipment

2.4.2 Data Collection

Initial HWD data collection took place on June 14 and 15, 1999. Engineering and Research International, Inc. (ERI) of Savoy, IL performed a series of Falling Weight Deflectometer (FWD) tests using a KUAB Model 150 FWD with a 12 inch (30.5 cm) load plate and a pulse width of approximately 27 msec. The Model 150 unit was used because at the time the FAA was still awaiting delivery of the larger Model 240 unit. Tests were performed at nominal load amplitudes of 9,000 lbs. (40 kN), 13,500 lbs. (60 kN), 18,500 lbs. (82 kN), and 25,900 lbs. (115 kN) on a 10 ft. grid within each of the test items. The FWD loading points included slab centers, corners, and transverse and longitudinal joints.

The Model 240 HWD was used for all subsequent Non-Destructive Testing (NDT) starting from October 1999. The FAA KUAB HWD unit has 7 sensors measuring deflections. For CC1 tests on rigid test items, one sensor was positioned at the center of the load plate (D0), and another sensor was positioned 12 inches in front of the plate along the path of the vehicle (D1). This allows the HWD unit to be positioned such that the D1 sensor is on the opposite side of a joint from the load plate to evaluate the load transfer efficiency. The remaining five sensors were positioned behind

the plate at 12 inch (305 mm) spacing (Figure 31). The HWD test plan consisted of four drop heights, a 36 kips (160 kN) seating drop followed by impact loads of 12, 24, and 36 kips (53, 106, and 160 kN). The first 36 kips (160 kN) drop seats the pavement by settling out the residual permanent deformations within the pavement structure and is discarded in the analysis. The peak loads and deflections were recorded for all four drops along with air and pavement surface temperatures.

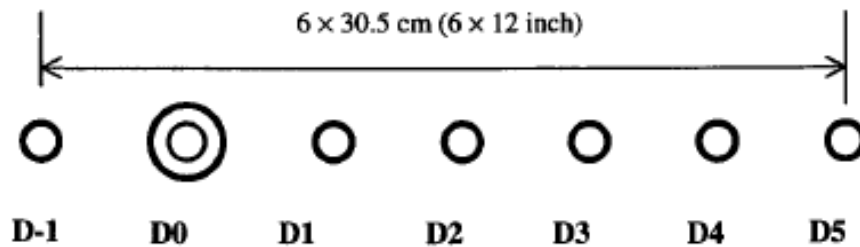


Figure 31. Location of the Deflection Sensors

2.4.3 Findings for Rigid Pavement

Table 8 summarizes the FWD test results for the rigid pavement test items at the center of slabs (deflection basin tests). The deflections are relatively uniform within each test item. The coefficients of variation (COVs) generally range from 3 to 8 %. One measurement on the high strength subgrade with COV value of 22 % appears to be an outlier.

Hayhoe, et al. (1999) analyzed D0 and D5 measurements at the center of the slabs for test items LRS, MRS, and HRS. D0 is an indicator of the overall stiffness of the pavement structure and D5 is an indicator of subgrade stiffness. They concluded that within each test item, the layer stiffness was uniform.

Table 8. Summary of FWD Basin Tests on Rigid Pavement Test Items (Hayhoe et al. 1999)

Item	Deflection (mils)	Load = 9000 lbs.			Load = 14000 lbs.			Load = 19000 lbs.			Load = 25500 lbs.		
		Mean	Std. Dev	COV (%)	Mean	Std. Dev	COV (%)	Mean	Std. Dev	COV (%)	Mean	Std. Dev	COV (%)
LRS	D0	2.56	0.14	5.43	4.07	0.29	7.07	5.56	0.37	6.73	7.44	0.55	7.38
	D1	2.43	0.14	5.85	3.75	0.29	7.82	5.17	0.37	7.21	6.89	0.53	7.66
	D2	2.26	0.14	6.12	3.53	0.23	6.42	4.75	0.33	6.95	6.34	0.47	7.42
	D3	2.06	0.12	5.89	3.2	0.21	6.67	4.3	0.29	6.82	5.79	0.45	7.72

Item	Deflection (mils)	Load = 9000 lbs.			Load = 14000 lbs.			Load = 19000 lbs.			Load = 25500 lbs.		
		Mean	Std. Dev	COV (%)	Mean	Std. Dev	COV (%)	Mean	Std. Dev	COV (%)	Mean	Std. Dev	COV (%)
MRS	D4	1.87	0.11	5.76	2.89	0.19	6.6	3.9	0.27	6.82	5.19	0.38	7.24
	D5	1.67	0.12	6.98	2.55	0.17	6.85	3.44	0.24	6.88	4.56	0.33	7.29
MRS	D0	2.45	0.14	5.71	3.85	0.21	5.28	5.31	0.26	4.87	7.2	0.37	5.07
	D1	2.22	0.1	4.36	3.5	0.18	5.24	4.81	0.25	5.27	6.5	0.35	5.43
	D2	1.97	0.09	4.46	3.06	0.15	4.98	4.17	0.23	5.52	5.66	0.28	5.01
	D3	1.71	0.08	4.54	2.64	0.13	5.06	3.61	0.17	4.66	4.92	0.24	4.92
	D4	1.48	0.05	3.37	2.28	0.1	4.37	3.09	0.14	4.44	4.14	0.19	4.66
	D5	1.24	0.05	4.12	1.9	0.08	4.34	2.57	0.12	4.72	3.43	0.16	4.6
HRS	D0	1.81	0.09	4.79	2.75	0.1	3.71	3.86	0.1	2.59	5.27	0.19	3.65
	D1	1.53	0.05	3.25	2.43	0.06	2.5	3.36	0.08	2.45	4.63	0.14	3.06
	D2	1.33	0.04	3.04	2.06	0.06	2.76	2.83	0.09	3.08	3.9	0.11	2.73
	D3	1.14	0.04	3.93	1.77	0.07	3.71	2.42	0.09	3.67	3.32	0.11	3.18
	D4	0.98	0.04	4.03	1.49	0.07	4.82	2.05	0.09	4.47	2.79	0.11	3.78
	D5	0.77	0.1	12.8	1.2	0.11	9	1.52	0.32	21.18*	2.26	0.12	5.52

* Outlier measurement

Figure 32 compares peak deflections D0 and D5 for the three rigid test items (Hayhoe et al. 1999). The rigid pavement test items on the low and medium strength subgrades showed similar D0 deflection responses, indicating that the stiffness of the two test items is comparable. But the rigid pavement test items on the high strength subgrade showed lower D0 deflections suggesting much higher structural capacity for HRS compared to LRS and MRS. Results from the D5 measurements also showed that the three subgrade types have significantly different stiffnesses.

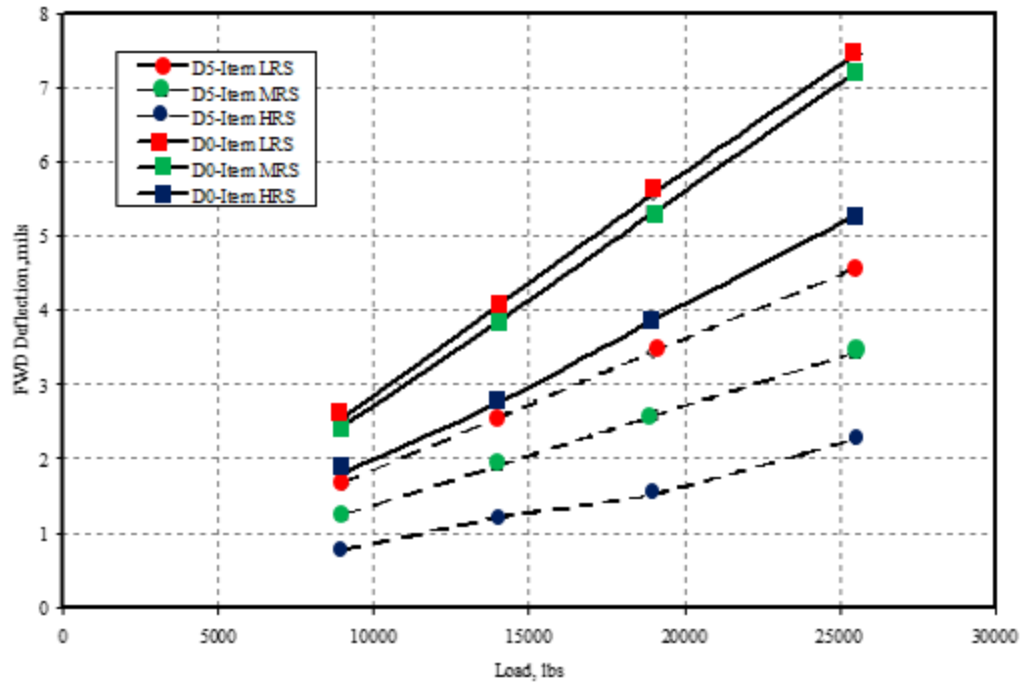


Figure 32. Comparison of FWD Deflections D0 and D5 at Center of Slab for the Three Rigid Test Items (Hayhoe, et al. 1999)

Figure 33 is a plan of a typical CC1 rigid pavement test item showing the locations of HWD tests relative to the joints (Brill and Guo 2000). All the longitudinal joints (L01-L20) were dowelled construction joints with 1 inch (2.54 cm) diameter dowel bars spaced at 10 inches (25.4 cm). All transverse joints (T01-T40) were undowelled construction (dummy) joints.

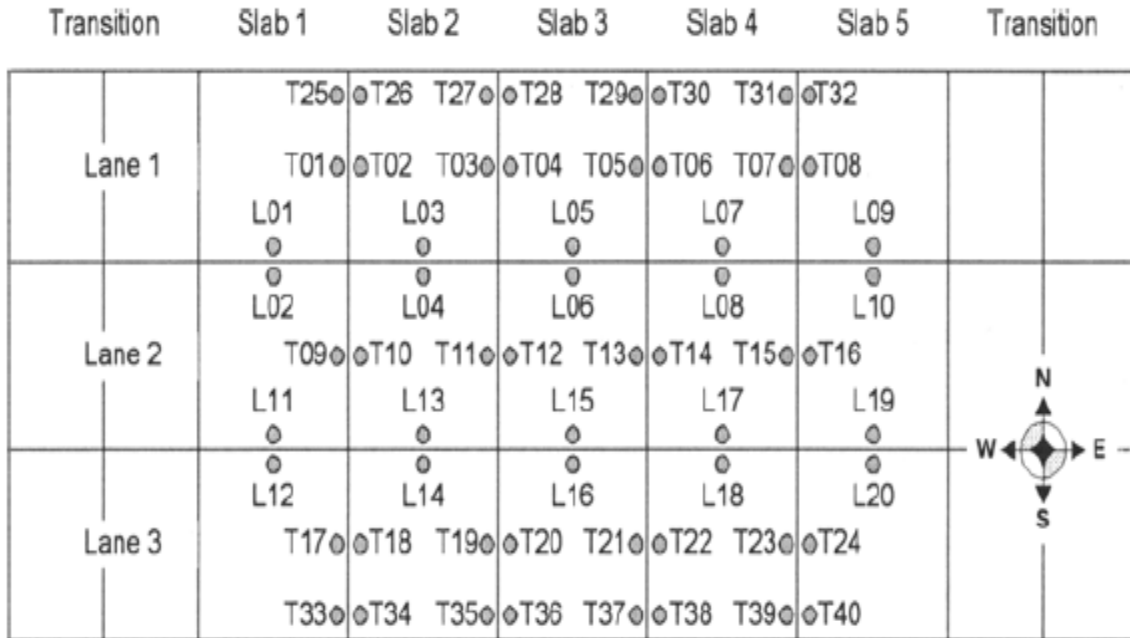


Figure 33. Locations of HWD Joint Tests for NAPTF Rigid Test Items (Brill and Guo 2000)

The mean of the measured deflections under the plate load (D0) and at 60 inches (D5) at the center of slabs are presented in Figure 34. The average D0 and D5 deflections were higher in the LRS sections with low strength subgrade. The average deflections from the June and October testing (see section 2.4.2) were relatively uniform within each test item.

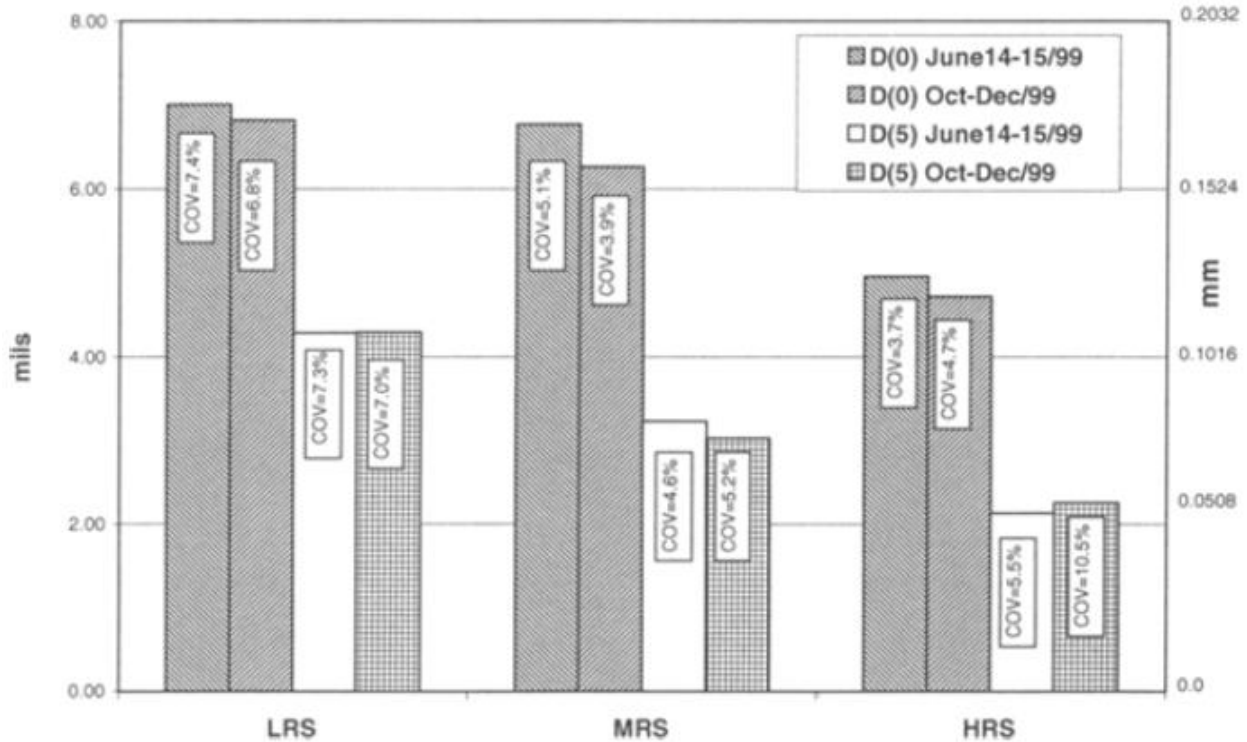


Figure 34. Average Deflections D0 and D5 at the Center of the Slabs (Guo and Marsey 2001)

Guo and Marsey (2001) evaluated deflections D0 at the joints and corners for LRS, MRS, and HRS test items. Deflection tests were conducted from June 1999 through January 2000. While the FWD loads were dropped on only one side of the joints in June 1999 testing, both sides of the joints were tested in the HWD testing in October 1999 to January 2000. The mean values of D0 at the joints and corners for LRS, MRS, and HRS test sections are displayed in Figure 35. It can be observed from the figure that the mean D0 measured at the transverse and longitudinal joints were fairly similar in June 1999 testing (4 months after construction). The deflections of transverse joints were higher than the longitudinal joints deflections in October, due to the lower load transverse efficiency of the dummy joints. The longitudinal and transverse joint deflections, as well as corner deflections, were higher in the winter testing compared to those during the summer testing. This can be attributed to higher upward slab curling in winter. The differences were more pronounced in the PCC slabs on top of the high strength subgrade.

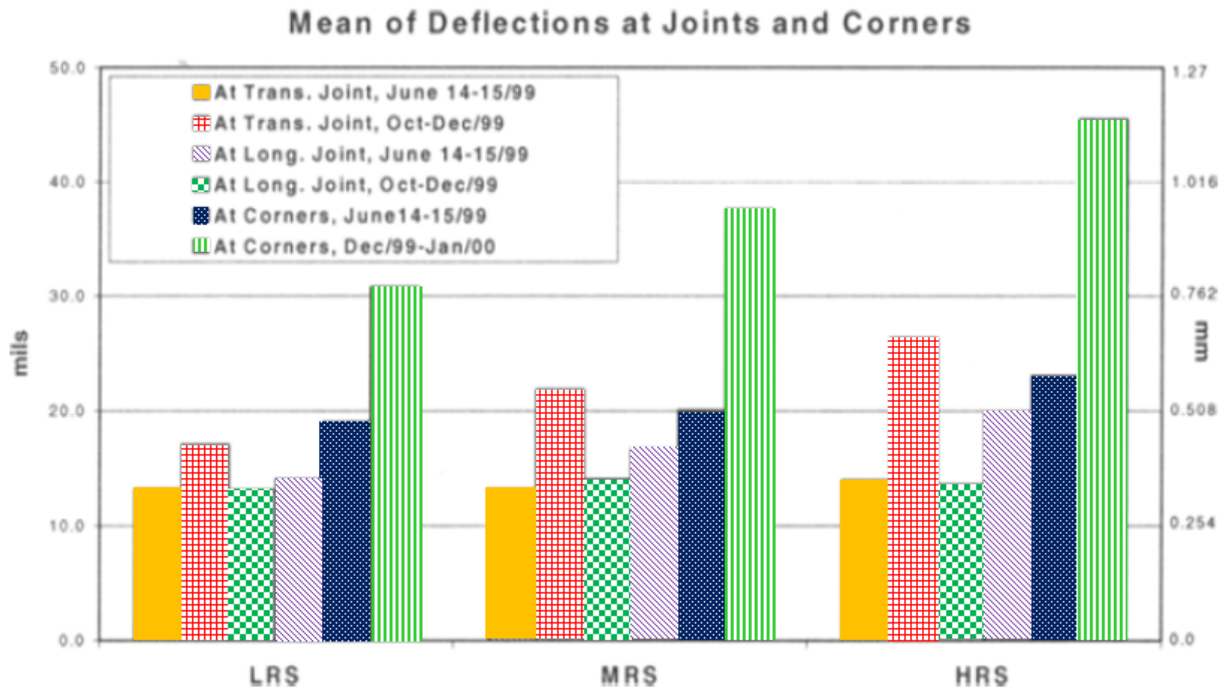


Figure 35. Deflection D0 at the Joints and Corners (Load = 24,000 lbs.) (Guo and Marsey 2001)

Joint load transfer efficiency (LTE_{δ}), is the ratio of the deflection of the slab on the unloaded side of the joint to the maximum deflection on the loaded side. Table 9 and 10 show calculated LTE_{δ} values for longitudinal and transverse joints, based on the 24 kip drops.

Table 9. LTE for NAPTF Longitudinal Joints (Doweled Joints) (Brill and Guo 2000)

Test Point	Load Transfer Efficiency			Test Point	LTE (%)		
	Subgrade Strength				Subgrade Strength		
	Low	Med	High		Low	Med	High
L01	76	77	90	L11	87	81	78
L02	91	77	89	L12	86	84	79
L03	80	81	90	L13	79	78	76
L04	76	77	77	L14	83	78	78
L05	86	77	86	L15	79	83	78
L06	73	77	80	L16	84	84	79
L07	78	85	96	L17	76	79	78
L08	81	92	80	L18	81	87	80
L09	77	85	87	L19	77	82	77
L10	80	91	82	L20	81	84	80
				Mean	81	82	82
				Standard Deviation	0.04	0.05	0.06

Table 10. LTE for NAPTF Transverse Joints (Dummy Joints) (Brill and Guo 2000)

Test Point	LTE (%)			Test Point	LTE (%)		
	Subgrade Strength				Subgrade Strength		
	Low	Med	High		Low	Med	High
T01	81	48	26	T13	59	78	76
T02	88	83	85	T14	74	77	26
T03	47	43	31	T15	79	77	45
T04	80	72	66	T16	24	77	77
T05	79	76	70	T17	84	75	44
T06	92	28	82	T18	90	74	90
T07	85	77	77	T19	53	21	49
T08	65	88	81	T20	74	56	55
T09	86	78	76	T21	87	42	78
T10	35	78	85	T22	78	10	81
T11	72	77	19	T23	85	58	73
T12	17	77	80	T24	8	8	85
				Mean	71	65	66
				Standard Deviation	0.21	0.21	0.2

From Table 9 and Table 10, doweled joints had a mean LTE_{δ} of 71% and standard deviation of 0.21 (approximately 5 times the standard deviation of 0.04 for doweled longitudinal joints). Comparing the statistical results, the LTE_{δ} highly uniform for doweled joints, but non-uniform for dummy joints where load transfer was accomplished primarily through aggregate interlock. Comparing the mean LTE_{δ} values for doweled joints for low, medium, and high strength subgrades, no significant influence of subgrade CBR on measured joint LTE can be observed. However, the LTE for dummy joints was lower for slabs on strong subgrades compared to those on weak subgrades, indicating more curling in higher-strength subgrade test items.

2.4.4 Findings for Flexible Pavement

Table 11 summarizes the mean, standard deviation, and COV for D0 and D5 measured on the flexible test items. Test items LFS and MFS showed lower COV values for D0 compared to LFC and MFC respectively, indicating better uniformity in the pavement structure. The COV values for D5 ranged from 1.4 to 5.5 %, which indicate the variation within the subgrade stiffness. The COVs for D5 of HFC test indicate high variation within the subgrade.

Table 11. Summary of Uniformity Tests on Flexible Pavements at the NAPTF (Garg and Marsey 2002)

Test Item	Load, kN	Deflection D0, mm		Deflection D5, mm	
		Mean	COV (%)	Mean	COV (%)
LFS	53	0.18	5.88	0.06	2.31
	106	0.35	5.91	0.12	2.37
	160	0.53	6.31	0.18	2.59
LFC	53	0.33	9.08	0.07	2.39
	106	0.65	7.82	0.13	2.56
	160	0.97	7.14	0.2	2.89
MFC	53	0.33	9.41	0.05	3.17
	106	0.65	9.13	0.1	3.3
	160	1.01	9.35	0.15	3.62
MFS	53	0.17	4.13	0.05	1.8
	106	0.33	3.61	0.09	1.36
	160	0.51	3.35	0.14	1.4
HFS	53	0.14	8.37	0.03	4.13
	106	0.28	8.42	0.06	3.73
	160	0.42	8.22	0.09	3.3
HFC	53	0.24	7.21	0.03	5.36
	106	0.47	7.99	0.06	5.48
	160	0.71	9.6	0.09	5.51

2.4.5 Summary

The HWD data collected prior to the application of traffic indicated significant increase of curling in the slabs from summer to the winter of 1999. Test items on low and medium strength subgrades showed similar deflection responses. Pavements on high strength subgrade showed lower deflections.

The deflections of transverse joints were higher than the longitudinal joints due to lower LTE of the dummy joints.

Comparing the average deflections for the center of slabs for winter and summer testing, values were fairly compatible within each test item. However, for the longitudinal and transverse joints, as well as corners, deflections were higher in the winter testing compared to summer due to the higher upward curling in winter time.

Comparing the joint LTE for low, medium, and high strength subgrades, no significant influence of subgrade CBR was observed for dowelled joints. In dummy joints, however, slabs on higher strength subgrade test items showed more curling compared to the lower strength subgrade test items.

Deflection D0 from FWD testing is generally a representative of pavement structure as a whole. Comparing the D0 values within each test item in flexible pavement sections, it was seen that

deflections were relatively uniform indicating that pavement structure was uniform within each test item.

3. PAVEMENT RESPONSE AND TRAFFIC TESTING

Two separate test protocols were established during the first year of testing in CC1: response testing and traffic testing (trafficking). The response testing consisted of a series of static load, slow rolling, and heavy weight deflectometer (HWD) testing conducted from August to September, 1999. The objectives of response testing were to determine the effects of static and moving load on pavement responses as well as the wheel load interaction effects for different wheel and gear spacing. Slow rolling tests were performed during August to September, 1999. In these tests, the testing vehicle was rolled at a speed of 0.5 ft./sec (0.15 m/sec) with 12,000 lbs. (53.4 kN) and 24,000 lbs. (106.8 kN) wheel loads for rigid pavements, and 24,000 lbs. (106.8 kN), 30,000 lbs. (133.5 kN) and 36,000 lbs. (160.1 kN) wheel loads for flexible pavements. Loads were selected such to minimize pavement damage.

To investigate the degree of load interaction, an analysis of slow rolling test data for different load levels, gear configuration, and transverse offsets was performed. Detailed analysis results can be found in a report by Gomez-Ramirez and Thompson (2001). To evaluate the effect of interaction between landing gears on pavement response, gear separation tests were performed as a part of the slow rolling tests. The effect of spacing between two 4-wheel gears, 4-wheel and 6-wheel gear, and two 6-wheel gears were studied by Garg and Dong (2002). A total of 822 response tests were conducted for the flexible test items with 137 tests for each item. A total of 252 response tests were also conducted on the rigid test items with 84 tests for each item (Hayhoe et al. 2001).

Traffic tests started after the completion of the response tests in February 2000. To simulate aircraft wander, a wander pattern consisting of a fixed sequence of 66 vehicle passes (33 in east to west and 33 in west to east directions) was defined. The 66 passes were arranged in nine equally spaced wander positions at intervals of 10.25 inches (260 mm) (Figure 36, Guo et al. 2002). Figure 37 shows the number of repetitions at each wander position in a complete wander cycle (Hayhoe and Garg 2002). The wander pattern was intended to approximate a normal distribution of aircraft traffic with a “wander width” of 70 inches; that is the normal distribution that results in 75% of traffic passes concentrated in a 70-inch wide width. It can be shown that the standard deviation of such a distribution is 30.54 inches (Ho song, 1975).

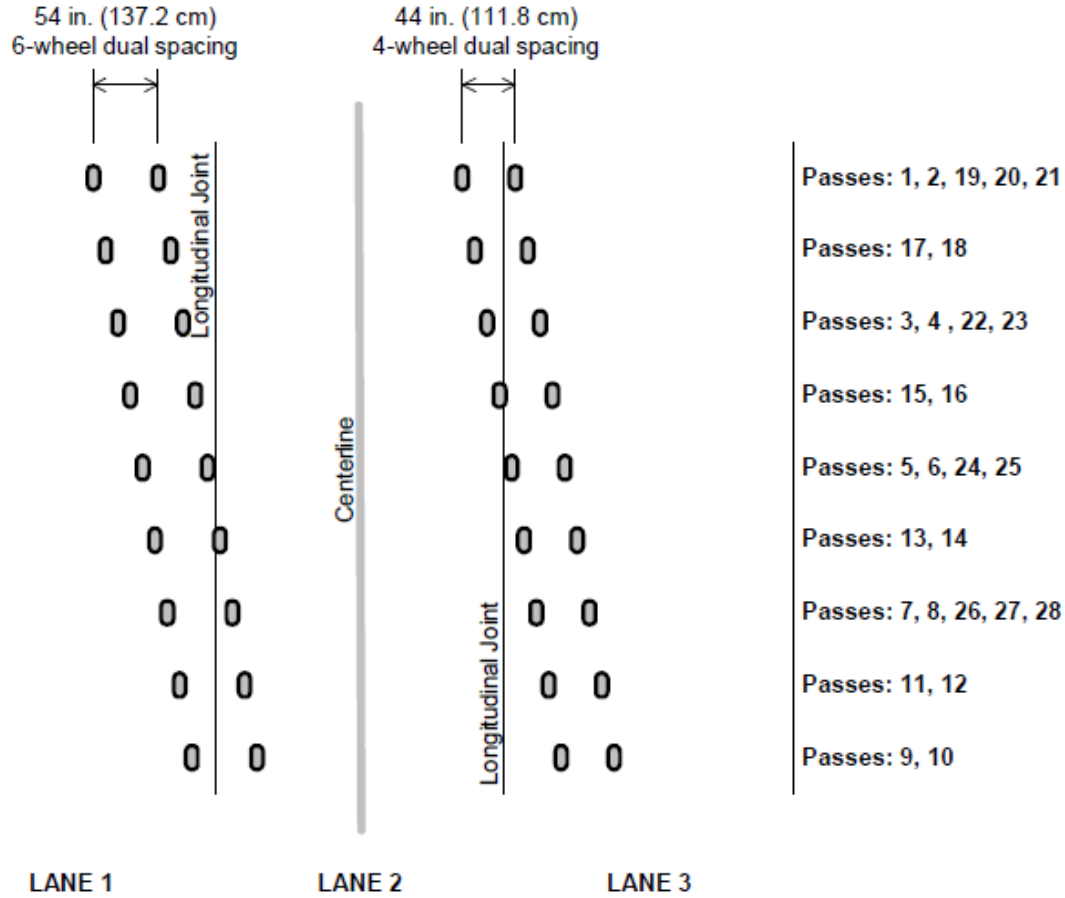


Figure 36. 6-Wheel and 4-Wheel Wander Patterns (Guo et al. 2002)

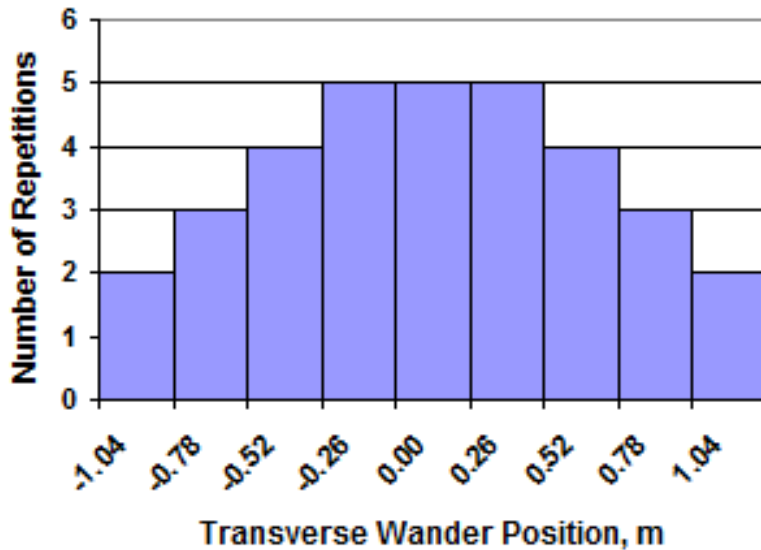


Figure 37. Wander Distribution (Hayhoe and Garg 2002)

Table 12 shows the transverse positions of the gear centers for each wander position in the cycle. Negative and positive positions of the gear centerlines correspond to the north and south of the pavement centerline, respectively. Travel direction is eastward for odd sequence numbers and westward for even sequence numbers. The transverse position of the gears was changed only at the start of the eastward repetitions. That is, westward repetitions always had the wheels following in the same paths as in the preceding eastward repetition. To minimize the interaction of gear loads at the subgrade level for the flexible pavement, the south and north carriages maintained an equal lateral distance at each step of the wander pattern. Since the traffic testing of rigid and flexible pavements were performed at the same time, this was applied for the rigid pavement as well.

Table 12. Transverse Gear Centerline (CL) Positions in a Complete Wander Cycle (Hayhoe et al. 2004)

Sequence No.	Track No.	North Gear Center Line Position, inch	South Gear Center Line Position, inch	Sequence No.	Track No.	North Gear Center Line Position, inch	South Gear Center Line Position, inch
1,2	-4	-194.4	107.0	35,36	-3	-184.2	117.3
3,4	-2	-174.0	127.5	37,38	3	-122.8	178.7
5,6	0	-153.5	148.0	39,40	1	-143.3	158.2
7,8	2	-133.0	168.5	41,42	-1	-163.7	137.8
9,10	4	-112.6	188.9	43,44	-3	-184.2	117.3
11,12	3	-122.8	178.7	45,46	-2	-174.0	127.5
13,14	1	-143.3	158.2	47,48	0	-153.5	148.0
15,16	-1	-163.7	137.8	49,50	2	-133.0	168.5
17,18	-3	-184.2	117.3	51,52	-2	-174.0	127.5
19,20	-4	-194.4	107.0	53,54	0	-153.5	148.0
21,22	-2	-174.0	127.5	55,56	2	-133.0	168.5
23,24	0	-153.5	148.0	57,58	1	-143.3	158.2
25,26	2	-133.0	168.5	59,60	-1	-163.7	137.8
27,28	4	-112.6	189.0	61,62	1	-143.3	158.2
29,30	3	-122.8	178.7	63,64	-1	-163.7	137.8
31,32	1	-143.3	158.2	65,66	0	-153.5	148.0
33,34	-1	-163.7	137.8				

The objective of traffic tests was to determine the effect of gear configuration, load level and wander on pavement life. Test items were loaded simultaneously with two gear configurations; a 6-wheel gear in one lane and a 4-wheel gear in the other lane. The pavement responses (strains, deflections, etc.) were monitored using embedded sensors as described in the previous chapter. Dynamic sensor data were recorded at 20 samples per second. Moisture and temperature readings

were recorded every 15 minutes. Throughout the test, the pavement condition was monitored by various methods:

- Heavy weight deflectometers (HWD): HWD tests were conducted at various stages of trafficking to track the structural deterioration of the pavement sections.
- Rut depth monitoring: this was done using several transverse surface profile (TSP) measuring devices including rolling inclinometer and straightedge.
- In-pavement sensors (MDDs) for measuring the permanent deformation of layers.

3.1 Traffic Testing of Rigid Pavement

3.1.1 Traffic Testing

3.1.1.1 Testing Method and Equipment

Figure 38 shows the gear load configuration for the rigid pavement traffic test. The north carriage (left) was configured to represent a B777 main gear. The south carriage (right) was configured to represent one truck of a B747 main gear. The 54-inch dual spacing at the north carriage deviates slightly from the actual dual spacing of a B777 main gear truck (which is 55 inches) due to the fixed spacing positions available on the NAPTF wheel modulus. For traffic testing, wheel loads were set at 45,000 lbs. (20.4 tonnes) with a target tire pressure of 188 psi (1296 kPa). The vehicle speed was 5 mph (8 km/h) during testing.

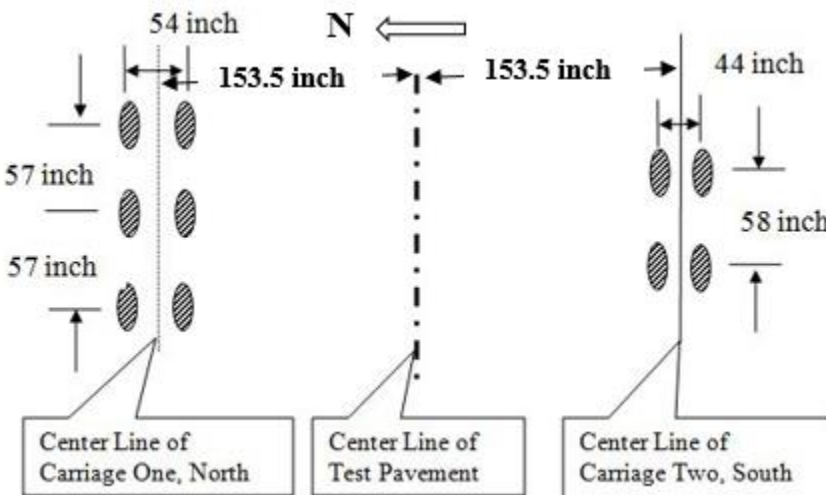


Figure 38. Gear Configurations

The coordinate system for rigid test items is displayed in Figure 39 (Hayhoe et al. 2001). The north (top) carriage is designated as “Carriage-1” and the south (bottom) carriage is designated as “Carriage-2”. The three load modules on Carriage-1 are designated 1-1, 1-2, and 1-3, respectively. Load module 1-1 (front) is toward the high-strength end of the facility and load module 1-3 (rear) is toward the low strength end of the facility. The three load modules on Carriage-2 are designated 2-1, 2-2, and 2-3 respectively. The transverse position of the load module was defined in terms of carriage offsets from the centerline.

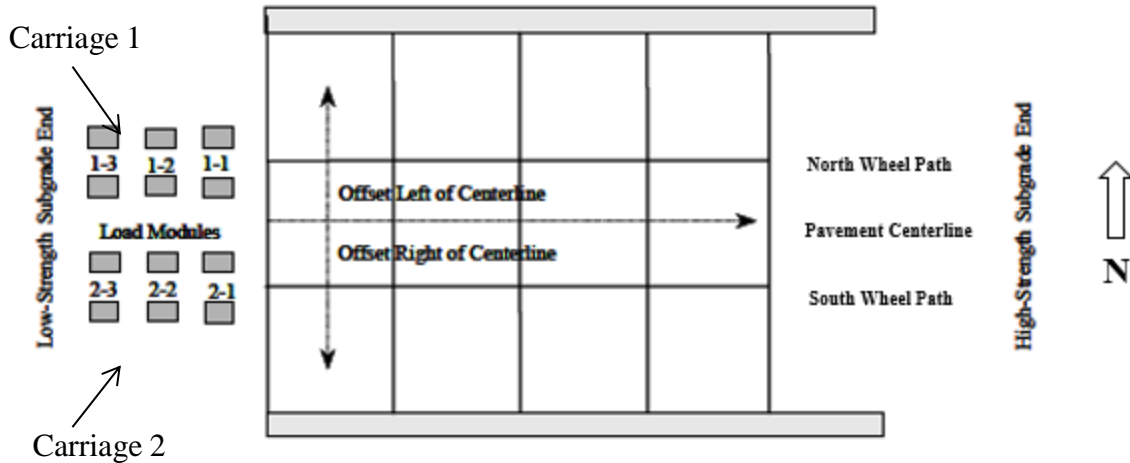


Figure 39. Coordinate System for Rigid Pavement Test Items (Hayhoe et al. 2001)

3.1.1.2 Data Collection

Table 13 shows the summary of traffic tests on rigid pavement test items. The first series of traffic tests was planned for February 2000 until July 2001. Using different failure models, the number of passes to failure was expected to be 1,000 to 10,000 passes. Testing started as planned on February 14, 2000. However, cracks were observed after only 28 passes and testing was stopped to evaluate the origin of the cracks on rigid test items (Guo and Marsey 2001). Almost all the slabs in MRS and HRS test items exhibited corner cracks. Longitudinal cracks were also observed in all the slabs in lane 2 of the LRS test item.

Traffic tests were resumed in March 2000 and continued until all the slabs failed. For rigid pavement test items, failure was defined in terms of structural cracking initiating at the joints at the bottom of the PCC layer (McQueen et al. 2002). Trafficking was stopped at 849 passes in HRS (March 31, 2000), 891 passes in MRS test item (April 6, 2000), and 1195 passes in LRS (April 10, 2000).

Table 13. Summary of Traffic Tests for Rigid Test Items in CC1

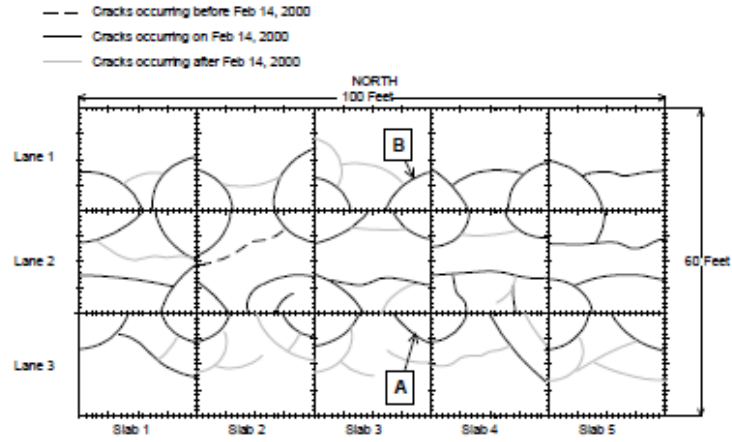
Test Item	Date	Load Level (kips)	Vehicle Speed (mph)	Accumulated Passes
HRS	Feb 2000 - Mar 2000	45	5	849
MRS	Feb 2000 - Apr 2000	45	5	891
LRS	Feb 2000 - Apr 2000	45	5	1,195

3.1.1.3 Findings

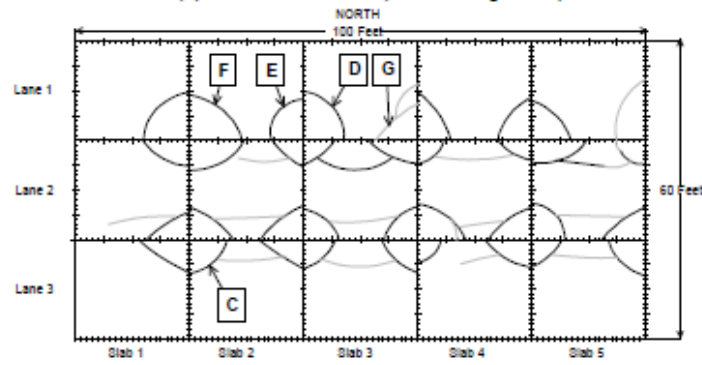
The distresses observed in the rigid test items are presented in Figure 40 (Guo 2008). In test item LRS, only four longitudinal cracks were observed after the initial 28 passes. After additional traffic was applied to test item LRS in March 2000, corner cracks started to develop. Figure 41 shows the definition of corner crack dimensions when reporting crack size (Guo et al. 2002). The “a” and “b” values were measured for the two sides of corner cracks and the average is presented in Table 14 for different test items (Guo et al. 2002). The largest and smallest corner cracks developed in the HRS and LRS test items, respectively.

Elevation surveys were done shortly after the pavement construction and four days prior to the start of traffic testing. Each slab elevation was measured at nine points (four corners, four joints, and one at the center). Analysis of the survey data revealed the presence of significant slab curling just prior to the start of traffic testing on February 14, 2000. The existence of curling was also verified by analyzing the HWD data at the centers, joints, and corners of each slab as explained in more detail in section 3.1.2. While curling was evident at the corners of all the pavement slabs, the HRS slabs exhibited the greatest amount of curling, and the LRS slabs exhibited the least amount of curling (Guo 2008).

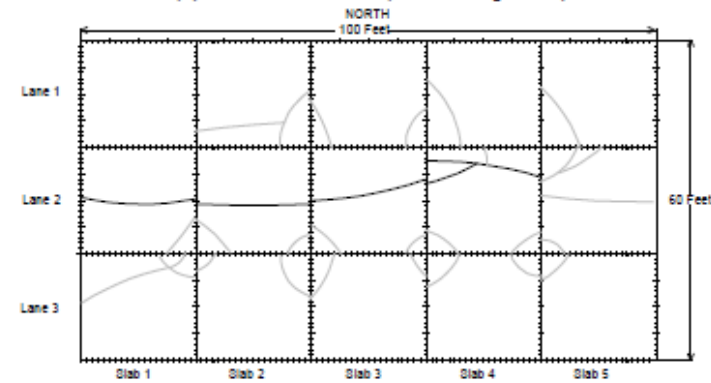
Indoor slabs were not exposed to typical field conditions. When CC1 was constructed, temperature-induced curling was not believed to be an issue of concern due to the fact that the test pavements were protected from sunlight exposure and temperature cycles. The measurements made after construction showed that the temperature gradients within the slabs were about one tenth of expected temperature gradients under typical field conditions. Therefore, it was concluded that the temperature gradient was not the major factor inducing upward curling. The manifestation of curling caused the FAA to rethink rigid test item design in subsequent construction cycles. Later, as a part of the CC2 effort, factors such as concrete mix, slab size, and curing procedure were examined for their potential in leading to the curling and premature corner breaks under traffic. Drying shrinkage and large vertical moisture gradients within the slab depth were found to be the root cause of slab upward curling in CC1 rigid test items. These factors were more pronounced in the relatively thin slabs in test item HRS (Hayhoe 2004).



(a) Test Item HRS (after 236 passes)



(b) Test Item MRS (after 646 passes)



(c) Test Item LRS (after 1164 passes)

Figure 40. Crack Patterns in Rigid Test Items (Guo et al. 2002)

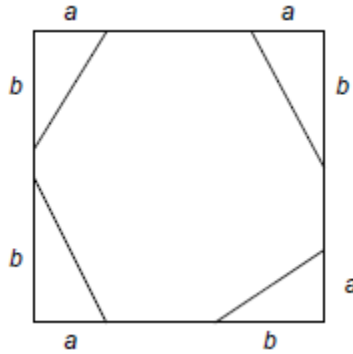
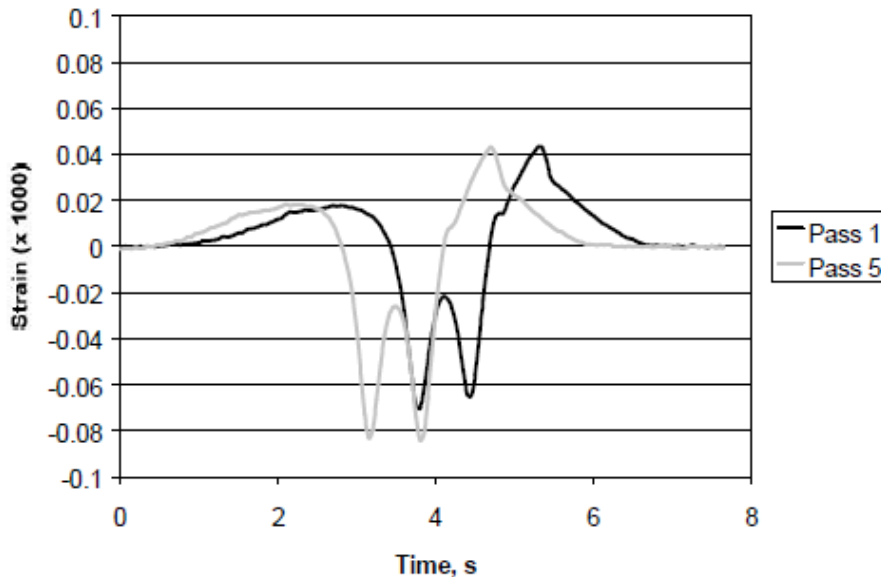


Figure 41. Definition of Corner Crack Dimensions in Table 14 (Guo et al. 2002)

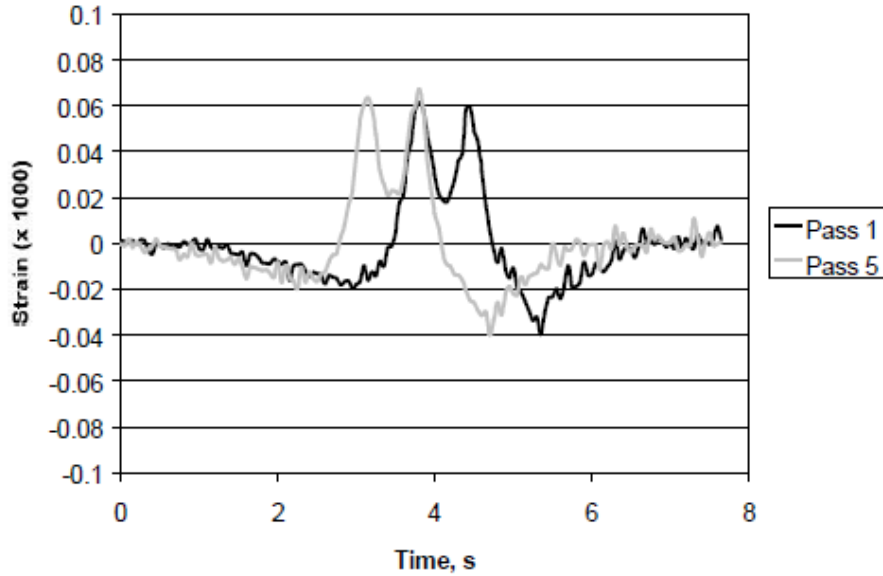
Table 14. Summary of Average Crack Sizes for Rigid Test Items (Guo et al. 2002)

Corner Crack Dimensions	Test Item		
	HRS	MRS	LRS
Average a, in. (cm)	78 (198)	72.5 (184)	54.9 (139)
Average b, in. (cm)	98.3 (250)	92.2 (234)	79.1 (201)

Guo et al. (2002) analyzed the strain gauge data from the first phase of CC1 rigid pavement traffic testing. Figure 42 (a) and (b) shows a typical strain gauge response before crack initiation for the top and bottom sensor during passes 1 and 5 of the 4-wheel load. The peak strains for pass 1 are smaller than those from pass 5, because in pass 5, both tires were on the same side of the longitudinal joint, while in pass 1 the tires straddled the joint and only a portion of the wheel load was transferred through the joint (see Figure 36).



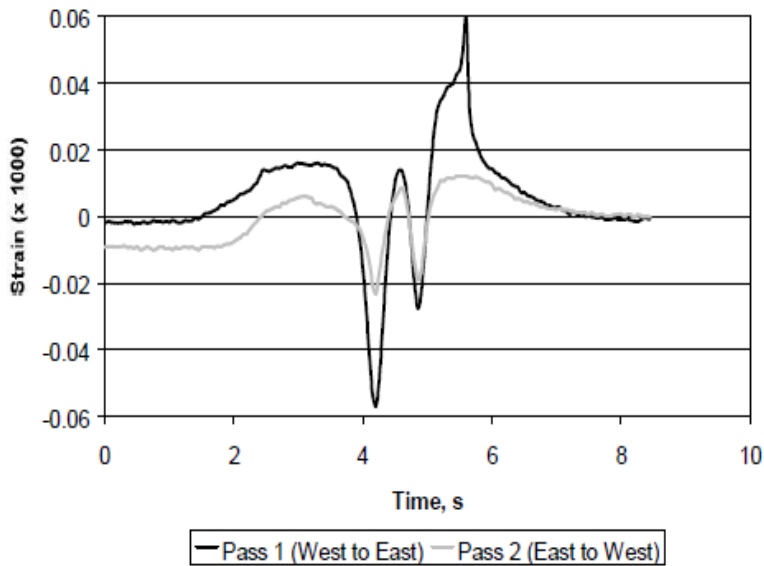
(a) Strain gauge at top of slab (CSG – 303)



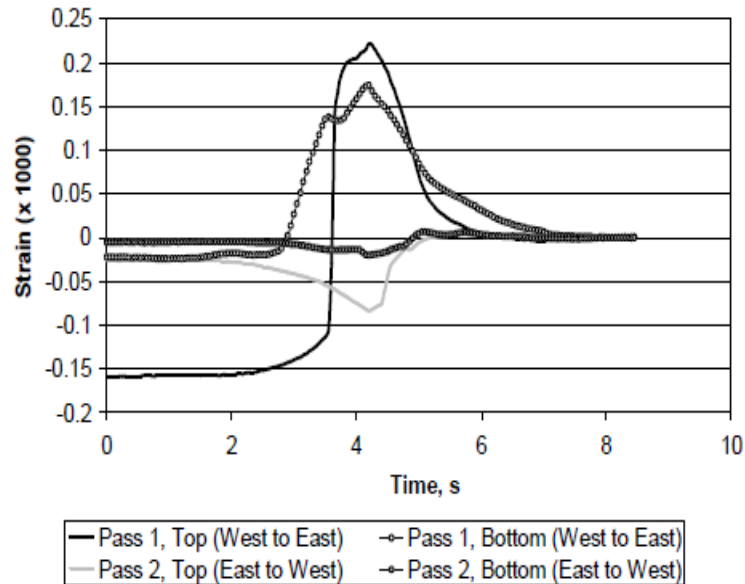
(b) Strain gauge at bottom of slab (CSG – 366)

Figure 42. Typical Strain Responses in LRS for the 4-Wheel Load (Guo et al. 2002)

Figure 43 (a) and (b) shows an example of strain gauge response after the corner crack developed (Guo et al. 2002). The unusually high strain readings are attributed to the crack passing through the strain gauge location. Guo et al. 2002 verified that crack A in Figure 40 (a) initiated during the first pass of the vehicle implying a lack of structural support attributable to curling, rather than a fatigue failure. Similarly, the majority of corner cracks identified in the HRS item along lane 3 developed during the first vehicle pass (Guo et al. 2002).



(a) Strain Gauge at Top of Slab, Longitudinal Joint (CSG – 109)



(b) Strain Gauges at Top (CSG –173) and Bottom (CSG – 192) of Slab, Transverse Joint

Figure 43. Strain Responses in HRS, Lane 3 (4-Wheel Load) (Guo et al. 2002)

Similar analyses performed on strain gauges in test items MRS and HRS showed that those slabs were subjected to high corner curling leading to early structure failure (Guo et al. 2002).

3.1.1.4 Summary

Traffic testing began on February 14, 2000. After completion of the initial 28 passes, corner cracks were observed in the test items MRS and HRS. No corner cracks were found in LRS after the first 28 passes. However, longitudinal cracks were observed in all slabs in lane 2 (centerline) of LRS. Trafficking was resumed in March 2000 and was continued until all the slabs were cracked.

Measurements of crack dimensions showed that the HRS slabs exhibited the largest, and the LRS slabs exhibited the smallest corner cracks. Furthermore, it was found that all pavement slabs were curled up at the corners, with the HRS slabs exhibiting the greatest amount of curling, and the LRS slabs exhibiting the least amount of curling. The high levels of slab curling were unexpected due to the protection from sunlight afforded by the NAPTF’s roof, which meant that the daily temperature cycles experienced by concrete slabs were minimal. Post-failure analysis found that slab curling was probably caused by relatively thin slabs combined with a PCC mixture susceptible to moisture-related shrinkage.

3.2 Pavement Response and Traffic Testing of Flexible Pavement

3.2.1 Static Response Test

3.2.1.1 Testing Method and Equipment

Static response tests are representative of stationary or very slow moving aircraft. In these tests, stationary loads are applied to the pavement with one of the wheels placed directly over an MDD.

Static response tests were performed on the flexible pavement test items using the 6-wheel gear of the NAPTF load modules as a stationary loading device over the centerline MDDs to examine the load deflection behavior of pavement component layers (Garg and Marsey 2002).

3.2.1.2 Data Collection

Static response tests were performed on March 3, 2000. The pavements were loaded by a 6-wheel gear at load levels of 12,000, 24,000, 36,000, 48,000, and 60,000 lbs. per gear, with one of the wheels placed directly above the centerline MDDs (Garg and Marsey, 2002). The MDD locations and gear configuration for static tests are shown in Figure 44. Each load was applied for 2 minutes and then removed. The MDD sensors continued to collect data for 2 minutes after removal of the load. Figure 45 shows an example of MDD time history from the static response test for test item LFC.

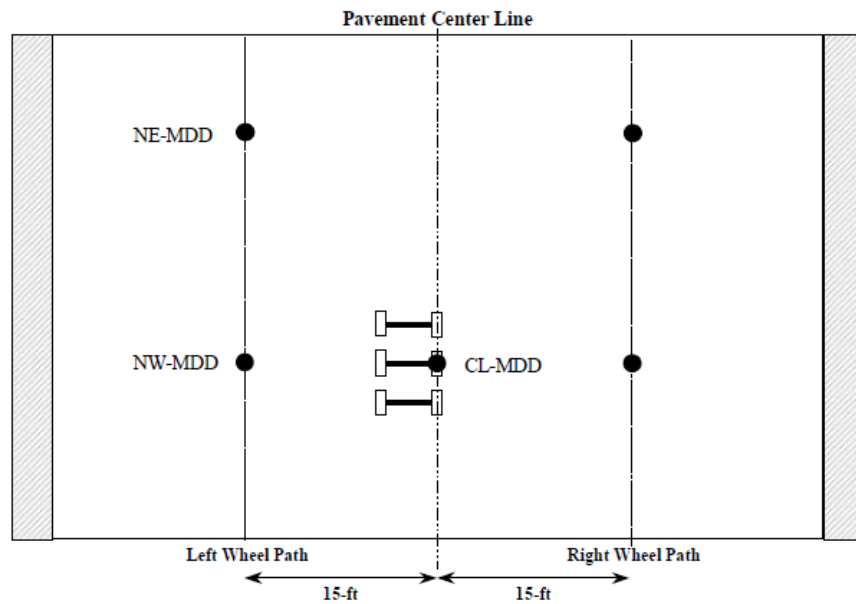


Figure 44. MDD Locations and Gear Configuration for Static Tests (Garg and Marsey 2002)

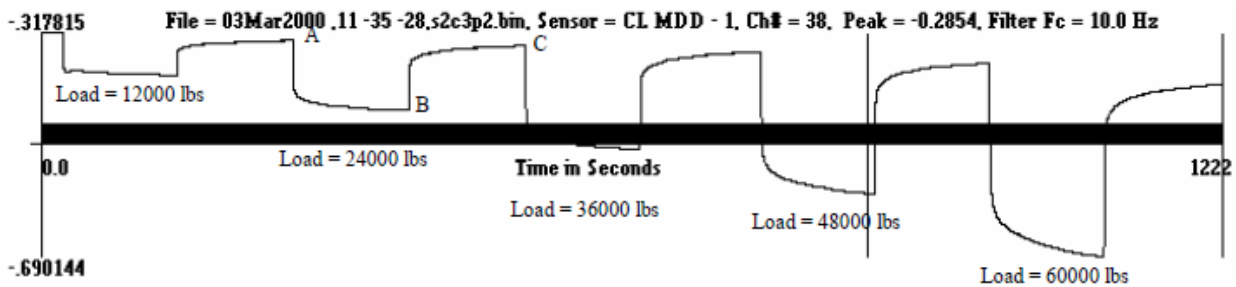


Figure 45. A Typical MDD Time History for Static Test (Test Item LFC) (Garg and Marsey 2002)

3.2.1.3 Findings

Figure 46 shows a typical MDD response. Three axles are clearly defined by distinct peaks in the response. The peak strain increases significantly from the first wheel to the last wheel. The last

wheel produces the maximum peak displacement. Each signal consisted of a steady response, a maximum response and a steady response after the peak. The difference between the initial response and the end response indicates unrecovered or permanent response. The unrecovered response was either negative (downward) or positive (upward) depending on the location of the wheel load in relation to the MDD. In some cases, the time history was such that the total response was equal to the unrecovered response. The net unrecovered strain over a single wander cycle represents the incremental contributions to the permanent deformation accumulated over that wander cycle. When accumulated over the complete test to failure, these small increments of permanent deformation represent the total rut accumulation. Further information on unrecovered response is provided in Section 3.2.2.

The recovered displacement corresponds to the difference between peak and unloaded displacement. Recovered responses provide a good measure of the elastic behavior of pavement materials (Ledbetter 1977, Crockford, Bendana et al. 1990, Bejarano 1999).

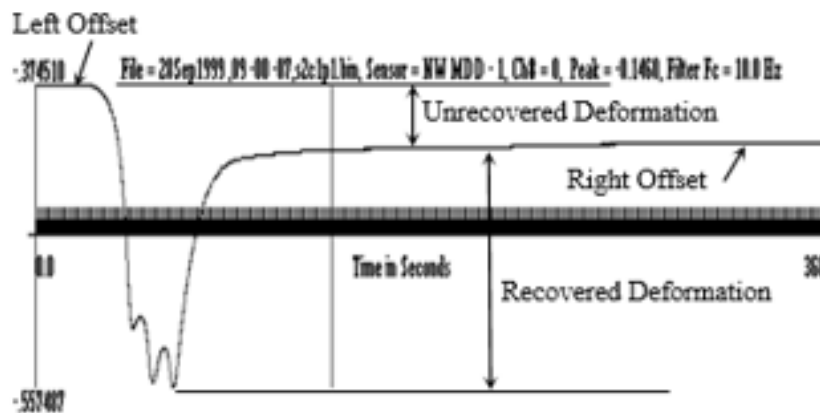


Figure 46. Typical Deflection Response from MDD for 6-Wheel Loading (Hayhoe et al. 2004)

Figure 47 shows the recovered surface deflections for the flexible test items at a range of load levels (Garg and Marsey 2002). The Micro Motion sensor Model DT, which was used to measure the total pavement deflection (Section 2.3.1), was not working in test item LFS during the static load testing, thus results for LFS are not included. As shown in Figure 47, test item LFC showed the highest deflection. Test item MFS had up to 10% higher recovered deflections compared to the MFC item. Test items HFS and HFC showed similar surface deflections (Garg and Marsey 2002).

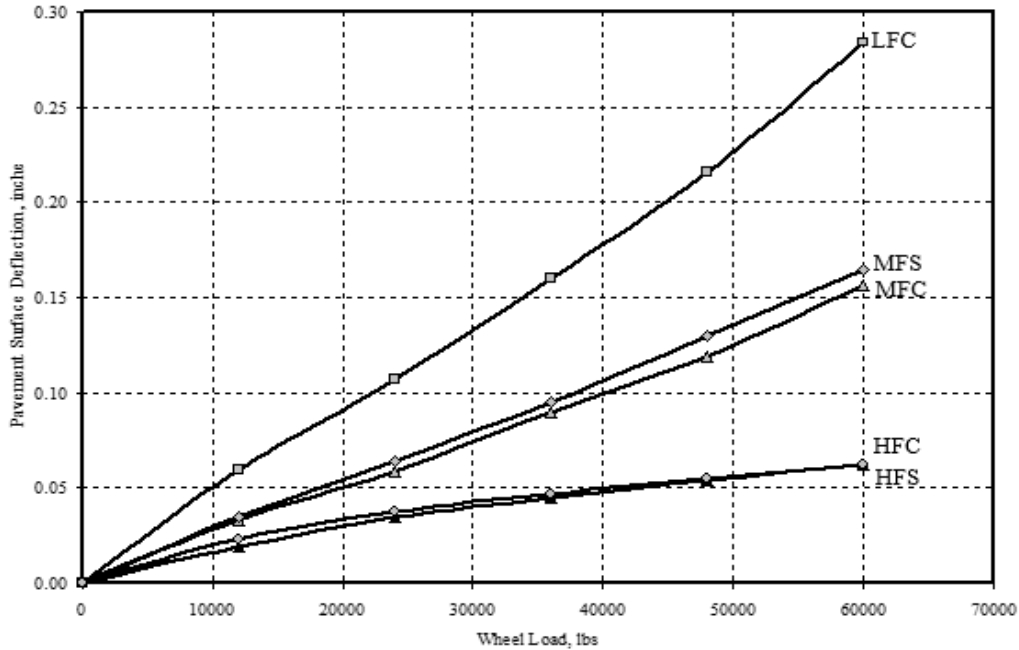


Figure 47. Recovered Surface Deflections from Static Load Tests for the Flexible Test Items (Garg and Marsey 2002)

Figure 48 shows the recovered subgrade deflections for the flexible test items except LFS at different load levels (Garg and Marsey 2002). Test item LFC showed the highest subgrade deflection. The difference in subgrade deflections between test items MFC and MFS became more with increasing load levels. Test items HFS and HFC showed almost similar subgrade deflections.

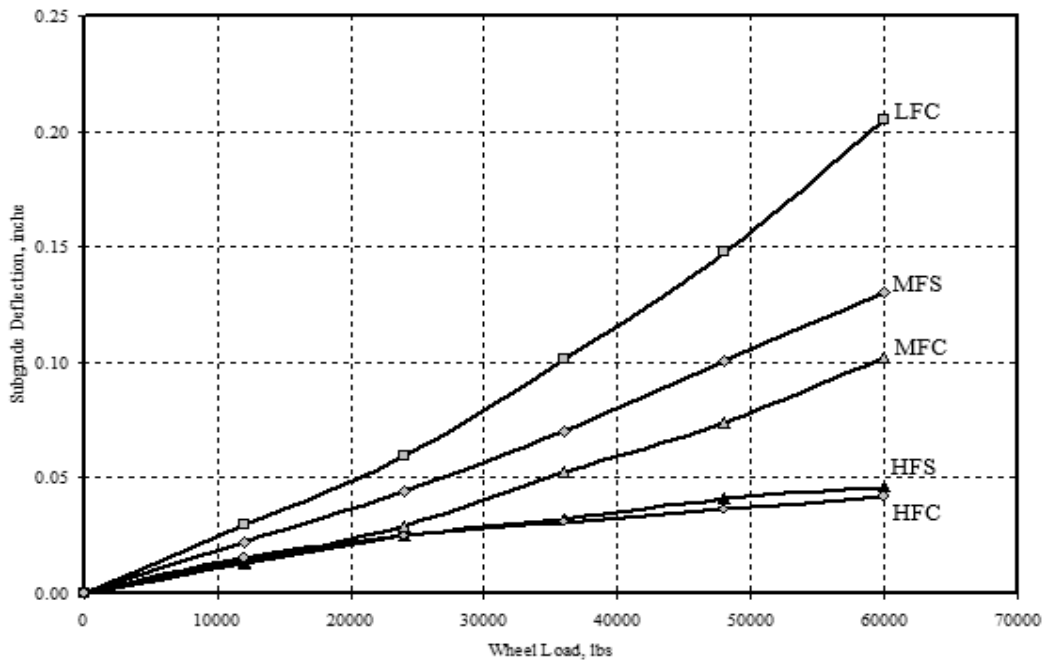


Figure 48. Recovered Subgrade Deflections for the Flexible Test Items from Static Load Tests (Garg and Marsey 2002)

Figure 49 shows the percentage of the subgrade layer contribution to the total surface deflection for five of the six flexible test items. Test items LFC, MFC, and MFS exhibit stress-softening of fine-grained subgrade, likely due to the silty-clay used in the LFC and the DuPont clay used in the MFC and MFS sections. Test items HFS and HFC exhibit stress-hardening of sandy subgrade (Garg and Marsey 2002).

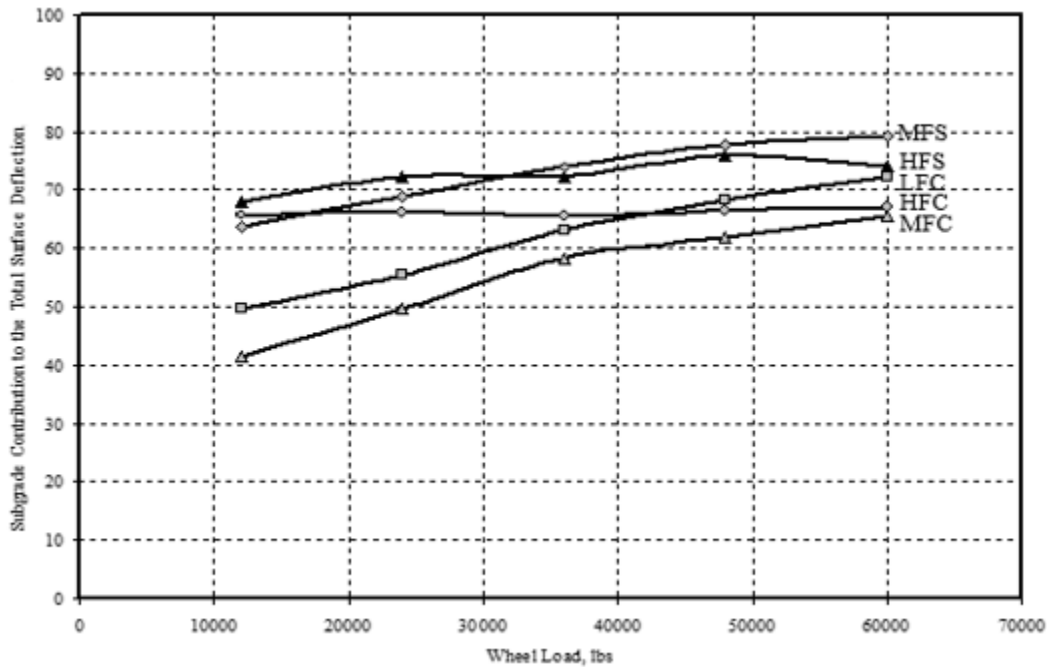


Figure 49. Subgrade Contribution to the Pavement Surface Deflection (Garg and Marsey 2002)

3.2.1.4 Summary

Static response tests were performed in all the flexible pavement test items to study the load deflection behavior of pavement component layers. In these response tests, the 6-wheel gear was positioned such that one of its wheels was directly over the MDD. Key findings were as follows:

- The highest recovered deflections at the surface were LFC, followed by MFS and MFC, followed by HFS and HFC.
- The highest recovered deflections at the subgrade level were LFC, followed by MFC and MFS, followed by HFS and HFC.
- HFS and HFC exhibited similar responses at both levels.
- The percent contributed by the subgrade to total surface recovered deflections was load-dependent for test items on clay subgrades.

3.2.2 Traffic Testing

Traffic tests on flexible pavement test items used the same gear configurations, vehicle speed, and programmed wander positions for the rigid pavement test items described in Section 3.1.1. As in

the rigid pavement tests, the initial load for flexible pavement traffic tests was 45,000 lbs. (20.4 tonnes) at a target tire pressure of 188 psi (1296 kPa).

3.2.2.1 Data Collection

Table 15 summarizes the traffic tests on flexible test items. Traffic testing began in February 2000 and was paused after 28 passes on February 14, 2000 due to premature failure of rigid pavement test items. This was a consequence of the plan, as the decision to test all the test items at once meant that premature failure of the rigid items caused delays in testing the flexible test items. Traffic resumed on March 30, 2000 on all test items. As indicated in Section 3.1.1, by April 10, 2000 all the rigid pavement test items had failed, but traffic continued on the flexible test items, skipping over the rigid items. Traffic on HFC and HFS ended after 3400 passes with no indication of damage, but continued on the low and medium strength subgrade flexible test items until November 2000. At that point, ambient temperatures became too low for representative testing on the asphalt layers. Testing resumed in May of 2001 and was completed in September 2001.

The criterion for failure of flexible pavements in the NAPTF was a minimum of 1 inch (25.4 mm) surface upheaval adjacent to the traffic lane. This is the same as the criterion used by the U.S. Army Corps of Engineers in previous full-scale tests of flexible airport pavements (Ahlvin et al. 1971). This failure mode is indicative of shear failure in the subgrade.

Test item MFC failed after 12,000 passes at the 45,000 lbs. wheel load in both north and south lanes. The straightedge rut depth measurements showed rut depth of 4 to 6 inches (101.6 to 152.4 mm) at failure. Upheavals and asphalt surface cracking were observed outside and inside the traffic lane, respectively (Hayhoe and Garg 2004).

In test item MFS, a localized failure was observed in the north traffic path (6-wheel) after 19,900 passes. The associated maximum rut depth was 3.5 inches (88.9 mm). No further trafficking was applied to the north side. Trafficking was resumed on the south side almost one year later with the same gear configuration and wheel load but with half of the previous speed 2.5 mph (4 km/h). The vehicle speed was decreased due to operational reasons. The lower speed was intended to avoid inducing rapid failure. After a total of 25,000 passes, the accumulation of rut depth started to increase considerably and failure occurred at 29,000 load repetitions (Hayhoe et al. 2004).

Test items LFC and LFS showed few signs of structural failure even after being subjected to 20,000 load repetitions. Therefore, the wheel load for LFS and LFC was increased to 65,000 lbs. (29.4 tonnes) after 20,000 passes and the speed changed to 2.5 mph (4 km/h). In order to maintain a similar footprint, the tire pressures were increased to 235 psi (1620 kPa) (Gervais 2004).

While aggregate base/subbase and subgrade failure was observed in the medium strength subgrade test items, LFC and LFS failed at surface layers as exhibited by formation of cracks (Gervais 2004). Trafficking was terminated in test item LFC after 42,000 passes. Hayhoe (2004) concluded that full structural failure did not occur in test items LFC and LFS, probably because the subgrade material contained a significant amount of silt and the upper layers of the subgrade lost moisture over the long period of time between the construction and start of traffic testing. In items with high strength subgrade, no damage was observed after 3400 passes and it was determined that structural

failure was unlikely to occur under the maximum loads that could be applied. Therefore, testing of high strength test items was terminated after 3400 passes in May 2000.

Table 15. Summary of Traffic Tests for Flexible Test Items in CC1

Test Item	Date	Load Level (kips)	Vehicle Speed (mph)	Accumulated Passes
LFC	Feb 2000-Jul 2001	45	5	20,000
		65	2.5	22,000
LFS	Feb 2000-Jul 2001	45	5	20,000
		65	2.5	25,000
MFC	Feb 2000-Jun 2000	45	5	12,000
MFS-North	Feb 2000-Nov 2000	45	5	19,900
MFS-South	Feb 2000-Sept 2001	45	5	29,000
HFC	Feb 2000-May 2000	45	5	3,400
HFS	Feb 2000-May 2000	45	5	3,400

3.2.2.2

3.2.2.3 Findings

3.2.2.4 Strain Gauges

Figure 50 shows a typical response signal for a longitudinal ASG with dual wheel loading (Garg and Hayhoe 2001). Longitudinal ASG response signal time histories were similar in shape even if the tire did not pass directly over the gauge. There was always negative strain first, then positive strain, and subsequently negative strain. After the axle had passed over the gauge, the strain level reduced rapidly with very little residual strain. In the case of 4- and 6-wheel loading, negative strain was always observed between axles. The longitudinal ASG response to 6-wheel loading is shown in Figure 51.

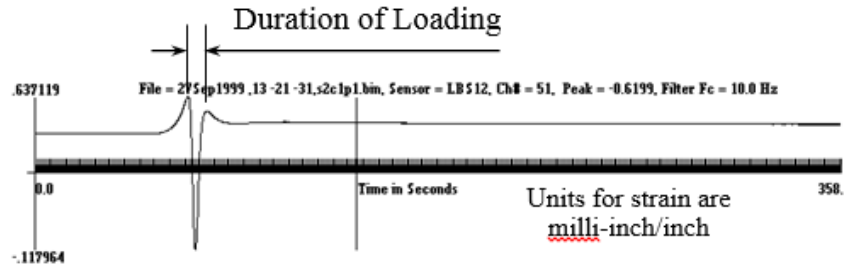


Figure 50. Longitudinal ASG Response Signal (Dual Loading) (Garg and Hayhoe 2001)

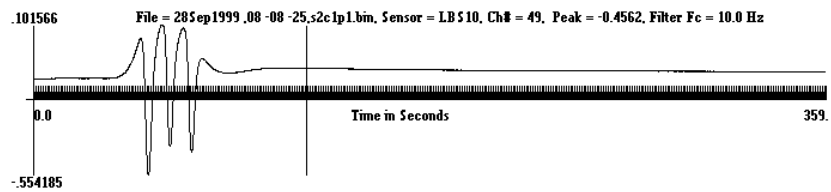


Figure 51. Longitudinal ASG Response Signal (6-Wheel Loading) (Garg and Hayhoe 2001)

Figure 52 shows a typical response signal from a transverse ASG subjected to a dual-wheel load (Garg and Hayhoe 2001). Figure 53 shows the response of a transverse ASG to a 6-wheel loading configuration. In contrast to the responses of the longitudinal gauges, the shape of the transverse gauge response was very sensitive to the lateral position of the gear. The transverse strain gauges did not show negative strain before or after the peak. Positive strain readings gradually diminished to an asymptotic value as the load moved away from the gauge. The difference between the asymptotic strain reading (offset right) and the starting value (offset left) represents the residual strain for that event. In general, multiple axle loads resulted in higher residual transverse strain than single axle loads. The presented plots are from the response testing data, but also present the general shape of responses from the traffic load phase.

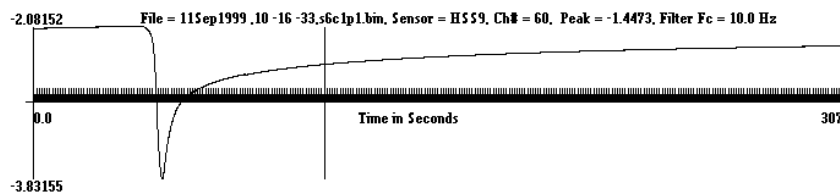


Figure 52. Transverse ASG Response Signal (Single Axle Load Gear) (Garg and Hayhoe 2001)

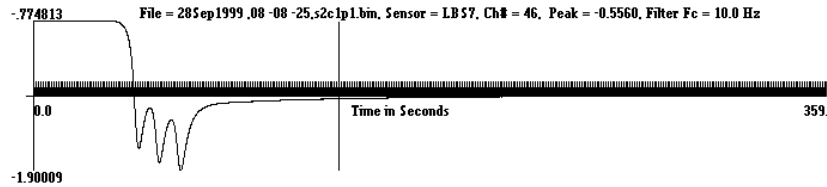


Figure 53. Transverse ASG Response Signal (6-wheel) (Garg and Hayhoe 2001)

3.2.2.5 MDDs

The average vertical strains in the subgrade were estimated by measuring the simultaneous deflections with the MDDs at two levels in the subgrade, taking the difference between them and dividing by the vertical distance between the sensors. The relationship between recovered and unrecovered strains at different positions in the wander cycle was found by the time histories (Hayhoe and Garg 2002). Comparing the measured recovered and unrecovered deflections for both six- and four-wheel gears shows a large fraction of deflection is unrecovered deflection. Hayhoe and Garg (2002) showed that both recovered and unrecovered strains increased significantly as the pavement structure deteriorated. Recovered strains were strongly dependent on the path of previously applied loads. This led to the conclusion that the pavement response is strongly path dependent and that wander is an important component. Net unrecovered strain over a complete wander cycle was very small both in absolute terms and relative to the unrecovered strains at individual wander positions.

3.2.2.6 Heavy Weight Deflectometer (HWD) Test

HWD tests were conducted on all flexible test items to monitor the pavement structural degradation with traffic and time. These tests were performed on the non-trafficked centerline (C/L), 6-wheel traffic lane (north), and 4-wheel traffic lane (south) at 10 ft. (3.05 m) offsets, as illustrated in Figure 54. Deflection basins were characterized by measuring deflections at the center of the load plate (D0) and at 12, 24, 36, 48, and 60 inch offsets (D1, D2, D3, D4, and D5).

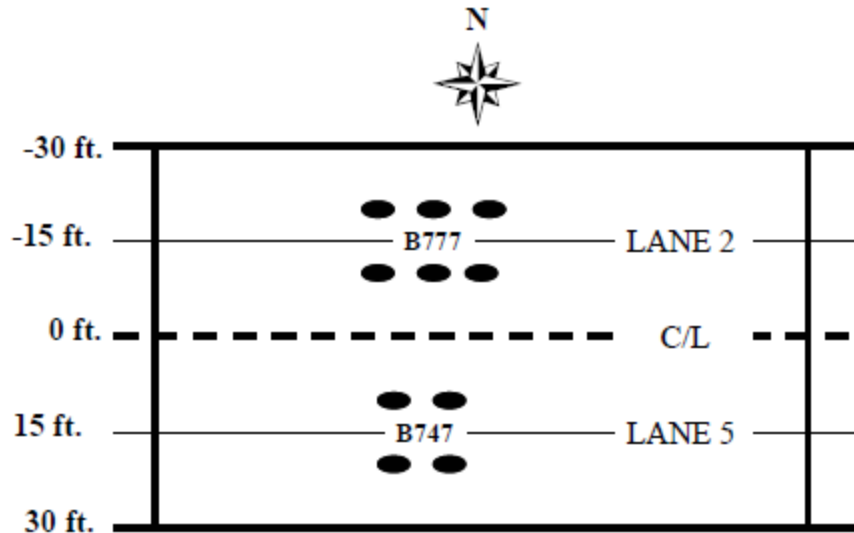


Figure 54. Location of HWD Test Lanes Results

Garg and Marsey (2004) evaluated the effect of traffic on pavement structure comparing the HWD deflection data for trafficked and non-trafficked (center lane) areas. They attributed any difference in HWD response between the non-trafficked and the traffic lane to the effects of traffic on the pavement structure (assuming that temperature effects on the stiffness of HMA layer was the same on the center lane and the traffic lanes). The following were found based on their study:

- For test item MFS, the non-dimensional ratio of D0 in the traffic lane to the corresponding D0 in the non-trafficked area for north-west locations of the test item increased significantly compared to the other test locations, suggesting premature failure in the 6-wheel traffic lane. As the ratio approached a value of 2, significant rutting and upheaval were also observed. The rest of the test item did not show any signs of failure. Traffic tests in the 6-wheel traffic path were terminated after 19,900 passes; however, the HWD tests were stopped after 12,814 passes because of severe rutting in the pavement structure that prevented the operation of HWD equipment.
- For test item LFS, the D0 Ratio increased slightly to approximately 1.2 after 20,000 passes. No significant amounts of rutting or failure signs were visible. When the load level for test items LFS and LFC was increased to 65,000 lbs. (29.4 tonnes) and the speed changed to 2.5 mph (4 km/h), the D0 ratio started increasing but did not reach levels similar to the MFS or MFC. The maximum value of D0 ratio observed for test item LFC was 1.65 and 1.5 for LFS.
- The ratio of D0 associated with the seating drop at 160 kN load (drop 4) for the traffic lane versus the non-trafficked area was also related to the pavement condition. This ratio reduced significantly for the two traffic lanes compared to the center lane as the pavement structure progressed towards failure.

In another study, Garg and Marsey (2002) compared the D0 and D5 values between the six flexible test items. Figure 55 and Figure 56 show the D0 and D5 values at different load levels for the six flexible test items, respectively. The following were observed from the figures:

- Deflections varied linearly with load.
- D0 values for test item HFC were smaller than those for test items LFC and MFC.

- Test items with asphalt stabilized base showed lower D0 values compared to the test items with crushed stone base.
- In low and medium strength subgrade test items, test items on crushed stone base exhibited higher D5 than test items on asphalt stabilized base. For test items HFS and HFC, deflection values were approximately the same.

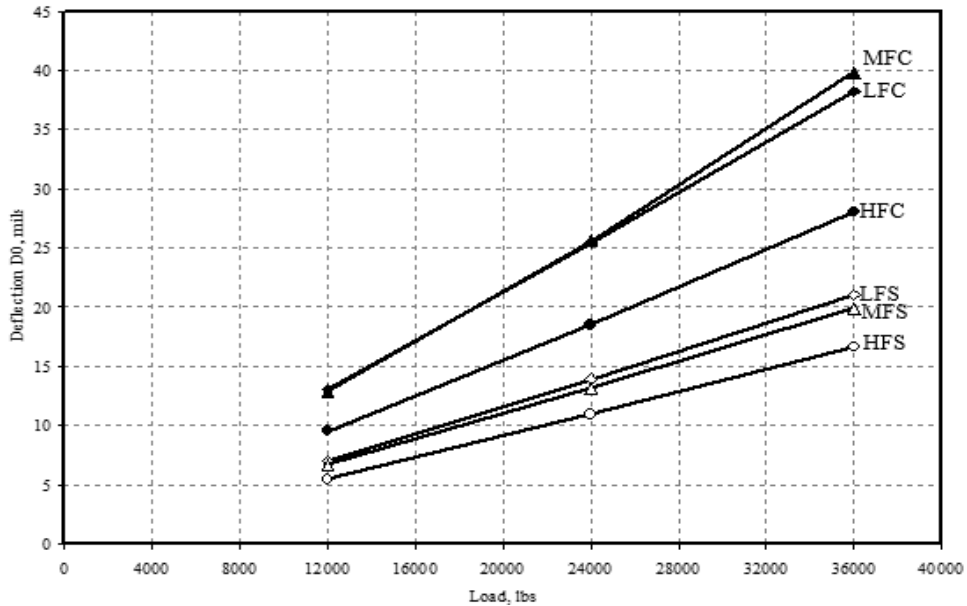


Figure 55. Comparison of Average Deflections D0 for Flexible Test Items (Garg and Marsey 2002)

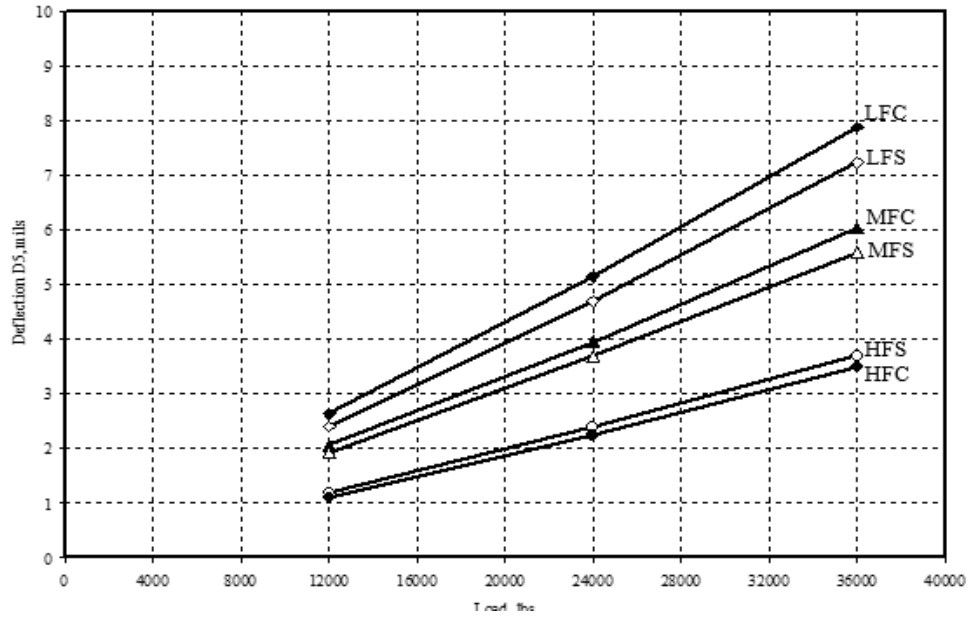


Figure 56. Comparison of Average Deflections D5 for Flexible Test Items (Garg and Marsey 2002)

3.2.2.7 Rut Depth Evaluation

3.2.2.8 Testing Method and Equipment

The progress of rut depth accumulation during trafficking was monitored using TSP measuring equipment and a physical straightedge. The MDD sensors embedded within the test pavements also were used to monitor the permanent deformations.

3.2.2.9 Data Collection

TSP measurements were made with a manually propelled inertial profiling device (CSC Profilair Profilite 300). Measurements were made at two longitudinal lines at the one-third points along the test items about 6 inches to the west of the MDDs perpendicular to the traffic direction (Figure 57). Profile elevations were recorded every 9.84 inches (250 mm) with an estimated speed of 1.2 mph (2 km/h) along the transverse lines.

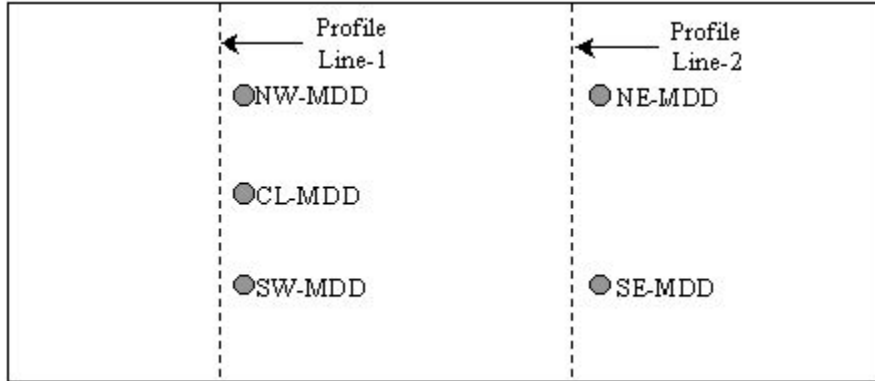


Figure 57. Profile Line Locations

The rut depth was measured initially with a 12 ft. (3.6 m) and later with a 16 ft. (4.9 m) long straightedge concurrent with TSP measurements. The straightedge was transverse to the traffic wheel path and placed on the center of wheel path (Figure 58). The recorded rut depth was the maximum deviation of the pavement surface from the straightedge. The traffic wheel path had the same width as the straightedge, therefore measurements indicated the permanent deformation inside the wheel path. To exclude the rut depth accumulated during the slow rolling tests, the final rut depth before the start of regular traffic testing was subtracted from the subsequent measurements.



Figure 58. Straightedge Used for Rut Depth Measurements in CC1

3.2.2.10 Findings

Figure 59 and Figure 60 plot rut depths from TSP measurements against passes for profile lines 1 and 2, respectively. The vertical dashed line at 20,000 passes indicates where the wheel load increased from 45,000 lbs. (20.4 tonnes) to 65,000 lbs. (29.4 tonnes). Rutting rates in test items with conventional base were higher compared to test items with stabilized base. The TSP rut depths are shown in Table 16. The rut depths under 4-wheel loads were higher than those from the corresponding 6-wheel loads. For both LFC and LFS test items, the rate of rut depth accumulation before 20,000 passes was very low, but increased significantly after the wheel load was increased to 65,000 lbs. (29.4 tonnes).

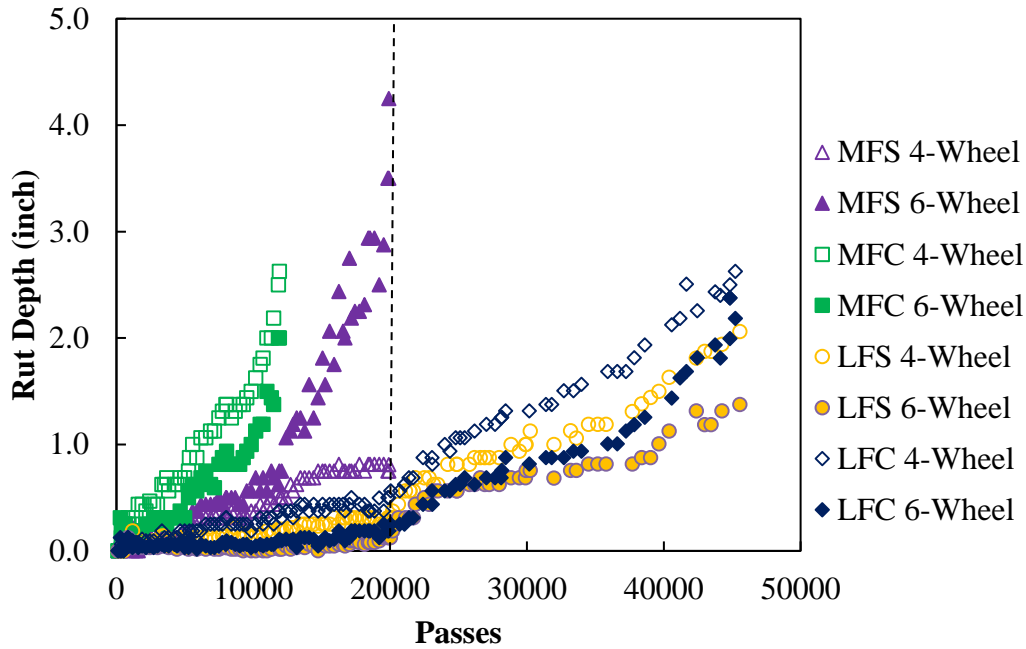


Figure 59. TSP Rut Depth vs. N for Profile Line 1

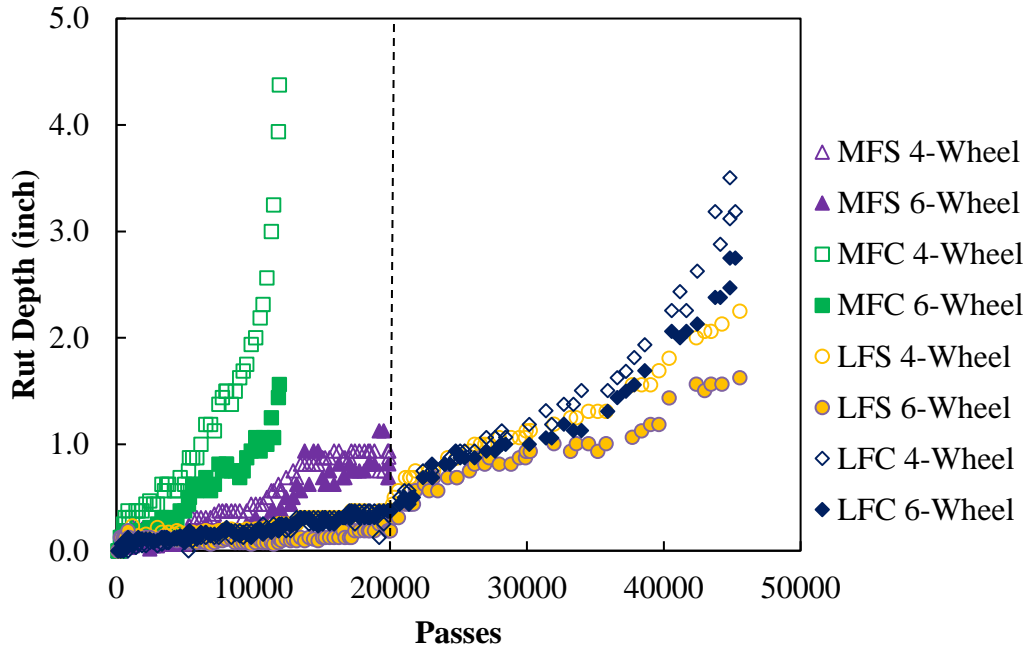


Figure 60. TSP Rut Depth Measurements

Table 16. TSP Rut Depth Measurements

Test Item	45 kips load			65 kips load		
	Accumulated Passes	RD 4-wheel (inch)	RD 6-wheel (inch)	Accumulated Passes	RD 4-wheel (inch)	RD 6-wheel (inch)
LFC	20,000	0.5	0.3	45,000	2.5	2
LFS	20,000	0.4	0.3	45,000	2	1.5
MFC	12,000	1.6-2	3-4.5	-	-	-
MFS	29,000	1-4.5	1	-	-	-

Figure 61 shows the cumulative rut depths from physical straightedge measurements for low-strength subgrade test items. Rut depth increased gradually while the wheel loads were 45,000 lbs. (20.4 tonnes), remaining less than 0.5 inch up to 20,000 passes. Rutting increased after the wheel load was increased to 65,000 lbs. (29.4 tonnes).

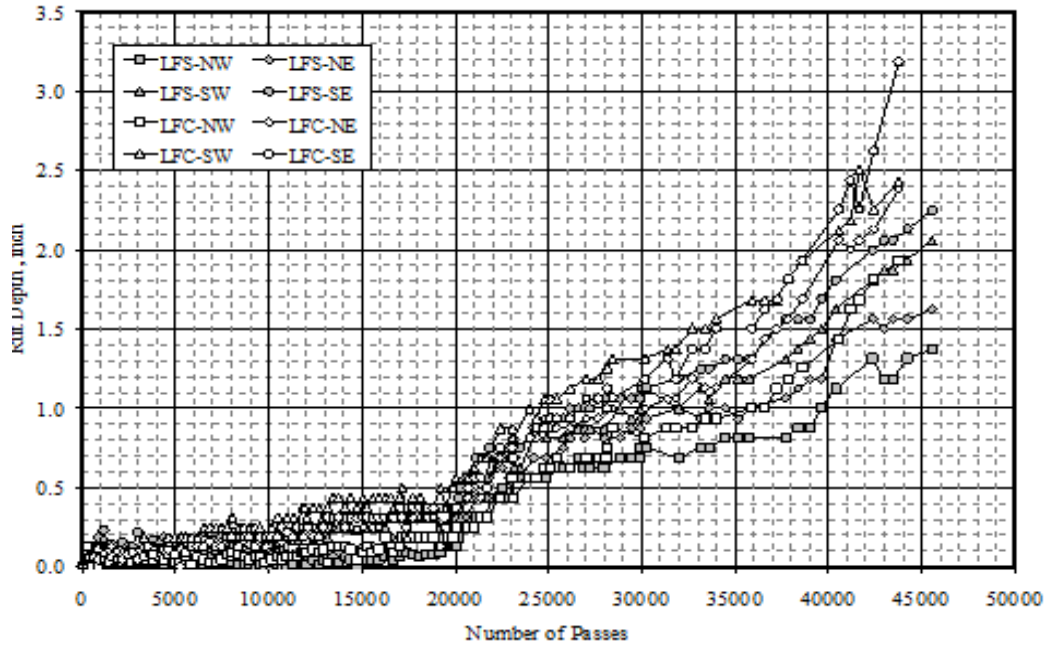


Figure 61. Straight Edge Rut Depth Measurements for Low Strength Subgrade Test Items (Hayhoe and Garg 2004)

Figure 62 shows cumulative rut depths obtained from physical straightedge measurements for medium strength subgrade test items. Test item MFC failed at approximately 12,000 passes with rut depths ranging from 2 to 4.5 inches. Test item MFS, localized failure was observed on the north traffic lane (6-wheel). The traffic tests were discontinued on the north, but continued on the south. The south lane failed after approximately 29,000 passes and exhibited severe rutting. The rutting rate was stable until about 10,000 passes but increased rapidly as test items MFS and MFC approached failure.

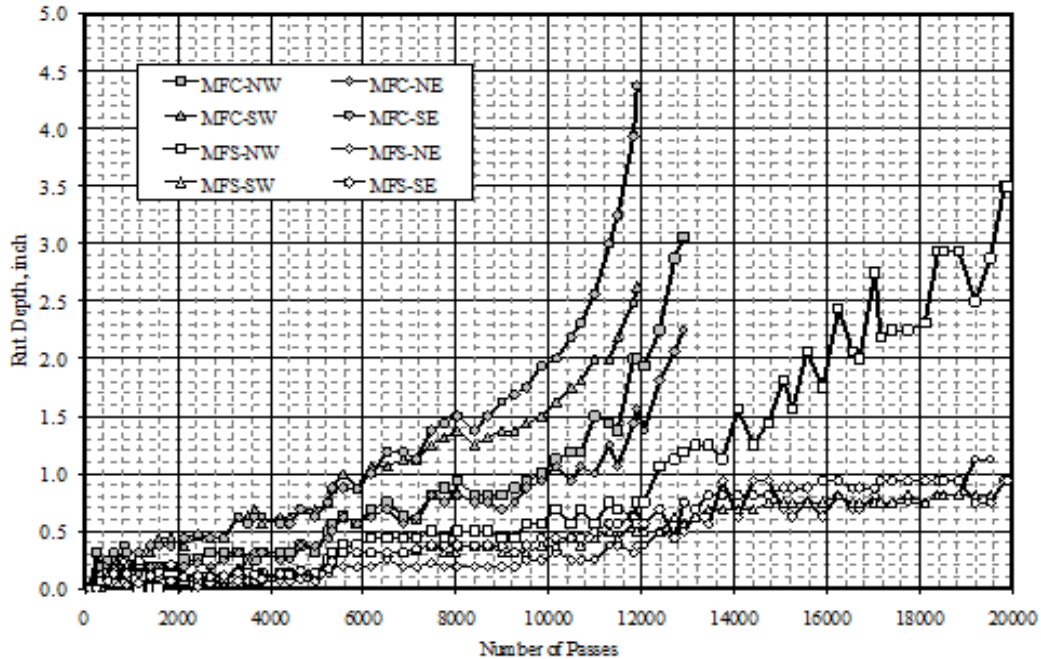


Figure 62. Straight Edge Rut Depth Measurements for Medium Strength Subgrade Test Items (Hayhoe and Garg 2004)

Where possible, the relative contribution of each structural layer to the total permanent (unrecovered) deformation was estimated using MDD data. The contributions of asphalt (P-401), aggregated subbase (P-154) and subgrade to the total permanent deformation are plotted against traffic passes for test item LFC-S (Figure 63), LFS-North (Figure 64), MFC North and South (Figure 65 and Figure 66), and MFS North and South (Figure 67 and Figure 68).

3.2.2.11 Low Strength Subgrade

The accumulation of permanent deformations measured with MDD under the 4-wheel loading are shown in Figure 63 for the LFC test item. The subbase P-154 layer contributed the most to the pavement deformation up to 20,000 passes. After 20,000 passes, when the wheel loads increased from 45 kips (20.4 tonnes) to 65 kips (29.4 tonnes), the rutting rate increased significantly and the subgrade started to contribute more to the total pavement deformation.

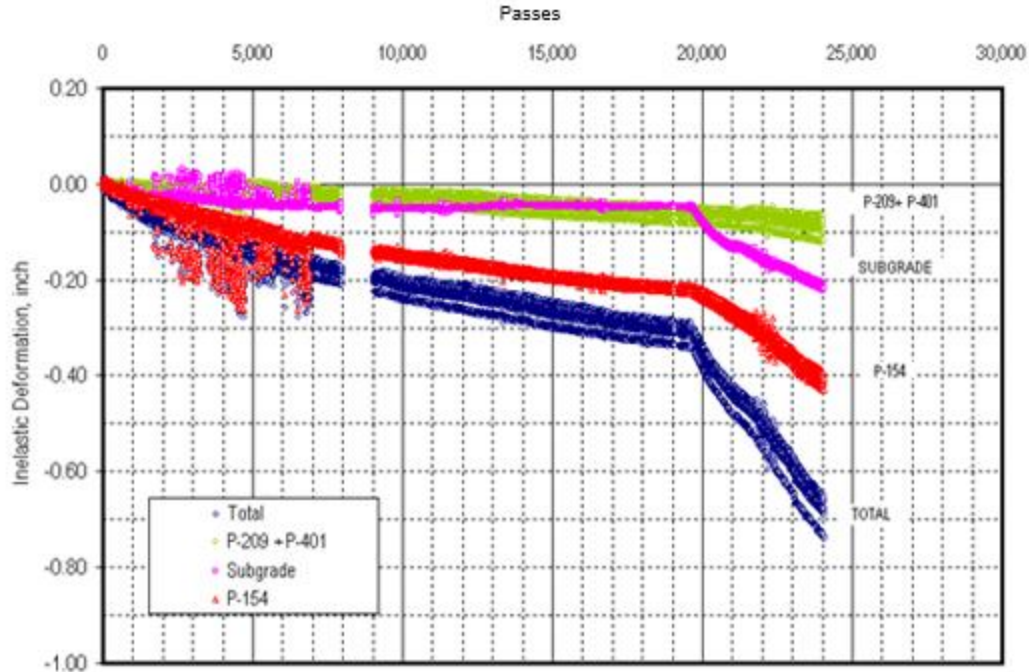


Figure 63. Permanent Deformation from MDD for Test Item LFC under 4-Wheel Loading (Hayhoe and Garg 2004)

Figure 64 shows the accumulation of permanent deformations from MDD data under 6-wheel loading for the LFS test item. As long as the wheel loads remained at 45 kips (up to 20,000 passes), the rutting of the P-209 base layer dominated the total deformation. As with the LFC test item, when the load was increased from 45 to 65 kips, there was a qualitative change, and the subgrade layer contribution became more significant. As shown in Figure 64, at failure the relative contributions of the subgrade and P-209 base layers were approximately the same.

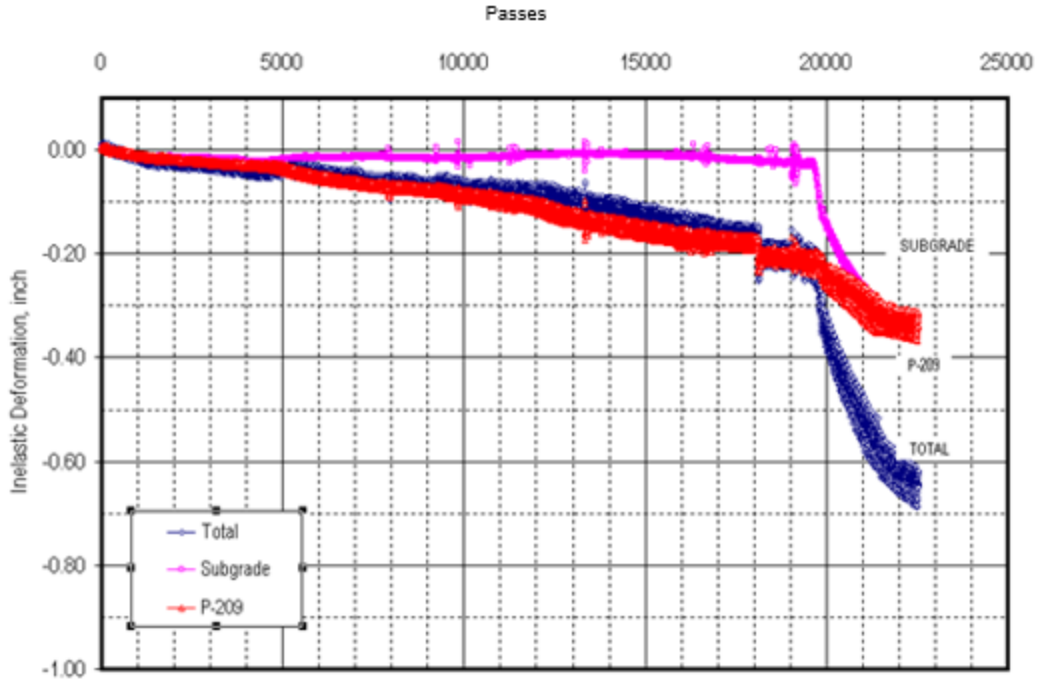


Figure 64. Permanent Deformation from MDD for Test Item LFS under 6-Wheel Loading (Hayhoe and Garg 2004)

3.2.2.12 Medium Strength Subgrade

The permanent deformation measurements from MDDs for the MFC test item are shown in Figure 65 and Figure 66 for the 6-wheel and 4-wheel loads respectively. Initially, the subgrade contributed the most to the permanent deformation under 6-wheel loading. At approximately 5,500 passes, subgrade deformation started to decrease. Hayhoe and Garg (2004) related this behavior to the transverse movement of the subgrade material as it undergoes shear flow when approaching failure.

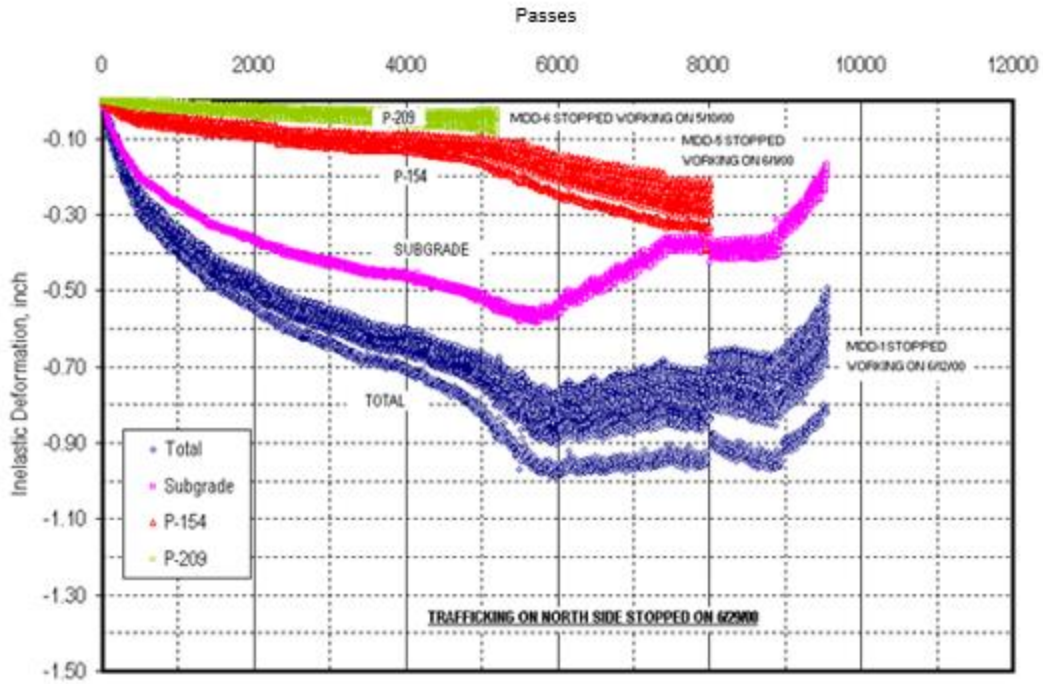


Figure 65. Permanent Deformation from MDD for Test Item MFC under 6-Wheel Loading (Hayhoe and Garg 2004)

Permanent deformation of the subgrade showed similar trends under 4-wheel loading, as shown in Figure 66. Subgrade deformation started to decrease at about 4,500 passes. The overall pavement deformation was mostly due to the deformation of the subbase layer.

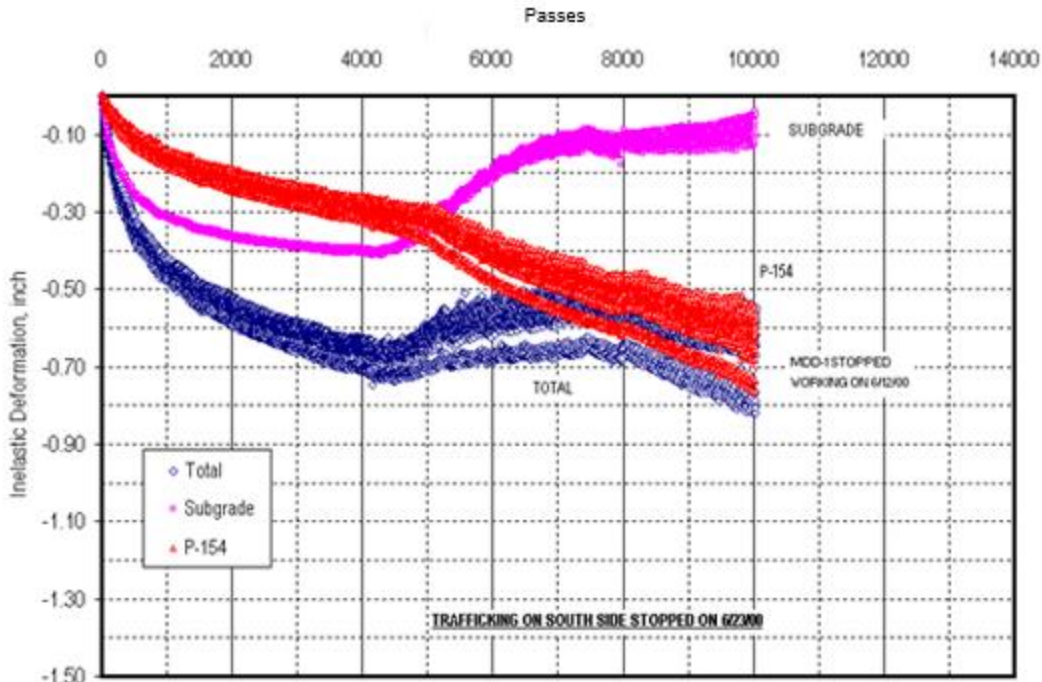


Figure 66. Permanent Deformation from MDD for Test Item MFC under 4-Wheel Landing Gear (Hayhoe and Garg 2004)

Hayhoe and Garg (2004) identified different stages in the failure of a flexible pavement including (1) initial shakedown period where rutting increases rapidly, (2) an extended period of consolidation where rutting approaches an asymptotic limit, (3) a period of increasing rate of deformation associated with the initiation of shear failure, and (4) a period of bulk transverse movement of the material in layers, undergoing shear flow until structural failure. The MDD results shown in Figure 65 and Figure 66 showed this characteristic stage from the apparent upward movement indicated and therefore verified the structural failure in test item MFC.

Figure 67 and Figure 68 show the permanent deformation measurements from MDDs for the test item MFS for the 6- and 4-wheel loading respectively. Hayhoe and Garg (2004) concluded that variations in the asphalt surface layer temperature during the testing impacted the permanent deformation behavior of the test item MFS. As shown in Figure 69, the average asphalt layer temperature was approximately 11°C up to 5,000 passes, and the surface layer deformation exhibited no sudden changes during this period. After 5,000 passes, the asphalt temperature (and consequently the rutting rate) started to increase. Another increase in asphalt temperature occurred at approximately 9,500 passes. This temperature increase was accompanied by another abrupt increase in the rutting rate. The same trends were observed for 4-wheel loading.

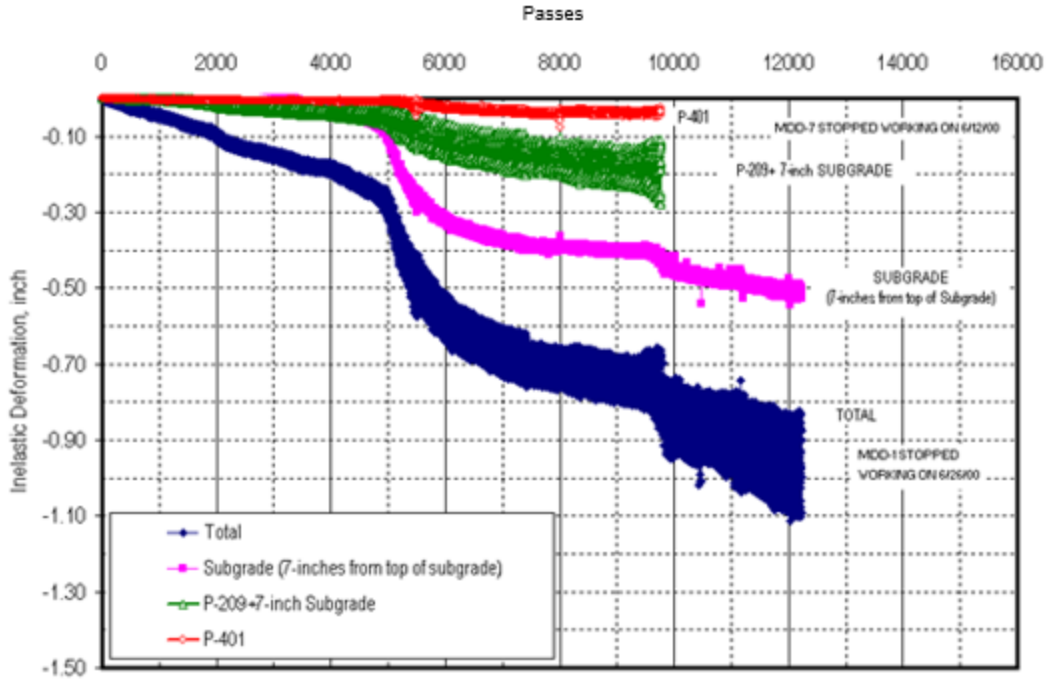


Figure 67. Permanent Deformation from Test Items MDD for MFS under 6-Wheel Loading (Hayhoe and Garg 2004)

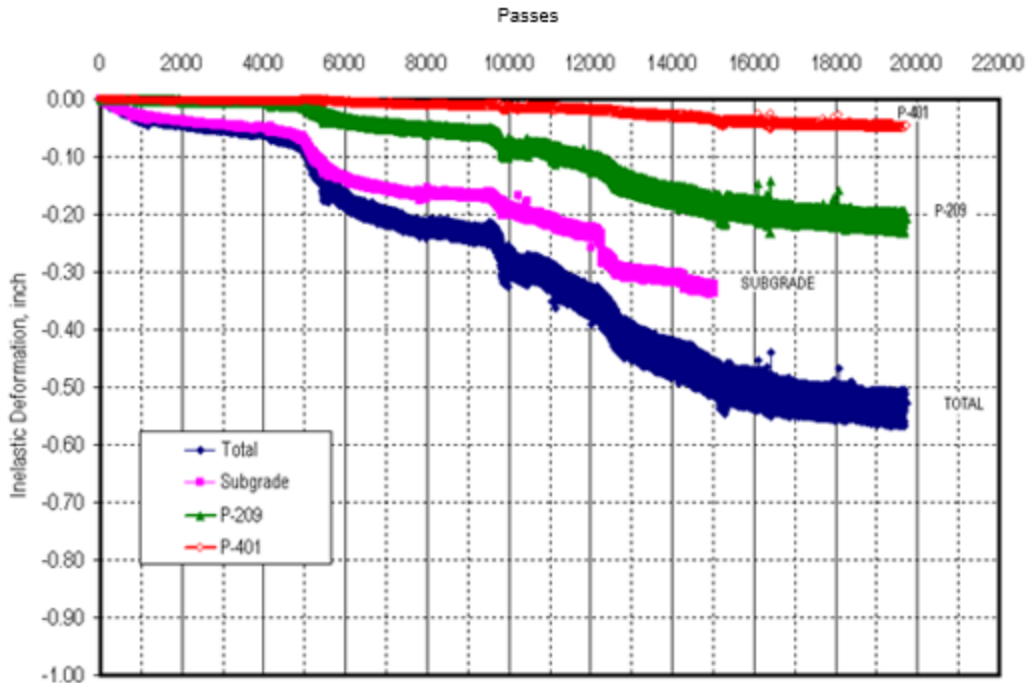


Figure 68. Permanent Deformation from MDD for Test Item MFS under 4-Wheel Loading (Hayhoe and Garg 2004)

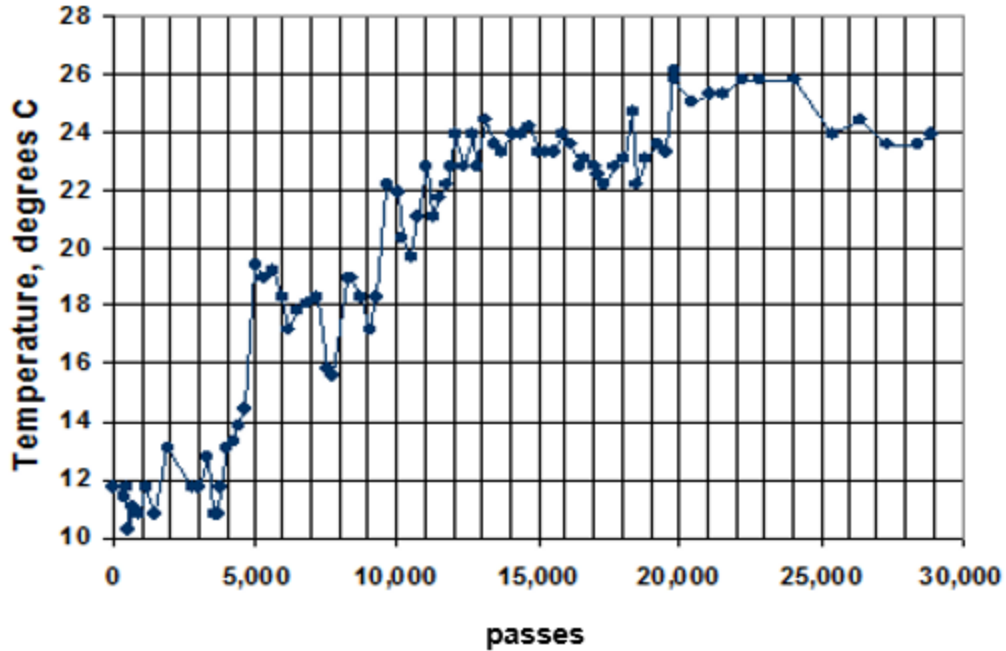


Figure 69. Average Temperature in the HMA Layer of Test Item MFS (Hayhoe and Garg 2004)

3.2.2.13 High Strength Subgrade

Testing was terminated at 5,000 passes in the test items with high strength subgrade. Figure 70 shows the permanent deformation of each layer of the HFC test item measured by MDD (Hayhoe and Garg 2004). As can be seen, the permanent deformation of the subgrade layer contributed the most to the overall permanent deformation of the section. The trend in permanent deformation tends to be asymptotic, indicating that the depth of deformation would not reach the 1-inch failure criteria. This further verifies the assumption that high strength subgrade test items were unlikely to fail. The pavement deformation after 3,400 passes was less than 0.2 inches (5 mm).

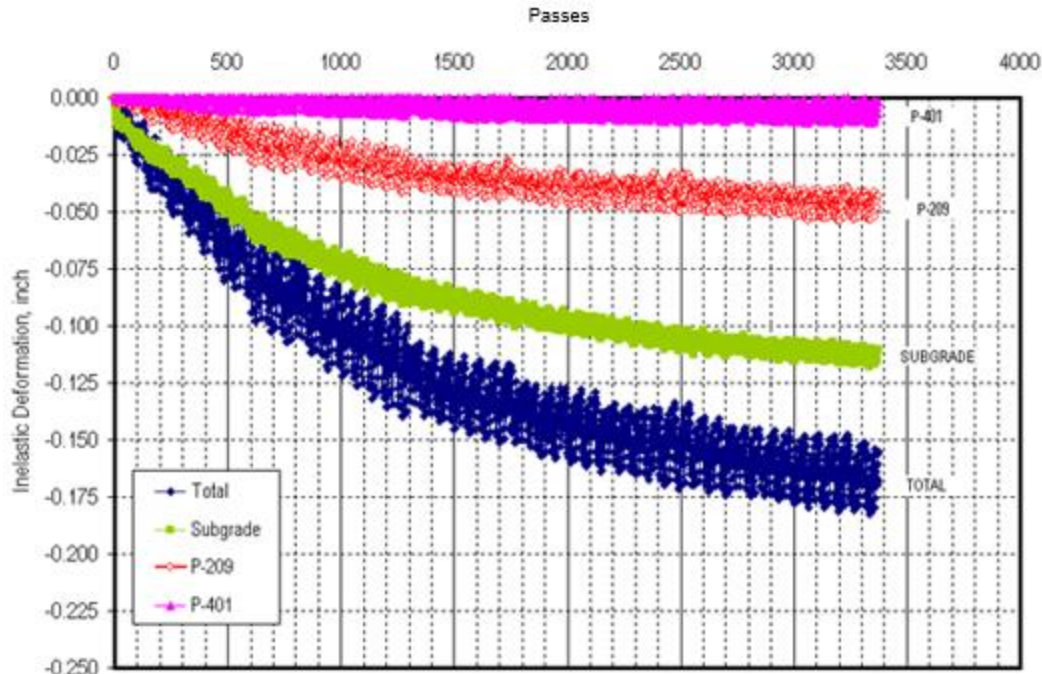


Figure 70. Permanent Deformation from MDD for HFC Test Item under 6-Wheel Loading (Hayhoe and Garg 2004)

3.2.3 Slow-Speed Traffic Tests

A series of additional traffic tests on high-strength subgrade test items were conducted in April 2000. The purpose of these additional tests was to gain data on the effect of vehicle speed on HMA layers. Tests were conducted at speeds of 0.25, 0.5, 0.75, 1.0, 2.0, 5.0, and 7.33 ft./sec (0.08, 0.15, 0.23, 0.3, 0.6, 1.5, and 2.2 m/sec) and wheel loads of 24,000, 30,000, and 36,000 lbs. (106.8, 133.5, and 160.2 kN) at each speed. To investigate the effects of vehicle speeds, peak HMA strains in test item HFS were measured at various speeds. Figure 71 and Figure 72 show the peak AC strains measured for test item HFS from longitudinal and transverse ASGs, respectively. The difference in gauge measurements could be due to the position of gauge with respect to the wheel. However as it can be seen from the figures, in all the gauges, higher speeds (lower load durations) result in lower strains. The rate at which measured strain reduces with speed, is higher at vehicle speeds lower than 2 feet/sec (0.6 m/sec).

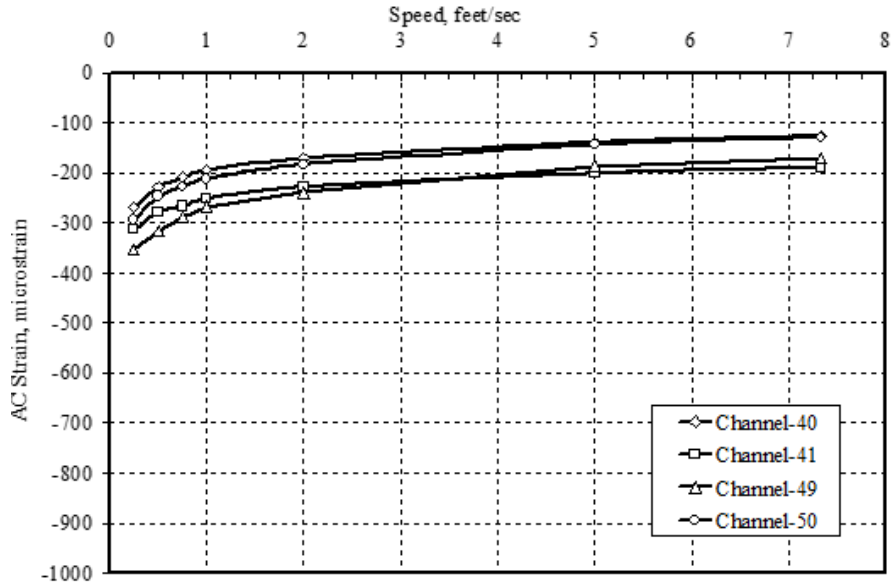


Figure 71. Peak AC Strains from Longitudinal ASGs for Test Item HFS (Test Date 4/20/00; Gauge Depth = 9.5 inches; Wheel Load = 36,000 lbs.) (Garg and Hayhoe 2001)

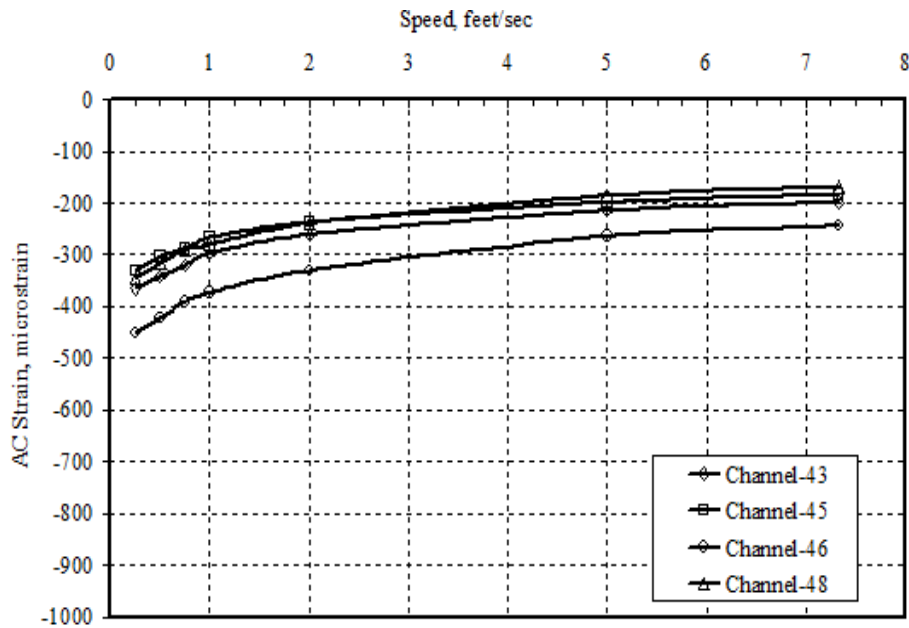


Figure 72. Peak AC Strains from Transverse ASGs for Test Item HFS (Test Date 4/20/00; Gauge Depth = 9.5 inches; Wheel Load = 36,000 lbs.) (Garg and Hayhoe 2001)

Figure 73 and Figure 74 show the relationship between time of loading and AC strains for three load levels of 24,000, 30,000, and 36,000 lbs. (106.8, 133.5, and 160.2 kN) for the longitudinal and transverse ASGs, respectively. Load durations range from 0.8 seconds (for a vehicle speed of 7.33 feet/sec (2.2 m/s)) to 18.6 seconds (for a vehicle speed of 0.25 feet/sec (0.08 m/s)).

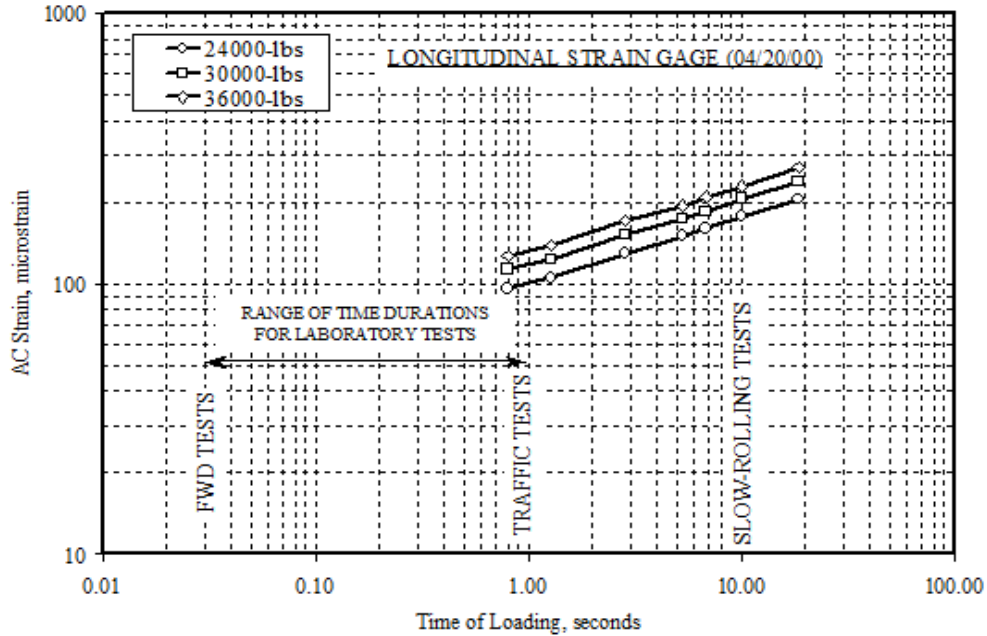


Figure 73. AC Strains – Time of Loading Relationship for Test Item HFS from Longitudinal ASGs (Test Date 4/20/00; Gauge Depth = 9.5 inches) (Garg and Hayhoe 2001)

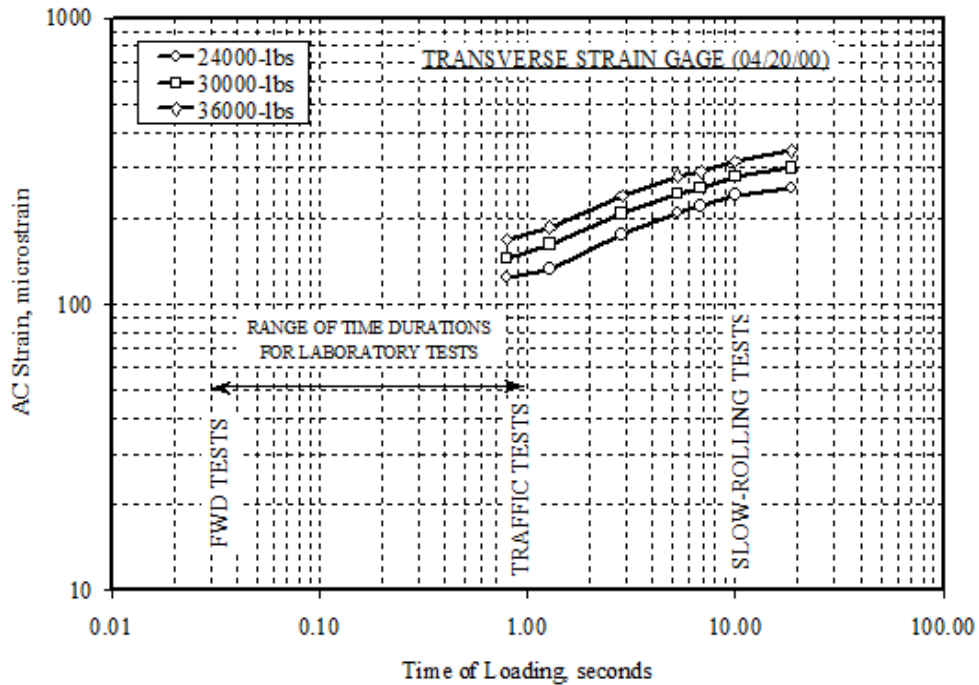


Figure 74. AC Strains – Time of Loading Relationship for Test Item HFS from Transverse ASGs (Test Date 4/20/00; Gauge Depth = 9.5 inches) (Garg and Hayhoe 2001)

3.2.3.1 Summary

The first series of traffic tests began in February 2000 and stopped after accumulating 28 passes on February 14, 2000. Trafficking restarted on March 30, 2000 and was completed in September 2001.

- MFC was the first test item to fail. Failure occurred after 12,000 passes. At failure, pavement surface was characterized by severe rutting between 2 and 6 inches.
- In MFS test item, localized failure was observed in the north side traffic path after 19,900 passes. The south side failed at 29,000 passes.
- The LFC and LFS showed few signs of structural failure after 20,000 passes. Therefore, the load level for LFS and LFC test items, was increased to 65,000 lbs. (29.4 tonnes) after 20,000 passes and the speed changed to 2.5 mph (4 km/h). In LFC and LFS test items, trafficking was stopped after 42,000 and 45,000 passes were completed, respectively.
- In HFC and HFS test items, tests were terminated after 3,400 passes due to a determination that these pavement sections were unlikely to fail.
- Both recovered and unrecovered strains increased significantly as the pavement structure deteriorated for test items on low and medium strength subgrade.
- The total accumulated permanent deformation in the pavement structure over a complete wander pattern was a small fraction of the total range of the unrecovered deformation occurring during a typical wander cycle.

HWD data collected during traffic testing was used to monitor the structural deformation of the flexible test items. Following summarizes the conclusions from the HWD data:

- The ratio of D0 in the traffic lane to the D0 in the non-trafficked area was used as an indicator of structural damage. This value increased with applied traffic passes, and generally tracked the observed structural failures.
- For test items MFC and MFS, the ratio approached a value of 2 and pavement structural failure was observed.
- For test items LFS and LFC that did not fail structurally during traffic tests, the ratio did not exceed 1.7.
- It was found that the ratio of the central deflection D0 for the fourth drop in the HWD sequence (drop-4), to the D0 value for the seating drop was also related to the observed pavement condition. This ratio decreased as the pavement structure progressed towards failure.

The progression of rut depth accumulation during trafficking was monitored using three methods: TSP measuring equipment, a physical straightedge, and analysis of MDD sensor data. Conclusions from the rut depth analysis were:

- In general, the maximum rut depth at failure was higher for conventional base flexible test items than for stabilized base flexible test items.

- The number of passes required to reach the 1-inch rut depth was similar for the 4-wheel and 6-wheel gears. In test item LFC, initially the subbase layer contributed the most to the pavement deformation. In test item LFS, however, the P-209 base layer contributed the most to the pavement deformation in initial passes. In both test items, subgrade started to contribute more to the total pavement deformation after the load was increased from 45 to 65 kips per wheel.
- For test item MFC, figure 65 and figure 66 show that in both 6-wheel and 4-wheel loading, the permanent deformation was dominated by the subgrade contribution up to about 5000 passes. Then there was a qualitative change, where the subgrade deformation trend reversed, while the P-154 subbase contribution continued to increase.
- For MFS test item, Figure 67 and Figure 68 show that all the layers contributed to rutting and the overall rutting level was very temperature dependent. It stands out to reason that these test items which had a greater depth of asphalt (temperature-dependent material) should be more sensitive to changes in temperature.
- In test item HFC, subgrade contributed the most to the overall rutting, but overall levels of rutting were very small.

Additional traffic testing was performed on HFS test item to investigate the effect of vehicle speed on HMA layers. The measured strains were found to vary strongly with test speed. Higher vehicle speeds (longer duration of loading) resulted in reduced asphalt stiffness and higher measured strain values.

4. POST-TRAFFIC TESTING

The purpose of post-traffic tests was to document the failure mechanism and to assign post-failure properties to each pavement layer. This was done by exposing test pits and trenches at various locations. Where trenches were exposed, they extended the full width of the test item from north to south. Test pits covered a smaller area of approximately 4 ft. by 4 ft. Characterization tests conducted at the top of each exposed layer typically included CBR, dynamic cone penetration (DCP), and in-situ density. Samples were removed to perform lab characterization tests including resilient modulus and moisture content. Table 17 presents a summary of post-traffic tests performed on each test item. The ‘E’ designation in the table denotes a trench excavated at the eastern MDD location of the test item while the ‘W’ designation denotes a trench excavated at the western MDD location.

The post-traffic testing data for flexible test items are provided in Appendix D. This chapter includes only the post-traffic testing on flexible test items. The post-traffic tests on the rigid pavement test items were performed as part of Construction Cycle 2 (CC2) and therefore are not included in this report.

Table 17. Summary of Tests Performed

Trench ID	Material	Test	No. of Samples
LFS-W	P-209	Sand Cone	2
	Subgrade	DCP	0
	Subgrade	CBR	27

LFS-E	P-209	Sand Cone	4
	Subgrade	DCP	0
	Subgrade	CBR	123
	Subgrade	Drive Cylinder	31
LFC-E	P-209	Sand Cone	5
	P-154	Sand Cone	5
	P-154	CBR	5
	P-154	DCP	3
	Subgrade	DCP	11
	Subgrade	CBR	120
	Subgrade	Drive Cylinder	31
MFC-W	P-209	Sand Cone	5
	P-154	Sand Cone	5
	P-154	CBR	5
	P-154	DCP	5
	Subgrade	DCP	16
	Subgrade	CBR	105
	Subgrade	Drive Cylinder	30
MFS-W	P-209	Sand Cone	5
	Subgrade	DCP	13
	Subgrade	CBR	102
	Subgrade	Drive Cylinder	33
MFS-E	P-209	Sand Cone	5
	Subgrade	DCP	17
	Subgrade	CBR	132
	Subgrade	Drive Cylinder	33
		Total No. of Tests	878

4.1 Trenching

4.1.1 Data Collections

After completion of the traffic testing, 7 trenches were dug in the flexible test items at the locations of the rut depth measurements to study the failure mechanism of each pavement component layer. Each trench was aligned with either the east or west MDD sensors in each test item and was designated with either 'E' or 'W' to denote this. Trenching involved removal of the asphalt pavement, base, and subbase layers to reveal the subgrade interface and subsequent layers below. The final trench dimensions were 60 ft. (18.3 m) long across the width of the test pavement, 4 ft. (1.22 m) wide, and 4 ft. (1.22 m) deep. Table 18 lists the trenches and their station locations and Figure 75 shows their layout within the test section. Within each trench, 4 ft. by 4 ft. test pits were dug to conduct the characterization tests. Figure 76 shows the layout of the test pits within a trench.

Table 18. Post-Traffic Trench Identification and Location

Trench ID	Trench Number	Station
LFC-E	4	1+75
LFS-W	1	2+50
LFS-E	2	2+75
MFC-W	3	3+45
MFC-E	5	3+67
MFS-W	6	4+33
MFS-E	7	4+55

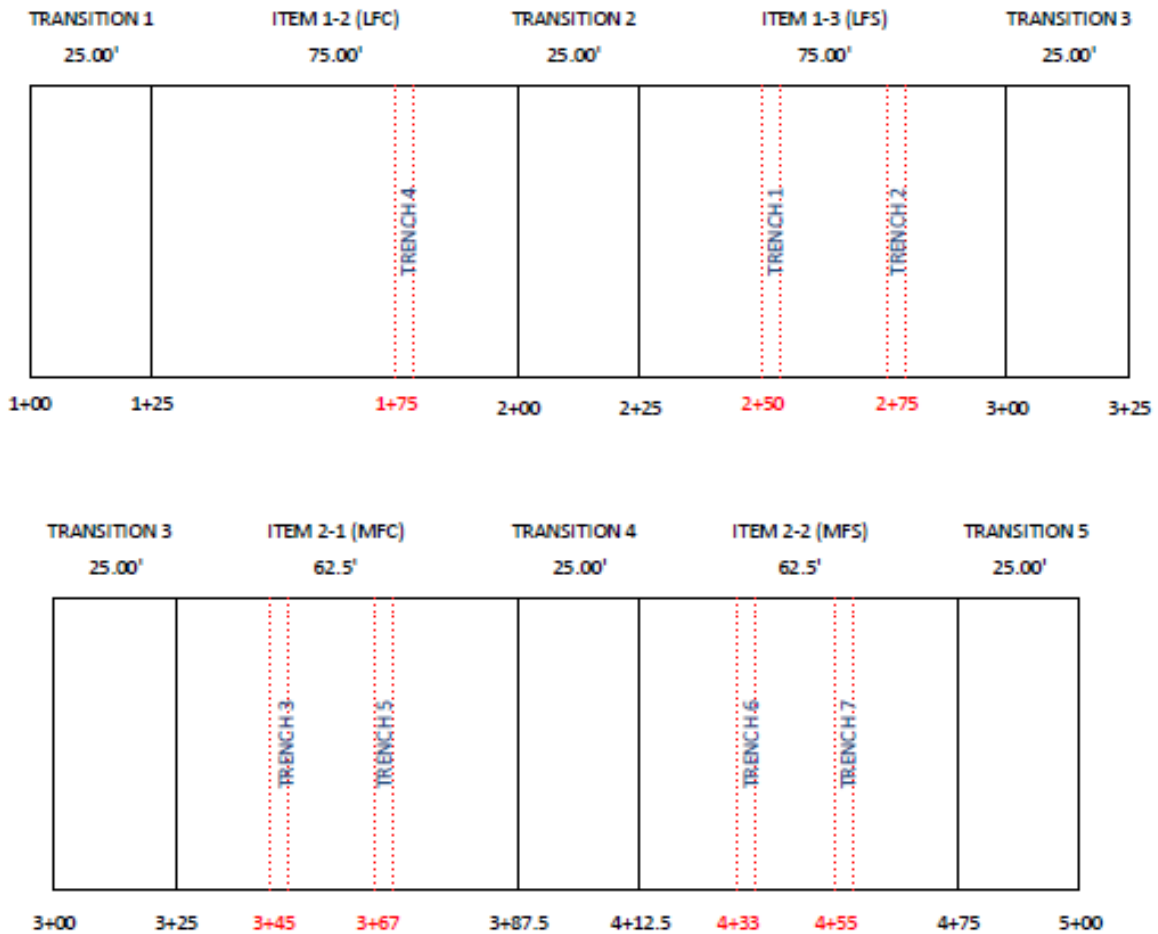


Figure 75. Post-Traffic Trench Locations

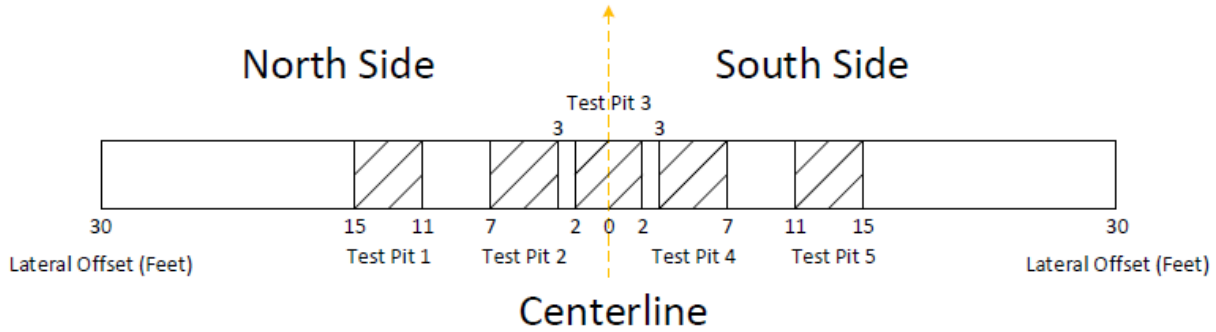


Figure 76. Post-Traffic Trench Test Pit Layout

Tests and measurements were performed on the various layers of the pavement structure. To measure the contribution of each component layer to the total pavement rutting and upheaval, pavement layer profile measurements were made. For layer profile measurements, a string line was run at the pavement surface from south to north along the west face of the trench. Figure 77 shows an example of profile measurement on a trench wall. The vertical distances between the string line and P-401 top (D1), P-401 bottom (D2), P-209/ P-401 base bottom (D3) (test items with conventional/stabilized base), and bottom of P-154/ P-209 (D4) (test items with conventional/stabilized base) at 1ft. (maximum) intervals were measured (figure 68). Within the two traffic lanes, measurements were made at maximum 6-inch intervals.

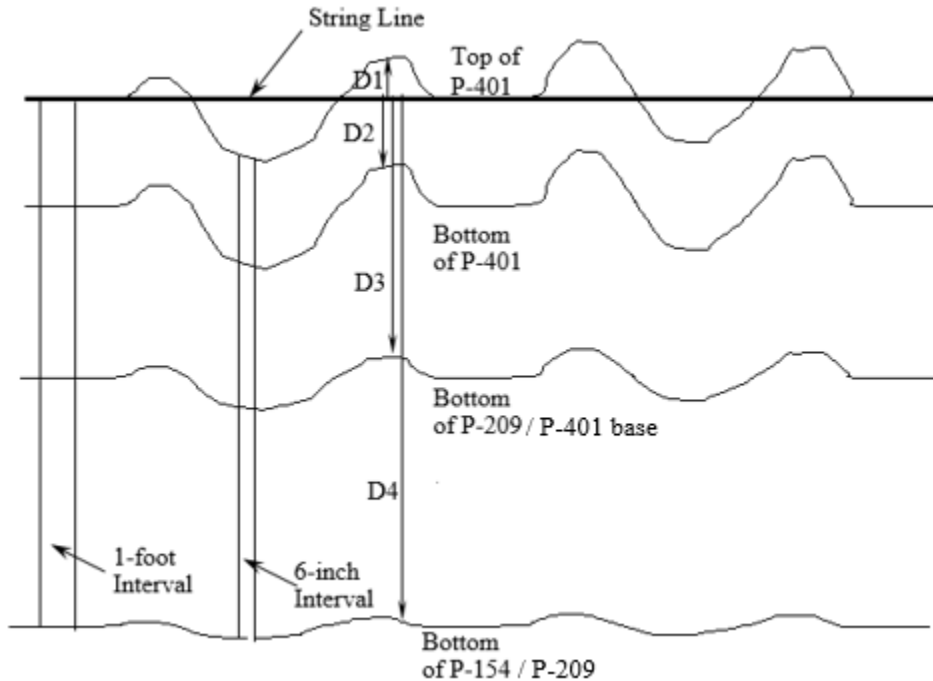


Figure 77. Profile Measurements on a Trench Wall

The CBR tests were performed at 2 ft. (0.6 m) intervals along the length of the trench with three penetrations for each CBR test as shown in figure 78. A minimum center-to-center spacing of 12 inches (305 mm) between the adjacent penetrations was used (U.S. Army Field Manual FM 5-430-00-2). Moisture samples were taken from the middle penetration of the CBR tests. Whenever a

significant difference between CBR values from adjacent penetrations was observed, the test was repeated. If the difference was still significant, an additional moisture sample was collected. In situ density was determined using the drive cylinder method (ASTM D 2937-94).

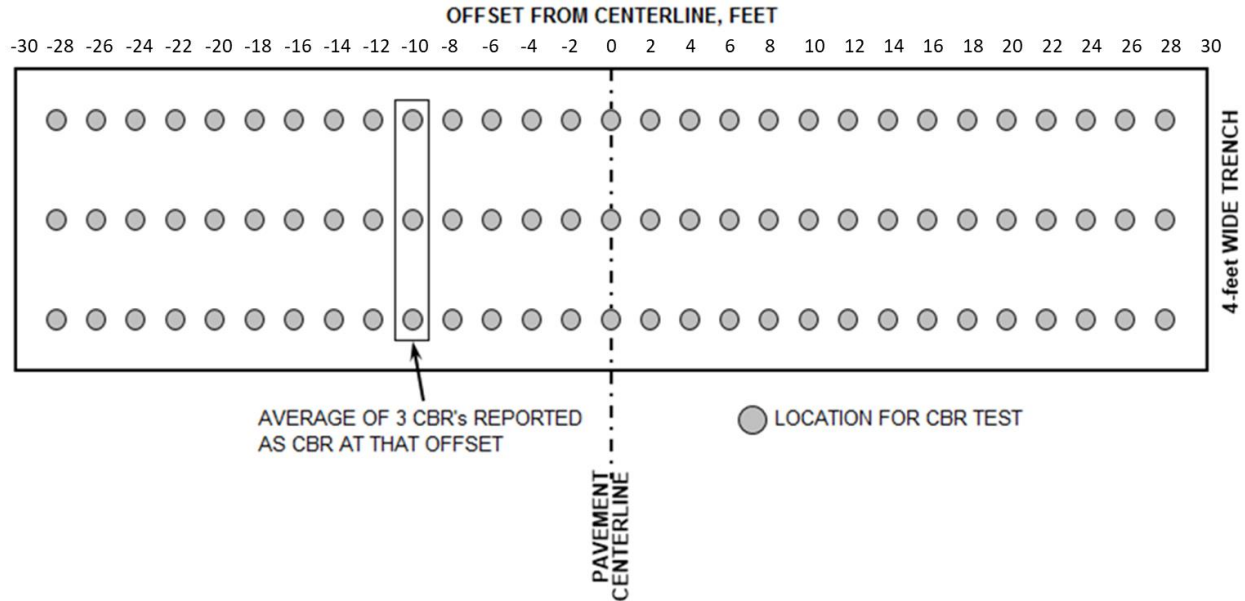


Figure 78. CBR Test Locations at the Subgrade Surface

4.1.2 Findings

4.1.2.1 LFC Test Item

As discussed before, during traffic testing the test items with low strength subgrade did not show any signs of failure at 20,000 passes and the wheel load was increased from 45 kip (20.4 tonnes) to 65 kip (29.4 tonnes). Trafficking was stopped in the LFC test item at approximately 22,000 passes with the final TSP rut depths of 3.2 inches (81 mm) in the 6-wheel traffic lane and 3.1 inches (79 mm) in the 4-wheel traffic lane. Following trafficking, Trench LFC-E was excavated at station 1+75. Figure 79 shows the LFC test item after trenching.



Figure 79. LFC Trench Section

The pavement layer profile measurements on the west and east faces of the LFC-E trench are shown in Figure 80 and Figure 81, respectively. The pavement layer profile thicknesses on the west and east faces of the LFC-E trench are shown in Figure 82 and Figure 83, respectively. LFC

experienced rutting in the P-401 AC layer within the traffic path, and shoving of the HMA layer, resulting in significant upheaval outside the traffic path.

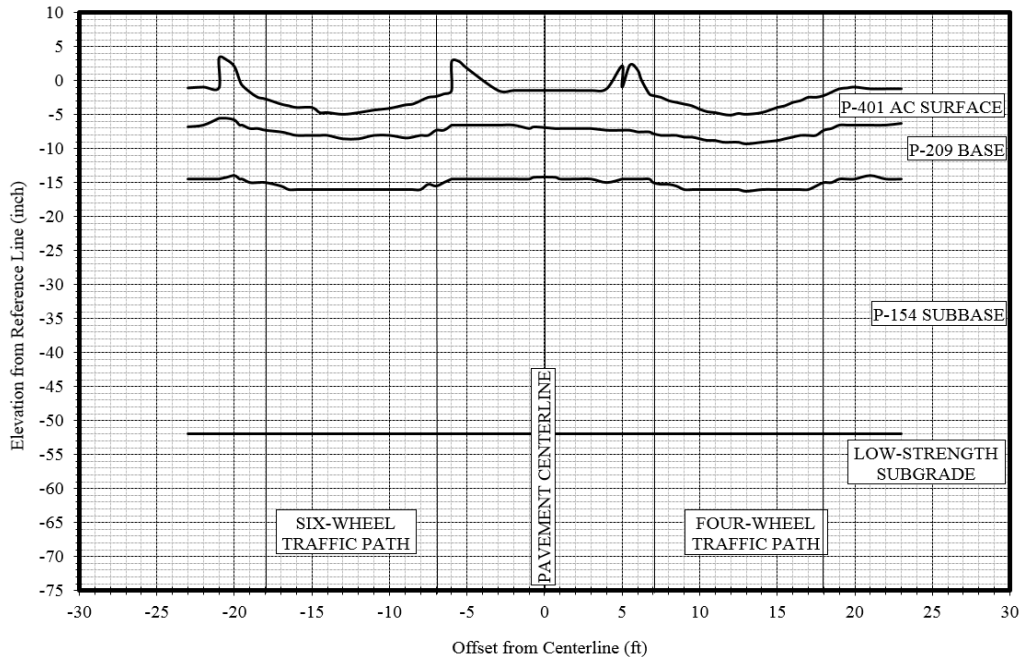


Figure 80. Trench Layer Interface Profiles, LFC-E (West Face of Trench)

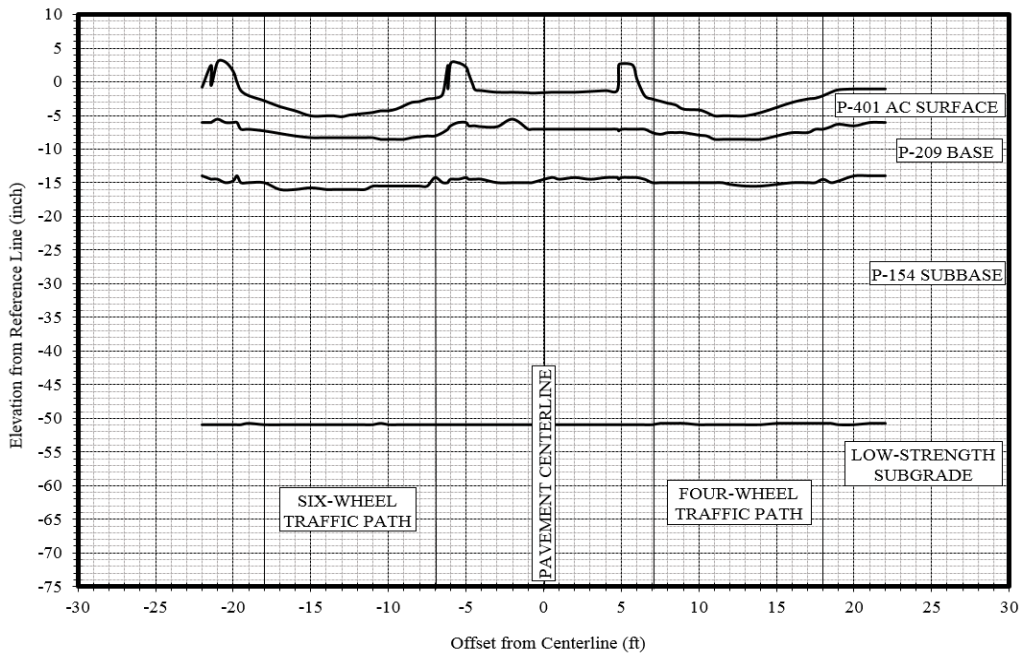


Figure 81. Trench Layer Interface Profiles, LFC-E (East Face of Trench)

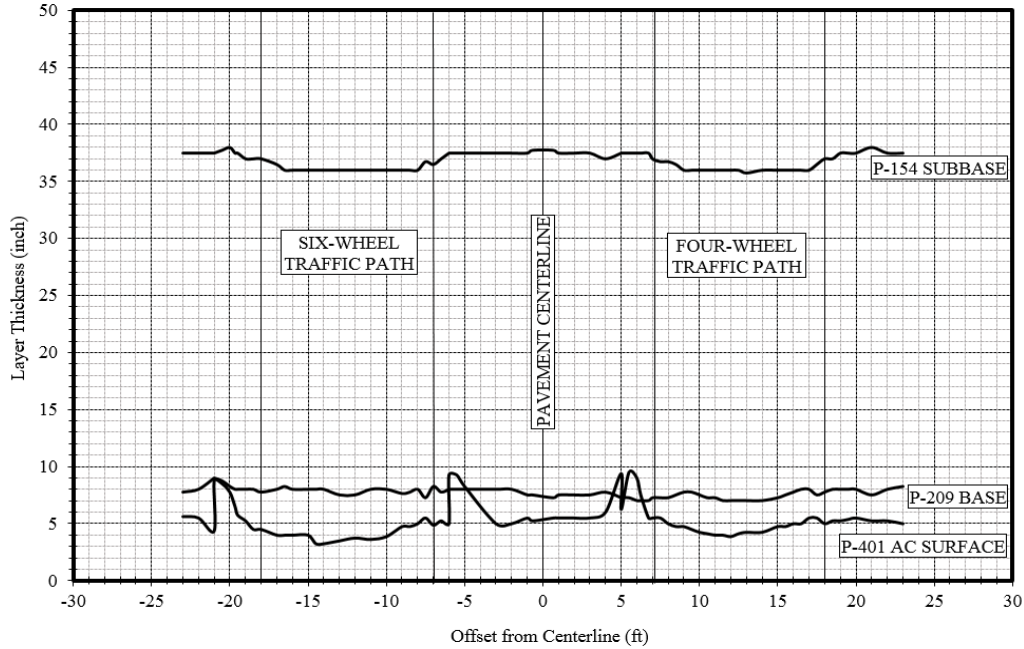


Figure 82. Trench Layer Thicknesses, LFC-E (West Face of Trench)

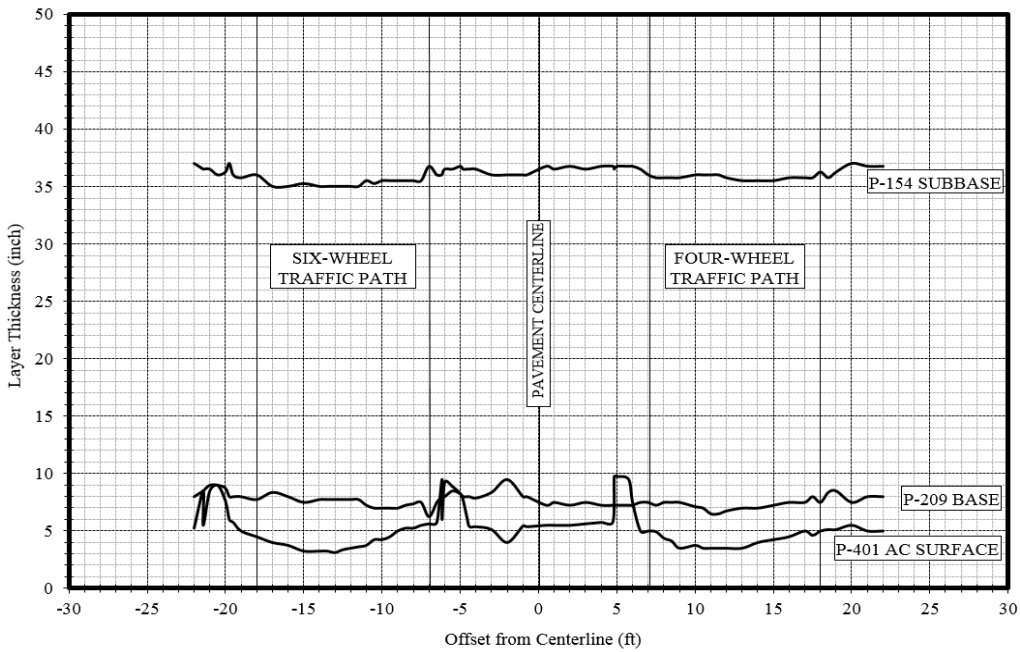


Figure 83. Trench Layer Thicknesses, LFC-E (East Face of Trench)

4.1.2.2 Test Item LFS

In the LFS item, traffic was stopped after 45,000 passes. At that point, the rut depth was 2.4 inches (61 mm) in the 6-wheel traffic path and 2.7 inches (69 mm) in the 4-wheel traffic path. The LFS test item did not meet the 1 inch (25.4 mm) surface upheaval failure criteria at the end of traffic

testing, thus it was not considered failed. Following trafficking, Trenches LFS-W and LFS-E were excavated at stations 2+50 and 2+75, respectively. Figure 84 shows LFS-E north and south of the centerline.



(a) North (6-Wheel) Side Looking West



(b) South (4-Wheel) Side Looking West
Figure 84. LFS-E Trench Views

Figure 85 and Figure 86 show pavement layer profiles for the west and east faces of the LFS-E trench. Layer profile thicknesses for the west and east faces of the LFS-E trench are shown in Figure 87 and Figure 88, respectively. Some rutting was observed in the P-401 AC and P-209 base layers in both traffic paths; however, as mentioned before, LFS failed at surface layer by the formation of cracks. In addition, shoving occurred in the P-401 AC layer resulting in upheaval outside the traffic path.

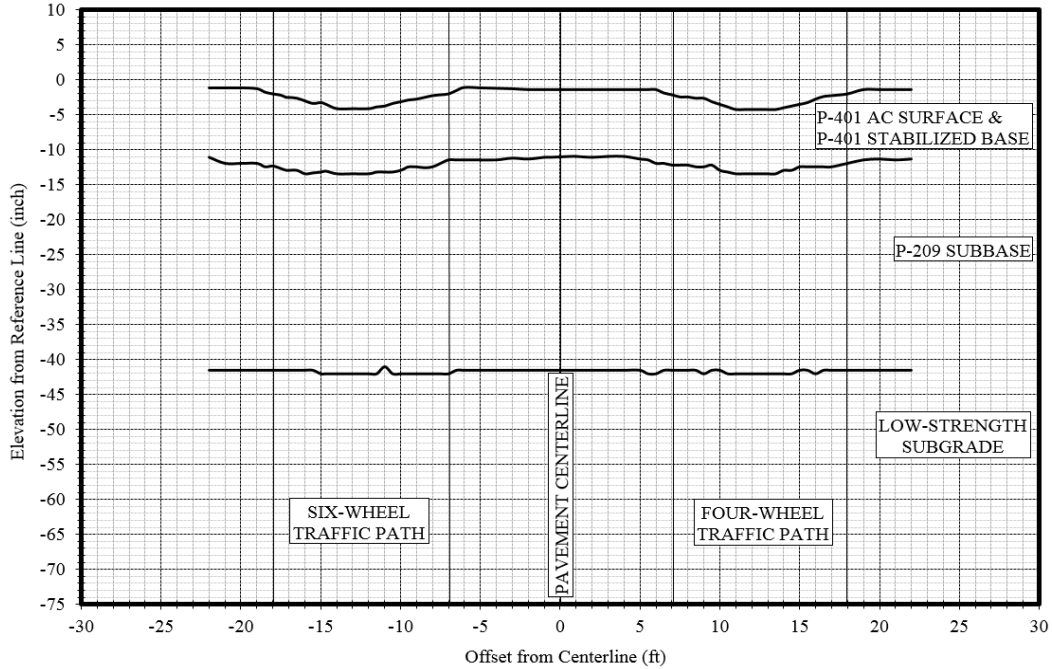


Figure 85. Trench Layer Interface Profiles, LFS-E (West Face of Trench)

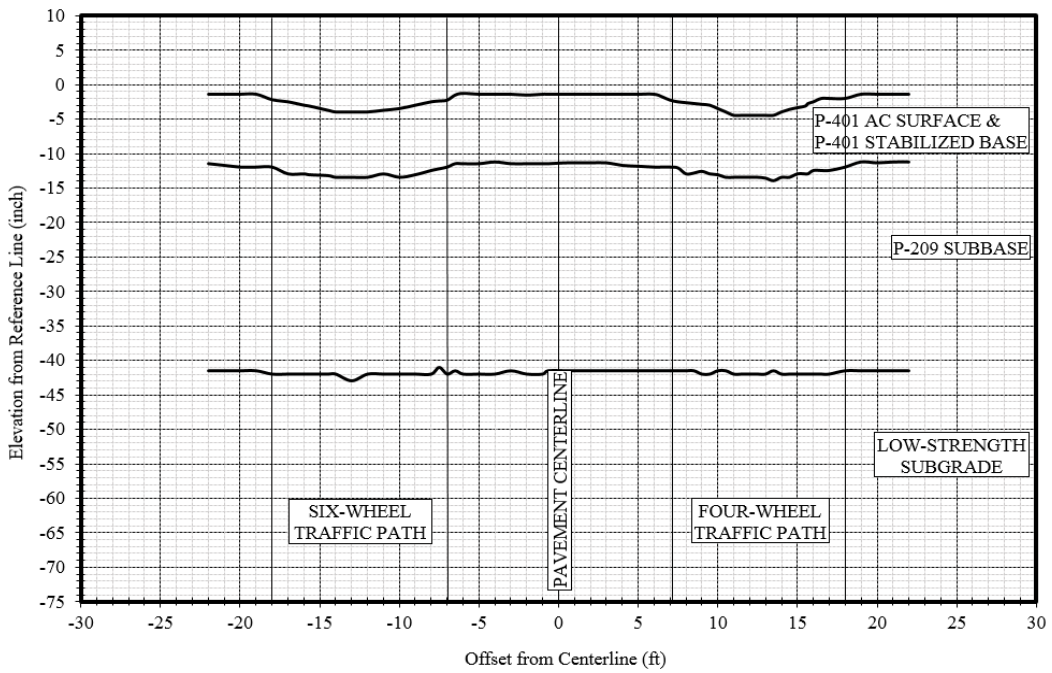


Figure 86. Trench Layer Interface Profiles, LFS-E (East Face of Trench)

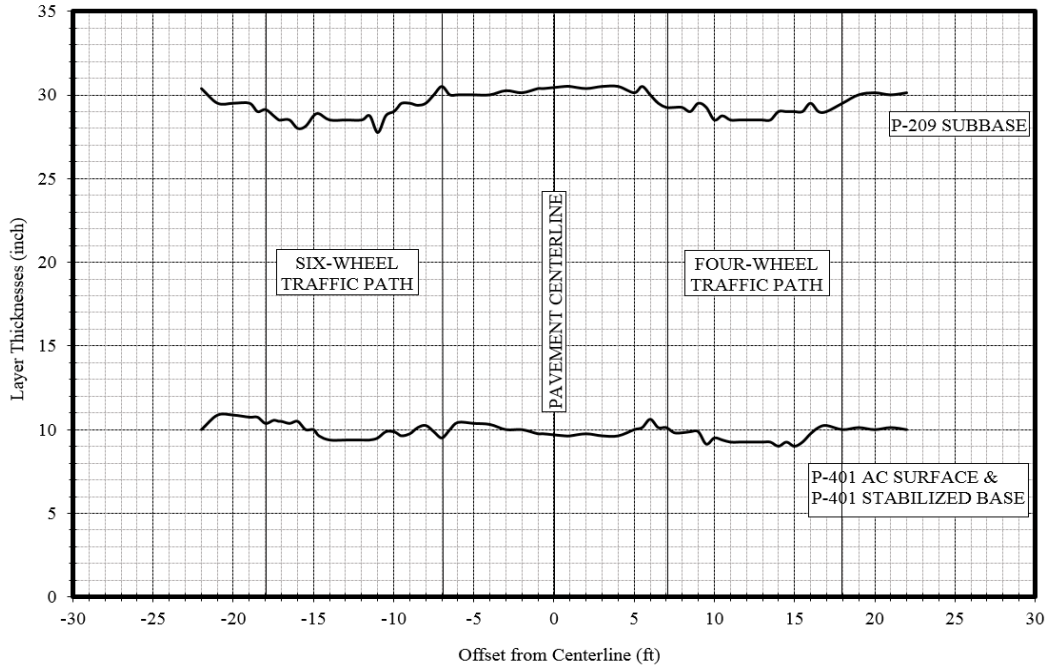


Figure 87. Trench Layer Thicknesses, LFS-E (West Face of Trench)

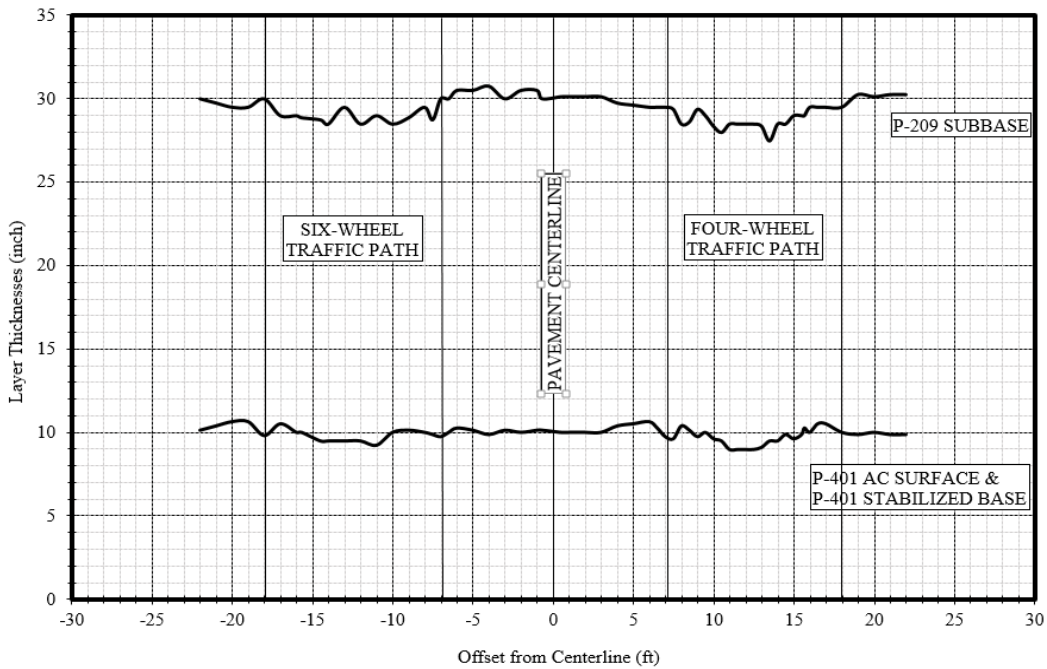


Figure 88. Trench Layer Thicknesses, LFS-E (East Face of Trench)

4.1.2.3 Test Item MFC

The MFC test item failed after 12,000 passes. At failure, rut depths ranged from 2 to 6 inches (50.8 to 152.4 mm) with asphalt cracking in the traffic lane and surface upheaval outside the traffic lane. Following trafficking, Trenches MFC-W and MFC-E were excavated at stations 3+45 and 3+67,

respectively, to investigate the failure mechanism of the pavement structure. Figure 89 and Figure 90 show the pavement layer profile measurements on the west and east faces of the east trench. The profiles clearly show intrusion of the subgrade material into the P-154 subbase in both traffic paths.

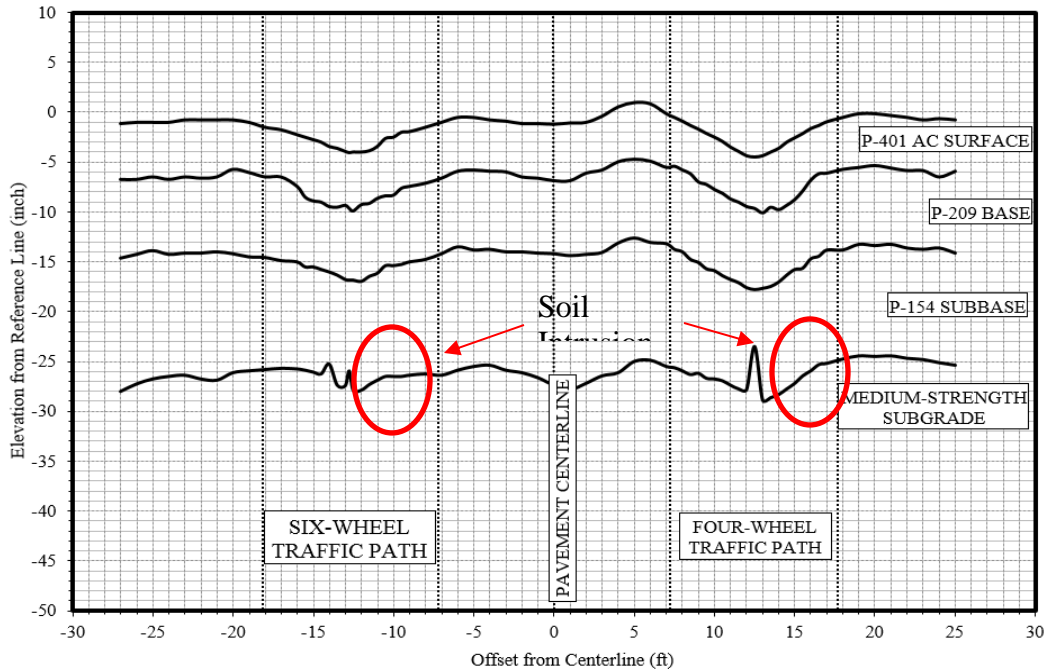


Figure 89. Pavement Layer Profile Measurements, MFC East (West Face of Trench)

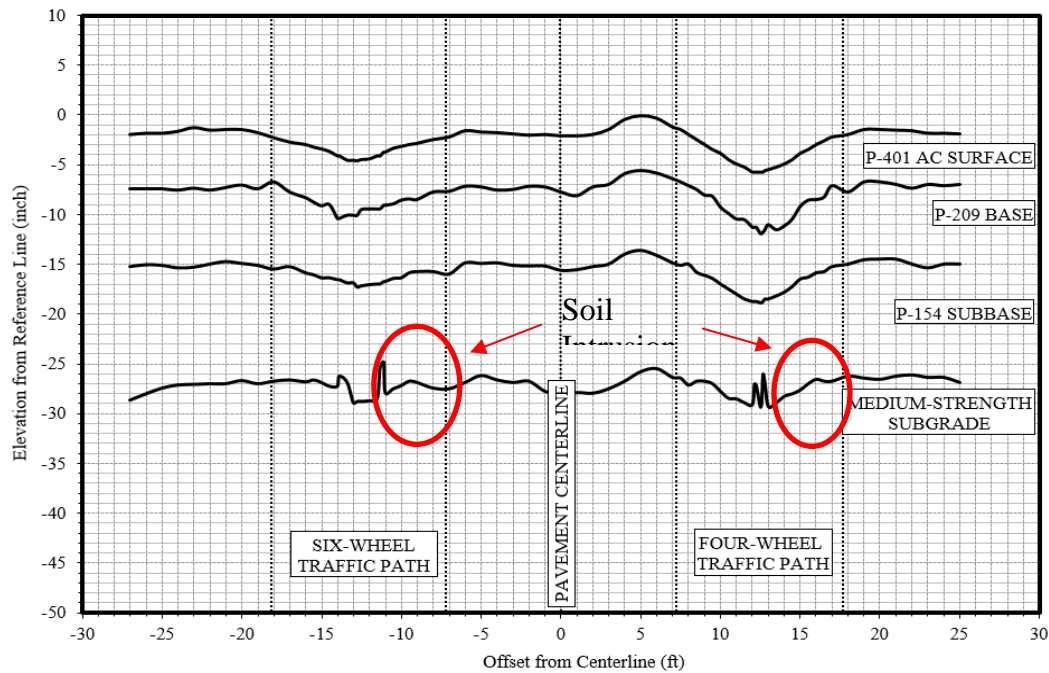


Figure 90. Pavement Layer Profile Measurements, MFC East (East Face of Trench)

Figure 91 and Figure 92 compare as-built layer thicknesses to post-traffic layer thicknesses determined from trench wall measurements. Post-construction (as-built) layer thicknesses were measured at 5 ft. (1.52 m) intervals. For trench measurements, layer thicknesses were measured at 1 ft. (0.3 m) intervals outside the wheel path areas and every 6 inches (0.15 m) inside the wheel path areas. As shown in the figures, the thickness of the P-154 subbase layer decreased in the wheel path area and increased in the upheaval area. Rutting was primarily contributed by the subgrade and the P-154 subbase. Shear flow, because of shear failure in the subgrade, contributed to the upheaval.

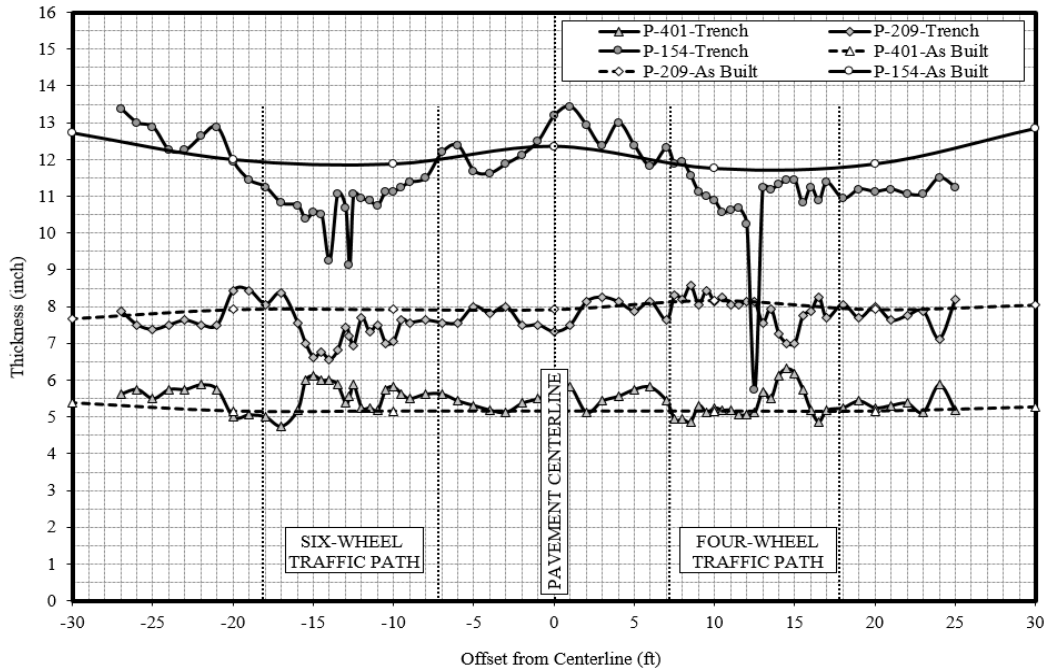


Figure 91. Pavement Layer Thickness in the MFC East Trench (West Face of Trench)

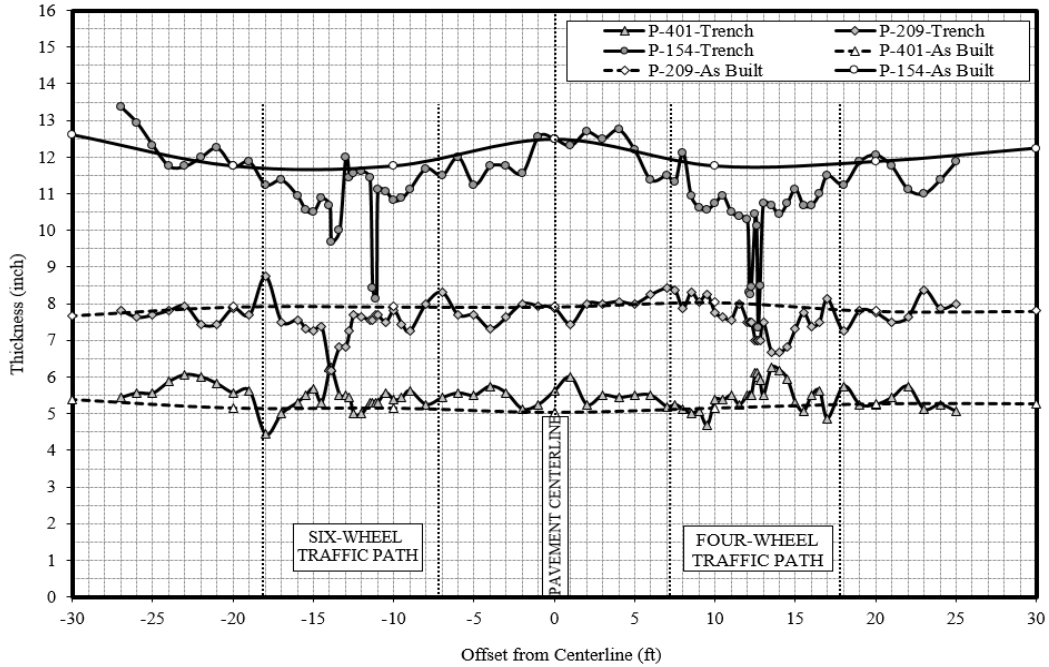


Figure 92. Pavement Layer Thickness in the MFC East Trench (East Face of Trench)

Figure 93 shows the P-401 layer at the location of maximum rutting (center of the 6-wheel traffic path). No signs of rutting in the P-401 layer were observed.



Figure 93. P-401 from Maximum Rutting Location (Center of 6-Wheel Traffic Path)

The loss of confining stress at the bottom of the granular material provided an opportunity for the clay subgrade material to intrude upwards into the subbase layer, which was observed at several locations in the trench (Figure 94 and Figure 95). Figure 94 shows the lateral movement of the subbase material at the subbase/subgrade interface at the center of 4-wheel traffic path.



Figure 94. Lateral Movement of P-154 Subbase in Test Item MFC at the Center of 4-Wheel Traffic Path (South Side) (Garg 2003)

Figure 95 shows penetration of subgrade material into the P-154 layer at the center of the 6-wheel traffic path.

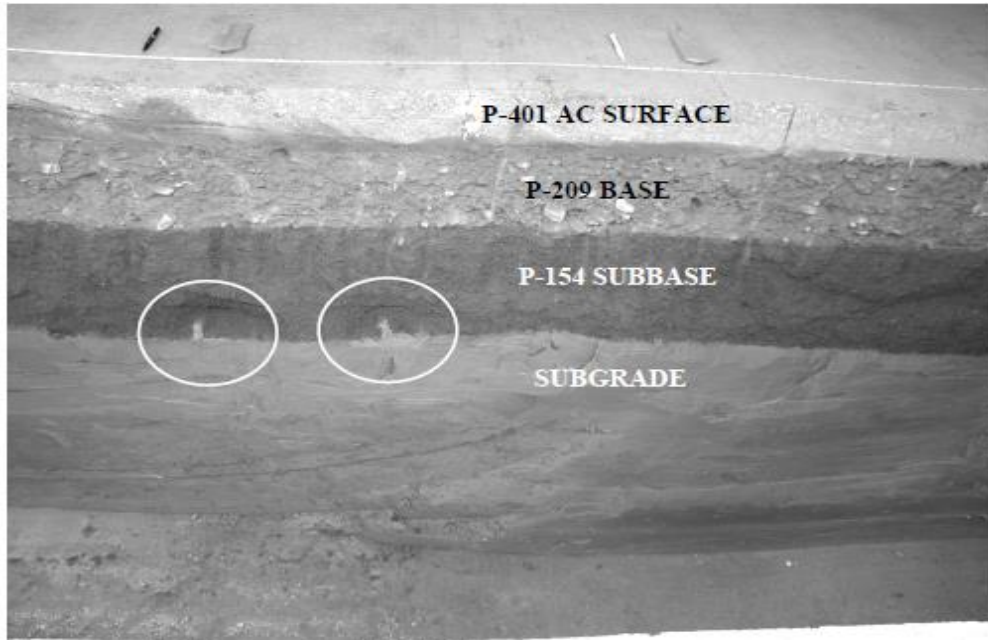


Figure 95. Lateral Movement of P-154 Subbase in Test Item MFC at the Center of 6-Wheel Traffic Path (Garg 2001)

Figure 96 shows the moisture content and CBR test results on the subgrade surface. The CBR values ranged from 4.9 to 8 with a mean value of 5.4 for both traffic paths. The post-constructed CBR value for test items with medium strength subgrade was 8. The decrease in the subgrade strength indicates the damage to the subgrade caused by traffic. The CBR values were higher outside the wheel path where there was no traffic. Moisture content ranged from 33.04% to 34.85%.

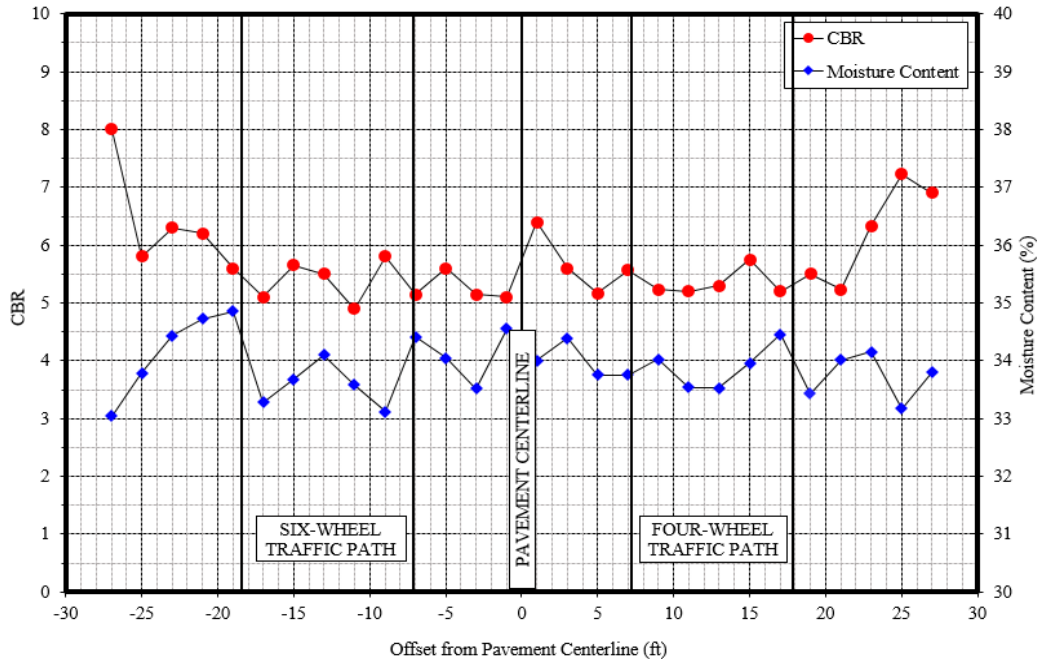


Figure 96. Post-Traffic CBR Results on Subgrade Surface in MFC-E Trench

4.1.2.4 MFS Test Item

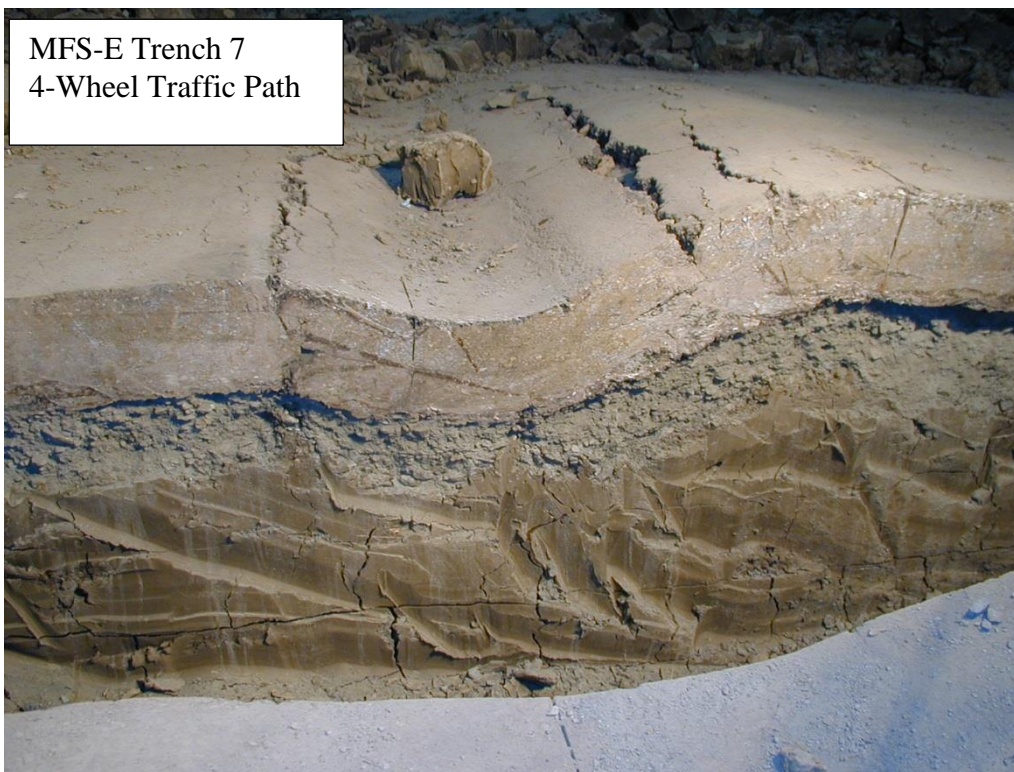
In the MFS test item, localized failure was observed in the north side traffic path (6-wheel) after 19,900 passes. Trafficking was continued only on the south side and was terminated after 29,000 passes. Following trafficking, Trenches MFS-W and MFS-E were excavated at stations 4+33 and 4+55, respectively, to investigate the failure mechanism of the pavement structure.

4.1.2.5 East Trench

The final rut depth on the east location was 0.7 inches (1.78 cm) under 6-wheel traffic (north) and 5.1 inches (12.95 cm) under 4-wheel traffic (south) (Hayhoe and Garg 2004). Figure 97 shows the MFS East trench section.



(a) North (6-Wheel) Side 0.7 Inch Rut



(b) South (4-Wheel) Side 5.1 Inch Rut

Figure 97. MFS East Trench Section

Figure 98 and Figure 99 show layer profile measurements for the west and east faces of the MFS east trench. Total rutting was significantly less under 6-wheel loading than under 4-wheel loading because of fewer passes. As with the MFC test item, intrusion of the clay subgrade into the weakened granular subbase occurred under the wheel path, as illustrated in Figure 98 and Figure 99.

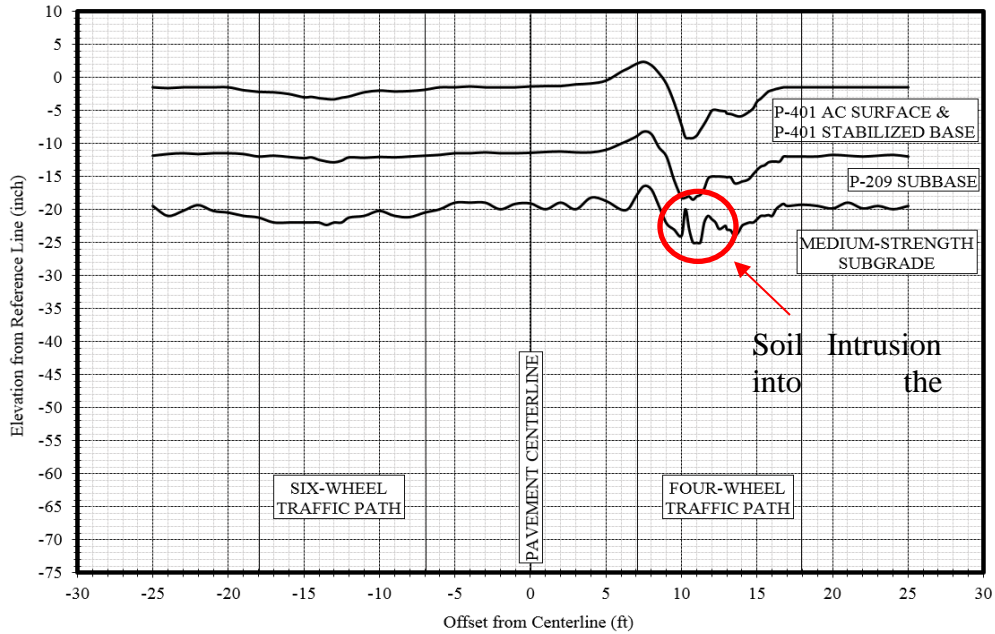


Figure 98. Layer Profile Measurements, MFS East (West Face of Trench)

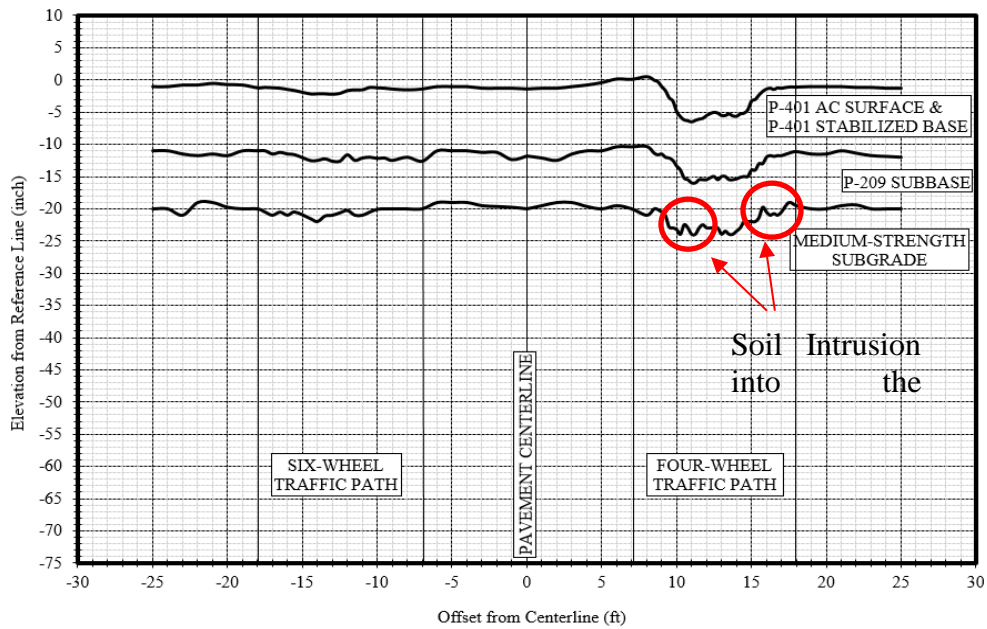


Figure 99. Layer Profile Measurements, MFS East (East Face of Trench)

4.1.2.6 West Trench

The P-401 surface and P-401 asphalt stabilized base were removed from the west trench to expose the P-209 subbase. Localized failure of the P-209 subbase was observed in the 6-wheel traffic path. A vertical crack was formed longitudinally in the P-209 subbase layer, which allowed subgrade material to intrude into the crack. The crack was approximately 2 inches (50 mm) wide at the bottom of the P-209 subbase and extended all the way up to the bottom of the asphalt base course. The longitudinal extent of the crack could not be determined, as it extended beyond the walls of the trench. Figure 100 shows the subgrade intrusion and shear failure in the subbase in the 6-Wheel traffic path. Similar behavior was observed in the 4-wheel traffic path but at a much lower severity (Figure 101).



Figure 100. MFS West Trench Section in the 6-Wheel Traffic Path (Hayhoe and Garg 2004)

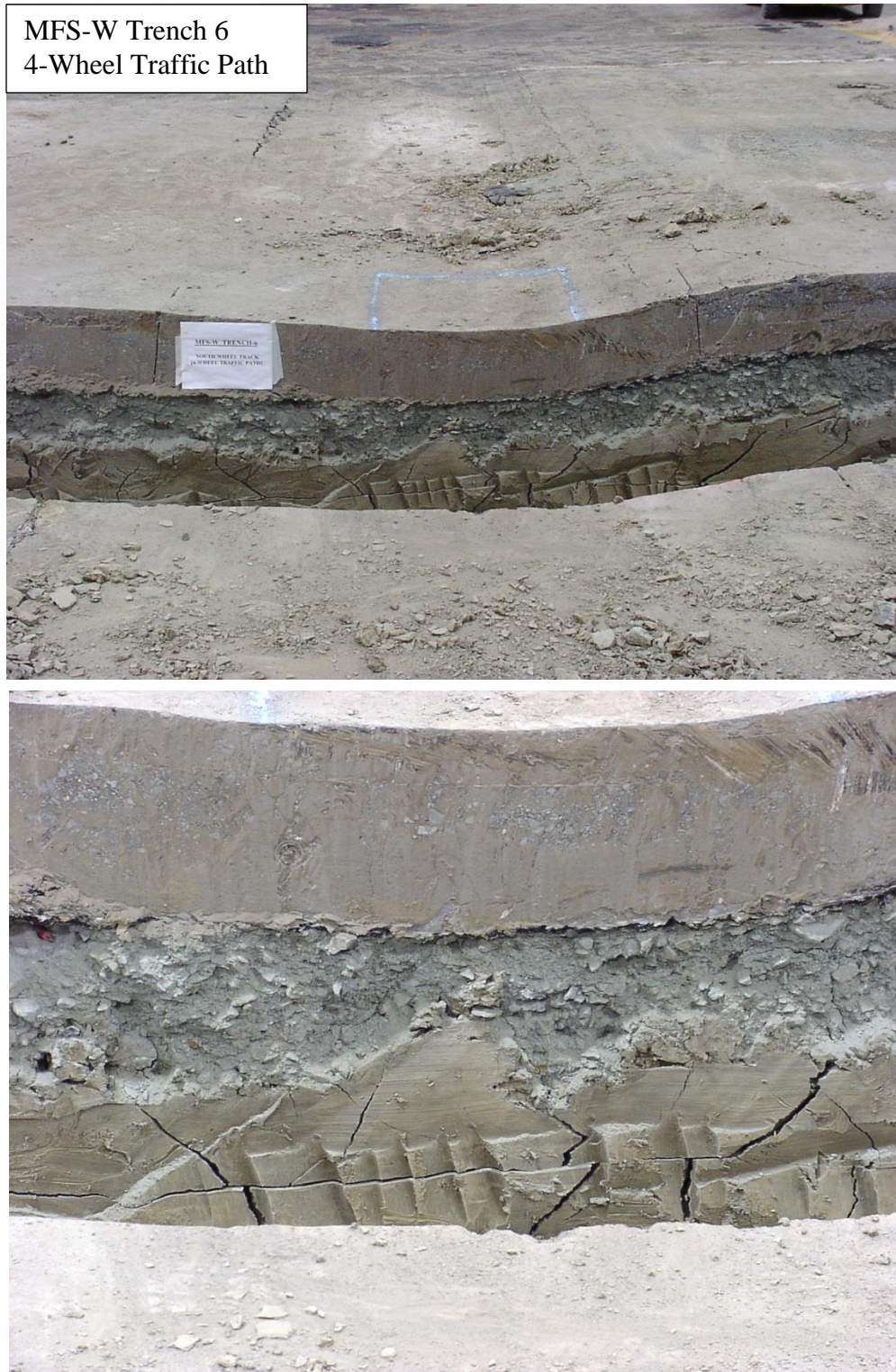


Figure 101. MFS West Trench Section in the 4-Wheel Traffic Path (Hayhoe and Garg 2004)

Figure 102 shows the pavement layer profile measurements for the MFS west trench. In the 6-wheel loading path, the failure of the P-209 subbase layer with subgrade intrusion is clearly visible. In the 4-wheel loading path, rutting was contributed by the P-209 subbase layer and the subgrade.

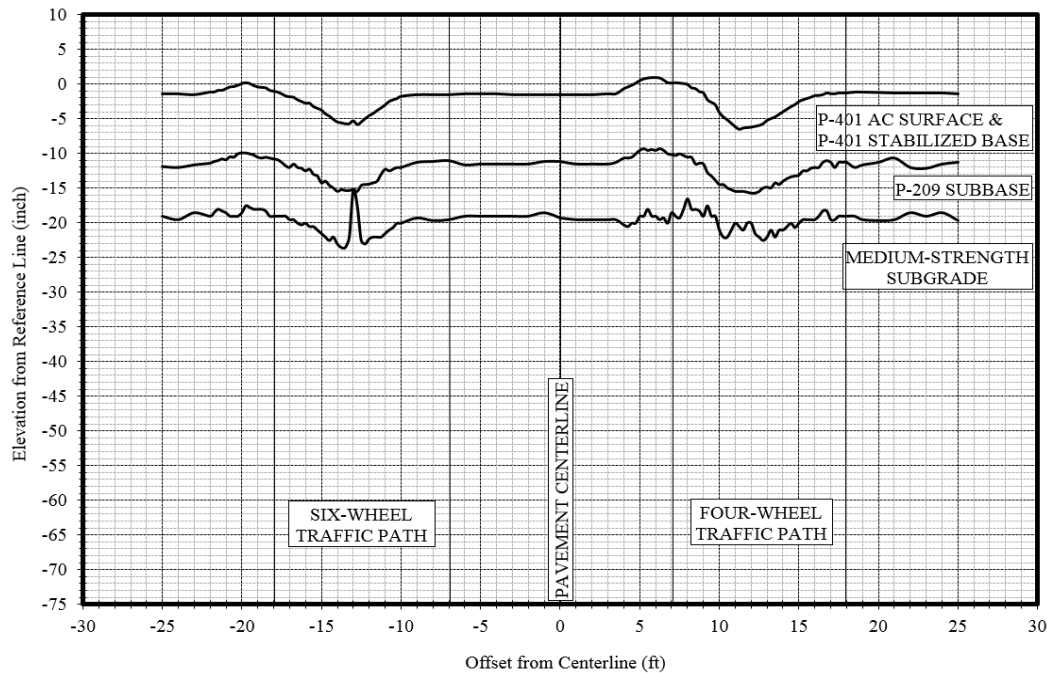


Figure 102. Layer Profile Measurements, MFS West (West Face of Trench)

4.2 Test Pit and Coring

4.2.1 Data Collection

The surface area for each of the 6 trenches was divided into five areas (Figure 103). Test areas 1 and 5 were the non-trafficked areas outside the traffic path. Test areas 2 and 4 were the areas under the 6-wheel and 4-wheel traffic loading, respectively. Test Area 3 was located in the centerline of the pavement between the two traffic paths. Five test pits with dimensions of approximately 4 ft. by 4 ft. were excavated in each layer of the trafficked and centerline areas (one in each trafficked area, 2 and 4, one on the pavement centerline, and two outside the wander path, area 3). Figure 104 shows the location of test pits in each area. Test pit locations were selected in critical locations (location of maximum rut depths, and maximum upheaval). Characterization tests such as CBR, dynamic cone penetration (DCP), and in-situ density were conducted on top of each exposed layer. DCP tests were performed to characterize strength variation with depth.

Test pits were initially excavated from P-401 AC surface before the removal of layer for the trench, to expose the surface of P-209 base. In-situ density measurements were made using the sand replacement method (ASTM D4914-89) to characterize density changes from the location of maximum rutting (center of each wander path) to the location of maximum upheaval (outside the wander path) and were also compared to the density of the non-trafficked area (pavement centerline). Figure 105 and Figure 106 show the location of sand cone tests within a test pit and

sand cone test in process, respectively. Moisture contents were determined using ASTM D 2216-92.

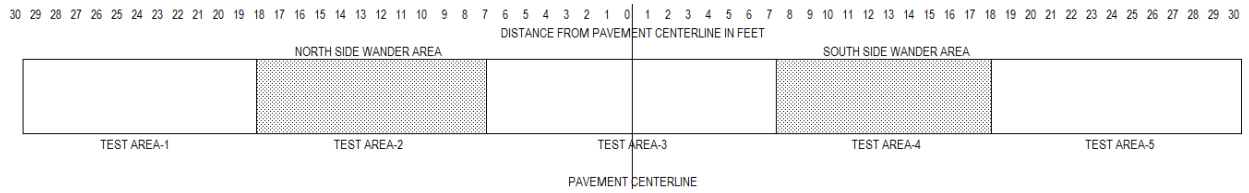


Figure 103. Schematic of Testing Areas

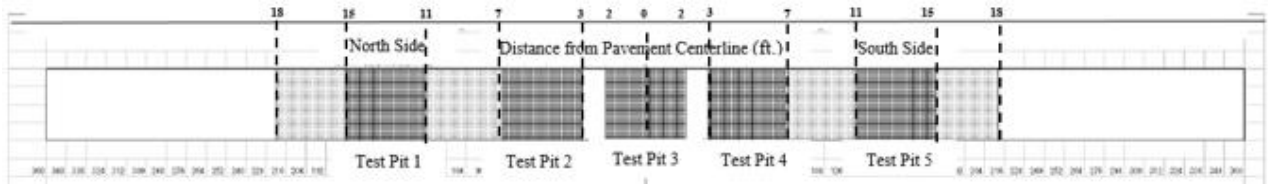


Figure 104. Location of Test Pits in Each Area

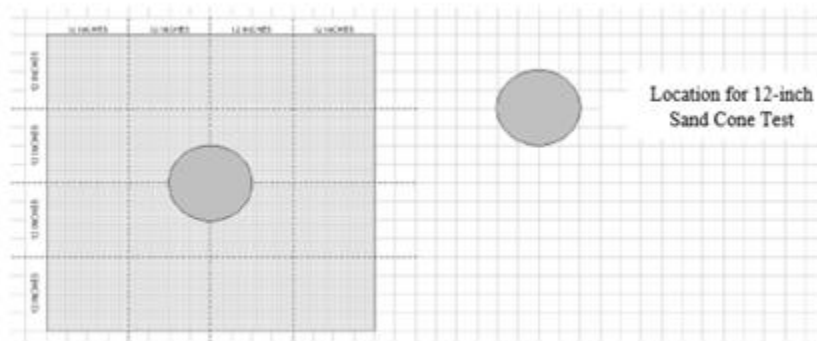


Figure 105. Location of 12-inch Sand Cone Density Tests in P-209 Crushed Stone Base



Figure 106. Sand Cone Test

After finishing the testing on the base layer, test pits were excavated at the same location from the P-209 base to expose the surface of the P-154 subbase. CBR tests were conducted on locations inside the test pits as shown in Figure 107. Each CBR test consisted of three penetrations. Based on guidance in FM 5-430-00-2 (U.S. Army Field Manual for Airfield Pavement Design), CBR tests were spaced in the pit so that areas covered by the surcharge weights of the individual tests did not overlap. A minimum center-to-center spacing of 12 inches (305 mm) was selected. Moisture samples were taken from the middle penetration of the CBR test. In situ density was measured using the sand cone method (ASTM D 1556-90).

Figure 107 also shows the locations of the sand cone test and DCP tests on P-154 test pit. The order in which the tests were performed was the CBR tests, followed by the sand cone, and then the DCP tests. As shown in Figure 108, DCP tests were performed in the diagonally opposite corners inside the test pit. A total of ten DCP tests were performed in each trench testing area using disposable cones.

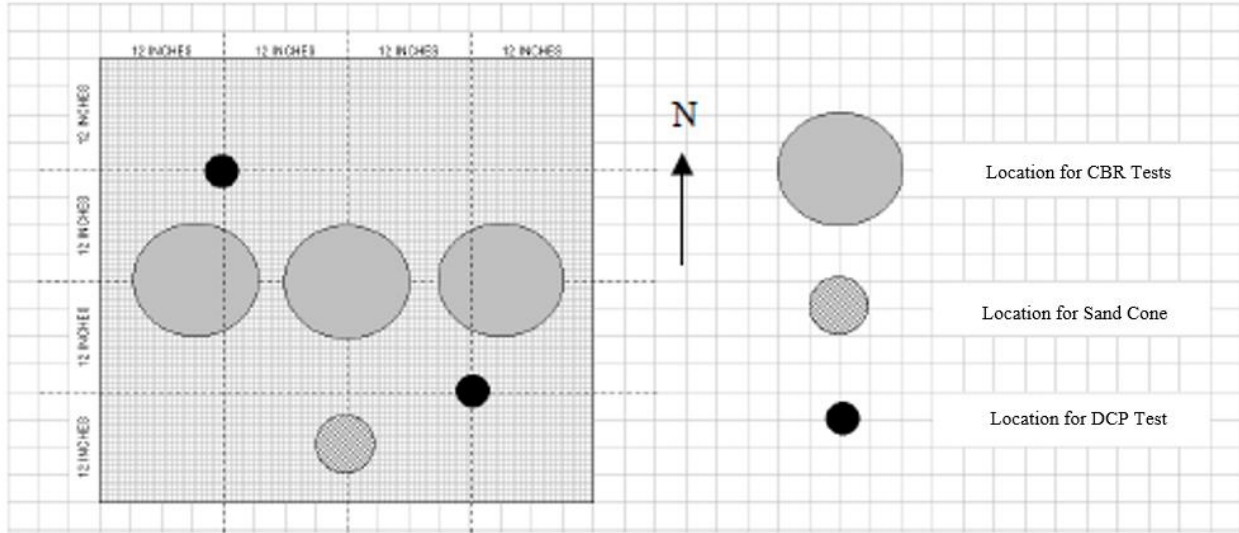


Figure 107. Schematic of Test Locations on P-154 in Test Pits

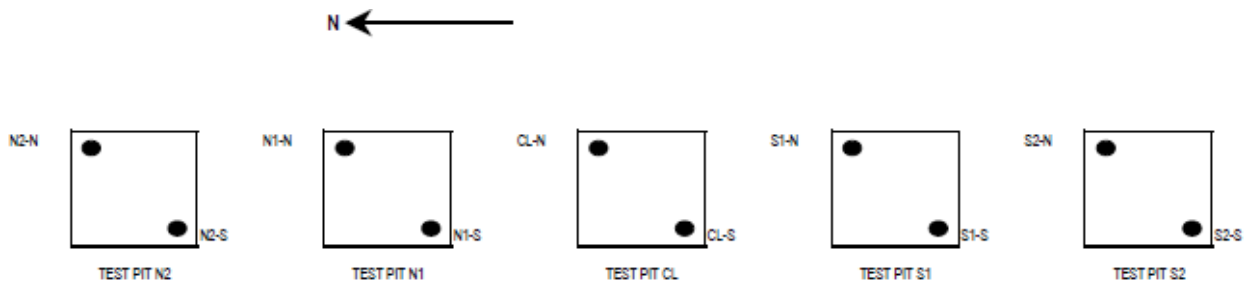


Figure 108. Location of DCP Tests on P-154 Layer

Then the P-154 subbase was excavated using a backhoe. Near the interface, material was hand excavated using shovels. After testing on the subgrade surface was completed, test pits were dug and testing was performed at 6-inch (15 cm) depth intervals. A 10.12 lb. (4.5 kg) hammer was used for the DCP tests in the subgrade, an ASTM permitted substitution for the standard 17.6 lb. (8.0 kg) hammer that might produce excess penetration in soft ground conditions. The DCP tests were performed on the surface of the subgrade and at 24 inches (610 mm) below the surface of the subgrade. The test locations within the test pits in the subgrade are shown in Figure 109. Thin-walled Shelby tube samples (ASTM D 1587-94) were stored and used for resilient modulus testing. Results of resilient modulus testing for each test item can be found in Appendix D.

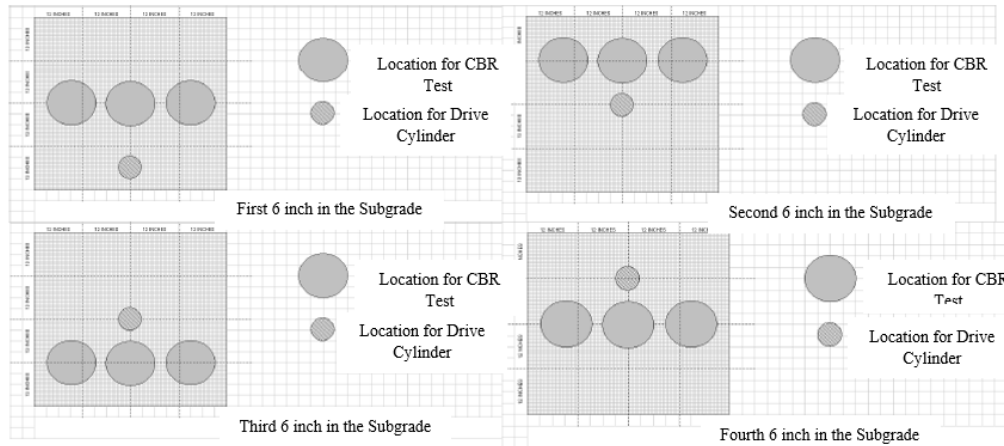


Figure 109. Test Locations within Test Pits in the Subgrade

In addition to the test pits, cores were obtained from the north wheel track, south wheel track, and the centerline in locations with the most severe cracks, hairline cracks, and medium intensity cracks within Test Item MFC. Core details are available in table D-28 of Appendix D. The number of extracted cores were selected based on examining the trafficked area in the two traffic lanes. The thickness of pavement component layers was measured from the cores. The cores were also inspected for separation at the interface of lifts and the depth of the cracks occurring in the pavement.

4.2.2 Findings from Test Pit Investigation

4.2.2.1 Test Item LFC

Findings from test pit investigations consist of two sets of data for each test item: post-traffic density data from sand cone tests and CBR data. Post traffic test results are presented in Appendix D. Summary of dry density and moisture results for each layer is presented in Table 19.

Table 19. Field Density and Moisture Results for LFC

Pavement Layer	Dry Density (Pcf)			Moisture Content (%)		
	Post-Traffic		Pre-Traffic	Post-Traffic		Pre-Traffic
	min	max		min	max	
P-209	150	154	157	2.6	3.6	-
P-154	145	151	129	2.1	4.8	6.0
subgrade	90	101	-	22.7	29.5	-

In the P-209 base layer, dry densities were higher in the wheel path compared to the outside wheel path. Lower moisture content was detected in the wheel paths compared to the outside wheel path areas.

In the P-154 subbase layer, dry densities were higher compared to the pre-traffic dry density whereas the moisture content decreased from the pre-traffic moisture content. The significant increase in the dry density and decrease in the moisture content can be attributed to the compaction of the P-154 subbase layer due to application of traffic.

The moisture and dry density changes with subgrade depth are shown in Figure 110. As it can be seen, the in-situ dry density values decreased with depth below the subgrade surface.

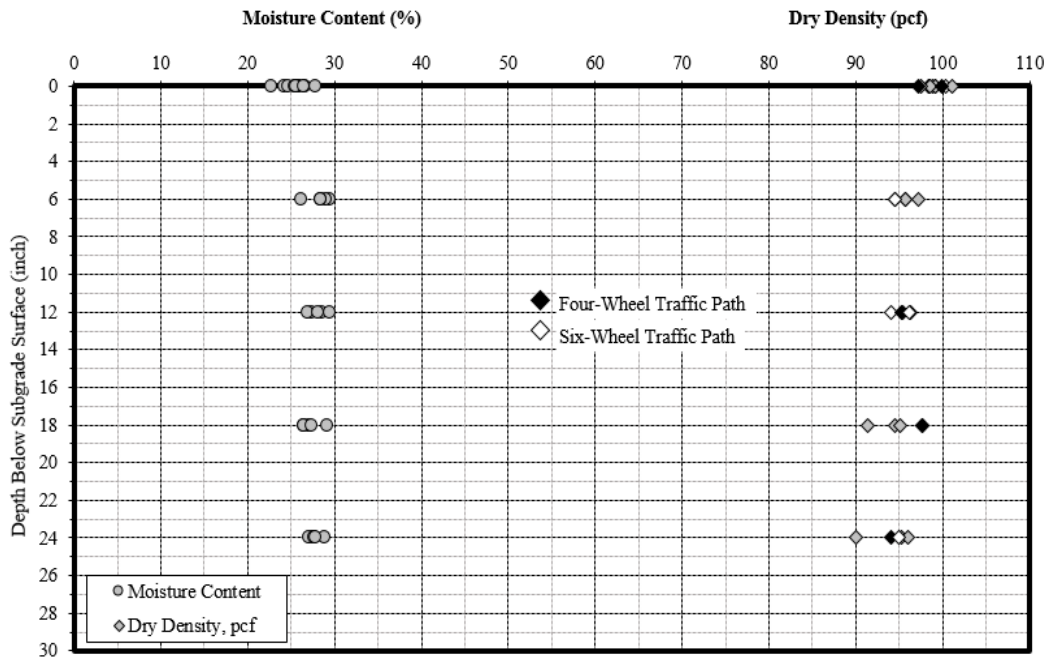


Figure 110. Moisture and Dry Density Variation with Depth in LFC East Trench

In the subgrade layer, the CBR variation within the subgrade depth is shown in Table 20. The CBR values generally were higher in traffic paths compared to non-trafficked area. The average CBR for both 6-wheel and 4-wheel traffic paths (5.5 and 6.5, respectively) showed an increase from the as-constructed CBR value of 4 indicating the compaction of subgrade due to trafficking.

Table 20. CBR Change with Depth in LFC East Trench

Depth from Subgrade Surface (inch)	6-Wheel Traffic Path	4-Wheel Traffic Path	Non-Trafficked Area
0	4.4	5.8	4.4
6	5.7	5.7	5.0
12	5.5	7.0	4.7
18	5.2	6.8	4.5
24	6.5	7.4	5.3

4.2.2.2 Test Item LFS

The variations in moisture content and dry density with depth in subgrade are shown in Figure 111.

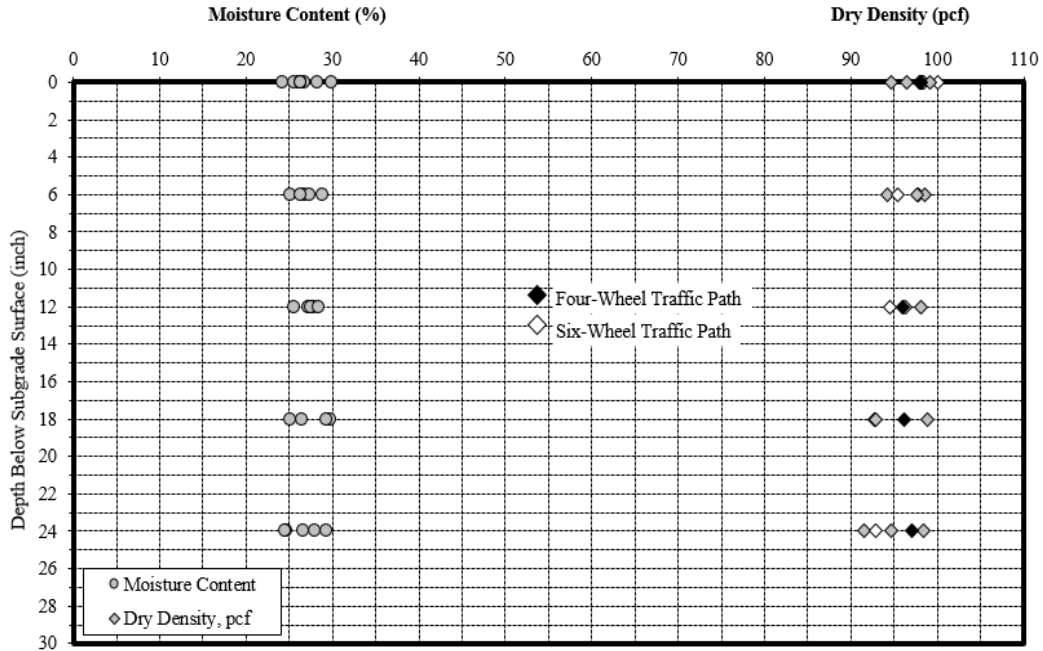


Figure 111. Moisture and Dry Density Change with Depth in LFS East Trench

The CBR changes with the increase in the subgrade depth are shown in Table 21. For both traffic paths, CBR values increased with depth. The average CBR for both 6-wheel and 4-wheel traffic paths (5.8 and 6.2, respectively) showed an increase from the as-constructed CBR value of 4 indicating the compaction of subgrade due to trafficking.

Table 21. CBR Change with Depth in LFS East Trench

Depth from Subgrade Surface (inch)	6-Wheel Traffic Path	4-Wheel Traffic Path	Non-Trafficked Area
0	5.0	5.3	5.4
6	5.5	6.0	5.3
12	5.3	7.5	5.4
18	6.1	5.8	5.1
24	7.1	6.4	5.6

4.2.2.3 Test Item MFC

Before the excavation of test pits, 4-inch diameter cores were extracted from the north wheel track and the south wheel track for thickness measurements. The cores were inspected for delamination/separation at the interfaces between lifts and for the depth of cracks occurring in the pavement. Core locations were chosen so as to include the most severe cracks, hairline cracks, and medium-intensity cracks. In total, nineteen cores were extracted and four measurements were made on each core at opposite sides. Delamination between the two lifts of the P-401 layer was observed in the 4-wheel traffic path cores. Only two cores from the 6-wheel traffic path showed delamination.

Figure 112 shows an example of delamination in the P-401 layer. A thin layer of dust between the two lifts could have caused the delamination (Garg 2001).



Figure 112. P-401 Surface Exhibiting Delamination

Investigation of cores showed that nearly all the cracks initiated from the top with the exception of one core that was cracked from the bottom. Figure 113 shows an example of a P-401 core with crack starting from the top. The P-401 core details can be found in table D- 28 in Appendix D.



Figure 113. Core Showing Crack Location

The P-401 layer was removed using a backhoe (Figure 114). During the removal, the two lifts of the P-401 layer in the four-wheel traffic path separated easily due to the delamination.



Figure 114. P-401 Removal

After the removal of the P-401 AC surface, the P-209 surface was exposed. In situ density was determined using the sand cone method (ASTM D 1556-90) with a 12-inch (305-mm) diameter cone. Figure 70 shows the location of the five test pits in the P-209 layer. Summary of dry density

and moisture results for each layer is presented in Table 22. Detailed test results can be found in Appendix D.

Table 22. Field Density and Moisture Results for MFC

Pavement Layer	Dry Density (Pcf)			Moisture Content (%)		
	Post-Traffic		Pre-Traffic	Post-Traffic		Pre-Traffic
	min	max		min	max	
P-209	153	158	158	2.2	2.9	3.6
P-154	118	135	131	3.8	4.7	6.4
subgrade	85	93	94	30.3	33.3	30.3

For the P-209 base and P-154 subbase, dry densities showed no significant change compared to the pre-traffic dry densities. The in-situ densities in the wheel tracks were slightly higher compared to the non-trafficked areas. For both layers, moisture contents were lower than the pre-traffic moisture content indicating the compaction of base layer due to trafficking.

After completing the tests in the P-154 test pits, the base and subbase were excavated using a backhoe. Figure 115 shows the penetration of clay subgrade into the P-154 subbase at the location of maximum rutting in the 4-wheel traffic path. For the subgrade, dry densities and moisture contents remained almost the same as pre-traffic values. In general, dry density and moisture content decreased with increasing depth. Figure 116 shows the variation of dry density and moisture content with subgrade depth.



Figure 115. Subgrade Penetration into P-154 Subbase in 4-Wheel Traffic Path

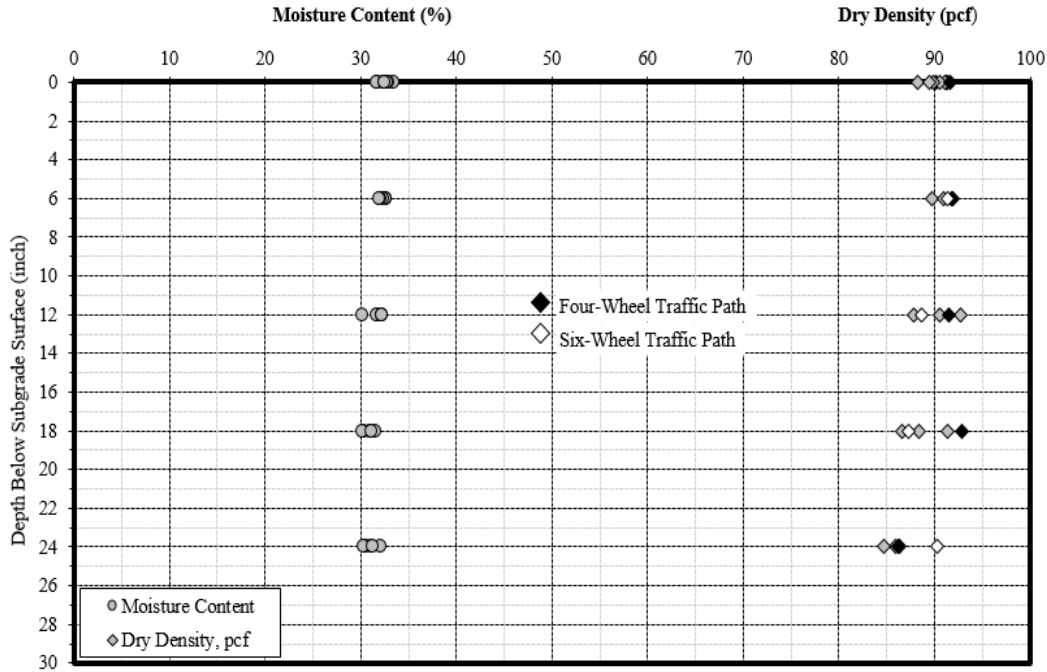


Figure 116. Variation in Subgrade Dry Density and Moisture Content with Depth in MFC East Trench

Table 23 shows the variation in CBR values with depth. CBR values were the highest at 12 inches (305 mm) below the subgrade surface. The average CBR for both traffic path were similar and slightly higher than the non-trafficked area. The DCP tests were also performed on the surface and at 24 inches (610 mm) below the surface of the subgrade using a 10.12 lb. (4.5 kg) hammer. The penetration rates ranged from 0.2 to 0.7 inch/blow (5 to 18 mm/blow) with higher penetration rates observed in the top 8 to 10 inches (203 to 254 mm) of the subgrade layer (Garg 2001).

Table 23. CBR Change with Depth in the MFC East Trench

Depth from Subgrade Surface (inch)	6-Wheel Traffic Path	4-Wheel Traffic Path	Non-Trafficked Area
0	5.4	5.4	6.0
6	6.7	6.6	5.7
12	8.4	9.2	8.8
18	6.9	7.2	6.0
24	7.8	6.2	6.6

4.2.2.4 Test Item MFS

4.2.2.5 East Trench

The P-209 dry density ranged from 142-148 pcf (2,275 - 2,371 kg/m³). Figure 117 shows the variation of dry density and moisture content with subgrade depth. The dry density and moisture content values both decreased with depth.

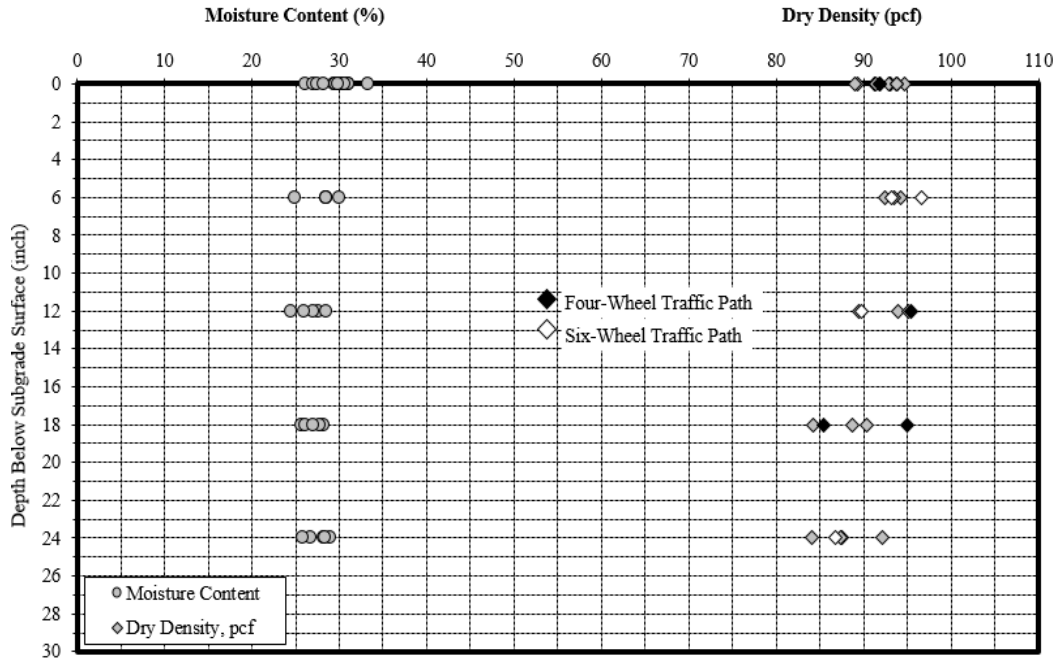


Figure 117. Variation in Subgrade Dry Density and Moisture Content with Depth in MFS East Trench

Subgrade CBR test results are summarized in Table 24. The average CBR value for the non-trafficked area was the same as the design CBR of 8. The average CBR for both 6-wheel and 4-wheel traffic path was 7.5 which was slightly lower than the design CBR of 8, showing the minimal effect of traffic on subgrade strength.

Table 24. Subgrade CBR in the MFS East Trench

Depth from Subgrade Surface (inch)	6-Wheel Traffic Path	4-Wheel Traffic Path	Non-Trafficked Area
0	7.1	6.2	8.6
6	10.9	7.3	10.5
12	7.2	8.9	7.4
18	5.8	7.5	6.4
24	6.7	8.0	7.1

4.2.2.6 West Trench

Figure 118 shows the variation of dry density and moisture content with subgrade depth. The P-209 dry densities ranged from 81 - 97 pcf (1,298 - 1,554 kg/m³).

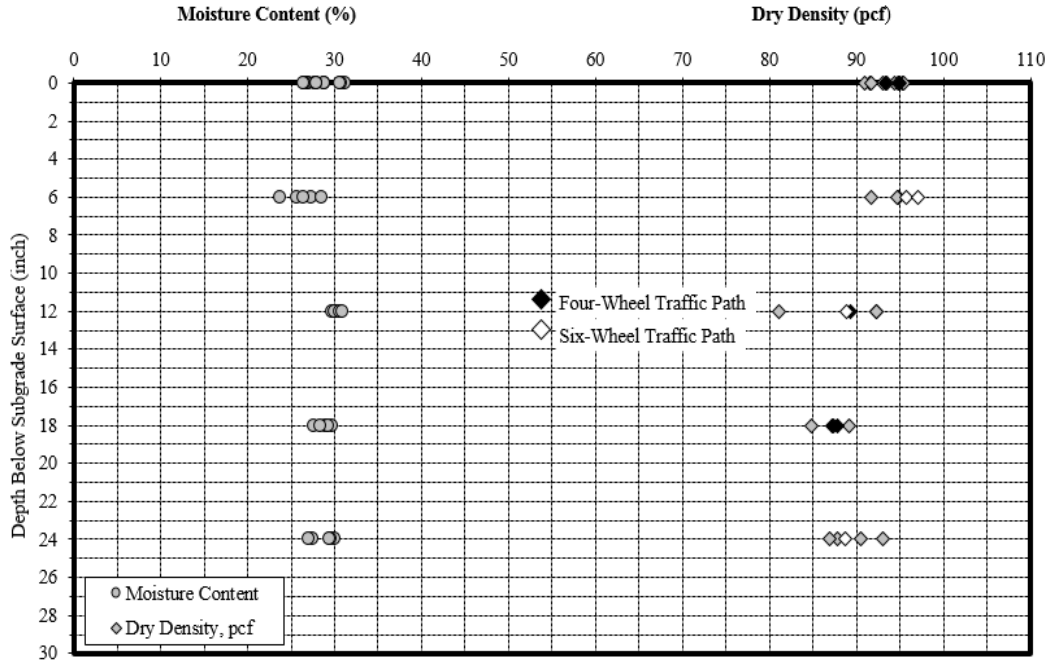


Figure 118. Moisture and Dry Density Change with Depth in the MFS West Trench

Table 25 summarizes the subgrade CBR test results. CBR values for the 6-wheel traffic path were lower than the 4-wheel traffic path. The CBR values for non-trafficked area and 4-wheel traffic path were close to the design CBR value of 8. However, for the 6-wheel traffic path, CBR with the average of 6.3, was 20% lower than the design CBR value as a result of failure in the subgrade.

Table 25. Subgrade CBR in the MFS West Trench

Depth Subgrade from Surface (inch)	6-Wheel Traffic Path	4-Wheel Traffic Path	Non-trafficked Area
0	6.2	6.9	7.5
6	6.5	9.5	7.9
12	7.2	7.7	7.9
18	6.2	8.8	6.1
24	5.5	7.7	6.7

4.3 Summary of Post-Traffic Testing

Post-traffic testing was performed on flexible test items after the termination of trafficking to characterize the failure mechanism of each component layer and assign post-failure properties to each pavement layer. This was done by test pits and trenches at the locations of rut depth measurements. Characterization tests such as CBR, moisture content, DCP, and in-situ density were conducted on top of each exposed layer.

The post-traffic trenches showed that overall all the cracks in the flexible pavement test items were top-down cracks. Most of the cracks appeared in the longitudinal direction parallel to the centerline of the pavement.

Test items with low strength subgrade, failed at surface layers as exhibited by formation of cracks. From the profile measurements, rutting was observed in the P-401 AC layer in both traffic paths. Shoving also occurred in the P-401 AC layer, resulting in upheaval outside the traffic path. Results of testing showed that dry densities were higher in the wheel path compared to the outside wheel path. Also, lower moisture content was detected in the wheel paths compared to the outside wheel path areas. The CBR values generally increased as a result of trafficking; however, there was no significant difference between the 4-wheel and 6-wheel traffic paths.

In MFC, failure was caused by the shear failure in the subgrade and P-154 subbase. The profiles showed clear intrusion of the subgrade material into the P-154 subbase in both traffic paths. From profile measurements, it was observed that the thickness of the P-154 subbase layer decreased in the wheel path area and increased in the upheaval area. Rutting was primarily contributed by the subgrade and the P-154 subbase. Excavated cores showed delamination between the two lifts of P-401 AC layer. From CBR testing on subgrade, the average CBR values for both traffic path was approximately similar and slightly higher than the non-trafficked area.

In the MFS west trench, localized failure was observed in the 6-wheel load path where the subgrade intruded into the P-209 subbase resulting in upheaval. In the 4-wheel traffic lane, rutting was contributed by subbase and subgrade. In the MFS east trench, significant rutting and AC cracking was observed in the 4-wheel traffic lane. From the CBR testing on the subgrade, non-trafficked area and 4-wheel traffic path had approximately similar values, whereas for 6-wheel traffic path, decreases in CBR values were observed as a result of failure in the subgrade.

5. SUMMARY

5.1 Rigid Pavement

Traffic testing was started on February 14, 2000. Corner cracks were observed in the MRS and HRS test items only after 28 passes. Testing was stopped to evaluate the origin of the cracks in the rigid pavement test items. Almost all the slabs in the MRS and HRS test items developed corner cracks. In the LRS test items, corner cracks were not observed during the February 2000 tests however, longitudinal cracks developed in all the slabs. In March 2000, traffic tests were resumed and continued until all slabs cracked. Corner cracks appeared in the LRS test item during the resumed phase of testing.

Crack measurements showed that the HRS slabs exhibited the largest cracks, and the LRS slabs exhibited the smallest corner cracks. Furthermore, it was found that all pavement slabs were curled up at the corners, with the HRS slabs exhibiting the greatest amount of curling and the LRS slabs exhibiting the least amount of curling. The cause of curling was studied further in CC2 experiments.

HWD test results before the start of traffic showed a significant increase of upward curling from the summer to the winter of 1999. The slabs on the higher strength subgrades were curled more than those on the lower strength subgrades. HWD tests at the slab corners and joints verified that there was an increase in upward curling. Additionally, the joint load transfer capability by deflection (LTD) was lower in winter.

5.2 Flexible Pavement

Traffic tests on flexible test items began February 14, 2000, simultaneously with the rigid pavement tests. All tests were paused after 28 passes on February 14, 2000 due to premature failure of rigid pavement test items. Trafficking of all test items restarted on March 30, 2000 and continued until the rigid test items were deemed failed. Trafficking then continued on the high-strength subgrade flexible test items until 5000 passes, and on low- and medium-strength subgrade flexible test items until November 2000 (when ambient temperatures became too low for representative testing on the asphalt layers). Testing of flexible pavement test items resumed in May of 2001 and was completed in July 2001.

From the MDD results it was seen that over a complete wander cycle, unrecovered strains varied from positive to negative relative to the mean value. Net unrecovered strain over a complete wander cycle was very small both in absolute terms and relative to the unrecovered strains at individual wander positions. Recovered strains were strongly dependent on the path of previously applied loads. Both recovered strains and unrecovered strains increased in magnitude as testing progressed to failure. Also, the ratio of unrecovered strain to recovered strain increased as testing progressed.

HWD tests were conducted at different stages of trafficking to monitor the effect of time and traffic on the structural condition of the pavement sections. To study the effects of traffic on pavement deterioration and minimizing the temperature effects, the ratio of D0 for the traffic lane to the D0 for center lane was identified for each test item. Results showed that as the pavement structure deteriorated under traffic loads, this ratio increased significantly.

Rutting was monitored manually throughout the traffic for flexible pavements using a TSP device, a rolling inclinometer, and straightedge rut depth measurements. Individual layer rut data were also collected automatically using MDDs. In general, the maximum rut depth at failure was higher for conventional base flexible test items than for stabilized base flexible test items. Compared to medium strength test items, the low-strength test items required more passes at higher wheel loads to reach failure.

After the completion of NAPTF traffic tests, post-traffic testing was conducted to investigate the failure mechanism of the pavement structures. In the medium strength flexible test items, failure was caused by the shear failure in the subgrade and P-154 subbase. Subgrade intrusion into the P-

154 subbase layer was observed. Test items with low strength subgrade, failed at the surface layer, as exhibited by the formation of cracks. From the profile measurements, rutting was observed in the P-401 AC layer in both traffic paths. Shoving also occurred in the P-401 AC layer, resulting in upheaval outside the traffic path.

The observations revealed that all the cracks in NAPTF test pavements were top-down cracks rather than bottom-up cracks. Most of the cracks appeared in the longitudinal direction parallel to the centerline of the pavement.

6. REFERENCES

AASHTO TP 8. Standard Test Method for Determining the Fatigue Life of Compacted Hot Mix Asphalt (HMA) Subjected to Repeated Flexural Bending.

ASTM D2937. Standard Test Method for Density of Soil in Place by the Drive-Cylinder Method.

ASTM D4429. Standard Test Method for CBR (California Bearing Ratio) of Soils in Place.

ASTM D1556. Standard Test Method for Density and Unit Weight of Soil in Place by the Sand-Cone Method.

ASTM D1587. Standard Practice for Thin-Walled Tube Sampling of Fine-Grained Soils for Geotechnical Purposes.

ASTM D2216. Standard Test Methods for Laboratory Determination of Water (Moisture) Content of Soil and Rock by Mass.

ASTM D2726. Standard Test Method for Bulk Specific Gravity and Density of Non-Absorptive Compacted Asphalt Mixtures.

ASTM D3665. Standard Practice for Random Sampling of Construction Materials.

AI MS-2. Asphalt Mix Design Methods. Asphalt Institute, 7th edition, Feb 2015.

Bejarano, M. O. (1999). Subgrade Soil Evaluation for the Design of Airport Flexible Pavements. *University of Illinois at Urbana-Champaign*.

Brill, D. R. and E. H. Guo (2000). Load Transfer in Rigid Airport Pavement Joints. The 2020 Vision of Air Transportation: Emerging Issues and Innovative Solutions: 13-24.

Crockford, W., et al. (1990). Modeling Stress and Strain States in Pavement Structures Incorporating Thick Granular Layers. Final Report. Contract F08635-87-C-0039, The Texas Transportation Institute, The Texas A&M University, College Station, Texas, April.

CTL (1998). National Airport Pavement Test Machine - Instrumentation/Data Acquisition. A Report Prepared for US Army Corps of Engineers. Construction Technologies Laboratories, Inc., Illinois.

FAA (1995). Advisory Circular 150/5320-6A. Airport Pavement Design and Evaluation. *Federal aviation administration, US Department of transportation: Maryland.*

FAA (2014). Advisory Circular 150/5320-6C. Airport Pavement Design and Evaluation. *Federal aviation administration, US Department of transportation: Maryland.*

FAA (1995). Airport Pavement Design for the Boeing 777 Airplane (LEDFAA). *Advisory Circular Number 150/5320-16.*

FAA, Advisory Circular (1989-2004). Standards for Specifying Construction of Airports. *AC 150/5370-10A.*

Gagnon, J. and N. Garg (2010). Predicting Rutting of Unbound Aggregate Layers Using Total Void Calculation under Full-Scale Testing at the FAA National Airport Pavement Test Facility. *Paving Materials and Pavement Analysis: 492-499.*

Garg, N. (1999). Pavement Material Characterization at the NAPTF. *FAA Working Group Meeting, November 1-3, 1999.*

Garg, N. and M. Dong (2002). Effect of Landing Gear Spacing on the Subgrade Deflection Response of Airport Pavements. Proceeding of the 6th International Conference on the bearing Capacity of the Roads and Airfields, Libson, Portugal, 24-26.

Garg, N. and G. F. Hayhoe (2001). Asphalt concrete strain responses at high loads and low speeds at the national airport pavement test facility (NAPTF). *Advancing Airfield Pavements: 1-14.*

Garg, N. and W. H. Marsey (2002). Comparison between falling weight deflectometer and static deflection measurements on flexible pavements at the National Airport Pavement Test Facility (NAPTF). *CD-ROM Proceedings of the 2002 FAA Airport Technology Transfer Conference, Citeseer.*

Garg, N. (2001). Posttrafficking testing at the National Airport Pavement Test Facility: Test item MFC. Rep. DOT/FAA/AR-TN01/49, U.S. Department of Transportation, Federal Aviation Administration, Washington, D.C.

Garg, N. (2003). Permanent Deformation Behavior of the Granular Layers Test at the FAA's National Airport Test Facility. 82nd Annual Meeting of the Transportation Research Board Modeling of Granular Bases for Flexible Pavements, Washington DC.

Garg, N. and W. H. Marsey (2004). Use of HWD to Study Traffic Effects on Flexible Airport Pavement Structure. *Road Materials and Pavement Design: Vol 5, 385-396.*

Gervais, Hayhoe, G. F. and N. Garg (2004). Towards a Permanent ACN Solution for 6-Wheel Landing Gear Aircraft. *Airfield Pavements: Challenges and New Technologies: 39-56.*

Gomez-Ramirez, F. M. and M. Thompson (2001). Aircraft Multiple Wheel Gear Load Interaction Effects on Airport Flexible Pavement Responses. *Advancing Airfield Pavements: 123-132*.

Guo, E. H., G. Hayhoe, D. Brill (2002). Analysis of NAPTF Traffic Test Data for the First-Year Rigid Pavement Test Items. *Presented for the 2002 Federal Aviation Administration Airport Technology Conference*.

Guo, E. H. and W. Marsey (2001). Verification of Curling in PCC Slabs at the National Airport Pavement Test Facility. *Advancing Airfield Pavements: 15-29*.

Hayhoe, G. F. (2004). Traffic Testing Results from the FAA's National Airport Pavement Test Facility. *Proceedings of the 2nd International Conference on Accelerated Pavement Testing, Citeseer*.

Hayhoe, G. F., R. Cornwell, N. Garg (2001). Slow-Rolling Response Tests on the Test Pavements at the National Airport Pavement Test Facility (NAPTF). *Advancing Airfield Pavements: 30-58*.

Hayhoe, G. F. and N. Garg (2001). Material Properties Database for the Test Pavements at the National Airport Pavement Test Facility (NAPTF). *Report, FAA Airport Technology Research and Development Branch, AAR-410, NJ*.

Hayhoe, G. F. and N. Garg (2002). Subgrade Strains Measured in Full-Scale Traffic Tests with Four-and Six-Wheel Landing Gears. *Presented for the 2002 Federal Aviation Administration Airport Technology Conference*.

Hayhoe, G. F. and N. Garg (2004). Posttraffic Testing on Medium-Strength Subgrade Flexible Pavements at the National Airport Pavement Test Facility. *Airfield Pavements: Challenges and New Technologies: 136-146*.

Hayhoe, N. Garg and M. Dong (2004). Permanent Deformations during Traffic Tests on Flexible Pavements at the National Airport Pavement Test Facility. *Airfield Pavements: Challenges and New Technologies: 147-169*.

Hayhoe, G. F., R. McQueen, E. Quo (1993). Airport Pavement Test Machine Design and Cost Study. *Galaxy, Scientific Corp Egg Harbor Township NJ*.

Hayhoe, G. F., N. Garg and E. Guo (2002). Falling Weight Deflectometer (FWD) Testing for Pavement Uniformity at the National Airport Pavement Test Facility (NAPTF). *Unpublished paper, Provided from FAA*.

Ledbetter, R. H. (1977). General Deformation (Elastic and Inelastic) and Stress Distribution Theory in Soils. *Army Engineer Waterways Experiment Station Vicksburg Geotechnical Lab*.

McQueen, R. D. (2000). Development of Requirements for Test Pavement Items for the National Airport Pavement Test Facility. *The 2020 Vision of Air Transportation: Emerging Issues and Innovative Solutions: 313-324*.

Contract No.: DTFACT-15-D-00007

McQueen, R. D., W. Marsey, J. Arze (2001). Analysis of Nondestructive Test Data on Flexible Pavements Acquired at the National Airport Pavement Test Facility. *Advancing Airfield Pavements*: 267-278.

Weinmann, T. L., A. Lewis, S. Tayabji (2004). Pavement Sensors used at Accelerated Pavement Test Facilities. *Proceedings of the second international conference on accelerated pavement testing*.

www.airporttech.tc.faa.gov. FAA Airport Technology Research and Technology Branch, AAR-410. *William J. Hughes Technical Center Atlantic City International Airport, New Jersey*

APPENDIX A—MATERIAL PROPERTIES

Table A-1 Laboratory Test Results on In-Situ Site Soil

Boring	Depth (in.)	In-Situ Moisture (%)	Plastic Index (PI)	Classification USC
B-13	0-2	5.1		
	2-4	9.1		
	4-6	10.2		
	6-4	9.3		
	8-10	6.6	NP	SP-SM
	10-12	5.7	NP	SP-SM
	12-14	6.6	NP	SP-SM
	14-16	7.3	NP	SW-SM
B-22	0-2	10.4		
	2-4	6.1	NP	SW-SM
	4-6	7.7		
	6-4	9.1		
	8-10	6.7	NP	SM
	10-12	7.8		
	12-14	8.5		
	14-16	7.3	NP	SP-SM
B-24	0-2	13.2	4.3	
	2-4	10.9	16.5	SC
	4-6	6.1	NP	SP-SM
	6-4	6.0	NP	SP-SM
	8-10	6.8	NP	SM
	10-12	5.4	NP	SP-SM
	12-14	6.5	NP	SP-SM
	14-16	6.2	NP	SP-SM

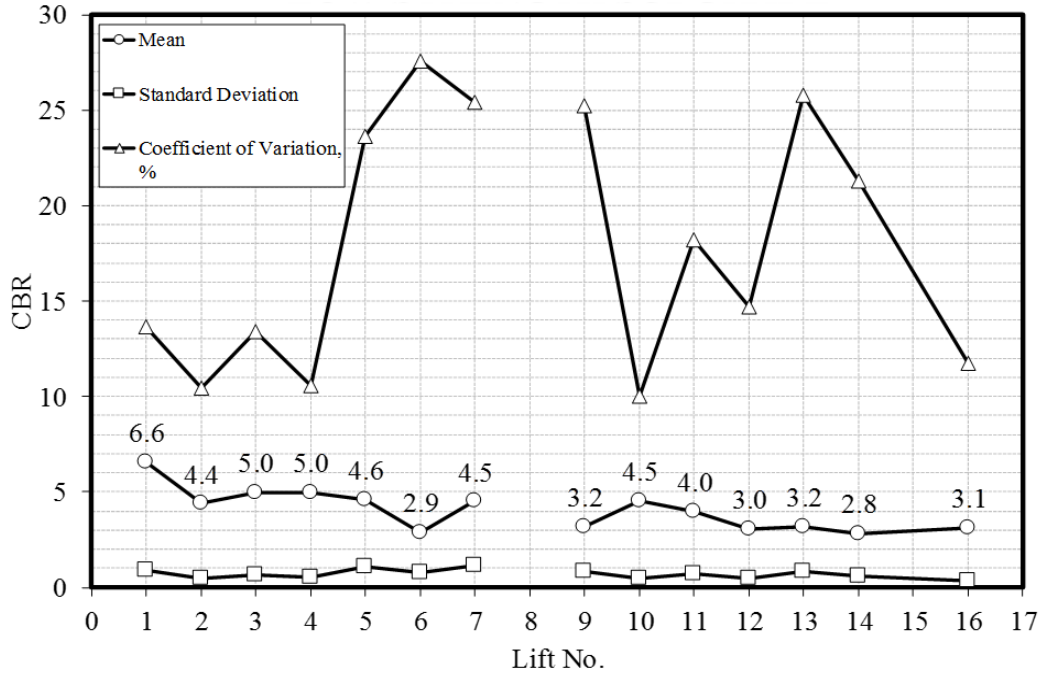


Figure A-1. CBR Summary for Low Strength Subgrade (Garg 1999)

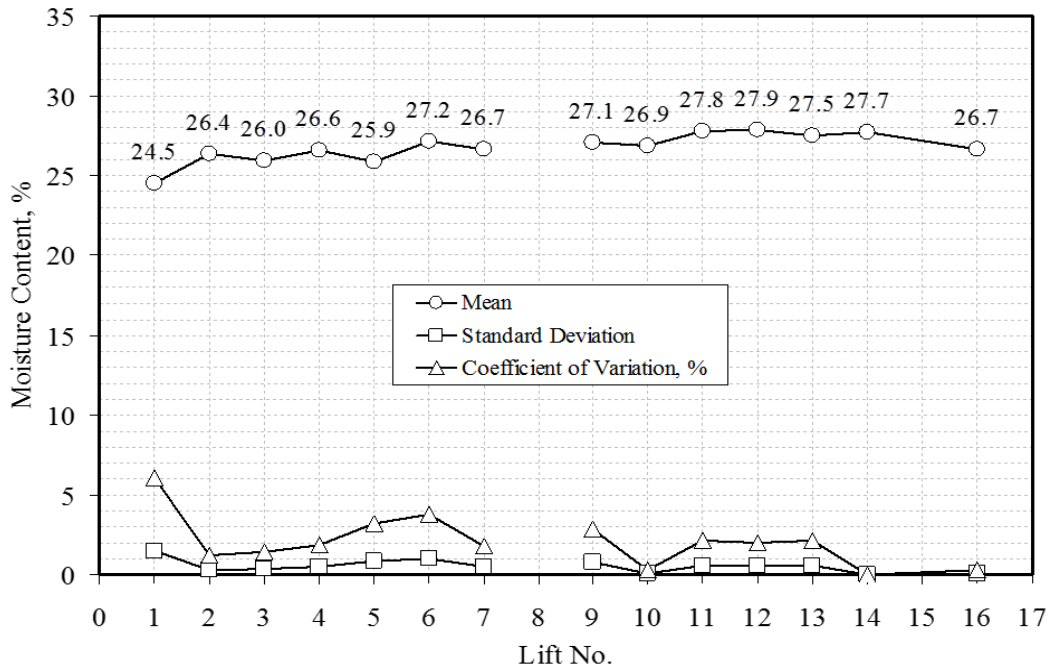


Figure A-2. Moisture Content Summary for Low Strength Subgrade (Garg 1999)

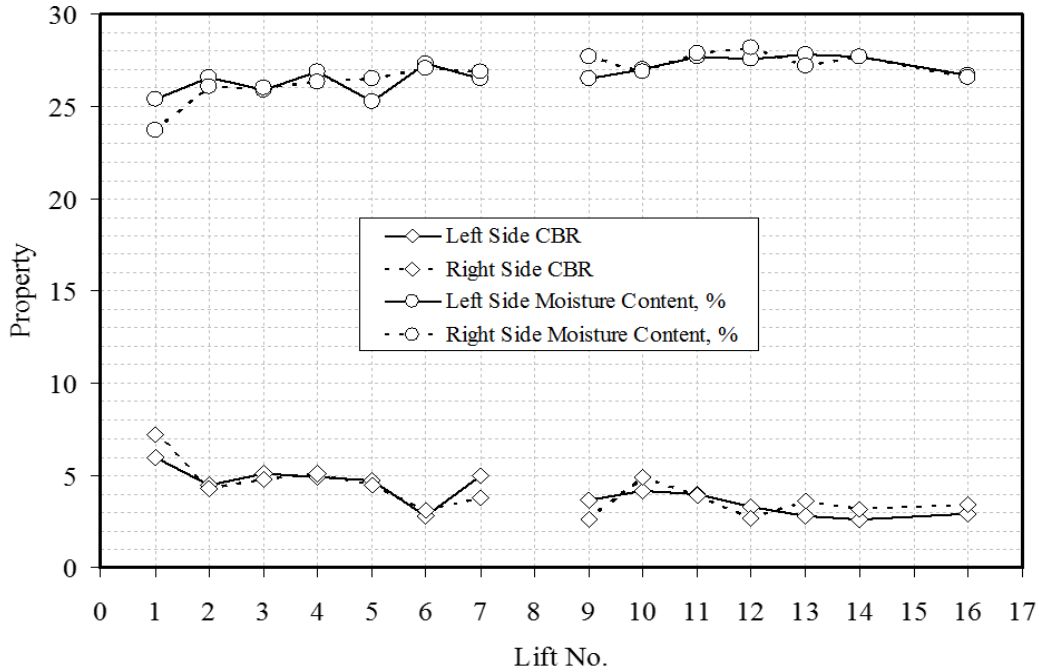


Figure A-3. CBR and Moisture Content on Either Side of CL for Low Strength Subgrade (Garg 1999)

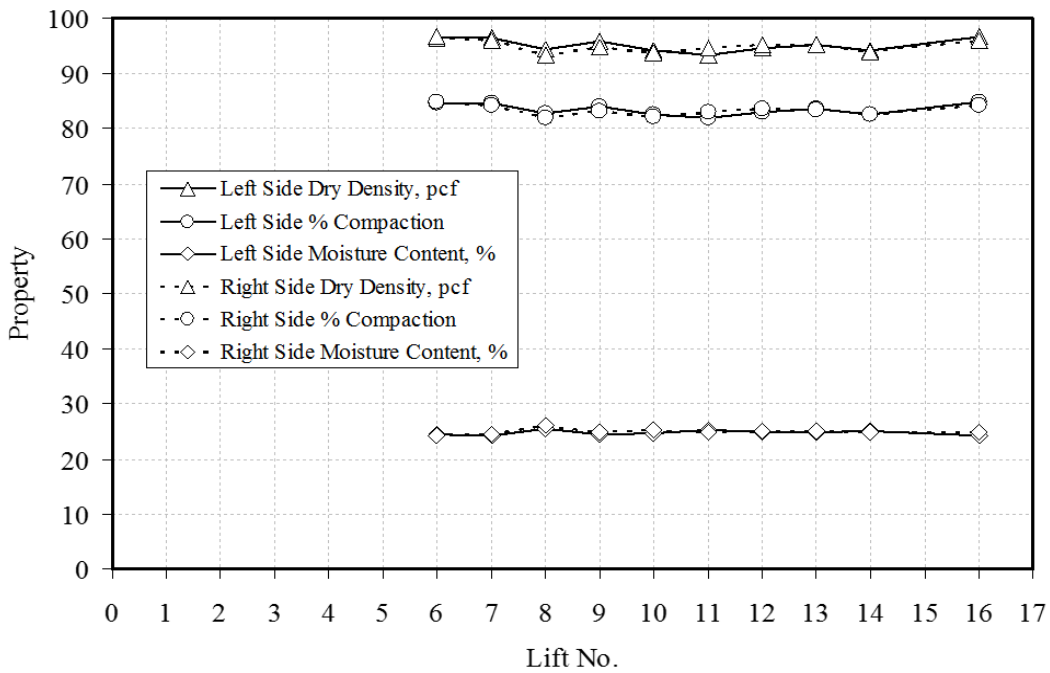


Figure A-4. Dry Density, Moisture Content and % Compaction on Either Side of CL for Low Strength Subgrade (Garg 1999)

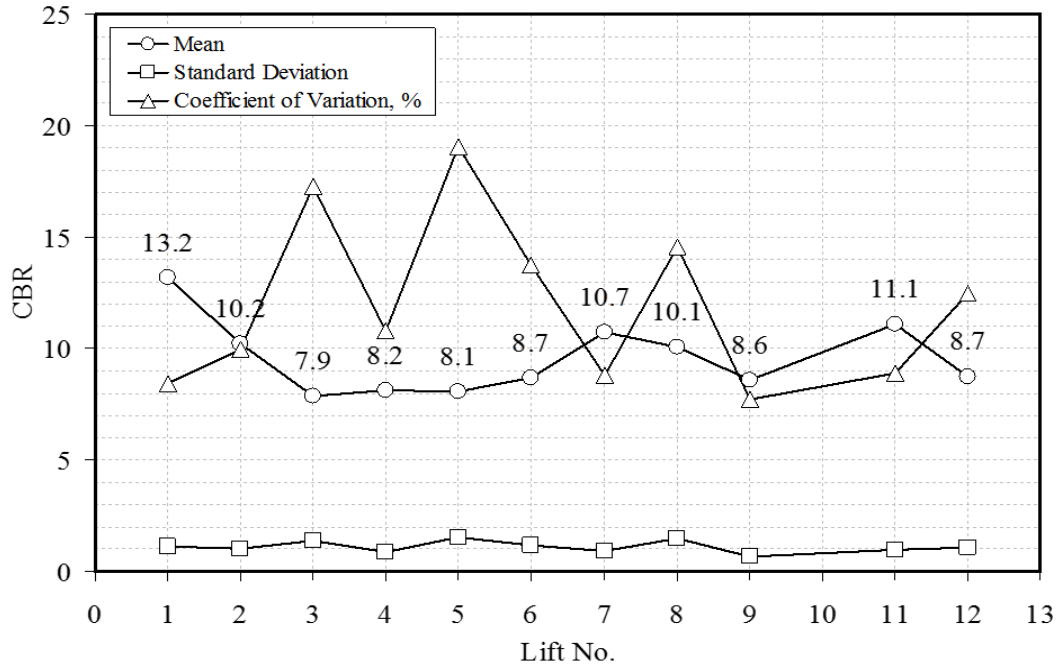


Figure A-5. CBR Summary for Medium Strength Subgrade (Garg 1999)

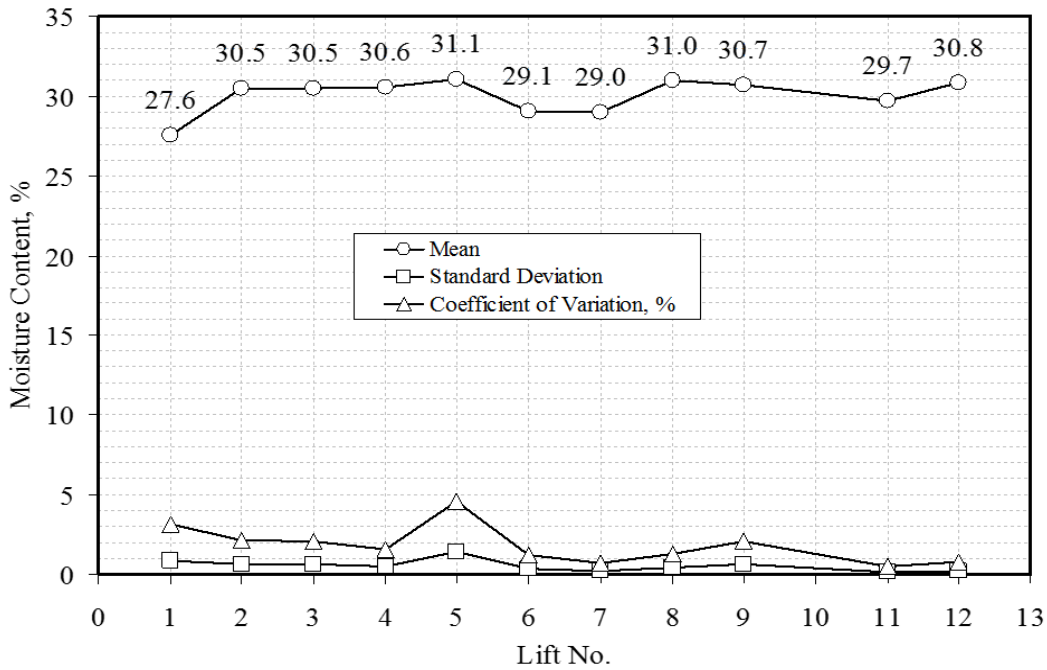


Figure A-6. Moisture Content Summary for Medium Strength Subgrade (Garg 1999)

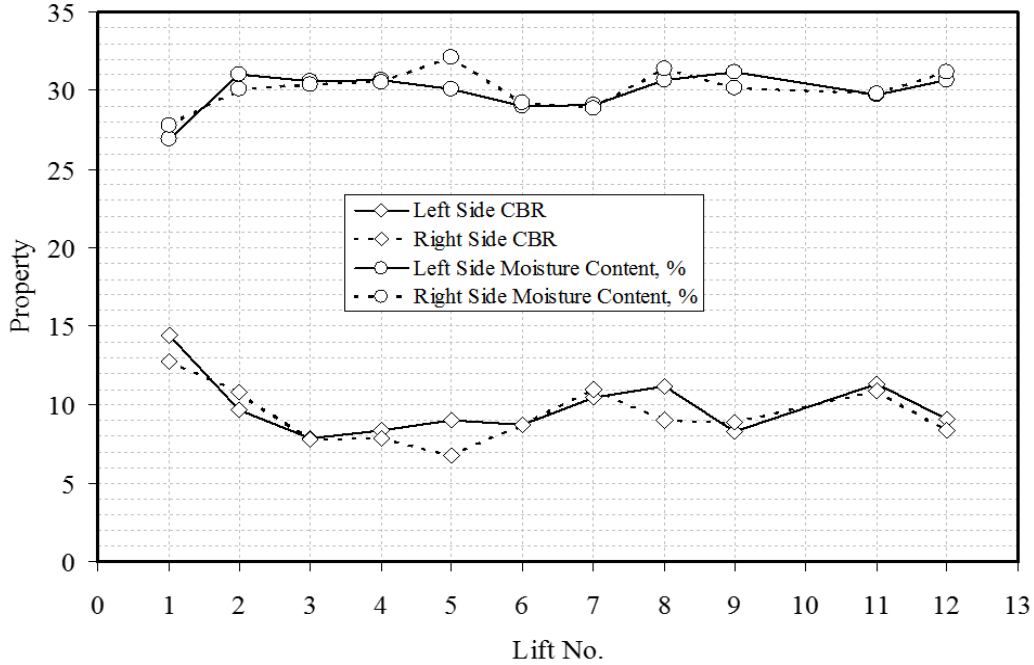


Figure A-7. CBR and Moisture Content on Either Side of CL for Medium Strength Subgrade (Garg 1999)

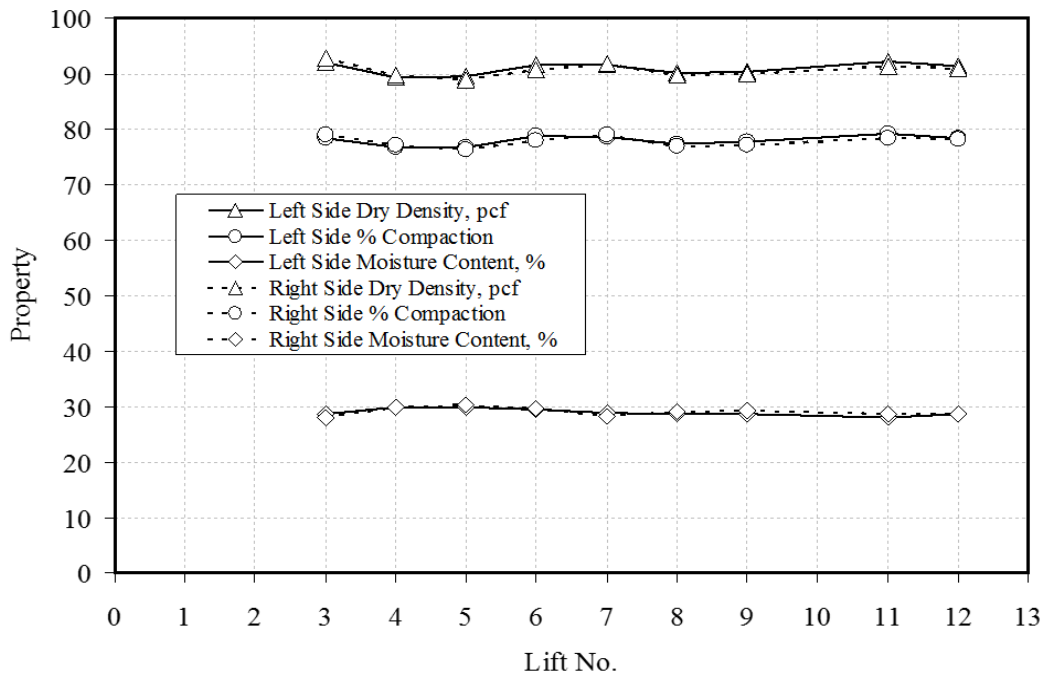


Figure A-8. Dry Density, Moisture Content and % Compaction on Either Side of CL for Medium Strength Subgrade (Garg 1999)

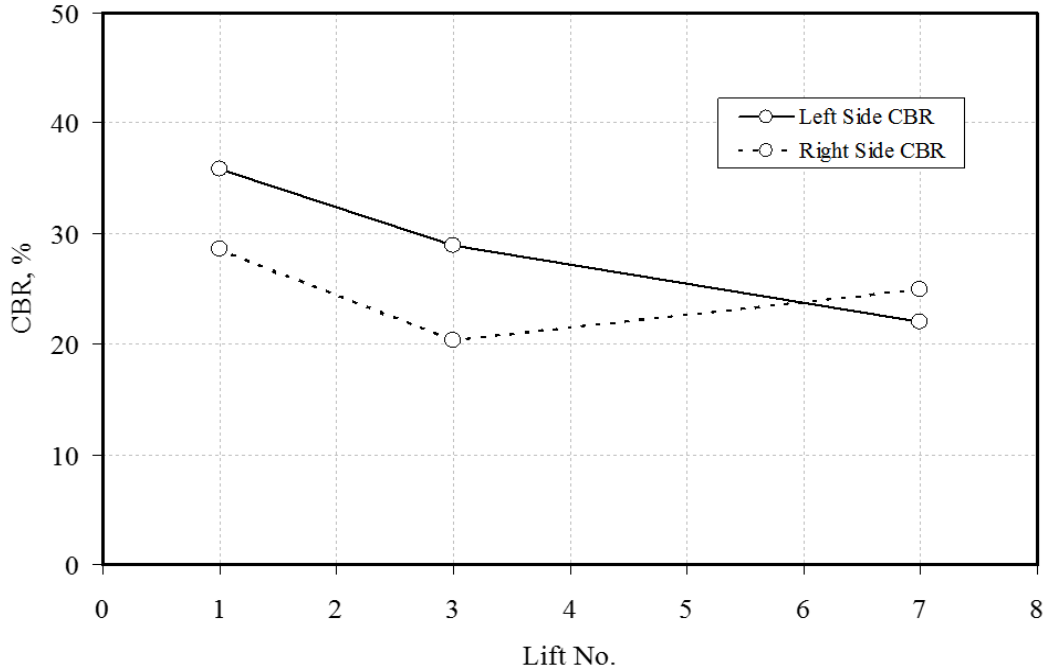


Figure A-9. CBR Summary for High Strength Subgrade (Garg 1999)

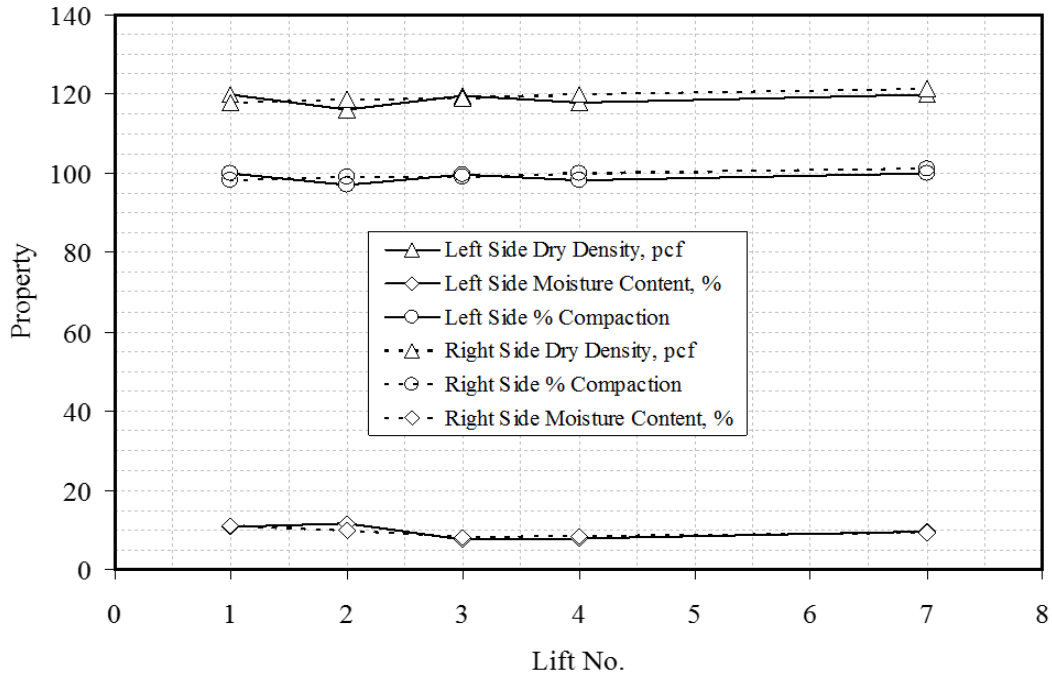


Figure A-10. Dry Density, Moisture Content and % Compaction on Either Side of CL for High Strength Subgrade (Garg 1999)

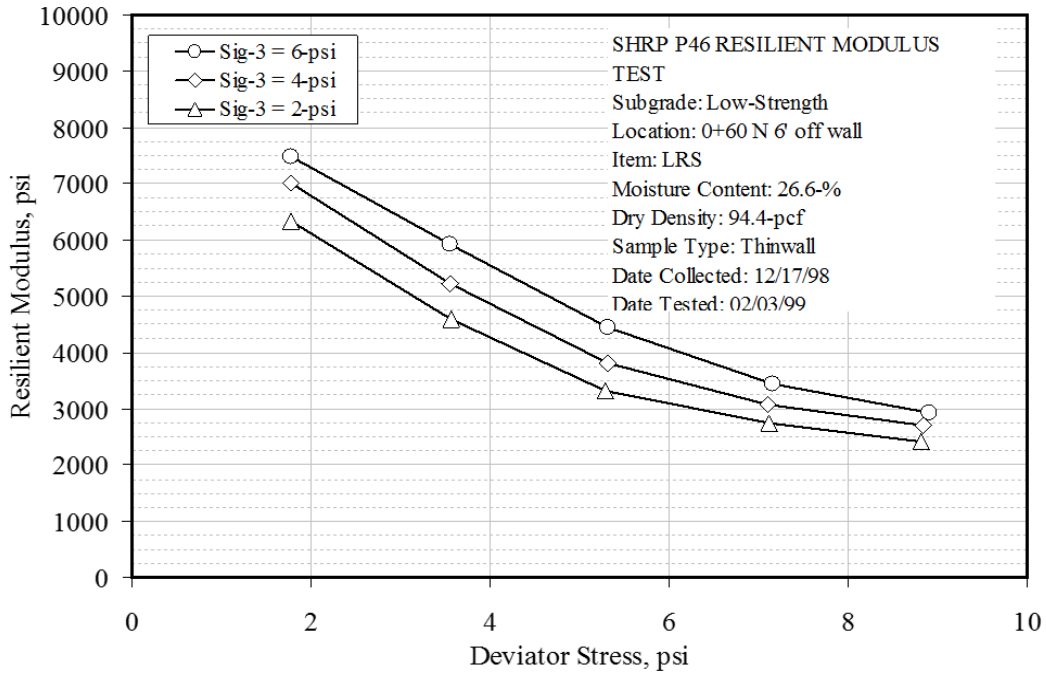


Figure A-11. Resilient Modulus Test Results for Low Strength Subgrade-LRS (Garg 1999)

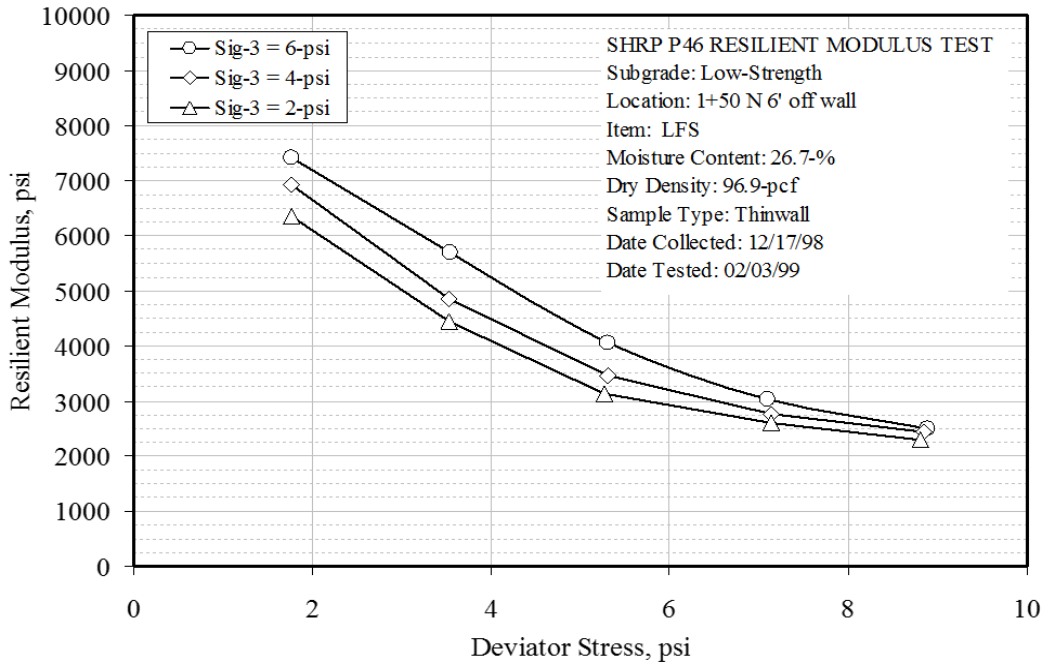


Figure A-12. Resilient Modulus Test Results for Low Strength Subgrade-LFS (Garg 1999)

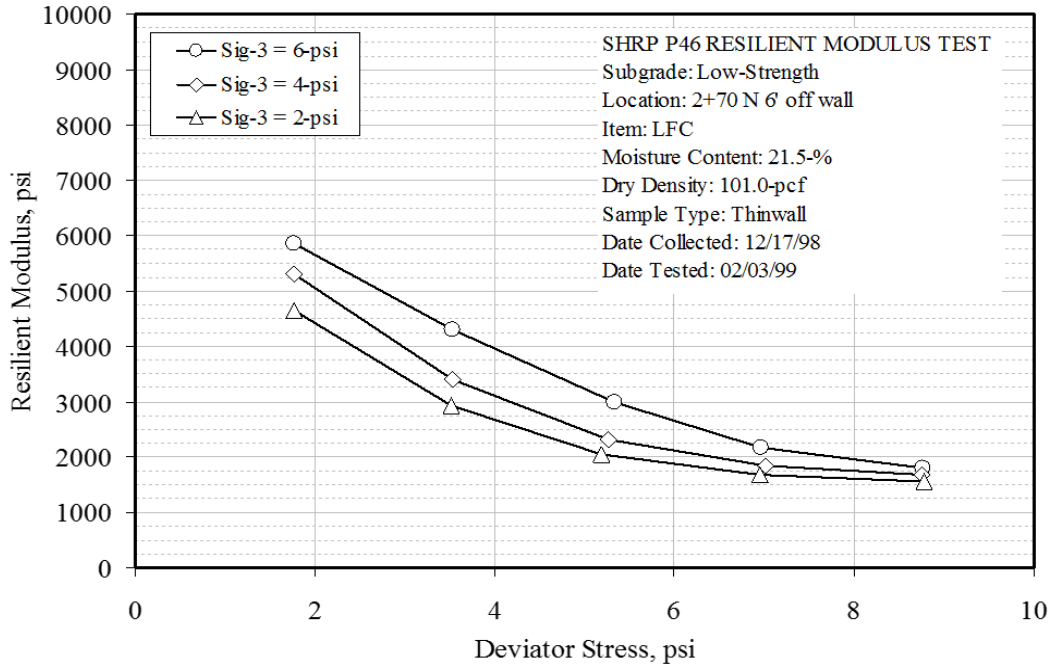


Figure A-13. Resilient Modulus Test Results for Low Strength Subgrade-LFC (Garg 1999)

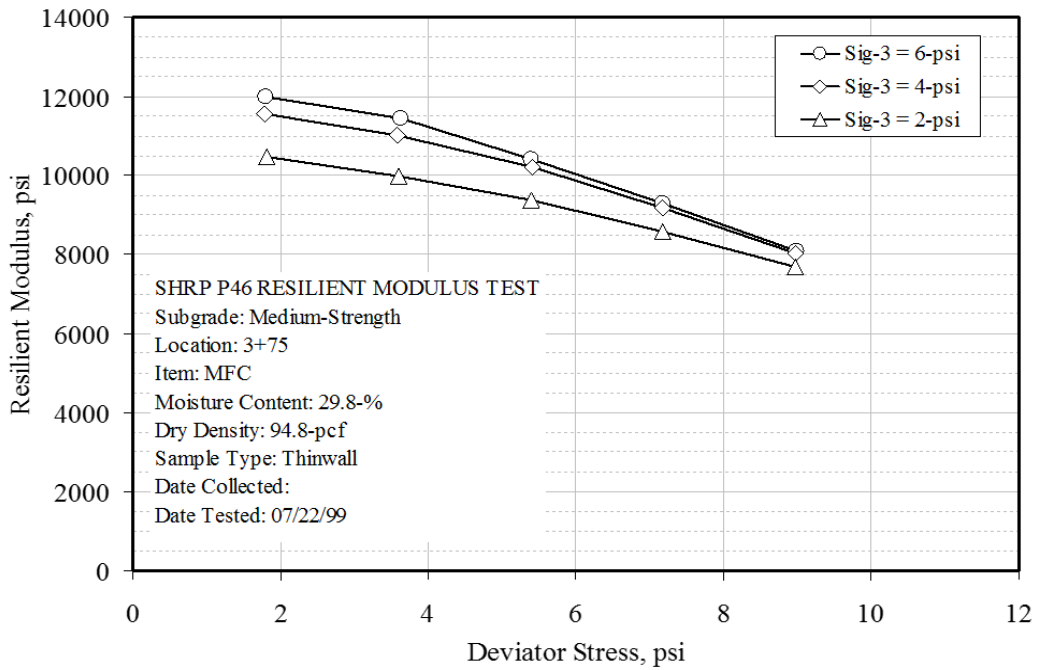


Figure A-14. Resilient Modulus Test Results for Medium Strength Subgrade-MFC (Garg 1999)

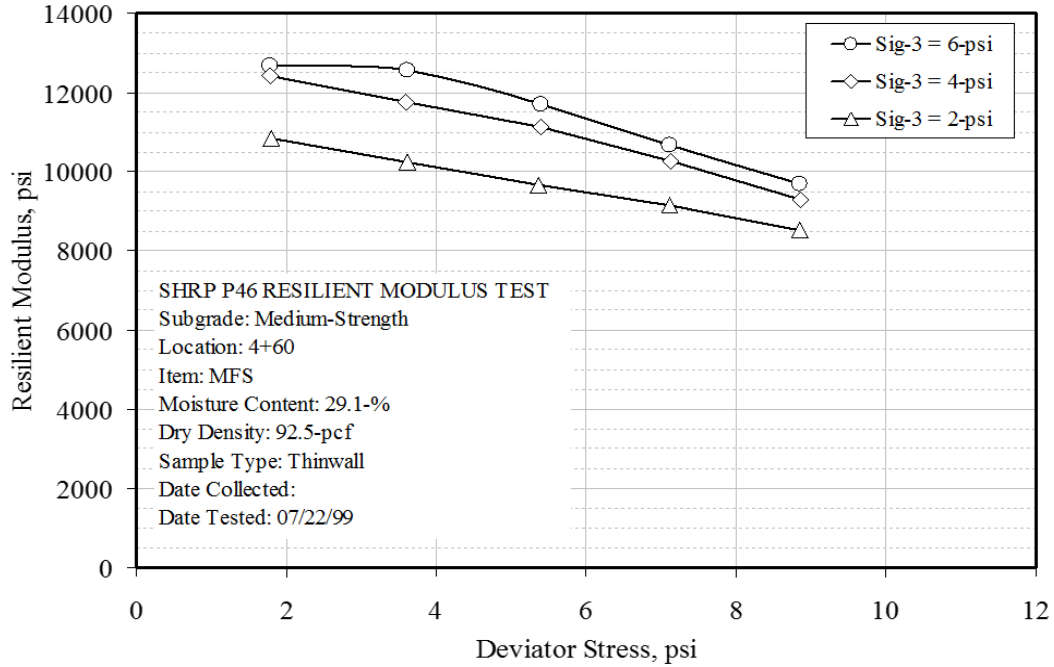


Figure A-15. Resilient Modulus Test Results for Medium Strength Subgrade-MFS (Garg 1999)

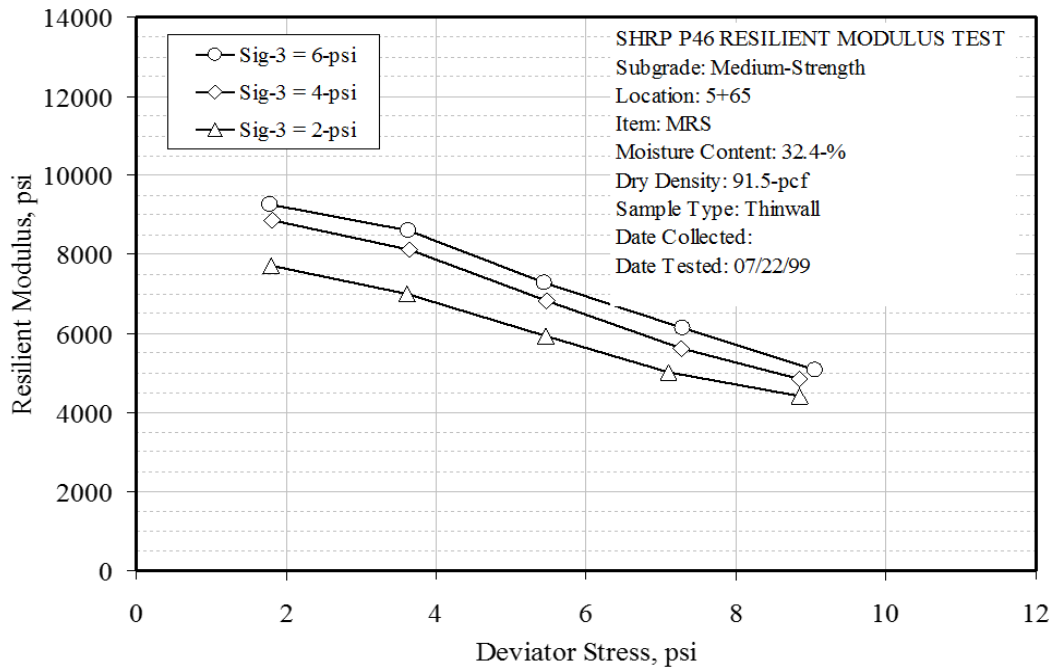


Figure A-16. Resilient Modulus Test Results for Medium Strength Subgrade-MRS (Garg 1999)

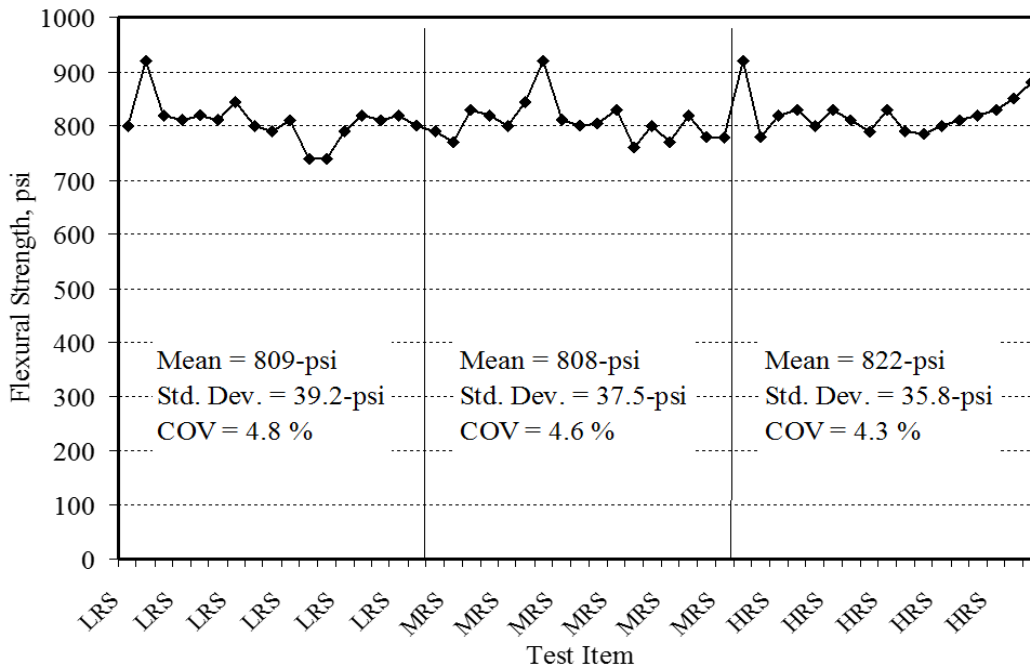


Figure A-17. 28-Day Flexural Strength Test Results for P-501 PCC Surface

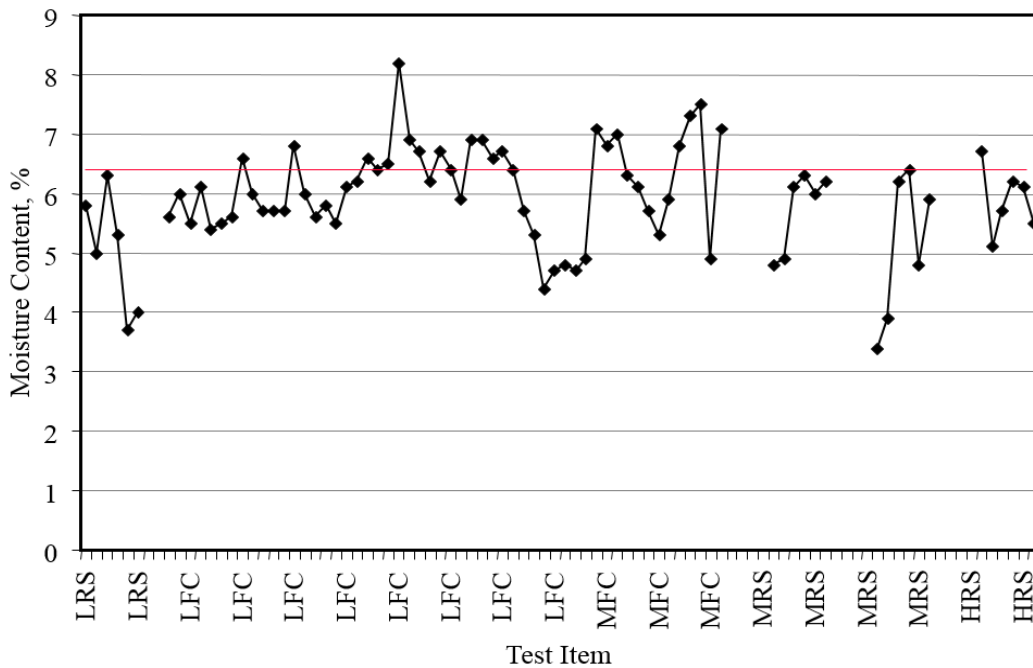


Figure A-18. Moisture Content for P-154 Subbase Material (Garg 1999)

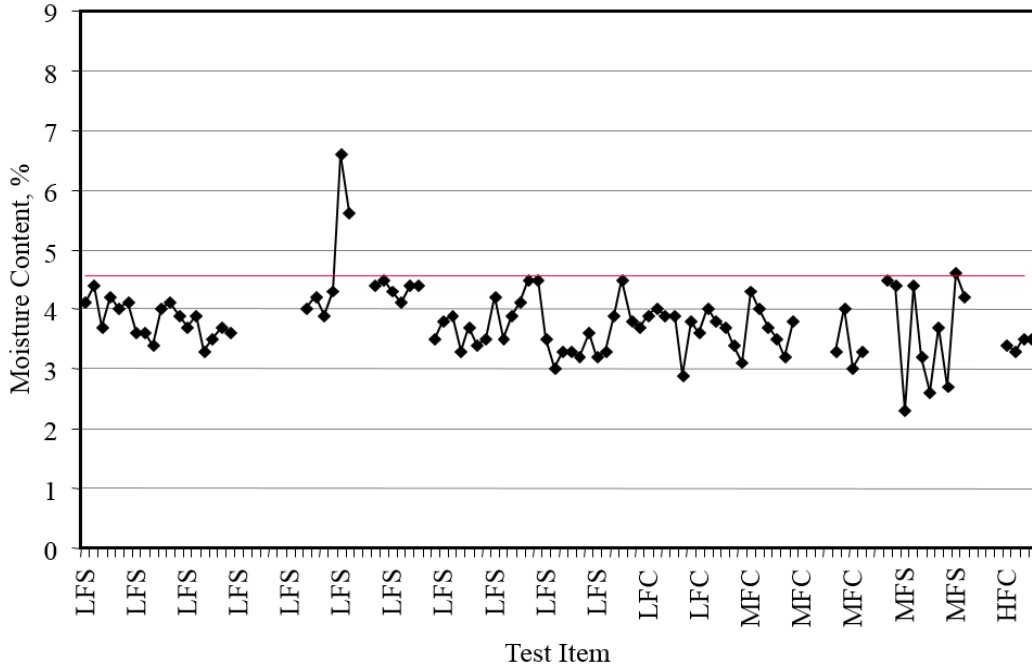


Figure A-19. Moisture Content for P-209 Base Material (Garg 1999)

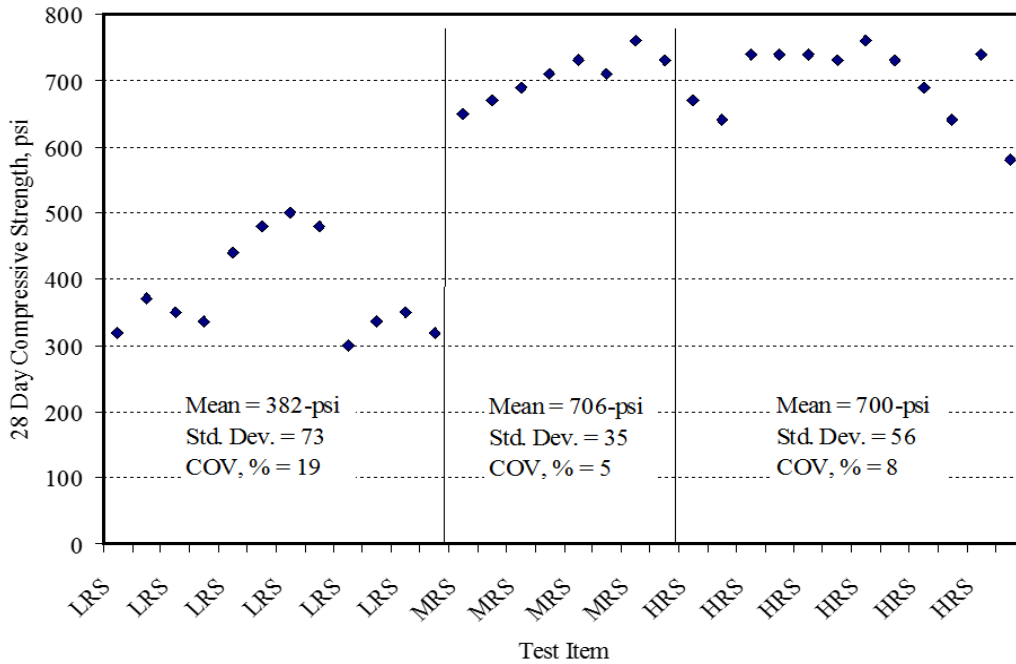


Figure A-20. 28-day Compressive Strength Test Results for P-306 Econocrete (Garg 1999)

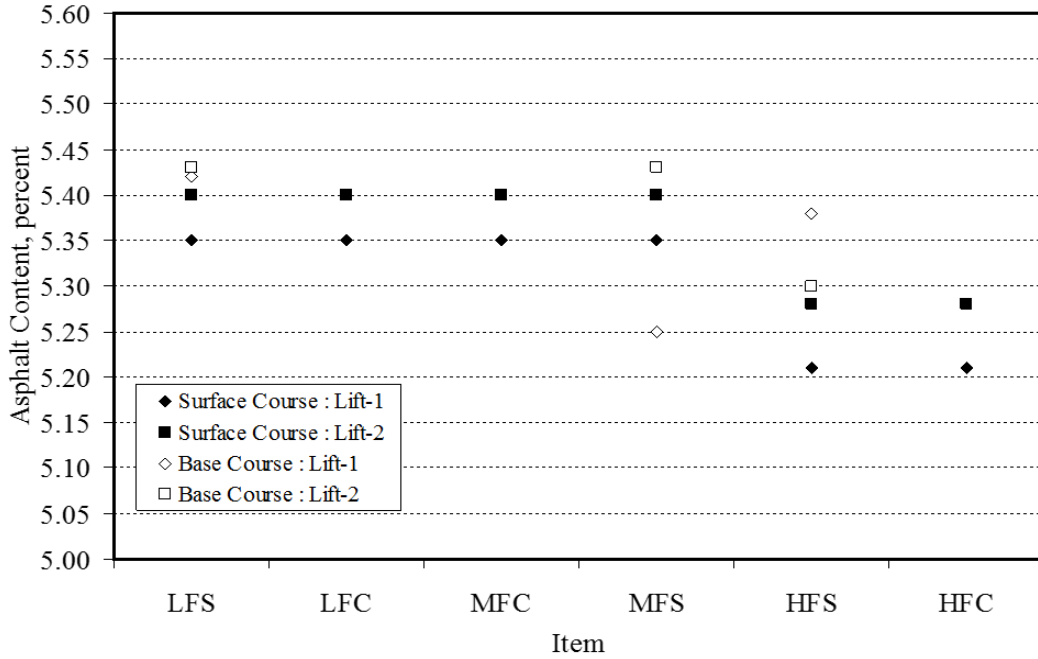


Figure A-21. P-401 Asphalt Content

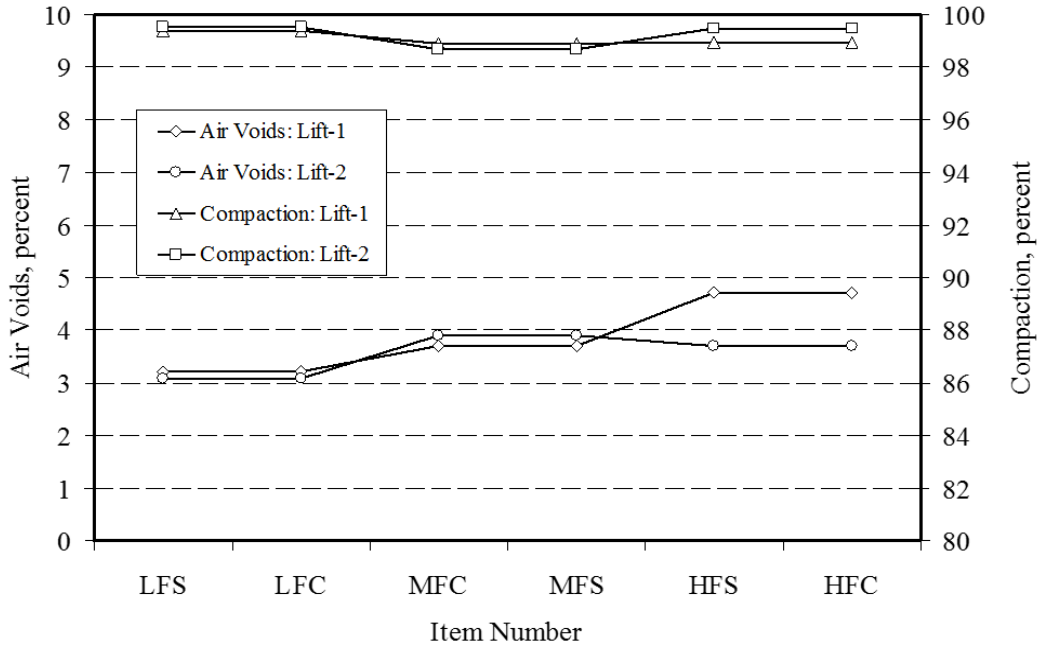


Figure A-22. P-401 AC Air Voids and % Compaction

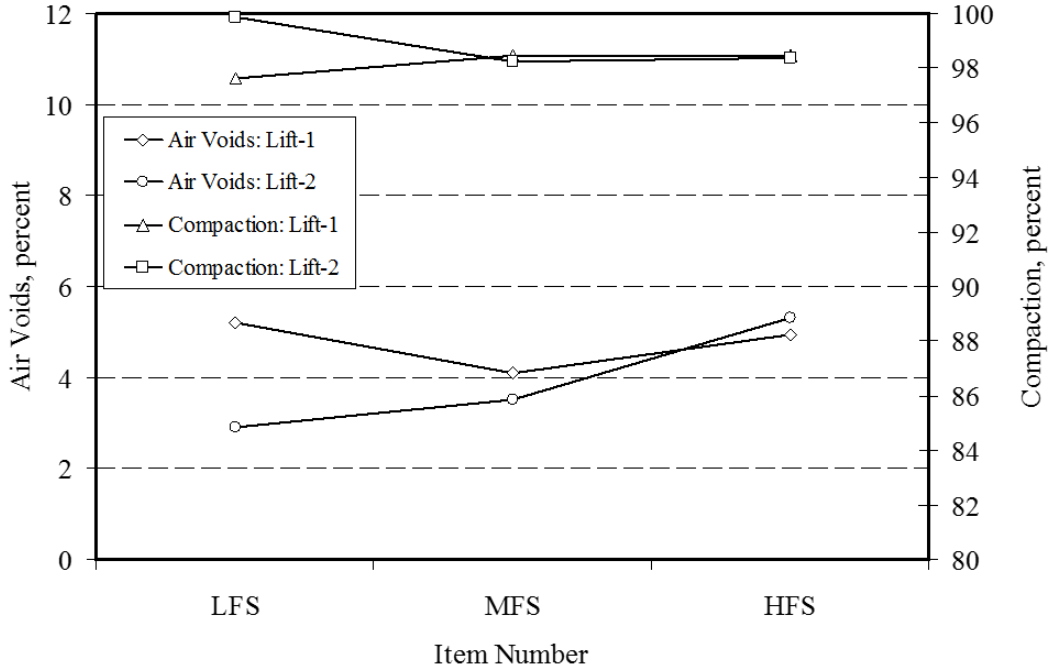


Figure A-23. P-401 Base Air Voids and % Compaction

APPENDIX B—STATIC SENSOR TYPES AND LOCATIONS

Sensor Name	Sensor Type	Location_x (ft.)	Location_y (ft.)	Location_z (ft.)
MG1	Moisture presently in place	50.0	0.0	2.333
MG2	Moisture presently in place	162.5	-10.0	
T1-A	Thermistor	90.0	29.5	0.042
T1-B	Thermistor	90.0	29.5	0.292
T1-C	Thermistor	90.0	29.5	0.625
T1-D	Thermistor	90.0	29.5	0.875
T2-A	Thermistor	92.0	22.0	0.042
T2-B	Thermistor	92.0	22.0	0.292
T2-C	Thermistor	92.0	22.0	0.625
T2-D	Thermistor	92.0	22.0	0.875
T4-A	Thermistor	92.0	-2.0	0.042
T4-B	Thermistor	92.0	-2.0	0.292
T4-C	Thermistor	92.0	-2.0	0.625
T4-D	Thermistor	92.0	-2.0	0.875
RG-9	resistance crack indicator			
RG-10	resistance crack indicator			
RG-11	resistance crack indicator			
RG-12	resistance crack indicator			
RG-13	resistance crack indicator			
RG-14	resistance crack indicator			
VSG-1	Vibrating Wire SG	92.0	10.5	0.125
VW THERM1	VWSG-Thermistor			
VSG-2	Vibrating Wire SG	92.0	10.5	0.792
VW THERM2	VWSG-Thermistor			
T5-A	Thermistor	39.0	19.0	0.042
T5-B	Thermistor	39.0	19.0	0.292
T5-C	Thermistor	39.0	19.0	0.625
T5-D	Thermistor	39.0	19.0	0.875
T6-A	Thermistor	39.0	1.0	0.042
T6-B	Thermistor	39.0	1.0	0.292
T6-C	Thermistor	39.0	1.0	0.625
T6-D	Thermistor	39.0	1.0	0.875

Sensor Name	Sensor Type	Location_x (ft.)	Location_y (ft.)	Location_z (ft.)
T7-A	Thermistor	7.5	2.5	0.042
T7-B	Thermistor	7.5	2.5	0.292
T7-C	Thermistor	7.5	2.5	0.625
T7-D	Thermistor failed before placement	7.5	2.5	0.875
T3-A	Thermistor	7.5	17.5	0.042
T3-B	Thermistor	7.5	17.5	0.292
T3-C	Thermistor	7.5	17.5	0.625
T3-D	Thermistor	7.5	17.5	0.875
T8	Thermistor above blanket			
T9	Thermistor above Burlap			
T10	Thermistor above Burlap			

APPENDIX C—DYNAMIC SENSOR TYPES AND LOCATIONS

Sensor Name	Test Item	Sensor Type	Location_X (ft.)	Location_Y (ft.)	Location_Z (in.)
JG-1	LRS	Joint Gage	20.00	-26.00	4.19
JG-9			20.00	26.00	4.75
CSG-225		Concrete Strain	21.00	-10.25	1.50
CSG-205			21.00	-10.25	9.50
CSG-297			21.00	10.25	1.50
CSG-300			21.00	10.25	9.50
CSG-235			24.00	-10.25	1.50
CSG-214			24.00	-10.25	9.50
CSG-288			24.00	10.25	1.50
CSG-282			24.00	10.25	9.50
CSG-230			27.00	-10.25	1.50
CSG-231			27.00	-10.25	9.50
CSG-315			27.00	10.25	1.50
CSG-293			27.00	10.25	9.50
CSG-206			30.00	-10.25	1.50
CSG-234			30.00	-12.00	1.50
CSG-208			30.00	-14.00	1.50
CSG-270			30.00	-16.00	1.50
CSG-222			30.00	-18.00	1.50
CSG-226			30.00	-20.00	1.50
CSG-213			30.00	-10.25	9.50
CSG-228			30.00	-12.00	9.50
CSG-221			30.00	-14.00	9.50
CSG-244			30.00	-16.00	9.50
CSG-236			30.00	-18.00	9.50
CSG-229			30.00	-20.00	9.50
CSG-384			30.00	10.25	1.50
CSG-296			30.00	12.00	1.50
CSG-375			30.00	14.00	1.50
CSG-386			30.00	16.00	1.50
CSG-357	30.00	18.00	1.50		
CSG-374	30.00	20.00	1.50		
CSG-283	30.00	10.25	9.50		
CSG-299	30.00	12.00	9.50		

Sensor Name	Test Item	Sensor Type	Location_X (ft.)	Location_Y (ft.)	Location_Z (in.)
CSG-379			30.00	14.00	9.50
CSG-368			30.00	16.00	9.50
CSG-359			30.00	18.00	9.50
CSG-360			30.00	20.00	9.50
CSG-233			33.00	-10.25	1.50
CSG-223			33.00	-10.25	9.50
CSG-303			33.00	10.25	1.50
CSG-366			33.00	10.25	9.50
CSG-204			36.00	-10.25	1.50
CSG-209			36.00	-10.25	9.50
CSG-308			36.00	10.25	1.50
CSG-218			36.86	-10.84	9.50
CSG-382			36.86	10.84	9.50
CSG-276			37.19	-11.63	9.50
CSG-391			37.19	11.63	9.50
CSG-216			37.70	-12.30	9.50
CSG-390			37.70	12.30	9.50
CSG-232			38.37	-12.81	9.50
CSG-394			38.38	12.81	9.50
CSG-274			39.00	-10.25	1.50
CSG-239			39.00	-10.25	9.50
CSG-295			39.00	10.25	1.50
CSG-361			39.00	10.25	9.50
CSG-272			39.16	-13.14	9.50
CSG-392			39.16	13.14	9.50
CSG-254			39.75	-12.00	1.50
CSG-252			39.75	-14.00	1.50
CSG-237			39.75	-16.00	1.50
CSG-224			39.75	-18.00	1.50
CSG-261			39.75	-20.00	1.50
CSG-251			39.75	-12.00	9.50
CSG-273			39.75	-14.00	9.50
CSG-258			39.75	-16.00	9.50
CSG-248			39.75	-18.00	9.50
CSG-278			39.75	-20.00	9.50
CSG-367			39.75	12.00	1.50

Sensor Name	Test Item	Sensor Type	Location_X (ft.)	Location_Y (ft.)	Location_Z (in.)
CSG-334			39.75	14.00	1.50
CSG-314			39.75	16.00	1.50
CSG-393			39.75	18.00	1.50
CSG-342			39.75	20.00	1.50
CSG-322			39.75	12.00	9.50
CSG-305			39.75	14.00	9.50
CSG-376			39.75	16.00	9.50
CSG-307			39.75	18.00	9.50
CSG-285			39.75	20.00	9.50
JG-2			Joint Gage	40.00	-26.00
JG-8		40.00		26.00	4.81
CSG-113		Concrete Strain	41.00	10.25	9.50
CSG-49			41.00	-10.25	1.50
CSG-71			41.00	-10.25	9.50
CSG-203			41.00	10.25	1.50
CSG-89			44.00	10.25	9.50
CSG-82			44.00	-10.25	1.50
CSG-29			44.00	-10.25	9.50
CSG-189			44.00	10.25	9.50
CSG-181			47.00	10.25	9.50
CSG-66			47.00	-10.25	1.50
CSG-51			47.00	-10.25	9.50
CSG-117			47.00	10.25	1.50
CSG-151			50.00	20.00	1.50
CSG-180			50.00	10.25	9.50
CSG-178			50.00	12.00	9.50
CSG-124			50.00	14.00	9.50
CSG-111			50.00	16.00	9.50
CSG-145			50.00	18.00	9.50
CSG-94			50.00	20.00	9.50
CSG-184			50.00	13.14	9.50
CSG-67			50.00	-10.25	1.50
CSG-85	50.00		-14.00	1.50	
CSG-27	50.00		-16.00	1.50	
CSG-77	50.00		-18.00	1.50	
CSG-28	50.00		-20.00	1.50	

Sensor Name	Test Item	Sensor Type	Location_X (ft.)	Location_Y (ft.)	Location_Z (in.)
CSG-46			50.00	-10.25	9.50
CSG-78			50.00	-12.00	9.50
CSG-84			50.00	-14.00	9.50
CSG-8			50.00	-16.00	9.50
CSG-79			50.00	-18.00	9.50
CSG-32			50.00	-20.00	9.50
CSG-186			50.00	10.25	1.50
CSG-165			50.00	12.00	1.50
CSG-101			50.00	14.00	1.50
CSG-202			50.00	16.00	1.50
CSG-99			50.00	18.00	1.50
CSG-93			53.00	10.25	9.50
CSG-58			53.00	-10.25	1.50
CSG-62			53.00	-10.25	9.50
CSG-185			53.00	10.25	1.50
CSG-201			56.00	10.25	9.50
CSG-73			56.00	-10.25	1.50
CSG-43			56.00	-10.25	9.50
CSG-136			56.00	10.25	1.50
CSG-123			56.86	10.84	9.50
CSG-69			56.86	-10.84	9.50
CSG-179			57.19	11.63	9.50
CSG-42			57.19	-11.63	9.50
CSG-129			57.70	12.30	9.50
CSG-65			57.70	-12.30	9.50
CSG-68			58.37	-12.81	9.50
CSG-140			58.38	12.81	9.50
CSG-150			59.00	10.25	9.50
CSG-59			59.00	-10.25	1.50
CSG-60			59.00	-10.25	9.50
CSG-188			59.00	10.25	1.50
CSG-53			59.16	-13.14	9.50
CSG-157			59.75	12.00	1.50
CSG-162			59.75	14.00	1.50
CSG-91			59.75	16.00	9.50
CSG-112			59.75	18.00	1.50

Sensor Name	Test Item	Sensor Type	Location_X (ft.)	Location_Y (ft.)	Location_Z (in.)
CSG-146			59.75	20.00	1.50
CSG-147			59.75	12.00	9.50
CSG-155			59.75	14.00	9.50
CSG-127			59.75	16.00	9.50
CSG-119			59.75	18.00	9.50
CSG-154			59.75	20.00	9.50
CSG-39			59.75	-12.00	1.50
CSG-38			59.75	-12.00	9.50
CSG-35			59.75	-16.00	1.50
CSG-80			59.75	-18.00	1.50
CSG-24			59.75	-20.00	1.50
CSG-54			59.75	-12.00	9.50
CSG-48			59.75	-14.00	9.50
CSG-31			59.75	-16.00	9.50
CSG-72			59.75	-18.00	9.50
CSG-3			59.75	-20.00	9.50
JG-3				Joint Gage	60.00
JG-7	60.00	26.00			4.75
JG-4	80.00	-26.00			4.69
JG-5	80.00	0.00			5.19
JG-6	80.00	26.00			4.75
NW MDD - 1	LFS	Deflection	150.38	-15.00	124.75
NW MDD - 2			150.38	-15.00	67.25
NW MDD - 3			150.38	-15.00	55.25
NW MDD - 4			150.38	-15.00	46.25
NW MDD - 5			150.38	-15.00	40.25
NW MDD - 6			150.38	-15.00	38.25
NW MDD - 7			150.38	-15.00	9.75
CL MDD - 1			150.38	0.00	124.75
CL MDD - 2			150.38	0.00	67.25
CL MDD - 3			150.38	0.00	55.25
CL MDD - 4			150.38	0.00	46.25
CL MDD - 5			150.38	0.00	40.25
CL MDD - 6			150.38	0.00	38.25
CL MDD - 7			150.38	0.00	9.75
SW MDD - 1			150.38	15.00	124.25

Sensor Name	Test Item	Sensor Type	Location_X (ft.)	Location_Y (ft.)	Location_Z (in.)		
SW MDD - 2			150.38	15.00	66.75		
SW MDD - 3			150.38	15.00	54.75		
SW MDD - 4			150.38	15.00	45.75		
SW MDD - 5			150.38	15.00	39.75		
SW MDD - 6			150.38	15.00	37.75		
SW MDD - 7			150.38	15.00	9.25		
NE MDD - 1			174.63	-15.00	124.75		
NE MDD - 2			174.63	-15.00	46.25		
NE MDD - 3			174.63	-15.00	40.25		
NE MDD - 4			174.63	-15.00	35.75		
NE MDD - 5			174.63	-15.00	24.25		
NE MDD - 7			174.63	-15.00	9.75		
NE MDD - 6			174.63	-15.00	15.75		
SE MDD - 1			174.63	15.00	124.88		
SE MDD - 2			174.63	15.00	46.38		
SE MDD - 3			174.63	15.00	40.38		
SE MDD - 4			174.63	15.00	35.88		
SE MDD - 5			174.63	15.00	24.38		
SE MDD - 6			174.63	15.00	15.88		
SE MDD - 7			174.63	15.00	9.88		
LSNW			2 inch Pressure	143.00	-15.00	41.75	
LSSW				143.24	15.00	40.00	
LSNE				145.62	-15.00	42.25	
LSSE				145.62	15.00	41.50	
LSNTH1				147.00	-15.00	40.75	
LSST-H1				147.00	15.00	41.00	
LSBN1				6 inch Pressure	148.00	-15.00	7.25
LSBN2					148.00	-12.69	7.25
LSBC					148.00	0.00	7.25
LSBS2					148.00	12.71	7.25
LSBS1			148.00		15.00	7.25	
LSSN1			148.00		-15.00	12.00	
LSSN2			148.00		-12.71	12.00	
LSSC			148.00		0.00	11.75	
LSSS2			148.00		12.71	12.00	
LSSS1	148.00	15.00	11.75				

Sensor Name	Test Item	Sensor Type	Location_X (ft.)	Location_Y (ft.)	Location_Z (in.)
LSNT-V		2 inch Pressure	148.00	-15.00	42.25
LSNTH2			148.00	-14.00	41.50
LSNM			148.00	-15.00	90.75
LSNB			148.00	-15.00	134.00
LSST-V			148.00	15.00	41.25
LSST-H2			148.00	14.00	41.50
LSSM			148.00	15.00	93.50
LSSB			148.00	15.00	133.00
LBS4			Asphalt Strain	152.75	-15.00
LBS5		152.75		-12.71	9.50
LBS6		152.75		-10.42	9.50
LBS7		152.75		10.42	9.50
LBS8		152.75		12.71	9.50
LBS9		152.75		15.00	9.50
LSS4		152.76		-15.00	4.50
LSS5		152.76		-12.71	4.50
LSS6		152.76		-10.42	4.50
LSS7		152.76		10.42	4.50
LSS8		152.76		12.71	4.50
LSS9		152.76		15.00	4.50
LBS3		155.13		-15.00	9.50
LBS10		155.13		15.00	9.50
LSS3		155.14		-15.00	4.50
LSS10		155.14		15.00	4.50
LBS11		157.5		15.00	9.50
LBS2		157.51		-15.00	9.50
LSS2		157.51		-15.00	4.50
LSS11		157.51		15.00	4.50
LBS1		159.88	-15.00	9.50	
LBS12	159.88	15.00	9.50		
LSS1	159.89	-15.00	4.50		
LSS12	159.89	15.00	4.50		
NW MDD - 1	LFC	Deflection	250.38	-15.00	124.00
NW MDD - 2			250.38	-15.00	78.25
NW MDD - 3			250.38	-15.00	66.25
NW MDD - 4			250.38	-15.00	57.25

Sensor Name	Test Item	Sensor Type	Location_X (ft.)	Location_Y (ft.)	Location_Z (in.)	
NW MDD - 5			250.38	-15.00	51.25	
NW MDD - 6			250.38	-15.00	49.00	
NW MDD - 7			250.38	-15.00	12.25	
CL MDD - 1			250.38	0.00	124.50	
CL MDD - 5			250.38	0.00	51.25	
CL MDD - 2			250.38	0.00	78.25	
CL MDD - 3			250.38	0.00	66.25	
CL MDD - 4			250.38	0.00	57.25	
CL MDD - 6			250.38	0.00	49.50	
CL MDD - 7			250.38	0.00	12.25	
SW MDD - 1			250.38	15.00	124.50	
SW MDD - 6			250.38	15.00	49.50	
SW MDD - 2			250.38	15.00	78.25	
SW MDD - 3			250.38	15.00	66.25	
SW MDD - 4			250.38	15.00	57.25	
SW MDD - 5			250.38	15.00	51.25	
SW MDD - 7			250.38	15.00	12.25	
NE MDD - 1			274.63	-15.00	124.25	
NE MDD - 2			274.63	-15.00	57.25	
NE MDD - 3			274.63	-15.00	51.75	
NE MDD - 4			274.63	-15.00	45.75	
NE MDD - 5			274.63	-15.00	30.75	
NE MDD - 6			274.63	-15.00	19.75	
NE MDD - 7			274.63	-15.00	12.25	
SE MDD - 1			274.63	15.00	124.50	
SE MDD - 2			274.63	15.00	57.25	
SE MDD - 3			274.63	15.00	51.75	
SE MDD - 4			274.63	15.00	45.75	
SE MDD - 5			274.63	15.00	30.75	
SE MDD - 6			274.63	15.00	20.00	
SE MDD - 7			274.63	15.00	12.25	
LCNW			2 inch Pressure	243.24	-15.00	52.25
LCSW				243.24	15.00	51.13
LCNE				245.62	-15.00	53.00
LSCE				245.62	15.00	51.38
LCNT-H1	247.00	-15.00		51.50		

Sensor Name	Test Item	Sensor Type	Location_X (ft.)	Location_Y (ft.)	Location_Z (in.)	
LCST-H1			247.00	15.00	50.50	
LCBN1		6 inch Pressure	248.00	15.00	7.25	
LCBN2			248.00	12.71	7.25	
LCBC			248.00	0.00	7.50	
LCBS2			248.00	-12.71	7.75	
LCBS1			248.00	-15.00	7.50	
LCSN1			248.00	-15.00	14.25	
LCSN2			248.00	-12.71	14.25	
LCSC			248.00	0.00	15.38	
LCSS2			248.00	12.71	15.50	
LCSS1			248.00	15.00	15.25	
LCNT-V			2 inch Pressure	248.00	-15.00	51.88
LCNT-H2				248.00	-14.00	51.50
LCNM		248.00		-15.00	92.88	
LCNB		248.00		-15.00	131.50	
LCST-V		248.00		15.00	51.00	
LCST-H2		248.00		14.00	50.50	
LCSM		248.00		15.00	92.88	
LCSB		248.00		-15.00	133.50	
LSC4		Asphalt Strain		252.76	-15.00	4.50
LSC5				252.76	-12.71	4.50
LSC6			252.76	-10.42	4.50	
LSC7			252.76	10.42	4.50	
LSC8			252.76	12.71	4.50	
LSC9			252.76	15.00	4.50	
LSC3			255.14	-15.00	4.50	
LSC10			255.14	15.00	4.50	
LSC2			257.51	-15.00	4.50	
LSC11			257.51	15.00	4.50	
LSC1			259.89	-15.00	4.50	
LSC12			259.89	15.00	4.50	
NW MDD - 1		MFC	Deflection	345.38	-15.00	100.25
NW MDD - 2				345.38	-15.00	53.00
NW MDD - 3	345.38			-15.00	41.00	
NW MDD - 4	345.38			-15.00	32.00	
NW MDD - 5	345.38			-15.00	26.00	

Sensor Name	Test Item	Sensor Type	Location_X (ft.)	Location_Y (ft.)	Location_Z (in.)	
NW MDD - 6			345.38	-15.00	24.00	
NW MDD - 1			345.38	-15.00	100.25	
CL MDD - 1			345.38	0.00	100.13	
CL MDD - 2			345.38	0.00	53.13	
CL MDD - 3			345.38	0.00	41.13	
CL MDD - 4			345.38	0.00	32.13	
CL MDD - 5			345.38	0.00	26.13	
CL MDD - 6			345.38	0.00	24.13	
CL MDD - 7			345.38	0.00	12.13	
SW MDD - 1			345.38	15.00	100.15	
SW MDD - 2			345.38	15.00	53.25	
SW MDD - 3			345.38	15.00	41.25	
SW MDD - 5			345.38	15.00	26.25	
SW MDD - 4			345.38	15.00	32.25	
SW MDD - 6			345.38	15.00	24.25	
SW MDD - 7			345.38	15.00	12.25	
NE MDD - 1			367.13	-15.00	100.25	
NE MDD - 2			367.13	-15.00	32.25	
NE MDD - 4			367.13	-15.00	24.25	
NE MDD - 3			367.13	-15.00	26.25	
NE MDD - 5			367.13	-15.00	14.25	
NE MDD - 6			367.13	-15.00	12.25	
NE MDD - 7			367.13	-15.00	6.75	
SE MDD - 1			367.13	15.00	100.25	
SE MDD - 6			367.13	15.00	12.25	
SE MDD - 5			367.13	15.00	14.25	
SE MDD - 2			367.13	15.00	32.25	
SE MDD - 3			367.13	15.00	26.25	
SE MDD - 4			367.13	15.00	24.25	
SE MDD - 7			367.13	15.00	6.75	
MCNW			2 inch Pressure	338.24	-15.00	26.75
MCSW				338.74	15.00	25.75
MCNE				340.62	-15.00	26.75
MCSE				340.62	15.00	26.00
MCNT-H1				342.00	-15.00	27.50
MCST-H1	342.00	15.00		27.25		

Sensor Name	Test Item	Sensor Type	Location_X (ft.)	Location_Y (ft.)	Location_Z (in.)	
MCBN1		6 inch Pressure	343.00	-15.00	7.00	
MCBN2			343.00	-12.71	7.00	
MCBC			343.00	0.00	7.25	
MCBS2			343.00	12.71	7.00	
MCBS1			343.00	15.00	6.75	
MCSN1			343.00	-15.00	15.25	
MCSN2			343.00	-12.71	14.88	
MCSC			343.00	0.00	15.25	
MCSS2			343.00	12.71	16.00	
MCSS1			343.00	15.00	15.75	
MCNT-V			2 inch Pressure	343.00	-15.00	28.25
MCNT-H2				343.00	-14.00	28.50
MCNM				343.00	-15.00	74.00
MCNB				343.00	-15.00	112.63
MCST-V		343.00		15.00	27.50	
MCST-H2		343.00		14.00	27.75	
MCSM		343.00		15.00	71.50	
MCSB		343.00		15.00	114.38	
MSC4		Asphalt Strain	347.76	-15.00	4.50	
MSC5			347.76	-12.71	4.50	
MSC6			347.76	-10.42	4.50	
MSC7			347.76	10.42	4.50	
MSC8			347.76	12.71	4.50	
MSC9			347.76	15.00	4.50	
MSC3			350.14	-15.00	4.50	
MSC10			350.14	15.00	4.50	
MSC2			352.51	-15.00	4.50	
MSC11			352.51	15.00	4.50	
MSC1	354.89		-15.00	4.50		
MSC12	354.89		15.00	4.50		
NW MDD - 1	MFS	Deflection	432.88	-15.00	100.50	
NW MDD - 2			432.88	-15.00	46.50	
NW MDD - 3			432.88	-15.00	34.50	
NW MDD - 4			432.88	-15.00	25.50	
NW MDD - 5			432.88	-15.00	19.50	
NW MDD - 6			432.88	-15.00	17.50	

Sensor Name	Test Item	Sensor Type	Location_X (ft.)	Location_Y (ft.)	Location_Z (in.)	
NW MDD - 7			432.88	-15.00	9.50	
CL MDD - 1			432.88	0.00	99.75	
CL MDD - 2			432.88	0.00	45.75	
CL MDD - 3			432.88	0.00	33.75	
CL MDD - 4			432.88	0.00	24.75	
CL MDD - 5			432.88	0.00	18.75	
CL MDD - 6			432.88	0.00	16.75	
CL MDD - 7			432.88	0.00	8.75	
SW MDD - 1			432.88	15.00	100.13	
SW MDD - 2			432.88	15.00	46.13	
SW MDD - 3			432.88	15.00	34.13	
SW MDD - 4			432.88	15.00	25.13	
SW MDD - 5			432.88	15.00	19.13	
SW MDD - 6			432.88	15.00	17.13	
SW MDD - 7			432.88	15.00	9.13	
NE MDD - 1			454.63	-15.00	100.25	
NE MDD - 2			454.63	-15.00	25.25	
NE MDD - 3			454.63	-15.00	19.25	
NE MDD - 4			454.63	-15.00	17.25	
NE MDD - 5			454.63	-15.00	11.25	
NE MDD - 6			454.63	-15.00	9.25	
NE MDD - 7			454.63	-15.00	6.75	
SE MDD - 1			454.63	15.00	100.13	
SE MDD - 2			454.63	15.00	25.13	
SE MDD - 3			454.63	15.00	19.13	
SE MDD - 4			454.63	15.00	17.13	
SE MDD - 5			454.63	15.00	11.13	
SE MDD - 6			454.63	15.00	9.13	
SE MDD - 7			454.63	15.00	6.63	
MSNW			2 inch Pressure	425.74	-15.00	20.25
MSSW				425.74	15.00	20.25
MSNE				428.00	-15.00	19.00
MSSE				428.12	15.00	19.88
MSST-H1				429.50	15.00	20.25
MSNT-H1				429.75	-15.00	20.50
MSBN1	430.50	-15.00		7.25		

Sensor Name	Test Item	Sensor Type	Location_X (ft.)	Location_Y (ft.)	Location_Z (in.)
MSBN2		6 inch Pressure	430.50	-12.71	7.25
MSBC			430.50	0.00	7.25
MSBS2			430.50	12.71	7.25
MSBS1			430.50	15.00	7.25
MSSN1			430.50	-15.00	11.25
MSSN2			430.50	-12.71	11.50
MSSC			430.50	0.00	11.63
MSSS2			430.50	12.71	11.75
MSSS1			430.50	15.00	12.00
MSNT-V			2 inch Pressure	430.50	-15.00
MSNT-H2		430.50		-14.00	20.00
MSNM		430.50		-15.00	73.50
MSNB		430.50		15.00	113.88
MSST-V		430.50		15.00	20.75
MSST-H2		430.50		14.00	20.38
MSSM		430.50		15.00	72.50
MSSB		430.50		15.00	113.13
MBS4		Asphalt Strain	435.25	-15.00	9.50
MBS5			435.25	-12.71	9.50
MBS6			435.26	-10.42	9.50
MBS7			435.26	10.42	9.50
MBS8			435.26	12.71	9.50
MBS9			435.26	15.00	9.50
MSS4			435.26	-15.00	4.50
MSS5			435.26	-12.71	4.50
MSS6			435.26	-10.42	4.50
MSS7			435.26	10.42	4.50
MSS8			435.26	12.71	4.50
MSS9			435.26	15.00	4.50
MBS3			437.63	-15.00	9.50
MBS10			437.64	15.00	9.50
MSS3			437.64	-15.00	4.50
MSS10			437.64	15.00	4.50
MBS2	440.00		-15.00	9.50	
MBS11	440.01		15.00	9.50	
MSS2	440.01	-15.00	4.50		

Sensor Name	Test Item	Sensor Type	Location_X (ft.)	Location_Y (ft.)	Location_Z (in.)
MSS11			440.01	15.00	4.50
MBS1			442.38	-15.00	9.50
MBS12			442.39	15.00	9.50
MSS1			442.39	-15.00	4.50
MSS12			442.39	15.00	4.50
JG-10		Joint Gage	520.00	-26.00	4.75
JG-18		520.00	26.00	4.94	
CSG-118	MRS	Concrete Strain	521.00	-10.25	1.50
CSG-418			521.00	-10.25	8.00
CSG-460			521.00	10.25	1.50
CSG-457			521.00	10.25	8.00
CSG-411			524.00	-10.25	1.50
CSG-397			524.00	-10.25	8.00
CSG-474			524.00	10.25	1.50
CSG-473			524.00	10.25	8.00
CSG-402			527.00	-10.25	1.50
CSG-417			527.00	-10.25	8.00
CSG-464			527.00	10.25	1.50
CSG-441			527.00	10.25	8.00
CSG-430			530.00	-10.25	1.50
CSG-280			530.00	-12.00	8.00
CSG-306			530.00	-14.00	1.50
CSG-414			530.00	-16.00	1.50
CSG-333			530.00	-18.00	1.50
CSG-347			530.00	-20.00	1.50
CSG-292			530.00	-10.25	8.00
CSG-432			530.00	-12.00	8.00
CSG-335			530.00	-14.00	8.00
CSG-435			530.00	-16.00	8.00
CSG-423			530.00	-18.00	8.00
CSG-415			530.00	-20.00	8.00
CSG-469			530.00	10.25	1.50
CSG-313			530.00	12.00	1.50
CSG-453			530.00	14.00	1.50
CSG-451	530.00	16.00	1.50		
CSG-450	530.00	18.00	1.50		

Sensor Name	Test Item	Sensor Type	Location_X (ft.)	Location_Y (ft.)	Location_Z (in.)
CSG-445			530.00	20.00	1.50
CSG-301			530.00	10.25	8.00
CSG-429			530.00	12.00	8.00
CSG-465			530.00	14.00	8.00
CSG-461			530.00	16.00	8.00
CSG-456			530.00	18.00	8.00
CSG-443			530.00	20.00	8.00
CSG-434			533.00	-10.25	1.50
CSG-387			533.00	-10.25	8.00
CSG-340			533.00	10.25	1.50
CSG-416			533.00	10.25	8.00
CSG-353			536.00	-10.25	1.50
CSG-346			536.00	-10.25	8.00
CSG-338			536.00	10.25	1.50
CSG-310			536.00	10.25	8.00
CSG-413			536.86	-10.84	8.00
CSG-455			536.86	10.84	8.00
CSG-406			537.19	-11.63	8.00
CSG-438			537.19	11.63	8.00
CSG-412			537.70	-12.30	8.00
CSG-452			537.70	12.30	8.00
CSG-336			538.37	-12.81	8.00
CSG-462			538.37	12.81	8.00
CSG-409			539.00	-10.25	1.50
CSG-284			539.00	-10.25	8.00
CSG-321			539.00	10.25	8.00
CSG-404			539.16	-13.14	8.00
CSG-436			539.16	13.14	8.00
CSG-371			539.75	-12.00	1.50
CSG-331			539.75	-14.00	1.50
CSG-421			539.75	-16.00	1.50
CSG-372			539.75	-18.00	1.50
CSG-408			539.75	-20.00	1.50
CSG-422			539.75	-12.00	8.00
CSG-341			539.75	-14.00	8.00
CSG-420			539.75	-16.00	8.00

Sensor Name	Test Item	Sensor Type	Location_X (ft.)	Location_Y (ft.)	Location_Z (in.)
CSG-396			539.75	-18.00	8.00
CSG-407			539.75	-20.00	8.00
CSG-472			539.75	12.00	1.50
CSG-440			539.75	14.00	1.50
CSG-468			539.75	16.00	1.50
CSG-466			539.75	18.00	1.50
CSG-471			539.75	20.00	1.50
CSG-454			539.75	12.00	8.00
CSG-463			539.75	16.00	8.00
CSG-439			539.75	18.00	8.00
CSG-458			539.75	20.00	8.00
JG-11			540.00	-26.00	5.06
JG-17			540.00	26.00	5.50
CSG-324			541.00	10.25	8.00
CSG-102			541.00	-10.25	1.50
CSG-115			541.00	-10.25	8.00
CSG-332			541.00	10.25	1.50
CSG-344			544.00	10.25	8.00
CSG-106			544.00	-10.25	1.50
CSG-100			544.00	-10.25	8.00
CSG-381			544.00	10.25	1.50
CSG-419			547.00	10.25	8.00
CSG-156			547.00	-10.25	1.50
CSG-90			547.00	-10.25	8.00
CSG-385			547.00	10.25	1.50
CSG-370			550.00	20.00	1.50
CSG-323			550.00	10.25	8.00
CSG-343			550.00	12.00	8.00
CSG-364			550.00	14.00	8.00
CSG-383			550.00	16.00	8.00
CSG-380			550.00	18.00	8.00
CSG-395			550.00	20.00	8.00
CSG-166			550.00	-10.25	1.50
CSG-120			550.00	-12.00	1.50
CSG-121			550.00	-14.00	1.50
CSG-130			550.00	-16.00	1.50

Sensor Name	Test Item	Sensor Type	Location_X (ft.)	Location_Y (ft.)	Location_Z (in.)
CSG-175			550.00	-18.00	1.50
CSG-138			550.00	-20.00	1.50
CSG-198			550.00	-10.25	8.00
CSG-197			550.00	-12.00	8.00
CSG-133			550.00	-14.00	8.00
CSG-105			550.00	-16.00	8.00
CSG-87			550.00	-18.00	8.00
CSG-92			550.00	-20.00	8.00
CSG-388			550.00	10.25	1.50
CSG-339			550.00	12.00	1.50
CSG-377			550.00	14.00	1.50
CSG-356			550.00	16.00	1.50
CSG-291			550.00	18.00	1.50
CSG-389			553.00	10.25	8.00
CSG-114			553.00	-10.25	1.50
CSG-98			553.00	-10.25	8.00
CSG-329			553.00	10.25	1.50
CSG-424			556.00	10.25	8.00
CSG-200			556.00	-10.25	1.50
CSG-97			556.00	-10.25	8.00
CSG-328			556.00	10.25	1.50
CSG-290			556.86	10.84	8.00
CSG-171			556.86	-10.84	8.00
CSG-311			557.19	11.63	8.00
CSG-142			557.19	-11.63	8.00
CSG-410			557.70	12.30	8.00
CSG-116			557.70	-12.30	8.00
CSG-289			558.37	12.81	8.00
CSG-195			558.37	-12.81	8.00
CSG-365			559.00	10.25	8.00
CSG-132			559.00	-10.25	1.50
CSG-169			559.00	-10.25	8.00
CSG-325			559.00	10.25	1.50
CSG-358			559.16	13.14	8.00
CSG-95			559.16	-13.14	8.00
CSG-294			559.75	12.00	1.50

Sensor Name	Test Item	Sensor Type	Location_X (ft.)	Location_Y (ft.)	Location_Z (in.)
CSG-425			559.75	14.00	1.50
CSG-320			559.75	16.00	1.50
CSG-362			559.75	18.00	1.50
CSG-319			559.75	20.00	1.50
CSG-400			559.75	12.00	8.00
CSG-403			559.75	14.00	8.00
CSG-378			559.75	16.00	8.00
CSG-350			559.75	18.00	8.00
CSG-354			559.75	20.00	8.00
CSG-126			559.75	-12.00	1.50
CSG-199			559.75	-14.00	1.50
CSG-108			559.75	-16.00	1.50
CSG-193			559.75	-18.00	1.50
CSG-177			559.75	-20.00	1.50
CSG-88			559.75	-12.00	8.00
CSG-104			559.75	-14.00	8.00
CSG-172			559.75	-16.00	8.00
CSG-148			559.75	-18.00	8.00
CSG-107			559.75	-20.00	8.00
JG-12				Joint Gage	560.00
JG-16	560.00	26.00			5.88
JG-13	580.00	-26.00			5.00
JG-14	580.00	0.00			5.25
JG-15	580.00	26.00			5.69
JG-19	HRS	Joint Gage	645.00	-26.00	5.19
JG-27		Joint Gage	645.00	26.00	5.56
CSG-110		Concrete Strain	646.00	-10.25	1.50
CSG-219			646.00	-10.25	7.50
CSG-286			646.00	10.25	1.50
CSG-348			646.00	10.25	7.50
CSG-271			649.00	-10.25	1.50
CSG-275			649.00	-10.25	7.50
CSG-281			649.00	10.25	1.50
CSG-373			649.00	10.25	7.50
CSG-267			652.00	-10.25	1.50
CSG-260			652.00	-10.25	7.50

Sensor Name	Test Item	Sensor Type	Location_X (ft.)	Location_Y (ft.)	Location_Z (in.)
CSG-317			652.00	10.25	1.50
CSG-355			652.00	10.25	7.50
CSG-255			655.00	-10.25	1.50
CSG-243			655.00	-12.00	1.50
CSG-240			655.00	-14.00	1.50
CSG-227			655.00	-16.00	1.50
CSG-253			655.00	-18.00	1.50
CSG-34			655.00	-20.00	1.50
CSG-242			655.00	-10.25	7.50
CSG-266			655.00	-12.00	7.50
CSG-269			655.00	-14.00	7.50
CSG-212			655.00	-16.00	7.50
CSG-36			655.00	-18.00	7.50
CSG-250			655.00	-20.00	7.50
CSG-428			655.00	10.25	1.50
CSG-401			655.00	12.00	1.50
CSG-337			655.00	14.00	1.50
CSG-345			655.00	16.00	1.50
CSG-427			655.00	18.00	1.50
CSG-352			655.00	20.00	1.50
CSG-433			655.00	10.25	7.50
CSG-431			655.00	12.00	7.50
CSG-318			655.00	14.00	7.50
CSG-309			655.00	16.00	7.50
CSG-326			655.00	18.00	7.50
CSG-302			655.00	20.00	7.50
CSG-259			658.00	-10.25	1.50
CSG-241			658.00	-10.25	7.50
CSG-351			658.00	10.25	1.50
CSG-349			658.00	10.25	7.50
CSG-265			661.00	-10.25	1.50
CSG-257			661.00	-10.25	1.50
CSG-238			661.00	-10.25	7.50
CSG-363			661.00	10.25	1.50
CSG-312			661.00	10.25	7.50
CSG-279			661.86	-10.84	7.50

Sensor Name	Test Item	Sensor Type	Location_X (ft.)	Location_Y (ft.)	Location_Z (in.)		
CSG-304			661.86	10.84	7.50		
CSG-220			662.00	-10.25	7.50		
CSG-211			662.19	-11.63	7.50		
CSG-330			662.19	11.63	7.50		
CSG-256			662.70	-12.30	7.50		
CSG-426			662.70	12.30	7.50		
CSG-246			663.37	-12.81	7.50		
CSG-405			663.37	12.81	7.50		
CSG-369			664.00	10.25	7.50		
CSG-207			664.16	-13.14	7.50		
CSG-398			664.16	13.14	7.50		
CSG-215			664.75	-12.00	1.50		
CSG-247			664.75	-14.00	1.50		
CSG-268			664.75	-16.00	1.50		
CSG-264			664.75	-18.00	1.50		
CSG-217			664.75	-20.00	1.50		
CSG-245			664.75	-12.00	7.50		
CSG-263			664.75	-14.00	7.50		
CSG-210			664.75	-16.00	7.50		
CSG-262			664.75	-18.00	7.50		
CSG-249			664.75	-20.00	7.50		
CSG-287			664.75	12.00	1.50		
CSG-316			664.75	14.00	1.50		
CSG-449			664.75	16.00	1.50		
CSG-442			664.75	20.00	1.50		
CSG-277			664.75	12.00	7.50		
CSG-467			664.75	14.00	7.50		
CSG-470			664.75	16.00	7.50		
CSG-444			664.75	20.00	7.50		
JG-20			Joint Gage		665.00	-26.00	5.19
JG-26					665.00	26.00	5.75
CSG-14			Concrete Strain		666.00	10.25	7.50
CSG-63					666.00	-10.25	1.50
CSG-56					666.00	-10.25	7.50
CSG-7	666.00	10.25			1.50		
CSG-143	669.00	10.25			7.50		

Sensor Name	Test Item	Sensor Type	Location_X (ft.)	Location_Y (ft.)	Location_Z (in.)
CSG-1			669.00	-10.25	1.50
CSG-25			669.00	-10.25	7.50
CSG-37			669.00	10.25	1.50
CSG-144			672.00	10.25	7.50
CSG-5			672.00	-10.25	1.50
CSG-11			672.00	-10.25	7.50
CSG-131			672.00	10.25	1.50
CSG-183			675.00	20.00	7.50
CSG-149			675.00	10.25	7.50
CSG-161			675.00	12.00	7.50
CSG-128			675.00	14.00	7.50
CSG-196			675.00	16.00	7.50
CSG-134			675.00	18.00	7.50
CSG-190			675.00	20.00	7.50
CSG-45			675.00	-10.25	1.50
CSG-41			675.00	-12.00	1.50
CSG-13			675.00	-14.00	1.50
CSG-4			675.00	-18.00	1.50
CSG-83			675.00	-20.00	1.50
CSG-52			675.00	-10.25	7.50
CSG-64			675.00	-12.00	7.50
CSG-44			675.00	-14.00	7.50
CSG-9			675.00	-16.00	7.50
CSG-21			675.00	-18.00	7.50
CSG-10			675.00	-20.00	7.50
CSG-174			675.00	10.25	1.50
CSG-125			675.00	12.00	7.50
CSG-170			675.00	14.00	7.50
CSG-153			675.00	16.00	1.50
CSG-135			675.00	18.00	1.50
CSG-182			678.00	10.25	7.50
CSG-50			678.00	-10.25	1.50
CSG-20			678.00	-10.25	7.50
CSG-109			678.00	10.25	1.50
CSG-194			681.00	10.25	7.50
CSG-6			681.00	-10.25	1.50

Sensor Name	Test Item	Sensor Type	Location_X (ft.)	Location_Y (ft.)	Location_Z (in.)
CSG-57			681.00	-10.25	7.50
CSG-168			681.00	10.25	1.50
CSG-159			681.86	10.84	7.50
CSG-18			681.86	-10.84	7.50
CSG-122			682.19	11.63	7.50
CSG-22			682.19	-11.63	7.50
CSG-167			682.70	12.30	7.50
CSG-76			682.70	-12.30	7.50
CSG-141			683.37	12.81	7.50
CSG-70			683.37	-12.81	7.50
CSG-103			684.00	10.25	7.50
CSG-81			684.00	-10.25	1.50
CSG-33			684.00	-10.25	7.50
CSG-96			684.00	10.25	1.50
CSG-176			684.16	13.14	7.50
CSG-2			684.16	-13.14	7.50
CSG-160			684.75	12.00	1.50
CSG-152			684.75	14.00	1.50
CSG-173			684.75	16.00	1.50
CSG-163			684.75	18.00	1.50
CSG-158			684.75	20.00	1.50
CSG-137			684.75	12.00	7.50
CSG-191			684.75	14.00	7.50
CSG-192			684.75	16.00	7.50
CSG-187			684.75	18.00	7.50
CSG-139			684.75	20.00	7.50
CSG-447			684.75	18.00	7.50
CSG-15			684.75	-12.00	1.50
CSG-30			684.75	-14.00	1.50
CSG-26			684.75	-16.00	1.50
CSG-12			684.75	-18.00	1.50
CSG-40			684.75	-20.00	1.50
CSG-23			684.75	-12.00	7.50
CSG-47			684.75	-14.00	7.50
CSG-61			684.75	-16.00	7.50
CSG-55			684.75	-18.00	7.50

Sensor Name	Test Item	Sensor Type	Location_X (ft.)	Location_Y (ft.)	Location_Z (in.)
CSG-16			684.75	-20.00	7.50
JG-21		Joint Gage	685.00	-26.00	4.88
JG-25			685.00	26.00	5.88
JG-22			705.00	-26.00	4.75
JG-23			705.00	0.00	5.19
JG-24			705.00	26.00	5.75
NW MDD - 1	HFS	Deflection	770.38	-15.00	87.63
NW MDD - 2			770.38	-15.00	73.13
NW MDD - 3			770.38	-15.00	37.13
NW MDD - 4			770.38	-15.00	25.13
NW MDD - 5			770.38	-15.00	16.13
NW MDD - 6			770.38	-15.00	10.13
NW MDD - 7			770.38	-15.00	8.13
CL MDD - 1			770.38	0.00	87.63
CL MDD - 2			770.38	0.00	73.13
CL MDD - 3			770.38	0.00	37.13
CL MDD - 4			770.38	0.00	25.13
CL MDD - 5			770.38	0.00	16.13
CL MDD - 6			770.38	0.00	10.13
CL MDD - 7			770.38	0.00	8.13
SW MDD - 1			770.38	15.00	87.63
SW MDD - 2			770.38	15.00	73.13
SW MDD - 3			770.38	15.00	37.13
SW MDD - 4			770.38	15.00	25.13
SW MDD - 5			770.38	15.00	16.13
SW MDD - 6			770.38	15.00	10.13
SW MDD - 7			770.38	15.00	8.13
NE MDD - 1			792.13	-15.00	88.25
NE MDD - 2			792.13	-15.00	73.75
NE MDD - 3			792.13	-15.00	16.75
NE MDD - 4			792.13	-15.00	10.75
NE MDD - 7			792.13	-15.00	6.75
NE MDD - 5			792.13	-15.00	8.75
NE MDD - 6			792.13	-15.00	7.50
SE MDD - 1			792.13	15.00	88.25
SE MDD - 2			792.13	15.00	73.75

Sensor Name	Test Item	Sensor Type	Location_X (ft.)	Location_Y (ft.)	Location_Z (in.)	
SE MDD - 3			792.13	15.00	16.75	
SE MDD - 4			792.13	15.00	10.75	
SE MDD - 5			792.13	15.00	8.75	
SE MDD - 6			792.13	15.00	7.50	
SE MDD - 7			792.13	15.00	6.75	
HSNW			2 inch Pressure	763.24	-15.00	15.00
HSSW				763.24	15.00	11.50
HSNE		765.62		-15.00	10.50	
HSSE		765.62		15.00	11.50	
HSNT-H1		767.00		-15.00	11.00	
HSST-H1		767.00		15.00	12.00	
HSBN1		6 inch Pressure		768.00	-12.71	6.50
HSBN2			768.00	-15.00	6.50	
HSBC			768.00	0.00	6.50	
HSBS2			768.00	12.71	6.50	
HSBS1			768.00	15.00	6.50	
HSSN1			768.00	-15.00	9.00	
HSSN2			768.00	-12.71	9.00	
HSSC			768.00	0.00	9.00	
HSSS2			768.00	12.71	9.00	
HSSS1			768.00	15.00	9.00	
HSNT-V		2 inch Pressure	768.00	-15.00	10.50	
HSNT-H2			768.00	-14.00	11.50	
HSNM			768.00	-15.00	70.50	
HSNB			768.00	-15.00	97.00	
HSST-V			768.00	15.00	11.50	
HSST-H2			768.00	14.00	11.50	
HSSM			768.00	15.00	68.50	
HSSB			768.00	15.00	99.63	
HBS4			Asphalt Strain	772.76	-15.00	9.50
HBS5	772.76			-12.71	9.50	
HBS6	772.76	-10.42		9.50		
HBS7	772.76	10.42		9.50		
HBS8	772.76	12.71		9.50		
HBS9	772.76	15.00		9.50		
HSS7	772.76	10.42		4.50		

Sensor Name	Test Item	Sensor Type	Location_X (ft.)	Location_Y (ft.)	Location_Z (in.)	
HSS8			772.76	12.71	4.50	
HSS9			772.76	15.00	4.50	
HBS3			775.14	-15.00	9.50	
HBS10			775.14	15.00	9.50	
HSS10			775.14	15.00	4.50	
HBS2			777.51	-15.00	9.50	
HBS11			777.51	15.00	9.50	
HSS11			777.51	15.00	4.50	
HBS1			779.89	-15.00	9.50	
HBS12			779.89	15.00	9.50	
HSS12			779.89	15.00	4.50	
NW MDD - 1			HFC	Deflection	857.88	-15.00
NW MDD - 2	857.88	-15.00			76.75	
NW MDD - 3	857.88	-15.00			40.75	
NW MDD - 4	857.88	-15.00			28.75	
NW MDD - 5	857.88	-15.00			19.75	
NW MDD - 6	857.88	-15.00			13.75	
NW MDD - 7	857.88	-15.00			11.75	
CL MDD - 3	857.88	0.00			41.25	
CL MDD - 1	857.88	0.00			87.25	
CL MDD - 2	857.88	0.00			77.25	
CL MDD - 4	857.88	0.00			29.25	
CL MDD - 5	857.88	0.00			20.25	
CL MDD - 6	857.88	0.00			14.25	
CL MDD - 7	857.88	0.00			12.25	
SW MDD - 1	857.88	15.00			88.25	
SW MDD - 2	857.88	15.00			78.25	
SW MDD - 3	857.88	15.00			42.25	
SW MDD - 4	857.88	15.00			30.25	
SW MDD - 5	857.88	15.00			21.25	
SW MDD - 6	857.88	15.00			15.25	
SW MDD - 7	857.88	15.00			13.25	
HCNW	2 inch Pressure	850.74			-15.00	15.00
HCSW		850.74			15.00	17.50
HCNE		853.12			-15.00	14.50
HCSE		853.12		15.00	16.50	

Sensor Name	Test Item	Sensor Type	Location_X (ft.)	Location_Y (ft.)	Location_Z (in.)
HCNT-H1			854.50	-15.00	14.00
HCST-H1			854.50	15.00	16.50
HCBN1			855.50	-15.00	6.50
HCBN2		855.50	-12.71	7.00	
HCBC		855.50	0.00	6.88	
HCBS2		855.50	12.71	6.75	
HCBS1		855.50	15.00	6.50	
HCSN1		855.50	-15.00	13.50	
HCSN2		855.50	-12.71	13.50	
HCSC		855.50	0.00	13.00	
HCSS2		855.50	12.71	13.00	
HCSS1		855.50	15.00	13.50	
HCNT-V		855.50	-15.00	14.00	
HCNT-H2		855.50	-14.00	16.50	
HCNM		855.50	-15.00	69.50	
HCNB		855.50	-15.00	96.00	
HCST-V		855.50	15.00	16.00	
HCST-H2		855.50	14.00	16.50	
HCSM		855.50	15.00	68.75	
HCSB		855.50	15.00	96.50	
HSC7		860.26	10.42	4.50	
HSC8		860.26	12.71	4.50	
HSC9		860.26	15.00	4.50	
HSC10		862.64	15.00	4.50	
HSC11		865.01	15.00	4.50	
HSC12		867.39	15.00	4.50	
NE MDD - 1		879.63	-15.00	87.38	
NE MDD - 2		879.63	-15.00	77.38	
NE MDD - 3		879.63	-15.00	20.38	
NE MDD - 4		879.63	-15.00	14.38	
NE MDD - 6	879.63	-15.00	8.88		
NE MDD - 5	879.63	-15.00	12.38		
NE MDD - 7	879.63	-15.00	5.88		
SE MDD - 1	879.63	15.00	87.50		
SE MDD - 2	879.63	15.00	77.50		
SE MDD - 3	879.63	15.00	20.50		

Contract No.: DTFACT-15-D-00007

Sensor Name	Test Item	Sensor Type	Location_X (ft.)	Location_Y (ft.)	Location_Z (in.)
SE MDD - 4			879.63	15.00	14.50
SE MDD - 5			879.63	15.00	12.50
SE MDD - 6			879.63	15.00	9.00
SE MDD - 7			879.63	15.00	6.00

APPENDIX D—POST-TRAFFIC TRENCH DATA

LFC-E

Table D-1. CBR Tests on Subgrade Surface in LFC-E Trench-4

Test No.	Depth from Pavement Surface (in.)	Offset from CL (ft.)	Moisture Content (%)	CBR			Mean	Std. Dev.	COV (%)
				Offset from East Face of Trench (in.)					
				12	24	36			
1	50.5	20.0	25.9	5.0	5.0	5.0	5.0	0.00	0.0
2	50.5	18.0	26.7	6.0	5.0	4.3	5.1	0.85	16.8
3	49.5	16.0	26.6	6.0	5.0	5.0	5.3	0.58	10.8
4	48.8	14.0	25.4	6.0	5.6	6.6	6.1	0.50	8.3
5	47.8	12.0	24.2	7.0	7.0	7.4	7.1	0.23	3.2
6	48.0	10.0	26.2	5.0	5.6	5.4	5.3	0.31	5.7
7	49.0	8.0	25.3	4.7	4.8	5.2	4.9	0.26	5.4
8	49.5	6.0	27.4	4.8	5.4	5.0	5.1	0.31	6.0
9	51.5	4.0	27.5	4.5	4.0	4.6	4.4	0.32	7.4
10	52.3	2.0	26.6	4.2	4.0	4.0	4.1	0.12	2.8
11	51.5	0.0	28.3	4.2	4.4	5.0	4.5	0.42	9.2
12	51.5	-4.0	26.7	4.4	4.2	3.6	4.1	0.42	10.2
13	50.3	-6.0	29.0	4.2	4.2	4.5	4.3	0.17	4.0
14	49.5	-8.0	28.1	4.8	4.2	4.2	4.4	0.35	7.9
15	48.5	-10.0	26.0	4.0	4.4	4.4	4.3	0.23	5.4
16	48.0	-12.0	26.7	4.6	4.8	4.8	4.7	0.12	2.4
17	48.0	-14.0	26.2	4.4	5.0		4.7	0.42	9.0
18	48.8	-16.0	27.9	4.4	4.4	4.0	4.3	0.23	5.4
19	49.3	-18.0	26.5	3.8	4.4	3.4	3.9	0.50	13.0
20	52.5	-20.0	26.1	3.0	3.0	3.0	3.0	0.00	0.0

Table D-2. CBR Tests at 6 inch Below Subgrade Surface in LFC-E Trench-4

Test No.	Depth from Pavement Surface (in.)	Offset from CL (ft.)	Moisture Content (%)	CBR			Mean	Std. Dev.	COV (%)
				Offset from East Face of Trench (in.)					
				12	24	36			
1	60.0	12.0	26.6	5.8	5.6	5.6	5.7	0.12	2.0
2	56.0	6.0	27.1	5.8	5.0	5.0	5.3	0.46	8.8
3	58.5	0.0	26.9	5.2	4.6	5.0	4.9	0.31	6.2
4	57.0	-6.0	26.8	5.4	4.8	4.0	4.7	0.70	14.8
5	55.0	-12.0	26.7	5.6	5.6	5.8	5.7	0.12	2.0

Table D-3. CBR Tests at 12 inch Below Subgrade Surface in LFC-E Trench-4

Test No.	Depth from Pavement Surface (in.)	Offset from CL (ft.)	Moisture Content (%)	CBR			Mean	Std. Dev.	COV (%)
				Offset from East Face of Trench (in.)					
				12	24	36			
1	66.0	12.0	25.89	7.0	7.0	7.0	7.0	0.00	0.0
2	62.5	6.0	27.58	4.8	5.5	5.2	5.2	0.35	6.8
3	64.2	0.0	28.99	3.6	4.0	3.5	3.7	0.26	7.2
4	53.0	-6.0	28.28	5.0	5.2	5.4	5.2	0.20	3.8
5	61.0	-12.0	-	5.5	5.4	5.5	5.5	0.06	1.1

Table D-4. CBR Tests at 18 inch Below Subgrade Surface in LFC-E Trench-4

Test No.	Depth from Pavement Surface (in.)	Offset from CL (ft.)	Moisture Content (%)	CBR			Mean	Std. Dev.	COV (%)
				Offset from East Face of Trench (in.)					
				12	24	36			
1	69.3	12.0	26.5	6.6	6.8	7.0	6.8	0.20	2.9
2	68.5	6.0	28.7	4.2	5.4	5.2	4.9	0.64	13.0
3	71.5	0.0	31.3	4.0	4.2	4.6	4.3	0.31	7.2
4	68.5	-6.0	30.2	3.6	4.4	4.6	4.2	0.53	12.6
5	67.0	-12.0	28.7	5.0	5.2	5.4	5.2	0.20	3.8

Table D-5. CBR Tests at 24 inch Below Subgrade Surface in LFC-E Trench-4

Test No.	Depth from Pavement Surface (in.)	Offset from CL (ft.)	Moisture Content (%)	CBR			Mean	Std. Dev.	COV (%)
				Offset from East Face of Trench (in.)					
				12	24	36			
1	74.0	12.0	26.8	7.6	7.8	6.8	7.4	0.53	7.2
2	75.0	6.0	27.7	5.5	5.8	5.0	5.4	0.40	7.4
3	76.5	0.0	27.2	5.5	5.4	5.8	5.6	0.21	3.7
4	76.5	-6.0	26.3	5.4	4.4	4.5	4.8	0.55	11.6
5	75.5	-12.0	27.1	6.4	6.6	6.4	6.5	0.12	1.8

Table D-6. Summary of Drive Cylinder Test Results on Trench-4 LFC-E

Test No.	Offset from Centerline (ft.)	Depth from Subgrade Surface (in.)	Wet Density (pcf.)	Moisture Content (%)	Dry Density (pcf.)	Summary	
						Dry Density	
1	20.0	0.0	123.820	25.76	98.45		
2	16.0	0.0	124.670	24.19	100.39		
3	12.0	0.0	124.480	25.89	98.88		
4	8.0	0.0	124.810	25.85	99.17	Minimum	94.5
5	4.0	0.0	123.620	24.63	99.19	Maximum	101.0
6	0.0	0.0	123.420	25.34	98.47	Mean	97.9
7	-4.0	0.0	123.090	26.60	97.23	Std. Dev.	2.04
8	-8.0	0.0	123.680	25.49	98.56	COV (%)	2.1
9	-12.0	0.0	123.950	22.66	101.05		
10	-16.0	0.0	126.324	26.44	99.91		
11	-20.0	0.0	124.542	27.82	97.44		
12	-12.0	6.0	122.628	26.12	97.23	Minimum	94.5
13	-6.0	6.0	122.430	29.45	94.58	Maximum	97.2
14	0.0	6.0	121.902	29.02	94.48	Mean	95.5
15	6.0	6.0	122.958	28.37	95.78	Std. Dev.	1.11
16	12.0	6.0	122.760	28.33	95.66	COV (%)	1.2
17	-12.0	12.0	123.948	28.62	96.37	Minimum	94.1
18	-6.0	12.0	121.902	29.51	94.12	Maximum	96.4
19	0.0	12.0	121.308	27.43	95.20	Mean	95.4
20	6.0	12.0	122.034	26.93	96.15	Std. Dev.	0.89
21	12.0	12.0	122.166	28.10	95.37	COV (%)	0.9
22	-12.0	18.0	119.526	26.40	94.56	Minimum	91.4
23	-6.0	18.0	120.912	27.07	95.15	Maximum	97.6
24	0.0	18.0	123.354	26.40	97.59	Mean	95.3
25	6.0	18.0	118.074	29.17	91.41	Std. Dev.	2.56
26	12.0	18.0	124.344	27.42	97.59	COV (%)	2.7

27	-12.0	24.0	120.054	27.53	94.14	Minimum	90.1
28	-6.0	24.0	114.444	27.06	90.07	Maximum	96.0
29	0.0	24.0	122.364	28.80	95.00	Mean	94.1
30	6.0	24.0	121.572	27.69	95.21	Std. Dev.	2.34
31	12.0	24.0	122.760	27.84	96.03	COV (%)	2.5

Table D-7. Field Density Test Results on P-209 Crushed Stone Base in LFC-W

Test No.	1	2	3	4	5
Offset from CL (ft.)	-13.42	-23.00	0.00	12.33	23.00
Moisture Content (%)	2.55	3.60	3.40	2.71	2.80
Dry Density (pcf.)	154.20	153.30	150.50	153.50	151.90

Table D-8. Field Density Test Results on P-154 Crushed Stone Subbase in LFC-E

Test No.	1	2	3	4	5
Offset from CL (ft.)	-23.00	-13.42	0.00	12.33	23.00
Moisture Content (%)	3.89	4.13	4.81	2.057	3.54
Dry Density (pcf.)	146.52	150.52	145.24	150.84	145.97

Table D-9. Resilient Modulus Test Results on Trench-4 LFC-E

Location	Depth from Subgrade Surface (in.)	Moisture Content (%)	Dry Density (pcf.)	Confining Stress (psi)	Deviator Stress (psi)	Resilient Strain	Resilient Modulus (psi)
NWT	7.0	27.3	96.8	6.00	1.80	0.00029	6314
					3.60	0.00079	4588
					5.40	0.00171	3160
					7.30	0.00306	2368
					9.00	0.00448	2015
				4.00	1.80	0.00033	5544
					3.60	0.00096	3758
					5.40	0.00197	2756
					7.30	0.00316	2297
					9.00	0.00436	2076
				2.00	1.80	0.00034	5306
					3.60	0.00100	3604
5.40	0.00205	2646					
7.30	0.00326	2226					

Location	Depth from Subgrade Surface (in.)	Moisture Content (%)	Dry Density (pcf.)	Confining Stress (psi)	Deviator Stress (psi)	Resilient Strain	Resilient Modulus (psi)
					9.10	0.00438	2067
CL	9.0	26.5	98.4	6.00	1.80	0.00022	8198
					3.60	0.00060	6093
					5.40	0.00133	4120
					7.20	0.00236	3055
					8.90	0.00364	2448
				4.00	1.80	0.00022	8172
					3.60	0.00063	5789
					5.50	0.00136	3997
					7.30	0.00235	3093
					9.00	0.00351	2572
				2.00	1.80	0.00025	7374
					3.60	0.00070	5196
					5.50	0.00148	3679
					7.20	0.00247	2932
					9.10	0.00356	2550
SWT	5.0	27.0	104.2	6.00	1.80	0.00021	8473
					3.60	0.00055	6498
					5.30	0.00110	4810
					7.10	0.00192	3689
					8.80	0.00296	2981
				4.00	1.80	0.00023	7961
					3.60	0.00061	5808
					5.30	0.00125	4292
					7.10	0.00204	3492
					8.90	0.00297	2998
				2.00	1.80	0.00024	7493
					3.60	0.00066	5452
					5.30	0.00129	4104
					7.10	0.00211	3363
					8.80	0.00299	2951

LFS-W

Table D-10. CBR Tests on Subgrade Surface in LFS-W Trench-1

Test No.	Depth from Pavement Surface (in.)	Offset from CL (ft.)	Moisture Content (%)	CBR					
				Offset from East Face of Trench (in.)			Mean	Std. Dev.	COV (%)
				12	24	36			
1	40.0	-18	27.3	5.0	4.8	5.0	4.9	0.12	2.3
2	40.0	-16	26.7	5.6	6.2	5.4	5.7	0.42	7.3
3	40.0	-12	25.7	5.0	6.0	6.0	5.7	0.58	10.2
4	40.0	-6	28.1	5.2	5.0	5.5	5.2	0.25	4.8
5	40.0	0	24.5	5.5	5.5	5.4	5.5	0.06	1.1
6	40.0	4	25.2	6.0	6.6	5.8	6.1	0.42	6.8
7	40.0	8	27.2	5.0	5.0	5.2	5.1	0.12	2.3
8	40.0	12	27.3	5.2	6.0	6.0	5.7	0.46	8.1
9	40.0	18	24.1	5.8	4.6	4.5	5.0	0.72	14.6

LFS-E

Table D-11. CBR Tests on Subgrade Surface in LFS-E Trench-2

Test No.	Depth from Pavement Surface (in.)	Offset from CL (ft.)	Moisture Content (%)	CBR					
				Offset from East Face of Trench (in.)			Mean	Std. Dev.	COV (%)
				12	24	36			
	41.5	20	26.8	5.5	6.0	6.2	5.9	0.36	6.1
2	41.3	18	25.6	5.8	6.2	5.8	5.9	0.23	3.9
3	41.0	16	25.8	6.2	5.8	6.2	6.1	0.23	3.8
4	40.5	14	26.7	3.5	5.5	4.2	4.4	1.01	23.1
5	39.0	12	24.7	5.6	5.8	5.5	5.6	0.15	2.7
6	40.5	10	25.8	4.4	6.0	6.4	5.6	1.06	18.9
7	40.5	8	25.7	5.5	5.0	4.6	5.0	0.45	9.0
8	41.5	6	26.3	5.0	5.5	5.4	5.3	0.26	5.0
9	41.5	4	26.4	4.8	5.5	5.4	5.2	0.38	7.2
10	42.0	2	25.8	5.0	5.8	6.0	5.6	0.53	9.4
11	42.8	0	27.4	6.2	7.0	5.8	6.3	0.61	9.6
12	43.3	-2	-	5.2	6.0	6.4	5.9	0.61	10.4
13	43.0	-4	28.4	4.8	4.4	5.0	4.7	0.31	6.5
14	42.0	-6	27.7	4.8	4.8	4.2	4.6	0.35	7.5
15	42.0	-8	25.9	4.0	4.6	5.2	4.6	0.60	13.0
16	41.0	-10	26.0	5.2	5.4	4.4	5.0	0.53	10.6
17	40.0	-12	26.0	5.4	5.6	5.2	5.4	0.20	3.7

18	39.5	-14	25.5	5.0	5.0	5.0	5.0	0.00	0.0
19	40.0	-16	25.8	5.8		5.8	5.8	0.00	0.0
20	40.0	-18	25.8	4.0	4.0	4.4	4.1	0.23	5.6
21	40.0	-20	26.7	5.0	4.6	4.2	4.6	0.40	8.7

Table D-12. CBR Tests at 6 inch Below Subgrade Surface in LFS-E Trench-2

Test No.	Depth from Pavement Surface (in.)	Offset from CL (ft.)	Moisture Content (%)	CBR					
				Offset from East Face of Trench (in.)			Mean	Std. Dev.	COV (%)
				12	24	36			
1	46.5	-12.0	27.9	5.2	5.8	5.4	5.5	0.31	5.6
2	48.0	-6.0	28.8	4.5	4.4	5.0	4.6	0.32	6.9
3	46.8	0.0	26.4	5.8	5.6	5.8	5.7	0.12	2.0
4	47.0	6.0	27.0	5.4	5.1	6.4	5.6	0.68	12.1
5	44.5	12.0	26.4	6.4	5.0	6.5	6.0	0.84	14.1

Table D-13. CBR Tests at 12 inch Below Subgrade Surface in LFS-E Trench-2

Test No.	Depth from Pavement Surface (in.)	Offset from CL (ft.)	Moisture Content (%)	CBR					
				Offset from East Face of Trench (in.)			Mean	Std. Dev.	COV (%)
				12	24	36			
1	52.5	28.9	28.9	5.6	5.0	5.2	5.3	0.31	5.8
2	56.0	27.3	27.3	5.5	5.4	5.4	5.4	0.06	1.1
3	55.8	26.8	26.8	5.6	5.5	5.4	5.5	0.10	1.8
4	53.5	28.3	28.3	4.8	5.2	5.4	5.1	0.31	6.0
5	53.0	-	-	7.6	7.8	7.2	7.5	0.31	4.1

Table D-14. CBR Tests at 18 inch Below Subgrade Surface in LFS-E Trench-2

Test No.	Depth from Pavement Surface (in.)	Offset from CL (ft.)	Moisture Content (%)	CBR					
				Offset from East Face of Trench (in.)			Mean	Std. Dev.	COV (%)
				12	24	36			
1	58.5	-12.0	26.0	6.0	5.8	6.4	6.1	0.31	5.0

2	62.5	-6.0	28.1	5.4	5.5	5.2	5.4	0.15	2.8
3	61.0	0.0	28.8	4.6	4.6	5.2	4.8	0.35	7.2
4	58.3	6.0	28.5	5.4	4.6	5.4	5.1	0.46	9.0
5	59.0	12.0	28.3	5.5	5.4	6.4	5.8	0.55	9.6

Table D-15. CBR Tests at 24 inch Below Subgrade Surface in LFS-E Trench-2

Test No.	Depth from Pavement Surface (in.)	Offset from CL (ft.)	Moisture Content (%)	CBR					
				Offset from East Face of Trench (in.)			Mean	Std. Dev.	COV (%)
				12	24	36			
1	64.0	-12.0	29.5	6.8	7.4	7.0	7.1	0.31	4.3
2	67.5	-6.0	29.2	5.4	5.0	5.6	5.3	0.31	5.7
3	69.0	0.0	29.1	4.0	4.4	5.0	4.5	0.50	11.3
4	64.0	6.0	27.1	7.6	6.6	7.0	7.1	0.50	7.1
5	67.0	12.0	28.9	6.5	6.6	6.0	6.4	0.32	5.0

Table D-16. Summary of Drive Cylinder Test Results on Trench-2 LFS-E

Test No.	Offset from CL (ft.)	Depth from Subgrade Surface (in.)	Wet Density (pcf.)	Moisture Content (%)	Dry Density (pcf.)	Summary	
						Dry Density	
1	20.0	0.0	124.41				
2	16.0		124.15	24.14	100.00		
3	12.0		124.48	26.69	98.25		
4	8.0		123.75	26.17	98.08	Minimum	94.7
5	4.0		123.82	28.30	96.51	Maximum	100.0
6	0.0		122.96	29.88	94.67	Mean	97.9
7	-4.0		123.75	26.35	97.94	Std. Dev.	1.45
8	-8.0		124.34	26.35	98.41	COV, %	1.5
9	-12.0		124.48	25.50	99.19		
10	-16.0		124.01	26.35	98.15		
11	-20.0		123.68	26.25	97.96		
12	-12.0	6.0	123.88	26.74	97.74	Minimum	94.2

13	-6.0		123.29	25.15	98.51	Maximum	98.5
14	0.0		121.44	27.35	95.36	Mean	96.7
15	6.0		121.37	28.85	94.20	Std. Dev.	1.82
16	12.0		123.22	26.24	97.61	COV, %	1.9
17	-12.0	12.0	122.76	27.82	96.04	Minimum	94.6
18	-6.0		122.43	27.21	96.24	Maximum	98.1
19	0.0		122.43	27.52	96.01	Mean	96.2
20	6.0		121.51	28.45	94.59	Std. Dev.	1.25
21	12.0		123.16	25.56	98.09	COV, %	1.3
22	12.0	18.0	122.96			Minimum	92.7
23	6.0		120.25	29.68	92.73	Maximum	98.8
24	0.0		121.64	26.44	96.20	Mean	95.2
25	-6.0		120.19	29.36	92.91	Std. Dev.	2.92
26	-12.0		123.68	25.14	98.84	COV, %	3.1
27	-12.0	24.0	121.04	24.64	97.12	Minimum	91.5
28	-6.0		118.34	29.32	91.50	Maximum	98.4
29	0.0		118.87	28.02	92.85	Mean	94.9
30	6.0		119.70	26.50	94.61	Std. Dev.	2.87
31	12.0		122.50	24.50	98.39	COV, %	3.0

Table D-17. Field Density Test Results on P-209 Crushed Stone Base in LFS-E

Test No.	1	2	3	4	5
Offset from CL (ft.)	-16.00	-23.00	0.00	AREA SEVERELY DISTURBED DURING P-401 REMOVAL - TEST WAS NOT PERFORMED	20.50
Moisture Content (%)	3.32	3.45	3.19		3.33
Dry Density (pcf.)	150.51	149.22	144.03		149.05

Table D-18. Resilient Modulus Test Results on Trench-2 LFS-E

Location	Depth from Subgrade Surface (in.)	Moisture Content (%)	Dry Density (pcf.)	Confining Stress (psi)	Deviator Stress (psi)	Resilient Strain	Resilient Modulus (psi)
NWT	16.0	26.7	96.7	6.00	1.80	0.000270	6787
					3.60	0.000730	4991
					5.40	0.001650	3302
					7.10	0.002970	2390
					9.10	0.004310	2108

Location	Depth from Subgrade Surface (in.)	Moisture Content (%)	Dry Density (pcf.)	Confining Stress (psi)	Deviator Stress (psi)	Resilient Strain	Resilient Modulus (psi)
				4.00	1.80	0.000260	6893
					3.60	0.000820	4401
					5.40	0.001820	2994
					7.20	0.003030	2369
					9.00	0.004470	2023
				2.00	1.80	0.000320	5732
					3.60	0.000950	3832
					5.40	0.001970	2753
					7.20	0.003230	2226
					9.00	0.004550	1986
CL	13.0	26.2	98.5	6.00	1.80	0.000260	7062
					3.60	0.000710	5089
					5.40	0.001590	3413
					7.20	0.003080	2331
					9.00	0.004490	2006
				4.00	1.80	0.000260	6961
					3.60	0.000800	4544
					5.50	0.001720	3195
					7.30	0.002860	2539
				2.00	9.00	0.004140	2185
					1.80	0.000290	6326
					3.60	0.000870	4185
					5.40	0.001850	2945
					7.20	0.003020	2398
				SWT	1.5	25.7	98.8
1.80	0.000280	6530					
3.60	0.000770	4710					
5.40	0.001700	3157					
7.10	0.003070	2315					
4.00	8.80	0.004600	1910				
	1.80	0.000310	5864				
	3.60	0.000940	3835				
	5.30	0.001970	2716				
	7.10	0.003230	2215				
2.00	8.90	0.004480	1984				
	1.80	0.000340	5394				

Location	Depth from Subgrade Surface (in.)	Moisture Content (%)	Dry Density (pcf.)	Confining Stress (psi)	Deviator Stress (psi)	Resilient Strain	Resilient Modulus (psi)
					3.60	0.001000	3580
					5.30	0.002080	2569
					7.10	0.003340	2120
					8.90	0.004540	1968

MFC-W

Table D-19. CBR Tests on Subgrade Surface in MFC-W Trench-5

Test No.	Depth from Pavement Surface (in.)	Offset from CL (ft.)	Moisture Content (%)	CBR			Mean	Std. Dev.	COV (%)
				Offset from East Face of Trench (in.)					
				12	24	36			
1	25.5	22.0	34.4	5.8	5.5	6.0	5.8	0.25	4.4
2	26.3	18.0	30.2	6.4	6.2	4.6	5.7	0.99	17.2
3	26.0	16.0	30.9	7.0	7.0	6.2	6.7	0.46	6.9
4	25.0	12.0	32.6	6.6	6.4	6.2	6.4	0.20	3.1
5	27.0	10.0	30.6	8.0	6.5	6.6	7.0	0.84	11.9
6	27.0	8.0	33.4	6.0	6.0	4.6	5.5	0.81	14.6
7	27.0	6.0	31.8	6.4	6.2	6.0	6.2	0.20	3.2
8	27.0	0.0	30.8	6.0	6.5	6.5	6.3	0.29	4.6
9	27.0	-6.0	32.3	6.4	5.5	5.0	5.6	0.71	12.6
10	27.5	-8.0	30.2	6.0	5.8	5.6	5.8	0.20	3.4
11	27.5	-10.0	29.3	8.0	7.0	8.0	7.7	0.58	7.5
12	25.3	-12.0	31.0	6.2	6.4		6.3	0.14	2.2
13	26.0	-14.0	32.7	6.0	5.5	6.2	5.9	0.36	6.1
14	26.0	-18.0	29.3	8.0	6.5	6.6	7.0	0.84	11.9
15	27.0	-20.0	31.2	8.0	7.2	6.5	7.2	0.75	10.4

Table D-20. CBR Tests at 6 inch Below Subgrade Surface in MFC-W Trench-5

Test No.	Depth from Pavement Surface (in.)	Offset from CL (ft.)	Moisture Content (%)	CBR			Mean	Std. Dev.	COV (%)
				Offset from East Face of Trench (in.)					
				12	24	36			
1	32.5	12.0	30.0	10.0	10.0	9.3	9.8	0.40	4.1

2	33.5	6.0	27.4	9.2	7.2	9.5	8.6	1.25	14.5
3	34.0	0.0	29.5	9.6	10.0	8.4	9.3	0.83	8.9
4	36.0	-6.0	26.3	9.0	9.0	9.5	9.2	0.29	3.1
5	31.5	-12.0	29.3	9.0	9.6	7.2	8.6	1.25	14.5

Table D-21. CBR Tests at 12 inch Below Subgrade Surface in MFC-W Trench-5

Test No.	Depth from Pavement Surface (in.)	Offset from CL (ft.)	Moisture Content (%)	CBR					
				Offset from East Face of Trench (in.)			Mean	Std. Dev.	COV (%)
				12	24	36			
1	38.25	12.0	30.3	10.2	9.2	10.0	9.8	0.53	5.4
2	39.25	6.0	29.6	10.0	8.8	8.8	9.2	0.69	7.5
3	39.00	0.0	30.3	8.4	7.2	8.8	8.1	0.83	10.2
4	40.00	-6.0	30.4	10.0	9.2	8.0	9.1	1.01	11.1
5	36.50	-12.0	30.8	9.2	8.4	8.8	8.8	0.40	4.5

Table D-22. CBR Tests at 18 inch Below Subgrade Surface in MFC-W Trench-5

Test No.	Depth from Pavement Surface (in.)	Offset from CL (ft.)	Moisture Content (%)	CBR					
				Offset from East Face of Trench (in.)			Mean	Std. Dev.	COV (%)
				12	24	36			
1	46.0	12.0	30.0	8.0	7.6	8.0	7.9	0.23	2.9
2	45.0	6.0	29.7	6.4	6.4	6.4	6.4	0.00	0.0
3	46.5	0.0	30.1	4.0	5.0	4.0	4.3	0.58	13.3
4	46.0	-6.0	29.9	6.5	6.5	6.2	6.4	0.17	2.7
5	42.0	-12.0	29.5	6.6	7.6	8.8	7.7	1.10	14.4

Table D-23. CBR Tests at 24 inch Below Subgrade Surface in MFC-W Trench-5

Test No.	Depth from Pavement Surface (in.)	Offset from CL (ft.)	Moisture Content (%)	CBR					
				Offset from East Face of Trench (in.)			Mean	Std. Dev.	COV (%)

				12	24	36			
1	52.0	12.0	29.7	6.0	7.5	7.5	7.0	0.87	12.4
2	52.0	6.0	29.1	7.0	6.5	9.0	7.5	1.32	17.6
3	52.5	0.0	29.4	4.8	7.8	10.0	7.5	2.61	34.6
4	51.0	-6.0	25.0	6.0	6.0	6.0	6.0	0.00	0.0
5	48.0	-12.0	28.7	6.0	6.4	5.8	6.1	0.31	5.0

Table D-24. Field Density Test Results on P-154 Crushed Stone Subbase in MFC-W Trench-5

Test No.	1	2	3	4	5
Offset from CL (ft.)	-23.00	-13.42	0.00	12.33	23.00
Moisture Content (%)	3.89	3.02	4.46	4.03	2.95
Dry Density (pcf.)	149.446	151.422	145.214	155.324	146.878

Table D-25. Field Density Test Results on P-209 Crushed Stone Base in MFC-W Trench-5

Test No.	1	2	3	4	5
Offset from CL (ft.)	-13.50	-26.08	0.00	11.67	25.58
Moisture Content (%)	2.39	3.28	2.48	2.12	2.83
Dry Density (pcf.)	151.8	144.8	144.3	150.3	144.8

Table D-26. Summary of Drive Cylinder Test Results on MFC-W Trench-5

Test No.	Offset from CL (ft.)	Depth from Subgrade Surface (in.)	Wet Density (pcf.)	Moisture Content (%)	Dry Density (pcf.)	Summary	
						Dry Density	
1	22.0	0.0	119.920	29.96	92.27		
2	18.0		118.930	30.38	91.22		
3	14.0		119.590	29.88	92.08		
4	12.0		119.660	28.07	93.43	Minimum	88.9
5	8.0		118.340	29.68	91.25	Maximum	93.4
6	4.0		119.530	29.75	92.12	Mean	91.7
7	0.0		117.410	32.02	88.94	Std. Dev.	1.10
8	-6.0		119.260	29.28	92.25	COV, %	1.2

9	-10.0		119.530	30.61	91.51		
10	-16.0		119.196	29.85	91.79		
11	-20.0		119.394	29.92	91.90		
12	-12.0	6.0	119.790	28.41	93.29	Minimum	92.0
13	-6.0		117.744	27.99	91.99	Maximum	93.6
14	0.0		120.318	29.37	93.00	Mean	93.0
15	6.0		119.328	28.00	93.22	Std. Dev.	0.60
16	12.0		120.252	28.54	93.55	COV, %	0.6
17	-12.0	12.0	116.622	28.84	90.52	Minimum	86.8
18	-6.0		114.510	29.04	88.74	Maximum	92.0
19	0.0		116.556	30.39	89.39	Mean	89.5
20	6.0		113.982	31.36	86.77	Std. Dev.	1.94
21	12.0		119.724	30.20	91.95	COV, %	2.2
22	-12.0	18.0	115.302	30.58	88.30	Minimum	83.8
23	-6.0		112.464	29.47	86.87	Maximum	88.3
24	0.0		109.956	30.42	84.31	Mean	85.7
25	6.0		108.834	29.92	83.77	Std. Dev.	1.86
26	12.0		110.220	28.95	85.47	COV, %	2.2
27	-12.0	24.0	118.206	29.79	91.08	Minimum	84.5
28	-6.0		109.098	29.18	84.46	Maximum	91.1
29	0.0		111.672	28.80	86.70	Mean	87.6
30	6.0					Std. Dev.	2.78
31	12.0			113.586	28.81	88.18	COV, %

Table D-27. Resilient Modulus Test Results on MFC-W Trench-5

Location	Depth from Subgrade Surface (in.)	Moisture Content (%)	Dry Density (pcf.)	Confining Stress (psi)	Deviator Stress (psi)	Resilient Strain	Resilient Modulus (psi)
NWT	3.5	30.2	92.6	6.00	1.80	0.000140	13402
					3.60	0.000290	12698
					5.40	0.000480	11290
					7.20	0.000720	9951
					9.00	0.001050	8566
				4.00	1.80	0.000140	13440
					3.60	0.000280	12883
					5.50	0.000460	11856

Location	Depth from Subgrade Surface (in.)	Moisture Content (%)	Dry Density (pcf.)	Confining Stress (psi)	Deviator Stress (psi)	Resilient Strain	Resilient Modulus (psi)
					7.20	0.000690	10397
					9.00	0.001030	8763
				2.00	1.80	0.000150	12357
					3.60	0.000310	11791
					5.40	0.000500	10900
					7.10	0.000740	9718
					9.00	0.001070	8431
CL	5.0	30.3	92.7	6.00	1.80	0.000140	13428
					3.60	0.000280	13001
					5.40	0.000460	11667
					7.10	0.000700	10170
					9.00	0.001030	8677
				4.00	1.80	0.000140	13097
					3.60	0.000280	12679
					5.50	0.000460	11805
					7.20	0.000690	10434
				2.00	9.00	0.001010	8892
					1.80	0.000150	12158
					3.60	0.000310	11791
					5.40	0.000490	11136
					7.20	0.000720	9999
				SWT	10.0	29.6	93.6
3.70	0.000260	14282					
5.50	0.000410	13431					
7.20	0.000600	12094					
8.90	0.000850	10498					
4.00	1.80	0.000120	14938				
	3.70	0.000240	14932				
	5.50	0.000380	14397				
	7.30	0.000550	13215				
	9.00	0.000780	11538				
2.00	1.80	0.000140	13447				
	3.70	0.000270	13414				
	5.50	0.000420	13032				
	7.30	0.000600	12180				

Location	Depth from Subgrade Surface (in.)	Moisture Content (%)	Dry Density (pcf.)	Confining Stress (psi)	Deviator Stress (psi)	Resilient Strain	Resilient Modulus (psi)
					9.00	0.000820	10991

MFC-E

Table D-28. P-401 Core Details

Core No.	Core ID	Core Location (ft.)		P-401	Comments
		Offset from CL	Y	Thickness in.	
1	N0	367'0.0"	-30'7.0"	5.6	Core intact; no cracks
2	N1	367'0.0"	-19'0.0"	5.3	Core intact; no cracks
3	N2	367'0.0"	-17'2.5"	5.1	Core intact; no cracks
4	N3	368'0.0"	-15'3.0"	5.0	Core intact; crack width-125 mils; crack depth-2.5 in; crack initiated from top
5	N4	367'0.0"	-14'1.0"	5.2	Core intact; crack width-40 mils; crack depth-0.5 in; crack initiated from top
6	N5	365'9.0"	-14'0.0"	5.0	Core intact; crack width-80 mils; crack depth-0.5 in; crack initiated from top
7	N6	367'0.0"	-13'0.5"	5.3	Core intact; no cracks
8	N7T	367'0.0"	-12'0.0"	5.6	Core separated; no cracks
8	N7B	367'0.0"	-12'0.0"		Core separated; no cracks
9	N8	367'0.0"	-10'9.0"	5.4	Core intact; crack width-40 mils; crack depth-0.5 in; crack initiated from top
10	N9T	367'0.0"	-9'0.0"	5.4	Core separated; hairline crack at top
10	N9B	367'0.0"	-9'0.0"		Core separated; no cracks
11	N10	367'0.0"	-5'9.5"	5.1	Core intact; no cracks
12	S1T	367'0.0"	17'11.5"	5.3	Core separated; no cracks
12	S1B	367'0.0"	17'11.5"		Core separated; no cracks

Core No.	Core ID	Core Location (ft.)		P-401	Comments
		Offset from CL	Y	Thickness in.	
1	N0	367'0.0"	-30'7.0"	5.6	Core intact; no cracks
13	S2T	367'0.0"	16'1.0"	5.2	Core separated; no cracks
13	S2B	367'0.0"	16'1.0"		Core separated; no cracks
14	S3T	367'0.0"	13'11.0"	4.9	Core separated; no cracks
14	S3B	367'0.0"	13'11.0"		Core separated; no cracks
15	S4T	367'0.0"	12'0.0"	4.8	Core separated; no cracks
15	S4B	367'0.0"	12'0.0"		Core separated; cracked the entire depth of bottom core
16	S5T	367'0.0"	9'10.5"	4.9	Core separated; no cracks
16	S5B	367'0.0"	9'10.5"		Core separated; no cracks
17	S6	367'0.0"	7'0.0"	5.2	Core separated; no cracks
18	S7	367'0.0"	4'11.0"	5.2	Core separated; no cracks
19	S0	367'0.0"	30'7.0"	5.6	Core separated; no cracks

Table D-29. CBR Tests on Subgrade Surface in MFC-E

Test No.	Depth from Pavement Surface (in.)	Offset from CL (ft.)	CBR			Mean	Std. Dev.	COV (%)
			Offset from East Face of Trench (in.)					
			12	24	36			
1	26.0	27		6.9	6.9	6.9	0.00	0.0
2	26.0	25	7.2	7.0	7.5	7.2	0.25	3.5
3	25.0	23	7.1	6.3	5.6	6.3	0.75	11.9
4	25.5	21	5.6	6.4	3.7	5.2	1.39	26.5
5	25.0	19	4.3	5.8	6.4	5.5	1.08	19.7
6	25.0	17	4.1	5.8	5.7	5.2	0.95	18.3
7	24.5	15	5.6		5.9	5.8	0.21	3.7
8	24.0	13	5.1	5.3	5.5	5.3	0.20	3.8
9	25.0	11	5.0	5.6	5.0	5.2	0.35	6.7
10	26.0	9	4.4	5.0	6.3	5.2	0.97	18.6
11	26.0	7	5.9	5.6	5.2	5.6	0.35	6.3
12	26.0	5	5.3	4.6	5.6	5.2	0.51	9.9
13	27.0	3	6.2	5.2	5.4	5.6	0.53	9.4
14	27.0	1		6.3	6.5	6.4	0.14	2.2

15	26.5	-1		4.2	6.0	5.1	1.27	25.0
16	25.5	-3		5.3	5.0	5.2	0.21	4.1
17	25.0	-5		5.6	5.6	5.6	0.00	0.0
18	26.0	-7		5.2	5.1	5.2	0.07	1.4
19	25.0	-9		5.8		5.8		
20	24.5	-11		4.9		4.9		
21	25.0	-13		5.5		5.5		
22	24.5	-15	5.4	5.9		5.7	0.35	6.3
23	25.0	-17		5.1		5.1		
24	26.0	-19		5.6		5.6		
25	26.0	-21		6.2		6.2		
26	26.0	-23		6.3		6.3		
27	26.0	-25		5.8		5.8		
28	27.5	-27		8.0		8.0		

Table D-30. CBR Tests at 6 inch Below Subgrade Surface in MFC-E

Test No.	Depth from Pavement Surface (in.)	Offset from CL (ft.)	CBR
1	29.75	13.5	7.2
2	29.25	12.5	6.4
3	29.75	11.5	6.1
4	32.00	6.3	6.0
5	32.00	5.3	6.3
6	32.00	4.3	5.4
7	31.00	1.0	5.0
8	31.00	0.0	6.8
9	31.00	-1.0	4.9
10	31.00	-4.3	6.5
11	31.50	-5.3	4.2
12	31.25	-6.3	6.6
13	30.00	-12.0	7.4
14	29.50	-13.0	6.6
15	29.50	-14.0	6.0

Table D-31. CBR Tests at 12 inch Below Subgrade Surface in MFC-E

Test No.	Depth from Pavement Surface (in.)	Offset from CL (ft.)	CBR
1	35.50	13.5	9.4
2	35.50	12.5	8.6
3	35.50	11.5	9.6
4	39.00	6.3	6.4
5	38.50	5.3	9.2
6	38.50	4.3	10.0
7	38.00	1.0	10.0
8	37.75	0.0	8.0
9	38.00	-1.0	8.6
10	37.00	-4.3	8.8
11	37.00	-5.3	10.4
12	37.00	-6.3	8.2
13	36.00	-12.0	9.6
14	36.00	-13.0	8.0
15	36.75	-14.0	7.6

Table D-32. CBR Tests at 18 inch Below Subgrade Surface in MFC-E

Test No.	Depth from Pavement Surface (in.)	Offset from CL (ft.)	CBR
1	42.25	13.5	6.0
2	41.25	12.5	6.5
3	42.50	11.5	9.0
4	45.25	6.3	4.4
5	44.75	5.3	5.5
6	44.50	4.3	6.3
7	44.25	1.0	6.2
8	42.00	0.0	5.5
9	42.00	-1.0	5.8
10	43.00	-4.3	7.8
11	43.00	-5.3	5.9
12	43.50	-6.3	7.0
13	42.00	-12.0	8.2
14	42.00	-13.0	6.0
15	43.00	-14.0	6.4

Table D-33. CBR Tests at 24 inch Below Subgrade Surface in MFC-E

Test No.	Depth from Pavement Surface (in.)	Offset from CL (ft.)	CBR
1	49.50	13.5	6.4
2	49.00	12.5	5.8
3	49.50	11.5	6.3
4	52.00	6.3	5.4
5	52.00	5.3	5.4
6	51.25	4.3	5.8
7	51.00	1.0	7.7
8	50.75	0.0	7.0
9	50.75	-1.0	7.2
10	49.75	-4.3	8.3
11	49.00	-5.3	6.0
12	49.75	-6.3	6.8
13	49.00	-12.0	9.6
14	49.25	-13.0	7.6
15	49.00	-14.0	6.2

Table D-34. Field Density Test Results on P-209 Crushed Stone Base on MFC-E

Test No.	1.00	2	3	4	5
Offset from CL (ft.)	-22.33	-13.00	0.00	12.33	22.33
Moisture Content (%)	2.85	2.19	2.58	2.69	2.77
Dry Density (pcf.)	152.90	158.00	155.00	153.50	152.70

Table D-35. Field Density Test Results on P-154 Crushed Stone Subbase on MFC-E

Test No.	1	2	3	4	5
Offset from CL (ft.)	26.25	11.50	0.00	-12.75	-25.33
Moisture Content (%)	3.83	4.21	4.40	3.79	4.65
Dry Density (pcf.)	122.64	121.07	117.76	118.68	135.05

Table D-36. Resilient Modulus Test Results on MFC-E

Test No.	Offset from CL (ft.)	Depth from Subgrade Surface (in.)	Wet Density (pcf.)	Moisture Content (%)	Dry Density (pcf.)	Summary
						Dry Density
1	-1.0	0.0	119.33	32.47	90.08	

2	-9.0	0.0	120.32	31.77	91.31		
3	-16.0	0.0	121.04	32.75	91.18	Minimum	88.2
4	-21.0	0.0	120.05	31.70	91.16	Maximum	91.6
5	0.0	0.0	117.68	33.43	88.19	Mean	90.4
6	9.0	0.0	120.32	32.95	90.50	Std. Dev.	1.10
7	17.0	0.0	121.44	32.51	91.65	COV (%)	1.2
8	19.0	0.0	119.26	32.76	89.83		
9	27.0	0.0	118.54	32.46	89.49		
10	12.5	6.0	121.90	32.67	91.88	Minimum	89.7
11	0.0	6.0	118.93	32.56	89.72	Maximum	91.9
12	5.3	6.0	120.32	32.33	90.92	Mean	91.1
13	-5.3	6.0	121.24	32.07	91.80	Std. Dev.	0.88
14	-13.0	6.0	120.45	31.90	91.32	COV (%)	1.0
15	5.3	12.0	119.33	31.86	90.50	Minimum	87.8
16	0.0	12.0	115.63	31.73	87.78	Maximum	92.7
17	-5.3	12.0	120.71	30.23	92.69	Mean	90.2
18	-13.0	12.0	117.08	32.15	88.60	Std. Dev.	2.03
19	12.5	12.0	120.98	32.19	91.52	COV (%)	2.2
20	-13.0	18.0	114.38	31.01	87.30	Minimum	86.6
21	0.0	18.0	115.17	30.28	88.40	Maximum	92.9
22	-5.3	18.0	120.12	31.49	91.35	Mean	89.3
23	5.3	18.0	112.73	30.20	86.58	Std. Dev.	2.70
24	12.5	18.0	121.77	31.13	92.86	COV (%)	3.0
25	0.0	24.0	112.27	30.63	85.94	Minimum	84.8
26	5.3	24.0	113.26	31.19	86.33	Maximum	90.3
27	12.5	24.0	113.92	32.07	86.25	Mean	86.7
28	-5.3	24.0	110.48	30.34	84.77	Std. Dev.	2.10
29	-13.0	24.0	118.54	31.25	90.31	COV (%)	2.4

MFS-W

Table D-37. CBR Tests on Subgrade Surface in MFS-W Trench-6

Test No.	Depth from Pavement Surface (in.)	Offset from CL (ft.)	CBR			Mean	Std. Dev.	COV (%)
			Offset from East Face of Trench (in.)					
			12	24	36			
1	19.0	22.0	27.9	7.5	8.2	7.7	0.40	5.2
2	19.3	16.0	28.7	8.5	8.4	8.4	0.06	0.7

3	18.3	14.0	26.7	8.0	6.0	7.0	1.00	14.3
4	18.0	12.0	26.5	6.4	6.4	6.3	0.23	3.7
5	20.3	10.0	26.5	5.0	6.0	5.9	0.90	15.2
6	21.3	6.0	27.8	7.0	8.4	7.8	0.72	9.2
7	18.5	0.0	29.9	7.0	7.0	7.0	0.00	0.0
8	20.0	-6.0	28.3	7.1	7.6	7.6	0.45	6.0
9	19.5	-8.0	27.7	6.5	6.0	5.8	0.76	13.1
10	18.8	-10.0	28.1	7.0	5.0	5.8	1.04	17.8
11	18.0	-14.0	28.5	6.0	6.0	6.2	0.29	4.7
12	18.8	-16.0	29.0	7.5	6.2	6.6	0.81	12.4
13	19.8	-18.0	28.2	7.0	6.0	6.7	0.58	8.7
14	19.5	-26.0	28.7	7.5	7.5	7.5	0.00	0.0

Table D-38. CBR Tests at 6 inch Below Subgrade Surface in MFS-W Trench-6

Test No.	Depth from Pavement Surface (in.)	Offset from CL (ft.)	CBR			Mean	Std. Dev.	COV (%)
			Offset from East Face of Trench (in.)					
			12	24	36			
1	24.0	0.0	26.4	6.4	7.0	6.8	0.35	5.1
2	30.0	8.1	24.3	10.0	8.4	9.5	0.92	9.8
3	24.0	12.0	27.5	9.6	9.0	9.5	0.50	5.3
4	27.0	-6.0	25.2	8.4	6.4	7.4	1.00	13.5
5	25.0	-14.0	25.1	6.0	6.5	6.5	0.50	7.7

Table D-39. CBR Tests at 12 inch Below Subgrade Surface in MFS-W Trench-6

Test No.	Depth from Pavement Surface (in.)	Offset from CL (ft.)	CBR			Mean	Std. Dev.	COV (%)
			Offset from East Face of Trench (in.)					
			12	24	36			
1	30.0	0.0	29.3	6.4	7.6	7.2	7.1	0.61
2	36.0	8.1	27.1	10.0	10.0	9.6	9.9	0.23
3	30.0	12.0	29.2	8.4	8.0	6.8	7.7	0.83
4	33.5	-6.0	28.5	5.5	7.0	8.0	6.8	1.26
5	31.0	-14.0	28.9	7.5	7.0	7.0	7.2	0.29

Table D-40. CBR Tests at 18 inch Below Subgrade Surface in MFS-W Trench-6

			CBR	Mean		
--	--	--	-----	------	--	--

Test No.	Depth from Pavement Surface (in.)	Offset from CL (ft.)	Offset from East Face of Trench (in.)				Std. Dev.	COV (%)
			12	24	36			
1	40.5	0.0	29.1	6.0	5.5	6.0	5.8	0.29
2	41.0	8.1	28.3	7.0	6.5	7.0	6.8	0.29
3	36.0	12.0	26.2	10.0	10.0	6.5	8.8	2.02
4	39.5	-6.0	30.3	5.5	5.5	5.5	5.5	0.00
5	38.3	-14.0	28.8	7.0	6.0	5.6	6.2	0.72

Table D-41. CBR Tests at 24 inch Below Subgrade Surface in MFS-W Trench-6

Test No.	Depth from Pavement Surface (in.)	Offset from CL (ft.)	CBR			Mean	Std. Dev.	COV (%)
			Offset from East Face of Trench (in.)					
			12	24	36			
1	47.0	0.0	26.85	6.5	6.0	9.0	7.2	1.61
2	46.3	8.1	27.79	8.0	6.0	7.0	7.0	1.00
3	41.0	12.0	29.77	7.0	8.0	8.0	7.7	0.58
4	45.5	-6.0	29.30	6.5	5.5	6.0	6.0	0.50
5	44.8	-14.0	29.49	4.5	6.0	6.0	5.5	0.87

Table D-42. Summary of Drive Cylinder Test Results on MFS-W Trench-6

Test No.	Offset from CL (ft.)	Depth from Subgrade Surface (in.)	Wet Density (pcf.)	Moisture Content (%)	Dry Density (pcf.)	Summary	
						Dry Density	
1	22.0	0.0	120.910	26.95	95.24		
2	16.0		121.040	27.68	94.80		
3	14.0		121.640	28.86	94.40		
4	12.0		120.710	26.50	95.43		
5	8.0		120.380	26.86	94.89		
6	6.0		117.810	26.59	93.06	Maximum	95.4
7	0.0		120.250	28.86	93.32	Mean	93.7
8	-6.0		120.050	31.20	91.51	Std. Dev.	1.55
9	-9.0		118.870	30.78	90.89	COV, %	1.7
10	-13.0		120.120	26.38	95.04		
11	-16.0		121.308	27.84	94.89		
12	-18.0		119.856	30.65	91.74		

13	-26.0		119.592	27.96	93.46		
14	-12.0	6.0	120.380	25.69	95.78	Minimum	91.7
15	-6.0		120.850	27.35	94.89	Maximum	97.1
16	0.0		117.880	28.52	91.72	Mean	94.9
17	6.0		119.790	26.45	94.73	Std. Dev.	2.00
18	12.0		120.120	23.65	97.15	COV, %	2.1
19	-12.0		12.0	115.830	29.69	89.32	Minimum
20	-6.0	115.760		30.18	88.93	Maximum	92.4
21	0.0	105.400		30.05	81.05	Mean	88.8
22	6.0	120.580		30.57	92.35	Std. Dev.	4.62
23	12.0	120.910		30.94	92.34	COV, %	5.2
24	-12.0	18.0		113.320	29.01	87.84	Minimum
25	-6.0		109.890	29.64	84.77	Maximum	89.2
26	0.0		111.470	27.64	87.33	Mean	87.3
27	6.0		112.860	29.30	87.28	Std. Dev.	1.61
28	12.0		114.440	28.29	89.21	COV, %	1.8
29	-12.0		24.0	115.430	30.06	88.75	Minimum
30	-6.0	111.900		27.40	87.83	Maximum	93.0
31	0.0	112.530		29.55	86.86	Mean	89.4
32	6.0	117.080		29.38	90.50	Std. Dev.	2.42
33	12.0	118.140		27.05	92.99	COV, %	2.7

Table D-43. Resilient Modulus Test Results on MFS-W Trench-6

Location	Depth from Subgrade Surface (in.)	Moisture Content (%)	Dry Density (pcf.)	Confining Stress (psi)	Deviator Stress (psi)	Resilient Strain	Resilient Modulus (psi)
NW T	15.0	29.5	94.5	6.00	1.90	0.000130	14288
					3.60	0.000260	14084
					5.60	0.000430	13156
					7.40	0.000630	11679
					9.10	0.000890	10144
				4.00	1.80	0.000120	14720
					3.80	0.000260	14473

Contract No.: DTFACT-15-D-00007

Location	Depth from Subgrade Surface (in.)	Moisture Content (%)	Dry Density (pcf.)	Confining Stress (psi)	Deviator Stress (psi)	Resilient Strain	Resilient Modulus (psi)				
					5.60	0.000410	13741				
					7.50	0.000600	12420				
					9.20	0.000860	10649				
				2.00	1.90	0.000160	12018				
					3.80	0.000300	12440				
					5.60	0.000460	12215				
					7.40	0.000650	11374				
					9.10	0.000880	10315				
				CL	6.0	28.8	95.4	6.00	1.80	0.000110	16365
									3.60	0.000220	16342
									5.40	0.000340	15902
									7.20	0.000470	15194
9.00	0.000630	14243									
4.00	1.80	0.000110	16508								
	3.60	0.000220	16260								
	5.40	0.000340	15899								
	7.20	0.000470	15246								
	9.00	0.000620	14376								
2.00	1.80	0.000120	14916								
	3.60	0.000240	14815								
	5.40	0.000370	14718								

Location	Depth from Subgrade Surface (in.)	Moisture Content (%)	Dry Density (pcf.)	Confining Stress (psi)	Deviator Stress (psi)	Resilient Strain	Resilient Modulus (psi)
SW T					7.20	0.000500	14358
					9.00	0.000650	13750
	4.0	28.7	95.4	6.00	1.90	0.000130	14914
					3.80	0.000260	14630
					5.50	0.000400	13978
					7.40	0.000560	13183
					9.20	0.000760	12187
				4.00	1.80	0.000130	14772
					3.70	0.000250	14637
					5.50	0.000390	14059
					7.40	0.000550	13372
					9.20	0.000740	12407
				2.00	1.80	0.000140	13394
					3.70	0.000280	13247
					5.60	0.000420	13190
					7.30	0.000590	12534
					9.20	0.000780	11785

Table D-44. Field Density Test Results on P-209 Crushed Stone Base on MFS-W Trench-6

Test No.	1	2	3	4	5
Offset from CL (ft.)	13.83	26.00	0.00	28.42	11.25
Moisture Content (%)	1.53	1.35	1.38	1.48	1.62
Dry Density (pcf.)	144.6	140.9	146.2	143.1	147.6

MFS-E

Table D-45. CBR Tests on Subgrade Surface in MFS-E Trench-7

Test No.	Depth from Pavement Surface (in.)	Offset from CL (ft.)	CBR			Mean	Std. Dev.	COV (%)
			Offset from East Face of Trench (in.)					
			12	24	36			
1	20.9	24.0	28.4		10.0	10.0		
2	21.2	22.0	28.8	10.0	10.0	10.1	0.12	1.1
3	20.7	20.0	28.8	10.0	8.8	9.6	0.69	7.2
4	20.4	18.0	28.0	10.0	10.0	9.2	1.39	15.1
5	20.2	16.0	26.9	9.2	6.8	8.3	1.33	16.0
6	19.2	14.0	26.5	6.0	4.8	5.7	0.83	14.5
7	19.4	12.0	27.2	3.6	7.2	5.8	1.93	33.3
8	20.4	10.0	27.9	4.7	6.6	5.9	1.04	17.7
9	21.4	8.0	29.8	3.6	5.5	5.1	1.35	26.4
10	22.1	6.0	29.7	6.5	9.0	7.0	1.84	26.5
11	19.7	4.0	28.4	8.0	9.6	8.6	0.87	10.1
12	19.7	2.0	27.8	7.2	10.0	9.1	1.62	17.8
13	20.2	0.0	28.0	9.0	9.0	9.4	0.69	7.4
14	19.5	-2.0	25.4	10.0	9.0	10.1	1.21	11.9
15	19.3	-4.0	27.7	7.8	9.0	9.0	1.15	12.8
16	19.6	-6.0	28.1	4.0	8.1	6.7	2.34	34.9
17	19.5	-8.0	28.6	6.0	6.8	6.9	1.01	14.5
18	19.0	-10.0	29.6	6.0	7.4	7.0	0.87	12.5
19	18.8	-12.0	28.7	6.0	7.8	7.0	0.92	13.1
20	20.3	-14.0	30.2	7.0	8.4	7.8	0.72	9.2
21	20.2	-16.0	28.7	7.3	7.8	7.6	0.25	3.3
22	20.2	-18.0	30.4	6.4	5.6	6.0	0.40	6.7
23	19.3	-20.0	27.8	6.5	6.6	7.0	0.72	10.4
24	20.2	-22.0	22.8	6.0	6.0	7.2	2.08	28.9
25	19.0	-24.0	29.4	7.2	6.4	7.1	0.61	8.6

Table D-46. CBR Tests at 6 inch Below Subgrade Surface in MFS-E Trench-7

Test No.	Depth from Pavement Surface (in.)	Offset from CL (ft.)	Moisture Content (%)	CBR			Mean	Std. Dev.	COV (%)
				Offset from East Face of Trench (in.)					
				12	24	36			

1	26.0	0.0	28.8	11.0	10.0	11.5	10.8	0.76	7.1
2	26.0	8.0	25.9	10.0	10.8	11.0	10.6	0.53	5.0
3	23.8	11.6	26.6	6.4	8.0	7.6	7.3	0.83	11.4
4	26.3	-5.3	26.3	10.0	11.0	9.6	10.2	0.72	7.1
5	24.8	-14.0	26.8	11.0	10.0	11.8	10.9	0.90	8.2

Table D-47. CBR Tests at 12 inch Below Subgrade Surface in MFS-E Trench-7

Test No.	Depth from Pavement Surface (in.)	Offset from CL (ft.)	Moisture Content (%)	CBR					
				Offset from East Face of Trench (in.)			Mean	Std. Dev.	COV (%)
				12	24	36			
1	31.0	0.0	25.9	10.0	9.0	7.0	8.7	1.53	17.6
2	30.0	11.6	28.2	9.0	8.8	9.0	8.9	0.12	1.3
3	33.0	8.0	29.3	9.0	8.0	7.8	8.3	0.64	7.8
4	32.3	-5.3	27.2	5.0	5.5		5.3	0.35	6.7
5	31.0	-14.0	28.2	6.6	8.4	6.5	7.2	1.07	14.9

Table D-48. CBR Tests at 18 inch Below Subgrade Surface in MFS-E Trench-7

Test No.	Depth from Pavement Surface (in.)	Offset from CL (ft.)	Moisture Content (%)	CBR					
				Offset from East Face of Trench (in.)			Mean	Std. Dev.	COV (%)
				12	24	36			
1	37.5	0.0	28.0	6.0	5.0	5.0	5.3	0.58	10.8
2	37.5	11.6	26.5	8.0	8.0	6.5	7.5	0.87	11.5
3	43.0	8.0	25.8	5.0	6.0	6.0	5.7	0.58	10.2
4	38.8	-5.3	26.8	10.0	8.4	6.0	8.1	2.01	24.8
5	37.2	-14.0	28.0	6.5	5.0	6.0	5.8	0.76	13.1

Table D-49. CBR Tests at 24 inch Below Subgrade Surface in MFS-E Trench-7

Test No.	Depth from Pavement Surface (in.)	Offset from CL (ft.)	Moisture Content (%)	CBR					
				Offset from East Face of Trench (in.)			Mean	Std. Dev.	COV (%)
				12	24	36			
1	45.0	0.0	29.5	8.0	8.0	8.0	8.0	0.00	0.0
2	43.5	11.6	28.7	7.0	7.0	10.0	8.0	1.73	21.7

3	50.0	8.0		5.5	5.5	5.5	5.5	0.00	0.0
4	44.0	-5.3	27.9	6.0	9.0	8.0	7.7	1.53	19.9
5	43.0	-14.0		7.0	6.5	6.5	6.7	0.29	4.3

Table D-50. Summary of Drive Cylinder Test Results on MFS-E Trench-7

Test No.	Offset from CL (ft.)	Depth from Subgrade Surface (in.)	Wet Density (pcf.)	Moisture Content (%)	Dry Density (pcf.)	Summary	
						Dry Density	
1	24.0	0.0	119.53	31.07	91.19		
2	20.0		118.21	26.04	93.78		
3	16.0		120.25	29.33	92.98		
4	12.0		120.32	27.07	94.68		
5	8.0		116.42	30.37	89.30	Minimum	89.0
6	4.0		120.91	29.94	93.05	Maximum	94.7
7	0.0		119.06	29.55	91.91	Mean	92.3
8	-4.0		119.66	31.00	91.34	Std. Dev.	1.73
9	-8.0		118.67	33.27	89.05	COV, %	1.9
10	-12.0			119.99	30.58	91.89	
	-16.0		120.71	29.92	92.91		
	-20.0		119.59	27.50	93.79		
11	-24.0		120.25	28.23	93.78		
12	-12.0	6.0	119.79	28.49	93.23	Minimum	92.4
13	-6.0		121.11	28.49	94.26	Maximum	96.6
14	0.0		118.73	28.49	92.41	Mean	94.0
15	6.0		121.51	30.02	93.45	Std. Dev.	1.59
16	12.0		120.58	24.85	96.58	COV, %	1.7
17	-12.0	12.0	118.93	24.53	95.50	Minimum	89.5
18	-6.0		114.51	27.57	89.76	Maximum	95.5
19	0.0		114.97	28.52	89.46	Mean	92.8
20	6.0		119.33	27.06	93.91	Std. Dev.	2.93
21	12.0		119.79	25.94	95.12	COV, %	3.2
22	-12.0	18.0	119.33	25.66	94.96	Minimum	84.3
23	-6.0		113.92	26.14	90.31	Maximum	95.0
24	0.0		108.11	28.24	84.30	Mean	88.7
25	6.0		109.10	27.76	85.39	Std. Dev.	4.24
26	12.0		112.66	27.00	88.71	COV, %	4.8
27	-12.0		24.0	111.94	29.01	86.77	Minimum
28	-6.0	107.65		28.13	84.01	Maximum	92.1
29	0.0	110.88		26.76	87.47	Mean	87.5

30	6.0		112.13	28.39	87.34	Std. Dev.	2.90
31	12.0		115.90	25.86	92.08	COV, %	3.3

Table D-51. Resilient Modulus Test Results on MFS-E Trench-7

Location	Depth from Subgrade Surface (in.)	Moisture Content (%)	Dry Density (pcf.)	Confining Stress (psi)	Deviator Stress (psi)	Resilient Strain	Resilient Modulus (psi)
NWT	10.0	28.6	92.2	6.00	1.80	0.000120	15397
					3.70	0.000240	15415
					5.50	0.000370	14922
					7.30	0.000510	14085
					9.20	0.000700	13036
				4.00	1.80	0.000120	14901
					3.80	0.000260	14779
					5.50	0.000380	14439
					7.60	0.000540	13949
					9.20	0.000700	13117
	2.00	1.80	0.000140	13611			
		3.80	0.000280	13603			
		5.50	0.000410	13379			
		7.30	0.000560	13005			
		9.20	0.000730	12521			
CL	4.0	28.8	94.0	6.00	1.80	0.000120	15887
					3.70	0.000240	15217
					5.50	0.000390	14183
					7.30	0.000560	12948
					9.00	0.000770	11689
				4.00	1.80	0.000120	15484
					3.70	0.000240	15505
					5.50	0.000380	14743
					7.40	0.000540	13667
					9.10	0.000750	12210
				2.00	1.80	0.000130	14585
					3.70	0.000260	14309
					5.50	0.000400	13931
					7.40	0.000560	13125
					9.10	0.000760	11986

Location	Depth from Subgrade Surface (in.)	Moisture Content (%)	Dry Density (pcf.)	Confining Stress (psi)	Deviator Stress (psi)	Resilient Strain	Resilient Modulus (psi)
SWT	6.0	28.9	93.7	6.00	1.80	0.000150	12073
					3.70	0.000320	11505
					5.50	0.000530	10264
					7.30	0.000790	9146
					9.10	0.001120	8124
				4.00	1.80	0.000150	12361
					3.60	0.000310	11641
					5.50	0.000510	10848
					7.20	0.000750	9675
					9.10	0.001090	8291
				2.00	1.80	0.000160	11733
					3.70	0.000330	10973
					5.40	0.000540	10108
					7.30	0.000800	9094
					9.10	0.001140	7983

Table D-52. Field Density Test Results on P-209 Crushed Stone Base on MFS-E Trench-7

Test No.	1	2	3	4	5
Offset from CL (ft.)	-13.00	-25.33	0.00	13.33	22.50
Moisture Content (%)	1.01	1.56	1.14	1.12	1.38
Dry Density (pcf.)	134.4*	148.3	144.2	145.2	141.6

- The P-209 aggregate surface in the north side was damaged during P-401 removal, which may have caused the lower density

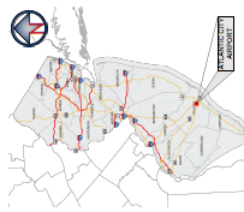
APPENDIX E—CONSTRUCTION CYCLE 1 HISTORICAL RECORD DRAWINGS

CONSTRUCTION CYCLE 1 HISTORICAL RECORD DRAWINGS

NATIONAL AIRPORT PAVEMENT TESTING FACILITY
WILLIAM J. HUGHES TECHNICAL CENTER
ATLANTIC CITY AIRPORT, NEW JERSEY

CONSTRUCTION PLAN DATE: 08/12/1998, DRAWINGS PREPARATION DATE: 05/23/2018

NEW JERSEY STATE MAP N.T.S.



VICINITY MAP N.T.S.



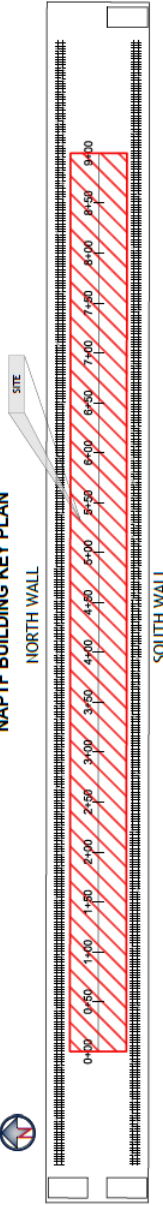
PROJECT LOCATION MAP N.T.S.



AERIAL VIEW OF THE NAPTF BUILDING N.T.S.



NAPTF BUILDING KEY PLAN



REFER TO :
Genlts. Highway, FF and N. Garp (2004), Towards
a Permanent ACN Solution for 6/17/04 Landing
Area at Atlantic City International Airport,
New Technologies: 38-56.

INDEX OF DRAWINGS

SHEET	SHEET TITLE	DATE
1 OF 12	COVER SHEET	05/23/2018
2 OF 12	SITE ACCESS, HANDING AND STAGING AREA PLAN	05/23/2018
3 OF 12	PLAN VIEW AND PROFILE VIEW	05/23/2018
4 OF 12	TEST PAVEMENT SECTIONS	05/23/2018
5 OF 12	SECTION 1 - LOW STRENGTH SUBGRADE ETA, 4+00 TO 5+00 INSTRUMENTATION PLAN	05/23/2018
6 OF 12	SECTION 2 - LOW STRENGTH SUBGRADE ETA, 5+00 TO 6+00 INSTRUMENTATION PLAN	05/23/2018
7 OF 12	SECTION 3 - MEDIUM STRENGTH SUBGRADE ETA, 6+00 TO 7+00 INSTRUMENTATION TABLE	05/23/2018
8 OF 12	SECTION 4 - MEDIUM STRENGTH SUBGRADE ETA, 7+00 TO 8+00 INSTRUMENTATION TABLE	05/23/2018
9 OF 12	SECTION 5 - HIGH STRENGTH SUBGRADE ETA, 8+00 TO 9+00 INSTRUMENTATION TABLE	05/23/2018
10 OF 12	SECTION 6 - HIGH STRENGTH SUBGRADE ETA, 8+00 TO 9+00 INSTRUMENTATION TABLE	05/23/2018
11 OF 12	CONSTRUCTION DETAILS	05/23/2018
12 OF 12	CONSTRUCTION DETAILS	05/23/2018

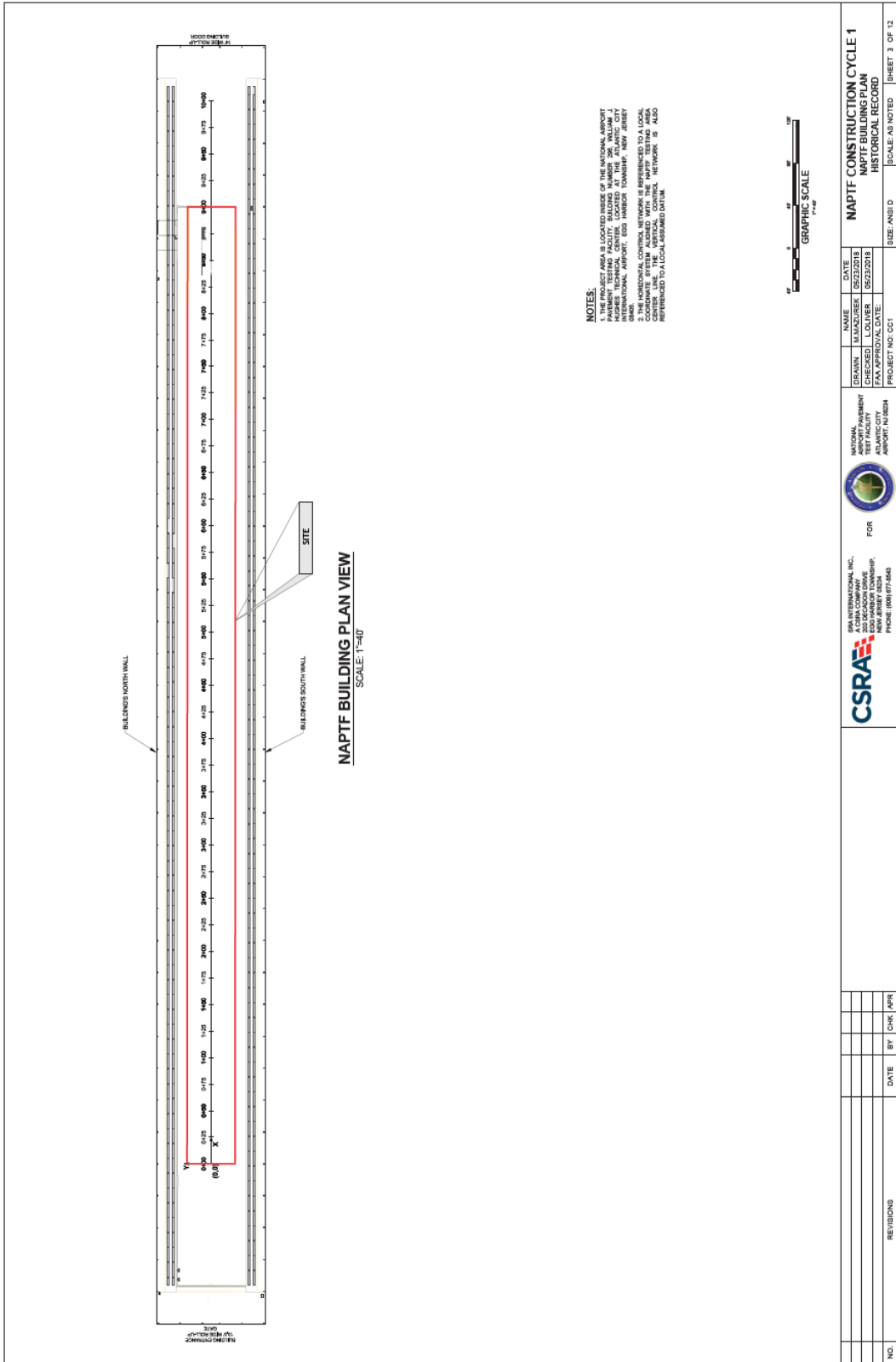
PREPARED BY:

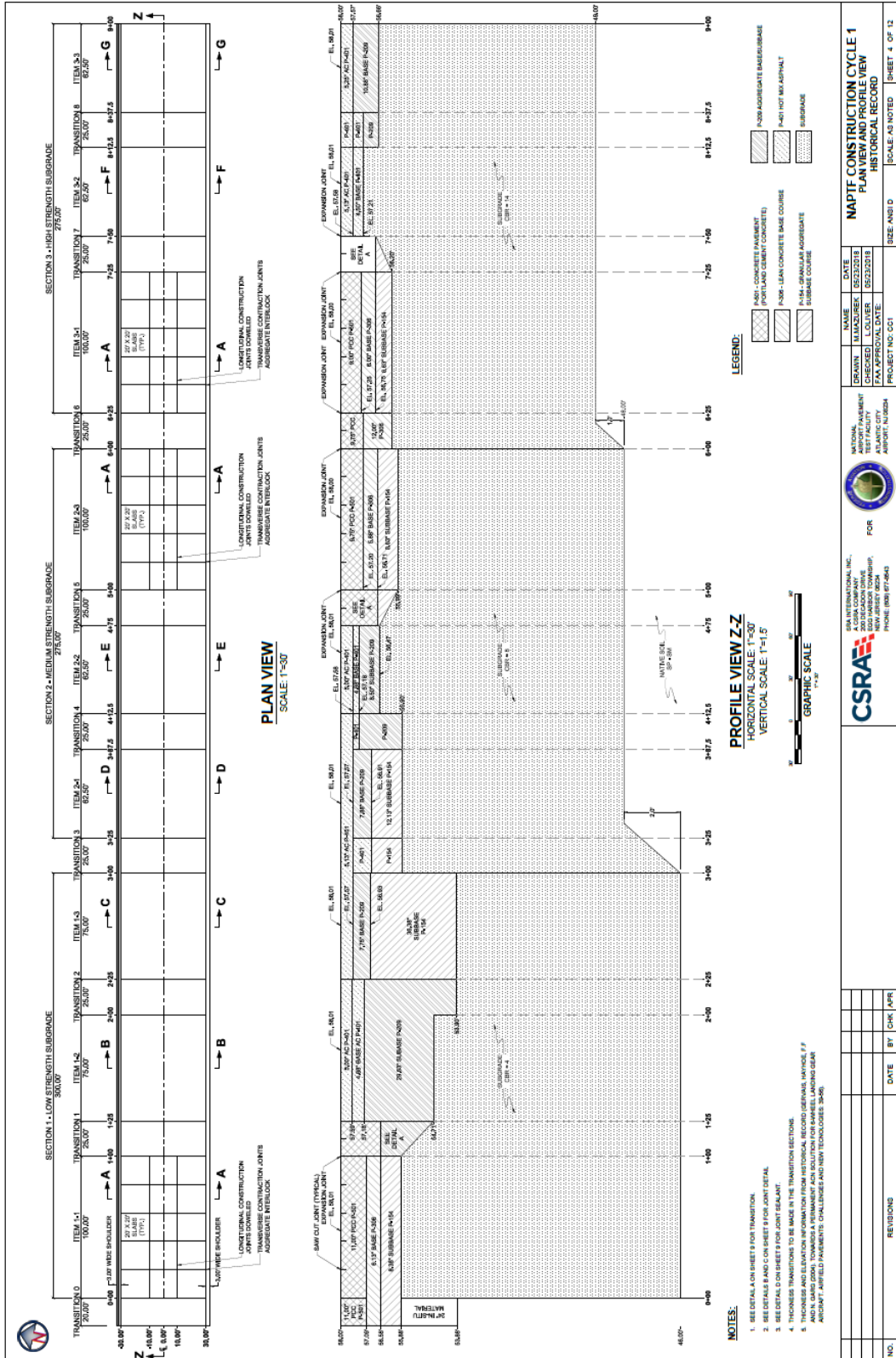


CSRA INTERNATIONAL, A CSRA COMPANY
800 HARBOR TOWNSHIP, NJ 08224
PHONE: (609) 877-5843

SHEET 1 OF 12







DRAWN		CHECKED		DATE		PROJECT NO.		SHEET NO.		SCALE	
NAME	AMAZUREK	NAME	LOUIER	DATE	02/20/2018	DATE	02/20/2018	NO.	001	OF	12
<p>NAPTIF CONSTRUCTION CYCLE 1 PLAN VIEW AND PROFILE VIEW HISTORICAL RECORD</p> <p>FOR NATIONAL TEST FACILITY ATLANTIC CITY MOUNTAIN TOP</p> <p>CSRA CONSTRUCTION SERVICES, INC. A CORA COMPANY 200 HARBOR TOWNSHIP NEW BRIDGE DELEN MOUNTAIN TOP, PA 18054</p> <p>CAD FILE: C01-CONE-PLAN.DWG</p>											

ID	SENSOR NAME	SENSOR TYPE	X (INCH)	Y (INCH)	Z (INCH)	ID	SENSOR NAME	SENSOR TYPE	X (INCH)	Y (INCH)	Z (INCH)	ID	SENSOR NAME	SENSOR TYPE	X (INCH)	Y (INCH)	Z (INCH)
1	M01	Maximum pressure in bulk	50.00	0.00	2.00	181	CS0401	Concrete Strain	50.00	-25.00	0.00	201	LS0101	Load Strain	150.00	0.00	0.00
2	M02	Maximum pressure in bulk	50.00	0.00	2.00	182	CS0402	Concrete Strain	50.00	-25.00	0.00	202	LS0102	Load Strain	150.00	0.00	0.00
3	T01	Temperature	50.00	0.00	0.00	183	CS0403	Concrete Strain	50.00	-25.00	0.00	203	LS0103	Load Strain	150.00	0.00	0.00
4	T02	Temperature	50.00	0.00	0.00	184	CS0404	Concrete Strain	50.00	-25.00	0.00	204	LS0104	Load Strain	150.00	0.00	0.00
5	T03	Temperature	50.00	0.00	0.00	185	CS0405	Concrete Strain	50.00	-25.00	0.00	205	LS0105	Load Strain	150.00	0.00	0.00
6	T04	Temperature	50.00	0.00	0.00	186	CS0406	Concrete Strain	50.00	-25.00	0.00	206	LS0106	Load Strain	150.00	0.00	0.00
7	T05	Temperature	50.00	0.00	0.00	187	CS0407	Concrete Strain	50.00	-25.00	0.00	207	LS0107	Load Strain	150.00	0.00	0.00
8	T06	Temperature	50.00	0.00	0.00	188	CS0408	Concrete Strain	50.00	-25.00	0.00	208	LS0108	Load Strain	150.00	0.00	0.00
9	T07	Temperature	50.00	0.00	0.00	189	CS0409	Concrete Strain	50.00	-25.00	0.00	209	LS0109	Load Strain	150.00	0.00	0.00
10	T08	Temperature	50.00	0.00	0.00	190	CS0410	Concrete Strain	50.00	-25.00	0.00	210	LS0110	Load Strain	150.00	0.00	0.00
11	T09	Temperature	50.00	0.00	0.00	191	CS0411	Concrete Strain	50.00	-25.00	0.00	211	LS0111	Load Strain	150.00	0.00	0.00
12	T10	Temperature	50.00	0.00	0.00	192	CS0412	Concrete Strain	50.00	-25.00	0.00	212	LS0112	Load Strain	150.00	0.00	0.00
13	T11	Temperature	50.00	0.00	0.00	193	CS0413	Concrete Strain	50.00	-25.00	0.00	213	LS0113	Load Strain	150.00	0.00	0.00
14	T12	Temperature	50.00	0.00	0.00	194	CS0414	Concrete Strain	50.00	-25.00	0.00	214	LS0114	Load Strain	150.00	0.00	0.00
15	T13	Temperature	50.00	0.00	0.00	195	CS0415	Concrete Strain	50.00	-25.00	0.00	215	LS0115	Load Strain	150.00	0.00	0.00
16	T14	Temperature	50.00	0.00	0.00	196	CS0416	Concrete Strain	50.00	-25.00	0.00	216	LS0116	Load Strain	150.00	0.00	0.00
17	T15	Temperature	50.00	0.00	0.00	197	CS0417	Concrete Strain	50.00	-25.00	0.00	217	LS0117	Load Strain	150.00	0.00	0.00
18	T16	Temperature	50.00	0.00	0.00	198	CS0418	Concrete Strain	50.00	-25.00	0.00	218	LS0118	Load Strain	150.00	0.00	0.00
19	T17	Temperature	50.00	0.00	0.00	199	CS0419	Concrete Strain	50.00	-25.00	0.00	219	LS0119	Load Strain	150.00	0.00	0.00
20	T18	Temperature	50.00	0.00	0.00	200	CS0420	Concrete Strain	50.00	-25.00	0.00	220	LS0120	Load Strain	150.00	0.00	0.00
21	T19	Temperature	50.00	0.00	0.00	201	CS0421	Concrete Strain	50.00	-25.00	0.00	221	LS0121	Load Strain	150.00	0.00	0.00
22	T20	Temperature	50.00	0.00	0.00	202	CS0422	Concrete Strain	50.00	-25.00	0.00	222	LS0122	Load Strain	150.00	0.00	0.00
23	T21	Temperature	50.00	0.00	0.00	203	CS0423	Concrete Strain	50.00	-25.00	0.00	223	LS0123	Load Strain	150.00	0.00	0.00
24	T22	Temperature	50.00	0.00	0.00	204	CS0424	Concrete Strain	50.00	-25.00	0.00	224	LS0124	Load Strain	150.00	0.00	0.00
25	T23	Temperature	50.00	0.00	0.00	205	CS0425	Concrete Strain	50.00	-25.00	0.00	225	LS0125	Load Strain	150.00	0.00	0.00
26	T24	Temperature	50.00	0.00	0.00	206	CS0426	Concrete Strain	50.00	-25.00	0.00	226	LS0126	Load Strain	150.00	0.00	0.00
27	T25	Temperature	50.00	0.00	0.00	207	CS0427	Concrete Strain	50.00	-25.00	0.00	227	LS0127	Load Strain	150.00	0.00	0.00
28	T26	Temperature	50.00	0.00	0.00	208	CS0428	Concrete Strain	50.00	-25.00	0.00	228	LS0128	Load Strain	150.00	0.00	0.00
29	T27	Temperature	50.00	0.00	0.00	209	CS0429	Concrete Strain	50.00	-25.00	0.00	229	LS0129	Load Strain	150.00	0.00	0.00
30	T28	Temperature	50.00	0.00	0.00	210	CS0430	Concrete Strain	50.00	-25.00	0.00	230	LS0130	Load Strain	150.00	0.00	0.00
31	T29	Temperature	50.00	0.00	0.00	211	CS0431	Concrete Strain	50.00	-25.00	0.00	231	LS0131	Load Strain	150.00	0.00	0.00
32	T30	Temperature	50.00	0.00	0.00	212	CS0432	Concrete Strain	50.00	-25.00	0.00	232	LS0132	Load Strain	150.00	0.00	0.00
33	T31	Temperature	50.00	0.00	0.00	213	CS0433	Concrete Strain	50.00	-25.00	0.00	233	LS0133	Load Strain	150.00	0.00	0.00
34	T32	Temperature	50.00	0.00	0.00	214	CS0434	Concrete Strain	50.00	-25.00	0.00	234	LS0134	Load Strain	150.00	0.00	0.00
35	T33	Temperature	50.00	0.00	0.00	215	CS0435	Concrete Strain	50.00	-25.00	0.00	235	LS0135	Load Strain	150.00	0.00	0.00
36	T34	Temperature	50.00	0.00	0.00	216	CS0436	Concrete Strain	50.00	-25.00	0.00	236	LS0136	Load Strain	150.00	0.00	0.00
37	T35	Temperature	50.00	0.00	0.00	217	CS0437	Concrete Strain	50.00	-25.00	0.00	237	LS0137	Load Strain	150.00	0.00	0.00
38	T36	Temperature	50.00	0.00	0.00	218	CS0438	Concrete Strain	50.00	-25.00	0.00	238	LS0138	Load Strain	150.00	0.00	0.00
39	T37	Temperature	50.00	0.00	0.00	219	CS0439	Concrete Strain	50.00	-25.00	0.00	239	LS0139	Load Strain	150.00	0.00	0.00
40	T38	Temperature	50.00	0.00	0.00	220	CS0440	Concrete Strain	50.00	-25.00	0.00	240	LS0140	Load Strain	150.00	0.00	0.00
41	T39	Temperature	50.00	0.00	0.00	221	CS0441	Concrete Strain	50.00	-25.00	0.00	241	LS0141	Load Strain	150.00	0.00	0.00
42	T40	Temperature	50.00	0.00	0.00	222	CS0442	Concrete Strain	50.00	-25.00	0.00	242	LS0142	Load Strain	150.00	0.00	0.00
43	T41	Temperature	50.00	0.00	0.00	223	CS0443	Concrete Strain	50.00	-25.00	0.00	243	LS0143	Load Strain	150.00	0.00	0.00
44	T42	Temperature	50.00	0.00	0.00	224	CS0444	Concrete Strain	50.00	-25.00	0.00	244	LS0144	Load Strain	150.00	0.00	0.00
45	T43	Temperature	50.00	0.00	0.00	225	CS0445	Concrete Strain	50.00	-25.00	0.00	245	LS0145	Load Strain	150.00	0.00	0.00
46	T44	Temperature	50.00	0.00	0.00	226	CS0446	Concrete Strain	50.00	-25.00	0.00	246	LS0146	Load Strain	150.00	0.00	0.00
47	T45	Temperature	50.00	0.00	0.00	227	CS0447	Concrete Strain	50.00	-25.00	0.00	247	LS0147	Load Strain	150.00	0.00	0.00
48	T46	Temperature	50.00	0.00	0.00	228	CS0448	Concrete Strain	50.00	-25.00	0.00	248	LS0148	Load Strain	150.00	0.00	0.00
49	T47	Temperature	50.00	0.00	0.00	229	CS0449	Concrete Strain	50.00	-25.00	0.00	249	LS0149	Load Strain	150.00	0.00	0.00
50	T48	Temperature	50.00	0.00	0.00	230	CS0450	Concrete Strain	50.00	-25.00	0.00	250	LS0150	Load Strain	150.00	0.00	0.00
51	T49	Temperature	50.00	0.00	0.00	231	CS0451	Concrete Strain	50.00	-25.00	0.00	251	LS0151	Load Strain	150.00	0.00	0.00
52	T50	Temperature	50.00	0.00	0.00	232	CS0452	Concrete Strain	50.00	-25.00	0.00	252	LS0152	Load Strain	150.00	0.00	0.00
53	T51	Temperature	50.00	0.00	0.00	233	CS0453	Concrete Strain	50.00	-25.00	0.00	253	LS0153	Load Strain	150.00	0.00	0.00
54	T52	Temperature	50.00	0.00	0.00	234	CS0454	Concrete Strain	50.00	-25.00	0.00	254	LS0154	Load Strain	150.00	0.00	0.00
55	T53	Temperature	50.00	0.00	0.00	235	CS0455	Concrete Strain	50.00	-25.00	0.00	255	LS0155	Load Strain	150.00	0.00	0.00
56	T54	Temperature	50.00	0.00	0.00	236	CS0456	Concrete Strain	50.00	-25.00	0.00	256	LS0156	Load Strain	150.00	0.00	0.00
57	T55	Temperature	50.00	0.00	0.00	237	CS0457	Concrete Strain	50.00	-25.00	0.00	257	LS0157	Load Strain	150.00	0.00	0.00
58	T56	Temperature	50.00	0.00	0.00	238	CS0458	Concrete Strain	50.00	-25.00	0.00	258	LS0158	Load Strain	150.00	0.00	0.00
59	T57	Temperature	50.00	0.00	0.00	239	CS0459	Concrete Strain	50.00	-25.00	0.00	259	LS0159	Load Strain	150.00	0.00	0.00
60	T58	Temperature	50.00	0.00	0.00	240	CS0460	Concrete Strain	50.00	-25.00	0.00	260	LS0160	Load Strain	150.00	0.00	0.00

LOCATION KEY

NO.	REVISIONS	DATE	BY	CHK	APP

SCALE AS NOTED

SECTION 1 - LOW STRENGTH SUBGRADE
SIA 000 TO 300 INSTRUMENTATION TABLE

CSRA
CONSTRUCTION SOFTWARE
300 BILKIN DRIVE
ATLANTA, GA 30328
PHONE: 800.878.0000

FOR
NATIONAL INSTRUMENT
TEST FACILITY
ATLANTA, GA 30328

DRAWN MAZUREK
CHECKED LOUIER
DATE 05/22/2018

PROJECT NO. **SCALE AS NOTED**

DATE **BY** **CHK** **APP**

NO. **REVISIONS** **DATE** **BY** **CHK** **APP**

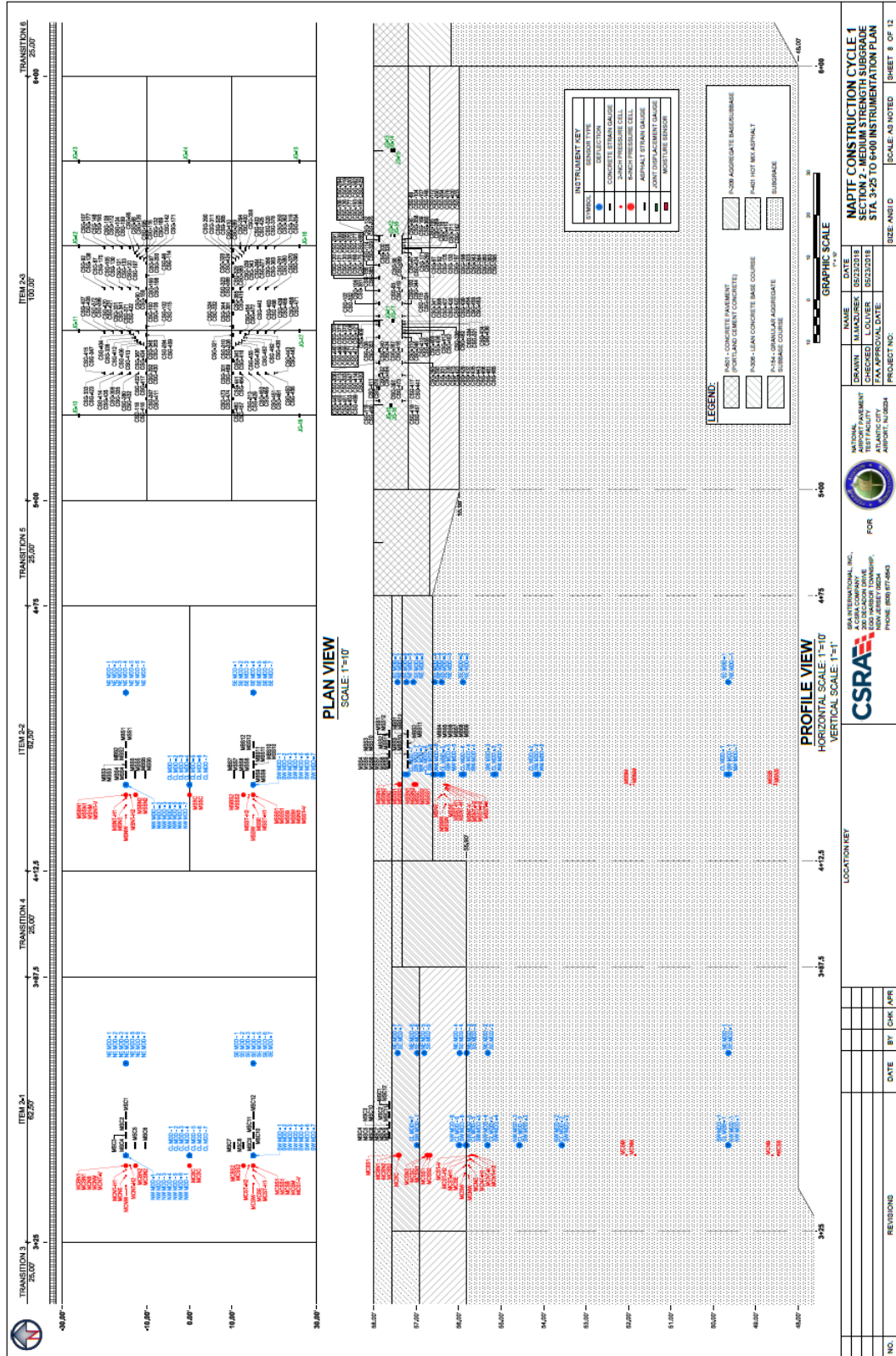
CSRA INTERNATIONAL, INC.
300 BILKIN DRIVE
ATLANTA, GA 30328
PHONE: 800.878.0000

GENERAL DYNAMICS
Information Technology

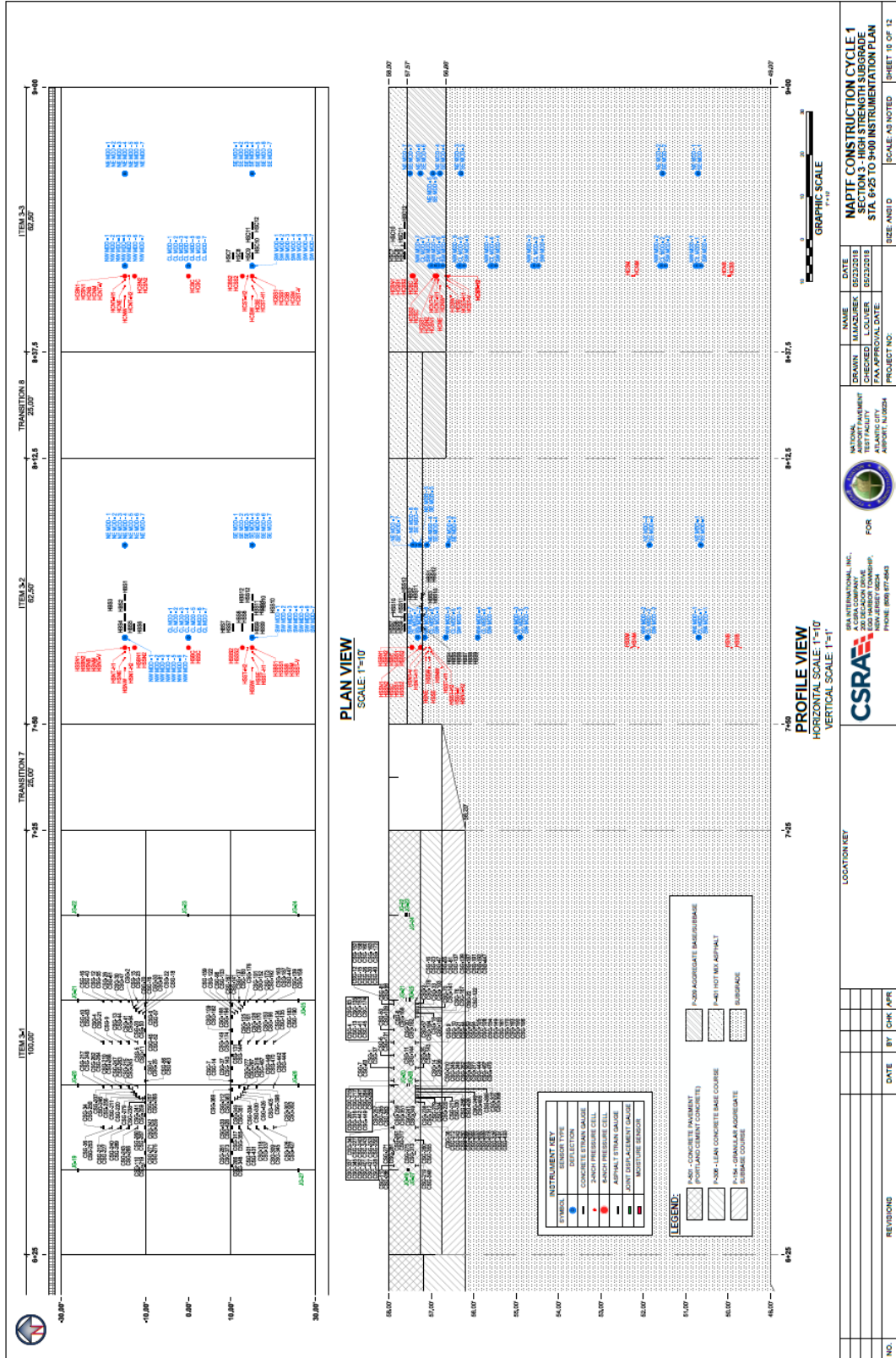
SECTION 1 - LOW STRENGTH SUBGRADE
SIA 000 TO 300 INSTRUMENTATION TABLE

SCALE AS NOTED

NO. **REVISIONS** **DATE** **BY** **CHK** **APP**



NO.	REVISION	DATE	BY	CHK	MR	LOCATION/KEY	CSRA	FOR	NATIONAL SECURITY AUTHORITY	CHECKED	LOUISER	DATE	NAME	DATE	SCALE	SHEET	OF
101	REV 000000-1	14/03/15	0000														
102	REV 000000-2	14/03/15	0000														
103	REV 000000-3	14/03/15	0000														
104	REV 000000-4	14/03/15	0000														
105	REV 000000-5	14/03/15	0000														
106	REV 000000-6	14/03/15	0000														
107	REV 000000-7	14/03/15	0000														
108	REV 000000-8	14/03/15	0000														
109	REV 000000-9	14/03/15	0000														
110	REV 000000-10	14/03/15	0000														
111	REV 000000-11	14/03/15	0000														
112	REV 000000-12	14/03/15	0000														
113	REV 000000-13	14/03/15	0000														
114	REV 000000-14	14/03/15	0000														
115	REV 000000-15	14/03/15	0000														
116	REV 000000-16	14/03/15	0000														
117	REV 000000-17	14/03/15	0000														
118	REV 000000-18	14/03/15	0000														
119	REV 000000-19	14/03/15	0000														
120	REV 000000-20	14/03/15	0000														
121	REV 000000-21	14/03/15	0000														
122	REV 000000-22	14/03/15	0000														
123	REV 000000-23	14/03/15	0000														
124	REV 000000-24	14/03/15	0000														
125	REV 000000-25	14/03/15	0000														
126	REV 000000-26	14/03/15	0000														
127	REV 000000-27	14/03/15	0000														
128	REV 000000-28	14/03/15	0000														
129	REV 000000-29	14/03/15	0000														
130	REV 000000-30	14/03/15	0000														
131	REV 000000-31	14/03/15	0000														
132	REV 000000-32	14/03/15	0000														
133	REV 000000-33	14/03/15	0000														
134	REV 000000-34	14/03/15	0000														
135	REV 000000-35	14/03/15	0000														
136	REV 000000-36	14/03/15	0000														
137	REV 000000-37	14/03/15	0000														
138	REV 000000-38	14/03/15	0000														
139	REV 000000-39	14/03/15	0000														
140	REV 000000-40	14/03/15	0000														
141	REV 000000-41	14/03/15	0000														
142	REV 000000-42	14/03/15	0000														
143	REV 000000-43	14/03/15	0000														
144	REV 000000-44	14/03/15	0000														
145	REV 000000-45	14/03/15	0000														
146	REV 000000-46	14/03/15	0000														
147	REV 000000-47	14/03/15	0000														
148	REV 000000-48	14/03/15	0000														
149	REV 000000-49	14/03/15	0000														
150	REV 000000-50	14/03/15	0000														
151	REV 000000-51	14/03/15	0000														
152	REV 000000-52	14/03/15	0000														
153	REV 000000-53	14/03/15	0000														
154	REV 000000-54	14/03/15	0000														
155	REV 000000-55	14/03/15	0000														
156	REV 000000-56	14/03/15	0000														
157	REV 000000-57	14/03/15	0000														
158	REV 000000-58	14/03/15	0000														
159	REV 000000-59	14/03/15	0000														
160	REV 000000-60	14/03/15	0000														
161	REV 000000-61	14/03/15	0000														
162	REV 000000-62	14/03/15	0000														
163	REV 000000-63	14/03/15	0000														
164	REV 000000-64	14/03/15	0000														
165	REV 000000-65	14/03/15	0000														
166	REV 000000-66	14/03/15	0000														
167	REV 000000-67	14/03/15	0000														
168	REV 000000-68	14/03/15	0000														
169	REV 000000-69	14/03/15	0000														
170	REV 000000-70	14/03/15	0000														
171	REV 000000-71	14/03/15	0000														
172	REV 000000-72	14/03/15	0000														
173	REV 000000-73	14/03/15	0000														
174	REV 000000-74	14/03/15	0000														
175	REV 000000-75	14/03/15	0000														
176	REV 000000-76	14/03/15	0000														
177	REV 000000-77	14/03/15	0000														
178	REV 000000-78	14/03/15	0000														
179	REV 000000-79	14/03/15	0000														
180	REV 000000-80	14/03/15	0000														
181	REV 000000-81	14/03/15	0000														
182	REV 000000-82	14/03/15	0000														
183	REV 000000-83	14/03/15	0000														
184	REV 000000-84	14/03/15	0000														
185	REV 000000-85	14/03/15	0000														
186	REV 000000-86	14/03/15	0000														
187	REV 000000-87	14/03/15	0000														
188	REV 000000-88	14/03/15	0000														
189	REV 000000-89	14/03/15	0000														
190	REV 000000-90	14/03/15	0000														
191	REV 000000-91	14/03/15	0000														
192	REV 000000-92	14/03/15	0000														
193	REV 000000-93	14/03/15	0000														
194	REV 000000-94	14/03/15	0000														
195	REV 000000-95	14/03/15	0000														
196	REV 000000-96	14/0															



ID	SENSOR NAME	SENSOR TYPE	STA (BLVD)	X	Y	Z	DATE	BY	CHK	APP
801	SRM M001-1	Deflection	801.00	10.00	10.00	10.00	11/27/15	MM		
802	SRM M001-2	Deflection	801.00	10.00	10.00	10.00	11/27/15	MM		
803	SRM M001-3	Deflection	801.00	10.00	10.00	10.00	11/27/15	MM		
804	SRM M001-4	Deflection	801.00	10.00	10.00	10.00	11/27/15	MM		
805	SRM M001-5	Deflection	801.00	10.00	10.00	10.00	11/27/15	MM		
806	SRM M001-6	Deflection	801.00	10.00	10.00	10.00	11/27/15	MM		
807	SRM M001-7	Deflection	801.00	10.00	10.00	10.00	11/27/15	MM		
808	SRM M001-8	Deflection	801.00	10.00	10.00	10.00	11/27/15	MM		
809	SRM M001-9	Deflection	801.00	10.00	10.00	10.00	11/27/15	MM		
810	SRM M001-10	Deflection	801.00	10.00	10.00	10.00	11/27/15	MM		

ID	SENSOR NAME	SENSOR TYPE	STA (BLVD)	X	Y	Z	DATE	BY	CHK	APP
811	SRM M002-1	Deflection	802.00	10.00	10.00	10.00	11/27/15	MM		
812	SRM M002-2	Deflection	802.00	10.00	10.00	10.00	11/27/15	MM		
813	SRM M002-3	Deflection	802.00	10.00	10.00	10.00	11/27/15	MM		
814	SRM M002-4	Deflection	802.00	10.00	10.00	10.00	11/27/15	MM		
815	SRM M002-5	Deflection	802.00	10.00	10.00	10.00	11/27/15	MM		
816	SRM M002-6	Deflection	802.00	10.00	10.00	10.00	11/27/15	MM		
817	SRM M002-7	Deflection	802.00	10.00	10.00	10.00	11/27/15	MM		
818	SRM M002-8	Deflection	802.00	10.00	10.00	10.00	11/27/15	MM		
819	SRM M002-9	Deflection	802.00	10.00	10.00	10.00	11/27/15	MM		
820	SRM M002-10	Deflection	802.00	10.00	10.00	10.00	11/27/15	MM		

ID	SENSOR NAME	SENSOR TYPE	STA (BLVD)	X	Y	Z	DATE	BY	CHK	APP
821	SRM M003-1	Deflection	803.00	10.00	10.00	10.00	11/27/15	MM		
822	SRM M003-2	Deflection	803.00	10.00	10.00	10.00	11/27/15	MM		
823	SRM M003-3	Deflection	803.00	10.00	10.00	10.00	11/27/15	MM		
824	SRM M003-4	Deflection	803.00	10.00	10.00	10.00	11/27/15	MM		
825	SRM M003-5	Deflection	803.00	10.00	10.00	10.00	11/27/15	MM		
826	SRM M003-6	Deflection	803.00	10.00	10.00	10.00	11/27/15	MM		
827	SRM M003-7	Deflection	803.00	10.00	10.00	10.00	11/27/15	MM		
828	SRM M003-8	Deflection	803.00	10.00	10.00	10.00	11/27/15	MM		
829	SRM M003-9	Deflection	803.00	10.00	10.00	10.00	11/27/15	MM		
830	SRM M003-10	Deflection	803.00	10.00	10.00	10.00	11/27/15	MM		

ID	SENSOR NAME	SENSOR TYPE	STA (BLVD)	X	Y	Z	DATE	BY	CHK	APP
831	SRM M004-1	Deflection	804.00	10.00	10.00	10.00	11/27/15	MM		
832	SRM M004-2	Deflection	804.00	10.00	10.00	10.00	11/27/15	MM		
833	SRM M004-3	Deflection	804.00	10.00	10.00	10.00	11/27/15	MM		
834	SRM M004-4	Deflection	804.00	10.00	10.00	10.00	11/27/15	MM		
835	SRM M004-5	Deflection	804.00	10.00	10.00	10.00	11/27/15	MM		
836	SRM M004-6	Deflection	804.00	10.00	10.00	10.00	11/27/15	MM		
837	SRM M004-7	Deflection	804.00	10.00	10.00	10.00	11/27/15	MM		
838	SRM M004-8	Deflection	804.00	10.00	10.00	10.00	11/27/15	MM		
839	SRM M004-9	Deflection	804.00	10.00	10.00	10.00	11/27/15	MM		
840	SRM M004-10	Deflection	804.00	10.00	10.00	10.00	11/27/15	MM		

ID	SENSOR NAME	SENSOR TYPE	STA (BLVD)	X	Y	Z	DATE	BY	CHK	APP
841	SRM M005-1	Deflection	805.00	10.00	10.00	10.00	11/27/15	MM		
842	SRM M005-2	Deflection	805.00	10.00	10.00	10.00	11/27/15	MM		
843	SRM M005-3	Deflection	805.00	10.00	10.00	10.00	11/27/15	MM		
844	SRM M005-4	Deflection	805.00	10.00	10.00	10.00	11/27/15	MM		
845	SRM M005-5	Deflection	805.00	10.00	10.00	10.00	11/27/15	MM		
846	SRM M005-6	Deflection	805.00	10.00	10.00	10.00	11/27/15	MM		
847	SRM M005-7	Deflection	805.00	10.00	10.00	10.00	11/27/15	MM		
848	SRM M005-8	Deflection	805.00	10.00	10.00	10.00	11/27/15	MM		
849	SRM M005-9	Deflection	805.00	10.00	10.00	10.00	11/27/15	MM		
850	SRM M005-10	Deflection	805.00	10.00	10.00	10.00	11/27/15	MM		

ID	SENSOR NAME	SENSOR TYPE	STA (BLVD)	X	Y	Z	DATE	BY	CHK	APP
851	SRM M006-1	Deflection	806.00	10.00	10.00	10.00	11/27/15	MM		
852	SRM M006-2	Deflection	806.00	10.00	10.00	10.00	11/27/15	MM		
853	SRM M006-3	Deflection	806.00	10.00	10.00	10.00	11/27/15	MM		
854	SRM M006-4	Deflection	806.00	10.00	10.00	10.00	11/27/15	MM		
855	SRM M006-5	Deflection	806.00	10.00	10.00	10.00	11/27/15	MM		
856	SRM M006-6	Deflection	806.00	10.00	10.00	10.00	11/27/15	MM		
857	SRM M006-7	Deflection	806.00	10.00	10.00	10.00	11/27/15	MM		
858	SRM M006-8	Deflection	806.00	10.00	10.00	10.00	11/27/15	MM		
859	SRM M006-9	Deflection	806.00	10.00	10.00	10.00	11/27/15	MM		
860	SRM M006-10	Deflection	806.00	10.00	10.00	10.00	11/27/15	MM		

MAPLE CONSTRUCTION CYCLE 1
SECTION 3 - HIGH SPEED RAIL UPGRADE
STA 9+25 TO 9+00 INSTRUMENTATION TABLE

SCALE AS NOTED SHEET 11 OF 12

LOCATION NET

NO.	REVISIONS	DATE	BY	CHK	APP



CSRA
CONSTRUCTION SERVICES, INC.
1000 WILSON ROAD, SUITE 100
FARMINGTON, CT 06030
PHONE 860 671-6800



MWH
CONSTRUCTION
TEST FACILITY
1000 WILSON ROAD, SUITE 100
FARMINGTON, CT 06030
PHONE 860 671-6800



FOR
MWH
CONSTRUCTION
TEST FACILITY
1000 WILSON ROAD, SUITE 100
FARMINGTON, CT 06030
PHONE 860 671-6800

NAME	DATE
DRAWN: MWH	05/22/2015
CHECKED: L. COLLIER	05/22/2015
APPROVED: MWH	05/22/2015

